THESE DE DOCTORAT

Soutenue le 08/07/2014 pour l'obtention du grade de docteur d'Aix-Marseille Université

Spécialité : Biogéochimie marine

Présentée par :

Nicolas FERRETTO

Étude de la matière organique dissoute fluorescente naturelle et anthropique en Méditerranée côtière nord-occidentale

Encadrée par :

Madeleine GOUTX, Directeur de recherche CNRS, MIO, Aix-Marseille Université

Stéphane MOUNIER, Maître de conférences, PROTEE, Université de Toulon

Marc TEDETTI, Chargé de recherche IRD, MIO, Aix-Marseille Université

Devant le jury composé de :

Edith PARLANTI, Chargée de recherche CNRS, EPOC, Université de Bordeaux

Claire RICHARD, Directeur de recherche CNRS, ICCF, Université Blaise Pascal

Richard SEMPERE, Directeur de recherche CNRS, MIO, Aix-Marseille Université

Oliver ZIELINSKI, Professeur, ICBM, Université d'Oldenburg

Résumé

La baie de Marseille, située en Méditerranée nord-occidentale, est impactée par des apports d'eau douce issus du Rhône et de ses effluents. Leur rôle dans la composition et la variabilité saisonnière de la matière organique dissoute (DOM) naturelle et anthropique (hydrocarbures et biocides), présente dans le delta du Rhône ainsi qu'en baie de Marseille est encore peu documenté. Une partie de la DOM possède des propriétés de fluorescence (la FDOM) et peut être caractérisée et quantifiée par spectrofluorimétrie. Le but de cette thèse est d'enrichir les connaissances sur la composition et la dynamique de la FDOM naturelle et anthropique dans les eaux continentales du bassin du Rhône et en Méditerranée côtière nord-occidentale.

Les propriétés de fluorescence (λ_{Ex}, λ_{Em}, temps de vie de fluorescence) et les limites de détection d'hydrocarbures aromatiques polycycliques (PAHs) et de biocides d'intérêt ont été déterminées à l'aide de solutions de composés standards. L'analyse factorielle parallèle (PARAFAC) appliquée sur les matrices de fluorescence 3 dimensions de solutions standards (mélanges de HAPs ou de biocides avec des substances humiques) puis d'échantillons naturels a montré les avantages (rapidité et simplicité des analyses) et les limites (sensibilité, effet de quenching) du couplage spectrofluorimétrie et analyse statistique multi-variée pour caractériser et quantifier la FDOM anthropique dans des milieux aquatiques contaminés. La recherche de ces composés anthropiques dans l'environnement côtier méditerranéen a fait l'objet d'un échantillonnage d'un an (février 2011-février 2012) dans les eaux du Rhône (station d'Arles), le delta du Rhône (étang de Vaccarès) et la baie de Marseille (stations Port de Bouc, Couronne et Sofcom). L'analyse des contaminants réalisée par techniques chromatographiques (GC-MS, LC-MS) a montré que seul le delta du Rhône était impacté par les biocides, avec la présence de bentazone à des concentrations allant de 20 à 970 ng L^{-1}. Un pic de contamination était observé en début d'été, qui correspondait à la période d'épandage de biocides pour la culture du riz. Les hydrocarbures étaient présents dans chaque site avec des concentrations en PAHs totaux allant de 8,1 à 405 ng L^{-1}. Les concentrations les plus élevées étaient enregistrées en hiver et étaient liées aux dépôts atmosphériques et aux apports du Rhône. La spectrofluorimétrie n'a pas pu mettre en évidence la présence de contaminants lors de cet échantillonnage, si ce n'est dans quelques échantillons de la zone industrielle du Golf de Fos pour lesquelles des signatures de fluorescence de PAHs pétrogéniques ont été détectées (naphtalène, phénanthrène, fluorène). Cependant, l'analyse de la FDOM naturelle a montré 1) que les substances humiques de sources terrigènes prédominaient dans les eaux continentales, tandis que le matériel de type protéique était plus abondant dans les eaux marines, produit par l'activité biologique autochtone, et 2) que le Rhône jouait un rôle majeur dans la baie de Marseille en augmentant la quantité de DOM réfractaire et labile par des apports directs, et en stimulant la production primaire par des apports de sels nutritifs.

Abstract

The Marseille bay, located in the North-western Mediterranean Sea, is impacted by important inputs of freshwater from the Rhône River and its effluents. Its role on composition and seasonal variability of anthropogenic (hydrocarbons and biocides) and natural dissolved organic matter (DOM), present in the Rhône delta and in the Marseille Bay is still poorly documented. A part of the DOM has fluorescence properties (FDOM) and can be characterised and quantified by spectrofluorimetry. The goal of this thesis was to supply knowledge about composition and dynamic of anthropogenic and natural FDOM in inland waters of the Rhône basin and in the North-western coastal Mediterranean Sea.

The fluorescence properties (λ_{Ex}, λ_{Em}, fluorescence lifetime) and detection limits of polycyclic aromatic hydrocarbons (PAHs) and targeted biocides were determined from standard solutions. The parallel factor analysis (PARAFAC) applied on 3 dimensions fluorescence matrices from standard solutions (mixture of PAHs or biocides with humic substances) and on contaminated field samples showed the relevances (quick and easy) and the limits (sensitivity, quenching effect) coupling spectrofluorimetry and statistical multi-way analysis to characterise and to quantify the anthropogenic FDOM in contaminated aquatic environments. The search for these anthropogenic compounds in the coastal Mediterranean environment has been the goal of a one year sampling series (February 2011- February 2012) of DOM in the Rhone River (Arles station), the Rhone delta (Vaccarès lagoon) and in the Marseille Bay (Port de Bouc, Couronne and Sofcom stations). Chromatography analyses (GC/MS, LC-MS) of contaminants showed that only the Rhône delta was impacted by biocides with the presence of bentazone with concentrations ranging from 20 to 970 ng L^{-1}. A contamination peak was observed at the beginning of the summer and corresponded to the biocide spreading period for rice culture. The hydrocarbons were bringing out in each site with total concentration PAHs ranging from 8.1 to 405 ng L^{-1}. The higher concentrations were recorded in winter and were linked to atmospheric deposition and to Rhône River inputs. The spectrofluorimetry did not succeed to bring out the presence of contaminants during the sampling period, except in some samples of the industrial zone of the Gulf of Fos where fluorescence signatures of petrogenic PAHs were detected (naphthalene, phenanthrene, fluorene). However, natural FDOM analysis showed 1) that humic substances from terrigenous sources predominated in inland waters, whereas protein like material were more abundant in marine waters, produced by autochthonous biological activity and 2) that the Rhône River played a major role in the Marseille Bay by increasing both refractory and labile DOM through direct inputs and by enhancing the primary production by nutrient inputs.

Remerciements

Cette thèse a été réalisée dans le cadre du projet « IBISCUS » (indicateurs biologiques et chimiques de contaminations urbaines), qui a été financé par l'agence nationale de la recherche (ANR), programme ECOTECH (projet ANR-09-ECOT-009-01), et du Work Package 3 du projet CNRS-MISTRALS « MERMEX ».

Je remercie Edith PARLANTI, Claire RICHARD, Richard SEMPERE, Oliver ZIELINSKI d'avoir accepté de faire partie de mon jury de thèse.

Je tiens à remercier le MIO et son équipe dirigeante pour leur accueil chaleureux au sein du laboratoire.

Je remercie Madeleine GOUTX pour m'avoir fait confiance pour mener à bien mes travaux de recherche ainsi que pour m'avoir fait partager son expérience scientifique tout au long de ma thèse et de m'avoir soutenu lors de la rédaction de ce manuscrit.

Je remercie Stéphane MOUNIER pour avoir accepté d'être mon codirecteur de thèse, pour m'avoir donné l'opportunité de dispenser des enseignements à l'université de Toulon, et pour m'avoir fait partager ses connaissances sur sa spécialité, la fluorescence.

Je remercie également Marc TEDETTI pour m'avoir formé à l'utilisation du spectrofluorimètre Hitachi F-7000 et de l'analyse PARAFAC et pour son aide précieuse qu'il m'a apporté dans la rédaction des articles et du manuscrit de thèse.

Je remercie Catherine GUIGUE pour m'avoir prêté main forte lors de la campagne de prélèvement IBISCUS.

Je remercie Caroline BACHET pour m'avoir aidé dans les échantillonnages réalisés dans les ports de Marseille et lors des deux missions DEWEX.

Je remercie Patrick RAIMBAULT et Nicolas GARCIA pour les analyses des paramètres biogéochimiques sur les échantillons de la campagne IBISCUS.

Je remercie Roland Redon et Cheikh Gadio du laboratoire PROTEE pour m'avoir formé sur le spectrofluorimètre laser et sur la technique de la fluorescence résolue en temps.

Et enfin, je remercie également tous les membres du labortatoire du MIO.

Glossaire

Ace: acénaphthène

Acy: acénaphtylène

ADOM: matière organique dissoute d'origine anthropique

AH: hydrocarbure aliphatique

ANR: Agence nationale de la recherche

Ant: anthracène

AR: Arles

BaA: benzo[a]anthracène

BaP: benzo[a]pyrène

BbF: benzo[b]fluoranthène

Ben: bentazone

BeP: benzo[e]pyrène

BIX: indice biolgique

BkF: benzo[k]fluoranthène

BP: benzo[g,h,i]perylène

CAMP: Centre d'analyses Méditerranée Pyrénées

Car: carbaryl

CDOM: matière organique dissoute chromophorique

CH_2Cl_2: dichlorométhane

CH_4: méthane

Chl *a:* chlorophylle *a*

Chr: chrysène

CNRS: Centre national de la recherche sc

CO: Couronne

CO_2: dioxyde de carbone

CTD: conductivity temperature depth

DBA: dibenz[a,h]anthracène

DBT: dibenzothiophène

DFlu : 1,8 diméthyl-9H-fluorène

DL: limite de détection

DNaph : 2,3 diméthyl naphthalène

DOC: carbone organique dissous

DOM: matière organique dissoute

DON: azote organique dissous

DOP: phosphore organique dissous

EEM: excitation and emission matrix

Em: emission

EPA: Environmental Protection Agency

Ex: excitation

FA: acides fulvique

FADOM: matière organique dissoute fluorescente d'origine anthropique

FDOM: matière organique dissoute fluorescente

FI: indice de fluorescence

Flt: fluoranthène

Flu: fluorène

FNDOM: matière organique dissoute fluorescente d'origine naturelle

GC/MS: chromatographie en phase gazeuse couplée à un spectromètre de masse

H_2SO_4: acide sulfurique

HA: acide humique

HCl: acide chlorhydrique

HIX: indice d'humification

HMW: haut poids moléculaire

HPLC: chromatographie liquide haute performance

HPLC-UV: chromatographie liquide haute performance couplée à un détecteur ultraviolet

HPAEC-PAD: chromatographie échangeuse d'anions à haute performance couplée à un détecteur ampérométrique pulsée

HS: substances humiques

IBISCUS: indicateurs biologiques et chimiques de contaminations urbaines en milieu marin

ICCD: dispositif à couplage de charges intensifiées

IFREMER: Institut français de recherche pour l'exploitation de la mer

IHSS: Humic Substances Society

InDP: indeno[1,2,3-cd]pyrène

INSU: Institut national des sciences de l'univers

JGOFS: Joint Global Ocean Flux Study

LC-MS: Chromatographie liquide couplée à un spectromètre de masse

LC-MS-MS: chromatographie liquide couplée à deux spectromètres de masse

LMW: faible poids moléculaire

LOICZ: Land-Ocean Interactions in the Coastal Zone

MARPOL: Marine pollution

MARS3D: modèle pour l'application à l'échelle régionale

MEEF: matrice d'excitation-émission de fluorescence

MERIS: Medium resolution imaging spectrometer

MERMEX: Marine ecosystems response in the Mediterranean experiment

MIO: Institut Méditerranéen d'Océanologie

MISTRALS: Mediterranean integrated studies at regional and local scales

MODIS: Moderate Resolution Imaging Spectroradiometer

NaCl: chlorure de sodium

Naph: naphthalène

Nd-Yag: grenat d'yttrium-aluminium dopé au néodyme

NDOM: matière organique dissoute d'origine naturelle

NO_2^-: nitrite

NO_3^-: nitrate

PAH: hydrocarbure aromatique polycyclique

PAR: rayonnement disponible pour la photosynthèse (400-700 nm)

PARAFAC: analyse factorielle parallèle

PB: Port de Bouc

PCA: analyse en composante principale

PCB: polychlorobiphényles

Phe: phénanthrène

Pho: 2-phénylphénol

Phy: phytane

PMT: photomultiplicateur

POC: carbone organique particulaire

POM: matière organique particulaire

PON: azote organique particulaire

POP: phosphore organique particulaire

PO_4^{3-}: phosphate

Pr: pristane

PREVIMER: observations et prévisions côtières

Pyr: pyrène

QL: limite de quantification

QSU: unité quinine sulfate

R: somme des concentrations des *n*-alkane à partir du *n*-C_{15} au *n*-C_{36}

SO et SOFCOM: station d'observation du Centre d'Océanologie de Marseille

Thi: thiabendazole

TLC-FID: chromtographie en couche mince couplée à un détecteur d'ionisation par flamme

TLL: transistor-transistor logic

TRFS: spectroscopie de fluorescence rés

UCM: mélange complexe non définis

UV: ultraviolet

UVR: rayonnement ultraviolet (280-400nm)

VA: Vaccarès

Vis: visible

Sommaire

Chapitre I: Etat de l’art – problématique scientifique

1. L'océan côtier : un compartiment biogéochimique majeur au niveau planétaire…mais encore difficile à appréhender

L'océan côtier est la région océanique qui couvre le plateau continental de 0 à ~ 200 m de profondeur (Figure I-1). Il inclue les systèmes littoraux comme les baies, les lagunes, les écosystèmes récifaux, les estuaires et les deltas. C'est une zone de transition et d'échanges entre les continents et l'océan ouvert. Bien qu'il ne représente que 7% de l'océan mondial en terme de surface et seulement 0,5% en terme de volume, l'océan côtier joue un rôle fondamental dans les cycles biogéochimiques du carbone, de l'oxygène et des éléments nutritifs (azote, phosphore, silicium) à l'échelle planétaire (Walsh, 1991 ; Frankignoulle et al., 1998 ; Rabouille et al., 2001 ; Chen et Borges, 2009). Il contribuerait à hauteur de 25% à la production primaire océanique totale, de 80% à l'enfouissement du carbone organique et de 40% au dépôt du carbonate de calcium dans les océans, et de 90% à la minéralisation réalisée au sein des sédiments marins (Wollast, 1991 ; Gattuso et al., 1998 ; Liu et al., 2000). Par ailleurs, l'océan côtier serait responsable de 18% de l'absorption nette du dioxyde de carbone (CO_2) atmosphérique par les océans (soit 0,3 Gt C[1] an^{-1}) (Borges, 2011). Aussi, notre vision du cycle global du carbone s'affinant au fil des années, en plus des boites réactives majeures que sont la biosphère terrestre, l'atmosphère et l'océan ouvert, il est aujourd'hui clairement reconnu le besoin d'inclure la boite « océan côtier » dans les bilans régionaux (Borges et al., 2006) et globaux (Thomas et al., 2004) (Figure I-2).

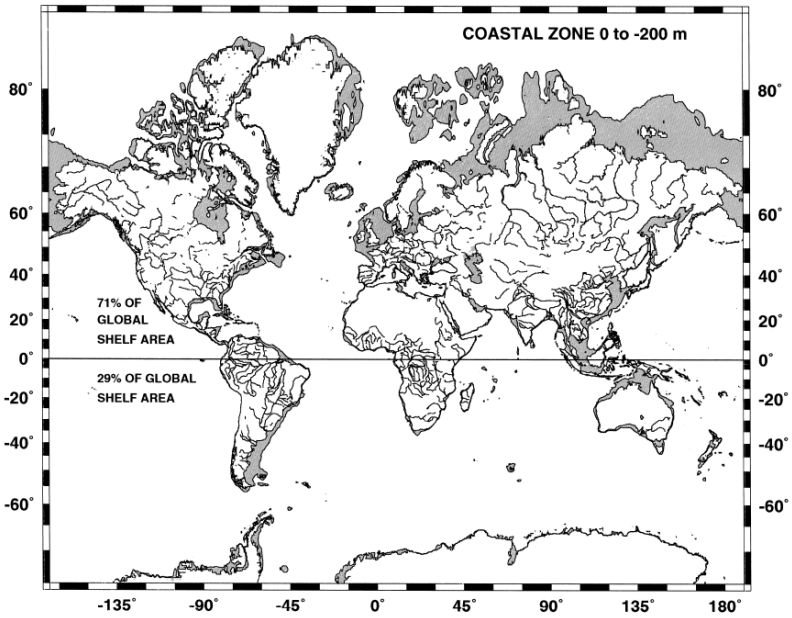

Figure I-1. L'océan côtier mondial (zone du plateau continental de 0 à 200 m de profondeur) et les principaux bassins fluviaux sur les continents. D'après Ver et al. (1999).

[1] 1 Gt C = 10^{15} g C.

Pourtant, malgré l'essor ces dernières années des études sur les cycles biogéochimiques dans l'océan côtier, en particulier *via* les programmes internationaux Joint Global Ocean Flux Study (JGOFS) et Land-Ocean Interactions in the Coastal Zone (LOICZ), le fonctionnement du système côtier reste encore difficile à appréhender et il n'est toujours pas représenté, ni dans les modèles terrestres, ni dans les modèles océaniques (Giraud et al., 2008 ; Liu et al., 2010). La difficulté d'étudier l'océan côtier et de l'intégrer aux bilans globaux provient du fait que dans cet environnement, les processus physiques, chimiques et biologiques sont très complexes et interagissent à des échelles spatiales et temporelles extrêmement variables. Les grandes disparités régionales et temporelles, qui sont la caractéristique principale du domaine côtier, sont sans équivoque un frein à la meilleure compréhension de son fonctionnement et des flux qui lui sont associés. La variété des processus hydrodynamiques, les forts gradients de salinité et de température, les fluctuations dans les apports fluviatiles en matière organique terrestre et en éléments nutritifs, et les propriétés de l'océan ouvert adjacent rendent chaque système côtier complexe et souvent unique.

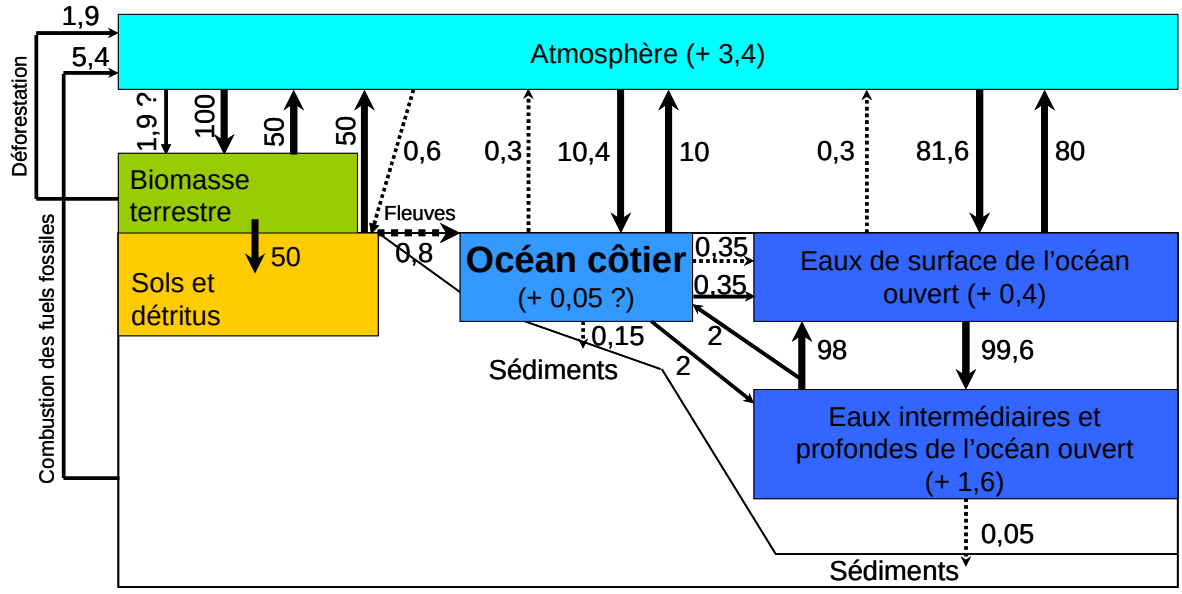

Figure I-2. Cycle du carbone à l'échelle globale (flux de carbone en Gt C an^{-1}). Schéma initial de Siegenthaler et Sarmiento (1993) modifié par Liu et al., (2000) pour inclure l'océan côtier. Dans ce système, l'absorption nette du CO_2 atmosphérique par l'océan côtier est de 10,4 - 10 - 0,3 = 0,1 Gt C an^{-1}. Borges (2011) attribue un rôle encore plus important à l'océan côtier avec une absorption nette de CO_2 de 0,3 Gt C an^{-1}.

D’autre part, l’océan côtier est soumis à de très fortes pressions anthropiques en raison de la concentration des activités urbaines, agricoles, industrielles et touristiques sur le littoral. Les perturbations qu’il subit sont multiples : eutrophisation liée à l’apport excessif de sels nutritifs, introduction de contaminants chimiques et microbiologiques, invasion d’espèces toxiques, aménagement au niveau des bassins versants, exploitation des nappes d’eau douce, aquaculture et pêche intensive (Nicholls et al., 2007). L’accroissement de la population (on estime que 60% de la population mondiale vivra à moins de 100 km des côtes d’ici 50 ans) et l’intensification des activités urbaines vont exacerber l’anthropisation du domaine côtier dans les prochaines années. L’océan côtier serait également très sensible aux effets du changement climatique global, qui est susceptible d’engendrer, ou de modifier l’occurrence des événements extrêmes tels que les crues, les inondations, les tempêtes et les sécheresses. Le caractère soudain de ces évènements rend difficile l’évaluation de leur impact sur le milieu (The MerMex group, 2011). L’environnement côtier pourrait aussi être affecté par l’augmentation du niveau de la mer, la stratification des eaux, l’acidification des océans et les changements de biodiversité (Borges, 2011).

Ainsi, bien que la communauté scientifique ait pris conscience depuis plusieurs années de la nécessité d’étudier l’océan côtier, la complexité et la diversité des échelles spatiales et temporelles des processus physiques et biogéochimiques s’y déroulant ont probablement contribué à ralentir l’émergence de recherches intégrées. Il apparaît aujourd’hui essentiel de mieux comprendre la structure et le fonctionnement de l’océan côtier pour estimer sa contribution réelle dans les flux de carbone globaux et pour évaluer son comportement et son évolution face aux pressions anthropiques locales et au changement climatique global.

2. La Méditerranée et les apports fluviaux. Cas du Rhône

La Méditerranée est une mer semi fermée ayant le détroit de Gibraltar comme principal lieu d’échange avec l’océan Atlantique. La Méditerranée borde à la fois les rives de l’Europe et du nord du continent africain. Elle a une circulation thermohaline propre (The MerMex group, 2011) et le temps de résidence de l’eau y est faible (environ 70 ans). Le littoral Méditerranéen est soumis à l’impact de rejets de contaminants toxiques industriels et de rejets urbains. Il est le siège d’une pollution inquiétante par les hydrocarbures pétroliers avec des rejets d’environ 80 000 tonnes/an. De plus, cette mer qui ne représente qu’une faible superficie des océans supporte à elle seule 28% du commerce mondial en hydrocarbures et 30% du trafic maritime mondial. Outre les

rejets accidentels, une quantité importante d'hydrocarbures se retrouve dans la zone côtière méditerranéenne suite à des rejets de raffinerie et de pétroliers, via les eaux usées, du déballastage, du dégazage et des vidanges. En Méditerranée nord-occidentale, les concentrations en PAHs totaux dans les eaux de surface varient de 226 à 321 ng L^{-1} (Pérez et al., 2003) et les concentrations PCB totaux varient entre 2 et 80 pg L^{-1} et entre 0 et 33 ng L^{-1} pour des biocides tels que le diuron, l'atrazine, l'irgarol et la simazine (Berrojalbiz et al., 2011a ; Munaron et al., 2012).

En Méditerranée, le Rhône contribue à hauteur de 50% aux apports d'eau douce en Méditerranée. Long de 812 km, son bassin de drainage a une superficie d'environ 97 800 km². Ce fleuve est impacté par des apports en biocides, avec des concentrations en biocides totaux dans les eaux de surface > 0,5 µg L^{-1} et comprenant 47% d'herbicides, 27% d'insecticides et 22% de fongicides (Olivier et al., 2009). Des études récentes reportent aussi des concentrations en hydrocarurbes significatives dans le Rhône : entre 12 et 3725 ng L^{-1} pour les PAHs et entre 7 et 20 ng L^{-1} pour les n-alcanes (Dachs et al., 1999 ; Sicre et al., 2008).

Le delta du Rhône couvre une zone d'environ 1 750 km², composée principalement de zones humides, d'étang et de marais salant. La partie centrale de son delta, appelée la Camargue (~ 750 km^2) est divisée en deux parties. Au nord-est se situent des zones agricoles où le riz est cultivé de façon intensive et où ont lieu l'élevage de taureaux et de chevaux. Au sud se situent des étangs salés où existent des écosystèmes spécifiques à la zone qui ont fait de cette zone une aire protégée depuis des décennies. Les eaux du Rhône peuvent être déviées afin d'irriguer les champs de riz à travers un système de canaux d'irrigation connecté à l'étang de Vaccarès, lui-même relié à la mer. L'eau provenant des canaux d'irrigation peut être renvoyée dans le Rhône grâce à des stations de pompage. Des échanges avec la mer peuvent se produire par le sud de l'étang de Vaccarès. Cet étang, qui mesure 12 km de long qui a une superficie de 6 500 km² et une profondeur inférieure à deux mètres, est le plus grand étang de Camargue. Il est également l'élément principal de contrôle des eaux du delta du Rhône. Cet étang, situé dans le parc national de Camargue, est resté un site préservé pour le biota. Cependant, bien que protégé, l'étang de Vaccarès est sujet à la fois à des apports de biocides en raison de l'agriculture intensive du riz et à des apports d'hydrocarbures *via* les zones industrielles voisines telles que le complexe

pétrochimique de Marseille-Fos (Ribeiro et al., 2005 ; Buet et al., 2006 ; Comoretto et al., 2007 ; Chiron et al., 2009 ; Roche et al., 2009).

Arrivées en mer, les eaux du Rhône, chargées en sels nutritifs et en carbone organique, vont impacter la production primaire et les flux biogéochimiques en Méditerranée nord-occidentale (Joux et al., 2009 ; The MerMex group., 2011). Habituellement, le panache du Rhône se dirige vers l'ouest en raison de l'influence du courant Liguro-Provençal (Courant Nord). Cependant, sous des conditions de vent de nord-est, il peut se diriger vers l'est et impacter le golfe de Fos-sur-mer et la baie de Marseille (Para et al., 2010 ; Pairaud et al., 2011).

3. La matière organique dissoute (DOM) océanique : un élément fondamental du cycle global du carbone

La matière organique dissoute (DOM) est communément définie comme étant la matière organique inférieure à 0,2 ou 0,7 µm. La DOM océanique représente l'un des réservoirs actifs de carbone organique les plus importants à la surface de la Terre. En effet, sa quantité (sous forme de carbone organique dissous, DOC) est évaluée à ~ 700 Gt C et elle participe pour plus de 95% au stock de carbone organique total de l'océan, alors que la matière organique particulaire (POM) ne représente que 5% de ce stock (Hedges, 2002 ; Battin et al., 2009). Le réservoir de carbone de la DOM océanique est donc comparable à celui du CO_2 atmosphérique (750 Gt C) et à celui de la biomasse terrestre (550 Gt C), et est environ 230 fois supérieur à celui de la biomasse marine (3 Gt C) (Siegenthaler et Sarmiento, 1993). La minéralisation de la DOM océanique est un facteur déterminant dans les flux de CO_2 à l'échelle de la planète. Par exemple, la minéralisation de seulement 1% du stock de DOM (soit 7 Gt C) correspond à une quantité de CO_2 plus importante que celle relarguée dans l'atmosphère en un an par la combustion des fuels fossiles (5,4 Gt C). Les concentrations en DOM (sous forme de DOC) sont relativement uniformes dans l'océan variant de 60-80 µM dans les eaux de surface à ~ 40 µM dans les eaux profondes (Carlson, 2002 ; Figure I-3).

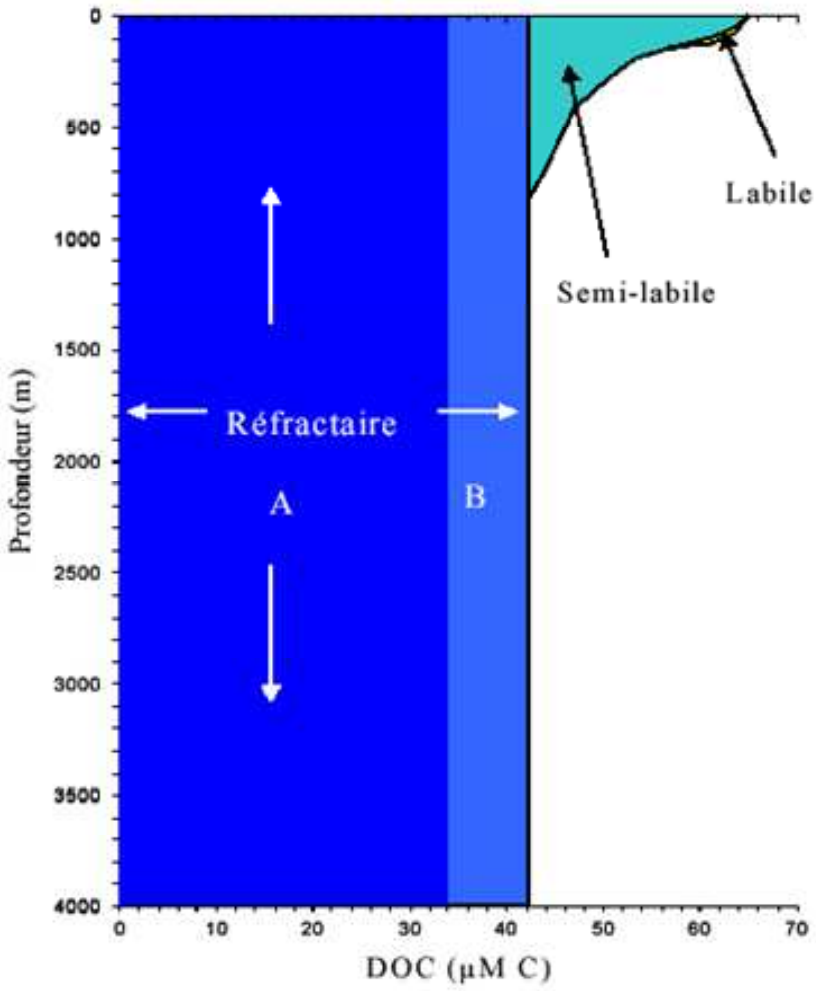

Figure I-3. Schéma conceptuel de la distribution de la DOM labile, semi-labile et réfractaire dans l'océan. Le stock réfractaire est séparé en DOM ayant un temps de résidence supérieur (A) et inférieur (B) à la durée du cycle de la circulation générale des océans (~ 1000 ans) (Carlson, 2002).

La DOM est à la base de la chaîne alimentaire (boucle) microbienne puisqu'elle est la source principale de carbone pour les procaryotes (bactéries et archéobactéries) hétérotrophes (Carlson, 2002). Ces derniers, en assimilant la DOM, en minéralisent une partie (~ 80%) en CO_2 et en sels nutritifs, alors que la fraction restante (~ 20%) est convertie en biomasse bactérienne et devient disponible pour les échelons trophiques supérieurs (Azam et al., 1983; Cho et Azam, 1990). La quantité de DOM ainsi assimilée par les procaryotes hétérotrophes correspondrait à un flux de

carbone équivalent à 50% de la production primaire océanique, soit 25 Gt C an^{-1} (Williams, 2000). De plus, le rôle de la DOM dans la pompe biologique de carbone[2] est très significatif. On estime que la DOM contribuerait à raison de 20% au flux total de matière organique transportée vers l'océan profond [80% du flux étant dû à la matière organique particulaire (POM)] (Hansell et al., 2009). Récemment, Jiao et al. (2010) ont introduit une composante conceptuelle à la pompe biologique de carbone qui permettrait d'expliquer l'accumulation de DOM dans l'océan : la pompe microbienne de carbone (Figure I-4). Celle ci met en exergue la production de DOM réfractaire par les procaryotes hétérotrophes, alors que ceux-ci étaient considérés jusqu'à lors comme d'uniques consommateurs de DOM. Cette DOM réfractaire serait stockée pendant des millénaires dans l'océan profond.

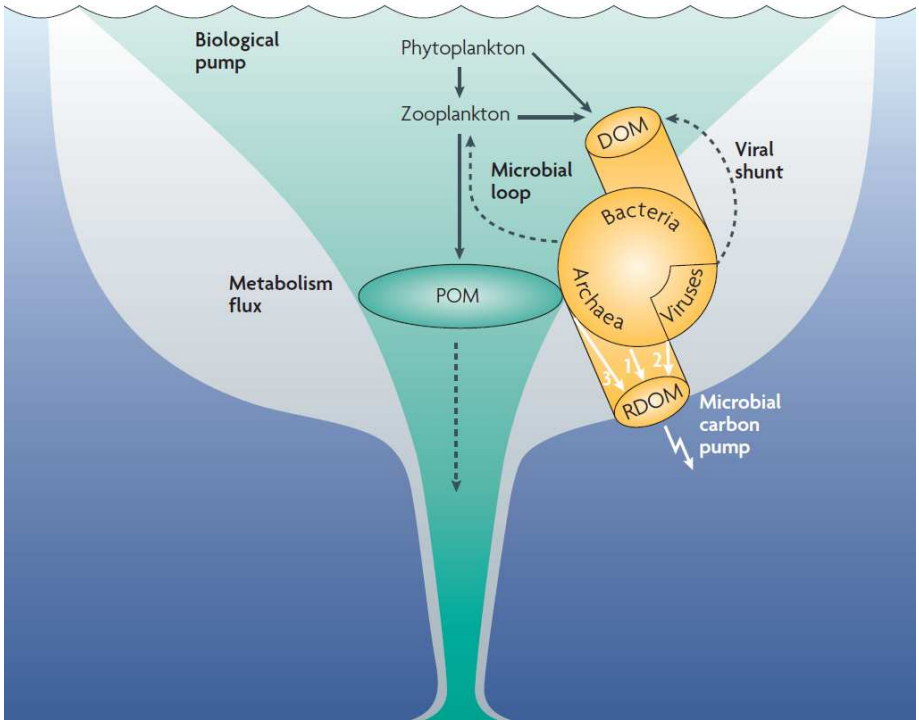

Figure I-4. Schéma conceptuel de la pompe microbienne de carbone au sein de laquelle la DOM (DOM dans la figure) occupe une place centrale (Jiao et al., 2010).

[2] La pompe biologique de carbone est l'ensemble des processus biologiques conduisant à transporter le carbone de la zone euphotique vers les fonds marins.

4. Importance biogéochimique et écologique de la DOM dans l'océan côtier

La DOM occupe une place centrale dans le cycle du carbone de l'océan côtier. Dans l'environnement côtier, la DOM à une multitude de sources autochtones et allochtones. Les sources autochtones (marines) comprennent essentiellement l'excrétion et l'exsudation par les producteurs primaires (phytoplancton, macrophytes), le broutage par le zooplancton, l'excrétion par les échelons trophiques supérieurs, la dégradation de la POM et la production de DOM réfractaire par les procaryotes hétérotrophes, et la lyse cellulaire (Nagata, 2000 ; Sempéré et al., 2000 ; Bertilsson et Jones, 2003 ; Jiao et al., 2010 ; Figure I-5). Les sources allochtones, quant à elles, incluent principalement les apports par les fleuves et les rivières (Para et al., 2010 ; Panagiotopoulos et al., 2012). L'apport de DOM fluviatile à l'océan côtier serait de l'ordre de 0,25 Gt C par an et représenterait 60% des apports de matière organique fluviatile (Cauwet, 2002). Cette DOM transportée par les fleuves proviendrait principalement des sols et des végétaux terrestres. Cet apport de 0,25 Gt C par an, qui représente 0,7% de la production primaire terrestre, suffirait à renouveler le réservoir de DOM océanique en seulement 2800 ans (Blough et Del Vecchio, 2002). En plus des fleuves et des rivières, des quantités non négligeables de DOM seraient apportées à l'océan côtier *via* les eaux souterraines, les effluents urbains, industriels et agricoles, les eaux de ruissellement des pluies, et l'océan ouvert (upwellings) (Cauwet, 2002 ; Hudson et Reynolds, 2007 ; Figure I-5). D'autre part, les sédiments seraient une source significative de DOM à l'océan côtier, par exemple lors d'épisodes de remise en suspension sédimentaire naturels (tempêtes) ou connectés aux activités humaines (trafic de grands navires, opérations de dragage) (Durrieu de Madron et al., 2008).

Comme pour ses sources, « les devenirs » de la DOM dans l'océan côtier seraient très variés. En plus d'être consommée par les procaryotes hétérotrophes pour être minéralisée en CO_2, convertie en biomasse ou transformée en matériel réfractaire, la DOM peut subir une minéralisation photochimique pour être oxydée en gaz d'intérêt climatique, comme le CO_2, le monoxyde de carbone (CO) et le sulfure de carbonyle (COS) (Mopper et Kieber, 2002 ; Figure I-5). Elle peut aussi être exportée vers l'océan ouvert adjacent par le biais de la circulation des masses d'eau, soit en surface (Druon et al., 2010), soit en profondeur lors des plongées d'eau dense (cascading) (Ulses et al., 2008). Enfin, la DOM côtière peut être séquestrée dans les sédiments *via* son adsorption sur les particules chutantes (Figure I-5).

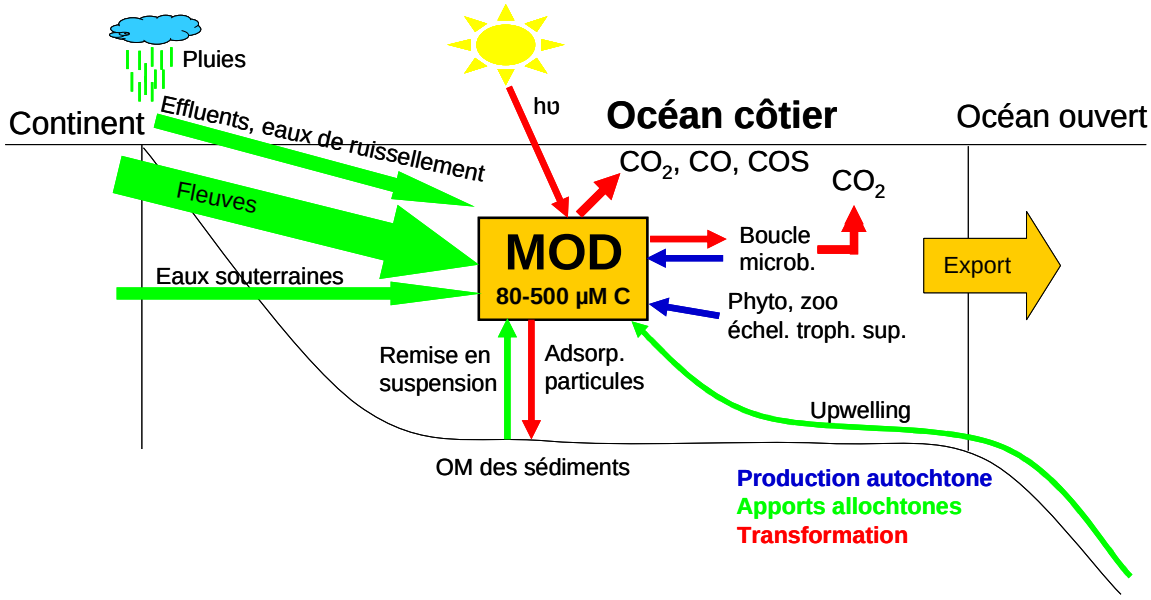

Figure I-5. Cycle biogéochimique de la DOM dans l'océan côtier.

Dans ce manuscrit, nous distinguons la DOM naturelle (NDOM), qui peut être d'origine marine (autochtone) ou d'origine terrestre (allochtone), et la DOM anthropique (ADOM) qui regroupe l'ensemble des composés organiques dissous introduits dans le milieu marin principalement ou exclusivement par les activités humaines.

La NDOM impacte la biogéochimie, l'écologie et la physique du domaine marin par ses propriétés optiques et chimiques. Tout d'abord, elle joue un rôle de premier ordre dans l'absorption du rayonnement solaire. En effet, la NDOM est le principal atténuateur du rayonnement ultraviolet (UVR : 280-400 nm) dont elle protège les organismes vivants des effets délétères (Tedetti et Sempéré, 2006). Elle intervient pour plus de 50 % dans l'atténuation du rayonnement disponible pour la photosynthèse (PAR : 400-700 nm) (Siegel et al., 2005). La communauté scientifique travaillant sur l'évaluation des biomasses phytoplanctoniques côtières à l'aide des outils de télédétection doit d'ailleurs s'affranchir du signal de luminance issue de la NDOM, qui « pollue » celui de la chlorophylle. Des quantités élevées de NDOM pourraient donc inhiber la production primaire en limitant le rayonnement PAR pour le phytoplancton. D'autre part, l'absorption du rayonnement solaire par la NDOM peut influencer la thermodynamique des eaux côtières « en piégeant » la chaleur dans les premiers mètres de la colonne d'eau (Pegau, 2002). En outre, la photodégradation de la NDOM dans les eaux de surface conduit à la

production de CO_2, de monoxyde de carbone (CO), de méthane (CH_4), de sels nutritifs et de composés organiques de faible poids moléculaire (Mopper et Kieber, 2002). Dans les systèmes côtiers, la DOM impacte aussi le cycle de nombreux contaminants inorganiques et organiques tels que les éléments traces métalliques, les PAHs et les biocides. En interagissant au niveau moléculaire avec ces contaminants, la NDOM modifie leur biodisponibilité, leur stabilité, leur transport et leur devenir (Akkanen et al., 2004 ; Mounier et al., 2010). Par exemple, elle peut contribuer à leur plus grande persistance dans le milieu et, dans le même temps, modifier leur toxicité envers les organismes vivants (Suffet et MacCarthy, 1989). Enfin, la NDOM a été utilisée avec succès comme traceur de mélange de masses d'eau (au même titre que la salinité) dans les zones côtières dans lesquelles elle présentait un comportement conservatif (Stedmon et al., 2010).

La ADOM est présente en d'importantes proportions dans les eaux côtières. Ces dernières sont soumises à une forte pression anthropique en raison de l'intensification des zones urbaines, industrielles, agricoles et des activités touristiques, ce qui peut avoir un impact sur le biota (Valiela, 2006; Nicholls et al., 2007).

4.1. Composition de la matière organique dissoute naturelle (NDOM)

La NDOM est issue de la dégradation et de la condensation de molécules provenant des êtres vivants (Frimmel et Christman, 1988 ; Walther, 1989). L'intégration de ces molécules au réservoir de matière organique peut s'effectuer de deux façons différentes : 1) *via* la dégradation d'un organisme après sa mort et 2) *via* la dégradation des composés produits par les organismes vivants. La NDOM peut être elle même séparée en deux catégories, avec d'un côté les biopolymères et de l'autre les géopolymères, appelés également substances humiques. Les biopolymères regoupent les protéines, les acides aminés, les sucres, les lipides, les acides nucléiques, les nucléotides et les acides phénoliques. Ils sont caractérisables au niveau moléculaire (Croué et al., 2003) et peuvent intervenir directement dans les processus métaboliques des organismes vivants. Ils proviennent de la dégradation d'organismes vivants par des mécanismes physiques (changement de température, pression, séchage), chimiques (hydrolyse, photolyse) ou biologiques (exsudation, consommation par les bactéries ou par la faune). Du fait de leur réactivité, ces composés ont une durée de vie bien inférieure aux géopolymères. Une fraction de ces biopolymères va d'ailleurs se transformer en géopolymères

tandis que la fraction restante sera minéralisée. Le second groupe, les géopolymères ou substances humiques proviennent donc de la dégradation des biopolymères mais aussi de leur recombinaison ou de leur condensation. Leur réactivité est plus faible que celle des biopolymères, et ils ont une durée de vie plus longue (entre quelques dizaines et quelques milliers d'années) (Williams et al., 1987). Les substances humiques ne sont pas totalement caractérisables contrairement aux biopolymères. Ce sont des molécules plus complexes, constituées de cycles aromatiques, de groupes phénoliques et carboxyliques. Les substances humiques peuvent être divisées en trois catégories en fonction de leur pH de solubilité : 1) les acides fulviques, solubles à tout pH, 2) les acides humiques, solubles à pH basique, et 3) les humines, insolubles à tout pH (Seitz, 1981 ; Aiken, 1985). En particulier, les acides humiques et fulviques se différencient par leurs propriétés optiques et chimiques, leur poids moléculaire et leur degré d'aromaticité (Harvey et al., 1983). Dans ces deux types de molécules, on peut retrouver des structures comme des aromatiques simples, des quinolinones, des coumarines et des falvones.

Parmis ces trois types de macromolécules, les acides fulviques possèdent le plus faible poids moléculaires. Ils peuvent se transformer en acides humiques par polymerisation. Les acides fulviques sont également plus réactifs que les acides humiques (Hedges, 1988). Ces derniers sont donc des macromolécules plus grosses et sont caractérisées par une moins grande proportion d'oxygène par rapports aux acides fulviques. Les acides humiques peuvent être différenciés des acides fulviques à l'aide du rapports O/C qui est de respectivement 0,5 et de 0,7 (Steelink, 1985). Les humines sont quant à elles des macromolécules de poids moléculaire plus élevé que les acides humiques et fulviques et sont formées à la fois par la polymerisation et par la dégradation des ces derniers (Hansell et Carlson, 2002).

4.2. La matière organique dissoute anthropique (ADOM) : source, toxicité et devenir

La ADOM regroupe plusieurs types de contaminants qui se retrouvent dans le milieu aquatique suites aux activités humaines. Il s'agit tout d'abord des hydrocarbures qui ont déjà été retrouvés en mer, dans les rivières, les ports, les effluents industriels et les eaux usées (Dabestani et Ivanov, 1999 ; Dachs et al., 2002 ; Wurl et Obbard, 2004 ; Goutx et al., 2009 ; Guigue et al., 2011 ; Montuori et Triassi, 2012). Les hydrocarbures sont des composés cancérigènes qui peuvent s'accumuler dans les organismes filtreurs tels que les moules et les huîtres (Kennish, 1992 ; Roche et al., 2002 ; Wetzel et Van Vleet, 2004 ; Ribeiro et al., 2005 ; Jeong et Cho, 2007). Ils

entrent dans les eaux marines *via* les fleuves (Fernandes et al., 1999), les dépôts atmosphériques (Pérez et al., 2003 ; Lim et al., 2007), les rejets d'eaux usées / effluents industriels (Wang et al., 2001) et le trafic maritime (Birpinar et al., 2009). Dans le pool d'hydrocarbures, les PAHs sont des molécules composées exclusivement de carbone, d'hydrogène et d'au moins deux cycles aromatiques. Les apports en PAHs dans l'environnement se font majoritairement par des rejets pétroliers (74%), on parle de contamination pétrogénique, le reste provient essentiellement de dépôts atmosphériques (22%), il s'agit dans ce cas de contaminations pyrogéniques (Ariese, 1999). Ils peuvent en effet être issus des rejets directs de pétrole brut ou de ses dérivés lors d'activités maritimes et pétrolières (transport, pollutions accidentelles, dégazages) ou provenir des déchets industriels et urbains (déversements de produits variés, combustion de carburants) acheminés par les fleuves, les eaux de lessivage, les eaux usées et l'atmosphère (pluies et aérosols) (Tolosa et al., 1996 ; Lipiatou et al., 1997). Les PAHs vont généralement se retrouver en quantité importante dans les ports. Les ports étant des zones closes où le trafic maritime est important, des apports de PAHs ont de grandes chances de se produire et ne seront pas évacués. Leur présence est due au fait que les ports sont généralement des endroits clos où le trafic maritime est important. Dans l'eau, ils ont tendance à se concentrer dans la micro-couche de surface (Marty et Saliot, 1976). Les PAHs présents dans les produits pétroliers sont des composés à seulement 2 ou 3 cycles comme le phénanthrène ou le naphtalène ainsi que leurs dérivés alkylés (Wang et al., 1999). Dans les produits pétroliers, les PAHs se sont formés très lentement, cependant leur processus de formation peut être bien plus rapide. Ces composés organiques peuvent se former à haute température grâce à une combustion incomplète de matière première comme des composés fossiles, du bois ou tout autre matière organique complexe (Harvey et al., 1983). Ils peuvent au gré des vents être transportés sur de longues distances et contaminer des environnements quasiment vierges comme les régions polaires (Weber et Goerke, 2003). La présence de PAHs dans l'environnement peut être également naturelle (feu de forêt, éruption volcanique) (Menzie et al., 1992). Dans ces cas là, les PAHs les plus présents possèdent 4 cycles au moins comme le pyrène et ne sont pas alkylés (Ariese, 1999). Pour déterminer si une contamination est d'origine pyrogénique ou pétrogénique, les rapports fluoranthène/pyrène et phénanthrène/anthracène sont utilisés. Si le rapport phénanthrène/anthracène est inférieur à 10 et que le rapport fluoranthène/pyrène est supérieur à 1 alors la contamination est pyrolytique. Par contre, si le rapport phénanthrène/anthracène est supérieur à 10 et que le rapport

fluoranthène/pyrène est inférieur à 1, dans ce cas la contamination est pétrogénique (Budzinski et al., 1997 ; Lim et al., 2007).

Les PAHs font parties des 45 substances prioritaires listées par le parlement Européen et par le conseil de l'union Européenne (Journal officiel de l'UE, 24/08/2013, Directive 2013/39/EU). Ils sont suspectés d'être cancérigènes, très toxiques et mutagènes (Kennish, 1992) et sont présents en grande quantité dans les produits pétroliers ainsi que dans leurs produits dérivés (Ariese, 1999). Pour qu'une eau soit potable, la somme des concentrations de tous les PAHs ne doit pas excéder 0,2 µg L^{-1} (Journal officiel de l'UE, 29/04/2004, Directive 2004/850/EU).

La somme des concentrations en PAHs dans l'eau peut varier du ng L^{-1} jusqu'au µg L^{-1} pour des eaux très contaminées (Valero-Navarro et al., 2007 ; Men et al., 2009 ; Guigue et al., 2011). En raison de leur faible solubilité dans l'eau et de leur coefficient de partition élevé, les PAHs s'absorbent sur la surface des particules, ce qui explique que leurs concentrations dans l'eau de mer soient faibles (Kim et al., 1999) et qu'ils s'accumulent dans les sédiments côtiers (Abarnou et al., 2000). Leur élimination dans l'environnement peut s'effectuer de plusieurs façons : par sorption, par biodégradation et par photodégradation qui est la principale voie d'élimination (Abarnou et al., 2000).

En plus des PAHs, la ADOM est constituée de biocides. Ces derniers sont divisés en trois classes différentes, les insecticides, les herbicides et les fongicides. Ils ont été mis en évidence dans les eaux souterraines, dans les affluents d'eaux usées, et dans les eaux douces et sont persistants dans l'environnement, bioaccumulables et affectent le biota (Nhan et al., 2001 ; Kolpin, Barbash et al., 2002 ; Gilliom et al., 2006 ; Kupper et al., 2006 ; Lindsey et al., 2006 ; Leong et al., 2007 ; McKinlay et al., 2008 ; Loos et al., 2009). L'utilisation de biocides n'a cessé d'augmenter lors de ces dernières années suite à la pratique de l'agriculture intensive. On les retrouve dans les zones agricoles mais également dans les zones forestières ainsi que dans les zones urbaines (Jia et al., 2007). Ils vont être présent à la fois dans les sols et dans l'environnement aquatique. Les apports de ces composés vers ce dernier s'effectuent principalement *via* les eaux de ruissellements (Richards et Baker, 1993) mais aussi par des lixiviats, par contaminations accidentelles et par le lavage d'équipement utilisé pour l'épandage (Konstantinou et al., 2006). Les apports de contaminants dans le milieu dépendent des quantités de précipitations, de la pratique agricole, de la saison, des caractéristiques du sol qui pourra retenir plus ou moins les composés et des

propriétés de chaque biocide (un composé soluble et résistant à la dégradation aura de forte chance de se retrouver dans les eaux marines et les rivières) (Konstantinou et al., 2006). Les herbicides et les insecticides sont les plus souvent retrouvés dans les eaux naturelles (Capel et al., 2001). Les zones les plus contaminées sont les rizières où les plans d'eau sont fortement impactés à cause de l'inondation des cultures facilitant ainsi le transport de contaminants (Konstantinou et al., 2006). Les biocides peuvent également être introduits dans les rivières *via* les dépôts secs et humides (Albanis et al., 1998 ; Charizopoulos et Papadopoulou-Mourkidou, 1999). Leur présence dans les eaux de surface est importante en période d'étiage (entre avril et août), après l'application des biocides sur les zones agricoles. La contamination en biocides se produit généralement au début du printemps et en juin suite aux épandages (Thurman et al., 1991 ; Griffini et al., 1997 ; Planas et al., 1997 ; Comoretto et al., 2007 ; Chiron et al., 2009). Cependant, Il se peut que des pics de pollutions apparaissent en automne (septembre-octobre) après un été sec (Konstantinou et al., 2006 ; Comoretto et al., 2007). En période de crue, les concentrations seront faibles à cause d'une dilution importante et du lessivage des sols. Les biocides dans l'eau vont se concentrer dans la microcouche de surface tout comme les PAHs (Wu et al., 1980). Certains biocides sont hautement toxiques et leur accumulation dans l'organisme peut engendrer de graves maladies. La directive de l'Union Européenne sur l'eau potable a établi une concentration maximale de 0,1 $\mu g\ L^{-1}$ pour des composés individuels et 0,5 $\mu g\ L^{-1}$ pour la somme des concentrations de tous les composés (Journal officiel de l'UE, 29/04/2004, Directive 2004/850/EU). Dans les environnements aquatiques, ces composés, qui sont résistants à la biodégradation, seront éliminés uniquement par photodégradation ou par hydrolyse (Benitez et al., 2002). Tout comme les PAHs, les biocides sont le plus souvent caractérisés et quantifiés par chromatographie (García Reyes et al., 2004 ; Comoretto et al., 2007 ; Jia et al., 2007 ; Chiron et al., 2009).

Outre ces deux familles appartenant à la ADOM, on retrouve également dans l'environnement des produits industriels qui sont composés d'antioxydants (cosmétiques, caoutchouc, conservateurs) de perfluorates (répulsifs, revêtements protecteurs), de phénols (peintures, textiles, détergents), de phtalates (plastiques), de triazoles (anticorrosifs) (Murray et al., 2010). Ces composés peuvent être présents et persistants dans l'environnement aquatique et affecter les organismes présents dans le milieu (Mantovani et al., 1999 ; Vos et al., 2000 ; Furlong et al., 2002 ; Sarafian et al., 2002 ; Jos et al., 2005 ; Oliver et al., 2007 ; Gasperi et al., 2008 ; Fromme

et al., 2009 ; Loos et al., 2009). Les produits pharmaceutiques font également partis des contaminants organiques présents dans le milieu aquatique. Des substances telles que des analgésiques, des antiépileptiques, des antihyperlipidémiques, des antibiotiques et des hormones de synthèses ont été mises en évidence dans les eaux de surfaces, dans les eaux usées, dans les effluents de stations d'épuration et peuvent impacter les organismes vivants présents dans le milieu (Daughton et Ternes, 1999 ; Peterson et al., 2000 ; Furlong et al., 2002 ; Kolpin et al., 2004 ; Kannan et al., 2005 ; Loos et al., 2009).

4.3. L'apport des techniques de spectroscopie de fluorescence à l'étude de la DOM

En raison des multiples sources et des nombreux processus de transformation qu'elle subit, la NDOM océanique est un pool de matière complexe, hétérogène, constitué d'une myriade de composés organiques de structure et de poids moléculaire différents, et qui restent pour la plupart (75 %) non identifiés au niveau moléculaire (Mopper et al., 2007). Jusqu'à présent, la caractérisation de la DOM dans le milieu marin s'est effectuée *via* des méthodes globales avec l'analyse du carbone ou de l'azote organique dissous (DOC et DON), ou des méthodes très fines, chromatographiques (analyses de composés individuels par HPLC-UV, HPAEC-PAD, TLC-FID et GC-MS) et isotopiques (analyses des isotopes stables ^{13}C et ^{15}N) (Mopper et al., 2007). Les analyses de DOC et DON, relativement simples à mettre en œuvre, peuvent être réalisées sur un nombre important d'échantillons. Même si elles permettent de quantifier le pool global de DOM, elles sont très limitées pour apprécier sa qualité et sa composition. Au contraire, les analyses fines fournissent des informations très pertinentes sur la composition moléculaire de la DOM, par exemple sur les teneurs en acides aminés, en sucres, en lipides ou en acides carboxyliques (chromatographie), et sur ses sources et processus de transformation (isotopie), mais ne peuvent pas être appliquées à un nombre élevé d'échantillons. Elles nécessitent généralement de gros volume d'eau (parfois plusieurs litres pour une seule analyse), un traitement et une préparation complexe de l'échantillon, avec des étapes d'extraction, de purification, de concentration ou de dérivatisation. Ces analyses fines sont donc longues, délicates, et de surcroît, coûteuses. Les techniques d'analyse faisant intervenir les propriétés optiques de la DOM représentent des alternatives intéressantes car elles sont rapides et ne nécessitent aucun traitement si ce n'est une filtration, sont simple à mettre en place et permettent d'avoir une vision globale de la DOM.

Parmi le pool de DOM, une partie possède des propriétés optiques. Ces molécules ont la capacité d'absorber une partie de l'énergie sous forme lumineuse, il s'agit de la matière organique dissoute chromophorique (ou colorée) (CDOM). Les spectres d'absorption de la CDOM montrent généralement une augmentation exponentielle des valeurs de coefficients d'absorption avec la diminution de la longueur d'onde (λ). Même s'ils fournissent une information précieuse sur la quantité de DOM, ils ne sont pas assez discriminants pour donner des renseignements précis sur sa composition (Blough et Del Vecchio, 2002). Parmi les molécules composant le pool de CDOM, une partie est capable de réémettre de la lumière et donc de fluorescer, c'est la matière organique dissoute fluorescente (FDOM). Ainsi on peut écrire la relation suivante :

$$DOM \supset CDOM \supset FDOM$$

Une molécule qui a des propriétés de fluorescence est appelée fluorophore. La spectroscopie de fluorescence permet de caractériser la matière organique d'un échantillon et de déterminer l'origine des fluorophores (Hudson et Reynolds., 2007 ; Henderson et al., 2009 ; Ishii et Boyer, 2012), les réactivité chimiques (Saar et Weber, 1980 ; Plaza et al., 2005) et biologiques (Rinnan et Rinnan, 2007 ; Yaheng Zhang et al., 2008). Depuis une quinzaine d'années, la FDOM a été abondamment étudiée grâce aux avancées récentes dans le domaine de la spectroscopie de fluorescence, en particulier grâce à la mise en place d'instruments permettant la mesure de matrices d'excitation-émission de fluorescence (MEEF) (Coble, 1996 ; Mounier et al., 1999 ; Parlanti et al., 2000). Ces dernières sont générées par l'enregistrement et la compilation de spectres d'émissions pour des longueurs d'ondes d'excitation fixes et permettent d'obtenir une cartographie détaillée sur un large domaine spectral (200-700 nm) de la composition en fluorophores d'un échantillon d'eau. Contrairement aux spectres d'absorption, les spectres de fluorescence (spectres d'excitation et d'émission) sont plus discriminants. En effet, ces derniers présentent un ou plusieurs pics sur la gamme de longueur d'onde UV et visible qui correspondent à un ou plusieurs fluorophores. Les spectres de fluorescence d'un composé dépendent de sa structure moléculaire, tandis que son intensité de fluorescence est fonction de sa concentration. La caractérisation de la DOM *via* les mesures de fluorescence présente plusieurs avantages par rapport aux autres types d'analyses. Cette dernière est très rapide, elle ne nécessite aucune étape de traitement sauf une étape de filtration, elle ne nécessite que peu de volume d'échantillons (~ 5

mL). Le faible temps de traitement et d'analyse permettant de caractériser la FDOM rend possible l'application de cette technique d'analyse à un nombre important d'échantillons.

5. La spectroscopie de fluorescence

5.1. Le principe de fluorescence

Pour qu'une molécule fluoresce, elle doit être capable dans un premier temps d'absorber de l'énergie sous forme de lumière (onde électromagnétique). L'énergie lumineuse va être absorbée par des groupements fonctionnels ayant des doubles ou des triples liaisons de type π ou des doublets d'électron non liants. Ces groupements sont dits chromophoriques, ils vont absorber l'énergie émise par une source lumineuse sous forme de photons. Un électron va alors passer sur une couche d'un niveau d'énergie supérieur, on dit alors que la molécule est dans un état excitée. Il existe alors différentes façons pour une molécule de retourner à l'état fondamental et notamment la fluorescence. Lorsque l'électron au niveau vibrationnel S^*_1 v_i retourne à l'état fondamental S_0 v_i (Figure I-6), il va restituer une partie de l'énergie qu'il a absorbée sous forme de lumière. L'énergie réémise est toujours inférieure à l'énergie qui a permis d'exciter la molécule en raison notamment de conversions internes. Étant donné la relation qui lie l'énergie à la longueur d'onde, les différences constatées entre les énergies expliquent pourquoi la longueur d'onde d'excitation est toujours plus faible que la longueur d'onde d'émission (Valeur, 2001).

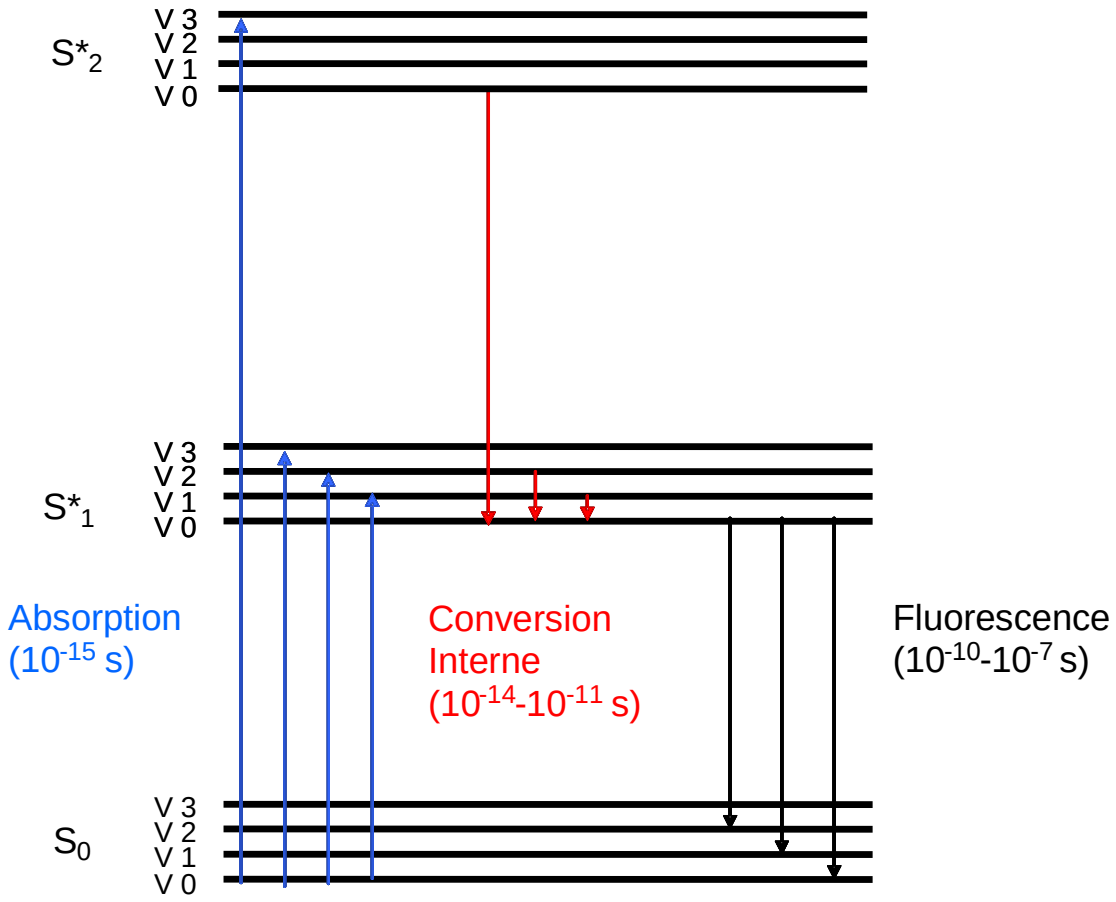

Figure I-6. Diagramme de Jablonski.

L'intensité de fluorescence émise par la molécule suit le modèle suivant :

$I_F(\lambda_{ex}, \lambda_{em}) = K F_{\lambda ex}(\lambda_{em})\, I_0(\lambda_{ex})\,(1-e^{2.303\varepsilon(\lambda ex)lC})$

Avec $I_F(\lambda_{ex}, \lambda_{em})$ étant l'intensité de fluorescence pour un couple de longueur d'onde d'excitation et d'émission données. K étant le produit du rendement quantique de fluorescence de la molécule et d'une constante qui dépend du système de mesure. $F_{\lambda ex}$ étant la densité de probabilité d'émission d'un photon une longueur donnée (le spectre d'émission). $I_0(\lambda_{ex})$ étant l'intensité incidente sur l'échantillon. $\varepsilon(\lambda_{ex})$ correspond au coefficient d'extinction molaire (en cm^{-1} mol^{-1} L) (spectre d'absorption). l correspond au trajet optique (en cm) et enfin C correspond à la concentration (mol L^{-1}) d'un fluorophore donné. Dans cette équation, ε (λex)lC représente les spectre d'absorption (Valeur, 2001).

Dans les milieux faiblement concentrés, cette équation peut être simplifiée et peut s'écrire de la façon suivante :

$I_F (\lambda_{ex}, \lambda_{em}) = 2.303\ KF_{\lambda ex} (\lambda_{em})\ I_0 (\lambda_{ex})\ A (\lambda_{ex})$

A (λ_{ex}) étant l'absorbance et correspond donc à $\varepsilon (\lambda_{ex}).l.C.$

Chaque fluorophore possède également un temps de vie de fluorescence qui lui est propre dans un environnement donné. La discrimination d'échantillon à l'aide du temps de vie permet de rajouter une dimension à la fluorescence et de pouvoir séparer des fluorophores différents qui pourraient avoir des signatures similaires telles que par exemple le tryptophane et le naphtalène.

Pour pouvoir déterminer le temps de vie de fluorescence, il faut pour cela avoir une source de lumière discontinue au cours du temps comme une source impulsionnelle (Valeur, 2001).

Pour une quantité [A] de fluorophore (en M), une lumière de très faible pulse à un temps 0 porte une certaine quantité de molécule à un état excité par absorption d'un photon. Les molécules excitées vont retourner à l'état fondamental par des voies qui sont à la fois radiative et non radiative. La décroissance de molécules excitées au fil du temps suivra l'équation suivante :

$[A^*] = [A^*]_0 \exp(-t/\tau)$

Avec $[A^*]_0$ la concentration en fluorophores excités à un temps 0, [A*] la concentration de fluorophores à l'état excités à un temps t et τ le temps de vie de fluorescence.

Avec $\tau = 1/(k_r+k_{nr})$

Avec k_r correspondant la constante de la désactivation radiative à et k_{nr} correspondant à la constante de la désactivation non radiative pour un retour à l'état fondamental de S^*_1 à S_0 (Valeur, 2001).

Pour passer de la concentration à une intensité en fonction du temps, il suffit de multiplier la concentration de fluorophore à un temps donné par une constante de désexcitation k_{sr} (Valeur, 2001). On obtient alors l'équation suivante :

$I_f (t) = k_{sr} [A^*] = k_{sr} [A^*]_0 \exp(-t/\tau)$

Un exemple de décroissance temporelle est présenté dans la Figure I-7.

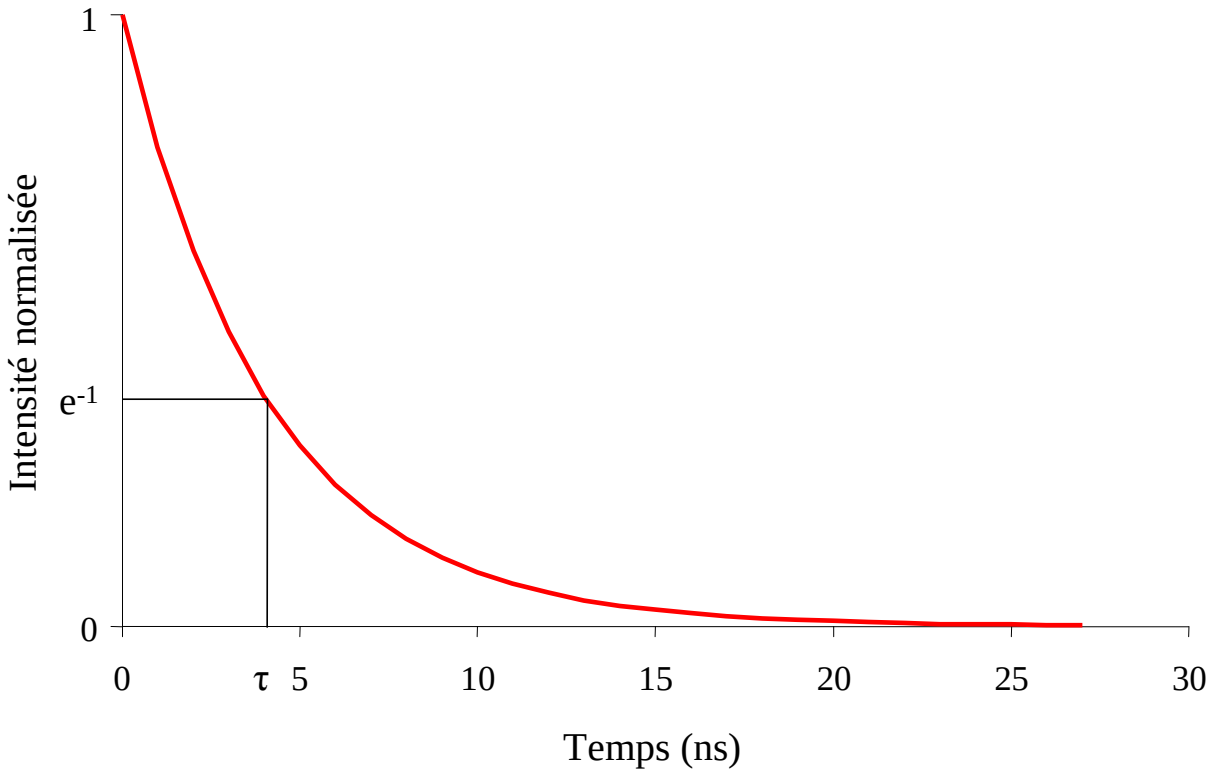

Figure I-7. Exemple de décroissance temporelle de fluorescence de la fluorescéine (τ = 4,1 ns et λex = 266 nm).

5.2. Les paramètres influençant la fluorescence

Plusieurs paramètres peuvent affecter le couple de longueurs d'onde d'excitation et d'émission ainsi que l'intensité de fluorescence des molécules.

5.2.1. Le quenching

Deux types de quenching existent, le quenching statique et le quenching dynamique. Ces phénomènes entraînent une sous-estimation de la quantité de fluorophore dans un échantillon (Howerton et al., 2002). Le quenching dynamique se produit lorsqu'un fluorophore à l'état excité retourne à un état stable par transfert d'énergie après collision avec un quencheur comme le dioxygène. Ce transfert d'énergie est non-radiatif, c'est-à-dire sans émission d'onde électromagnétique.

Ce phénomène réduit également le temps de vie moyen de fluorescence et s'exprime selon l'équation de Stern-Volmer :

$F_0/F=1+k_q t_0 [Q] = 1+K_D [Q]$

F_0 correspond à l'intensité de fluorescence du fluorophore considéré sans quencheur.

F correspond à l'intensité de fluorescence du fluorophore dans un échantillon contenant une certaine quantité de quencheur.

k_q représente la constante de quenching bimoléculaire (en L/mol.s ou en L/g.s).

t_0 correspond au temps de vie de fluorescence du fluorophore considéré (en s) en l'absence de fluorophore.

[Q] correspond à la concentration de quencheur (en g L^{-1} ou en mol L^{-1}) et K_D (en L g^{-1} ou en L mol^{-1}) (Lakowicz et Weber, 1973 ; Lakowicz, 2006).

Le quenching statique est provoqué par la réaction entre un fluorophore et un désactivateur qui va former un complexe. Les propriétés du complexe sont différentes du fluorophore d'origine et de ce fait, l'intensité du signal de fluorescence du fluorophore cible va diminuer (Lakowicz, 2006).

Contrairement au quenching dynamique, le quenching statique n'aura aucun effet sur le temps de vie de fluorescence d'un fluorophore. Ce phénomène se traduit par une autre équation de Stern-Volmer :

$F_0/F=1+K_{sv} [Q]$

F_0 correspond à l'intensité de fluorescence du fluorophore considéré sans quencheur.

F correspond à l'intensité de fluorescence du fluorophore dans un échantillon contenant une certaine quantité de quencheur.

[Q] correspond à la concentration de quencheur (en g L^{-1} ou en mol L^{-1}) et K_{sv} (en L g^{-1} ou en L mol^{-1}) correspond à la constante de Stern-Volmer relative au pouvoir de complexation des espèces considérées (Lakowicz, 2006).

Cette relation est représentative des interactions et de la diminution du signal de fluorescence entre un fluorophore et un quencheur lors d'une complexation et la constante de Stern-Volmer sera utilisée afin de déterminer les constantes d'équilibres de réaction :

$F + Q \leftrightarrow F\text{-}Q$

$K_{sv} = [F\text{-}Q]/ [F] [Q]$

La matière organique naturelle et notamment les substances humiques (Hudson et Reynolds, 2007) ont la capacité de réagir avec les métaux pour former des complexes. De telles réactions entre les métaux et les substances humiques peuvent avoir une influence sur les propriétés optique de ces dernières. La formation de complexes organométalliques va changer la structure de la molécule et pourra avoir pour conséquence un changement des propriétés optiques affectant à la fois le spectre d'absorbance mais aussi le spectres d'émission (Elkins et Nelson, 2002). L'impact sur l'intensité de fluorescence varie selon le type de métal considéré. Les métaux paramagnétiques tels que le cuivre, le fer, le mercure, le nickel, le zinc ou le palladium réduisent significativement l'intensité de fluorescence (Hudson et Reynolds., 2007 ; Henderson et al., 2009). Les métaux diamagnétiques tels que l'aluminium, le magnésium, le calcium et le cadmium peuvent à la fois réduire, augmenter ou n'avoir que peu d'effet sur la fluorescence. L'ajout d'aluminium par exemple augmente l'intensité de fluorescence des substances humiques à pH 5 mais cet effet n'est pas valable à tous les pH : au dessus de pH 7,5, du quenching est observé à cause de la précipitation du complexe formé (Cabaniss, 1992). Le tryptophane peut également être sensible à la présence d'ions métalliques. Le nickel, le cuivre, le fer et l'aluminium peuvent réduire l'intensité de ce fluorophore alors que le zinc, le manganèse, le chrome, le cobalt, le calcium et le sodium n'ont aucun effet sur cet acide aminé (Henderson et al., 2009).

D'un autre côté, les substances humiques, en interagissant lorsqu'ils s'associent avec des contaminants fluorescents (PAHs, biocides) peuvent réduire la fluorescence de ces derniers. Une étude a montré que des biocides tels que le carbaryl, le carbofuran, l'aldicarb ou encore le naphthol peuvent être complexés par différents types de matière organique (sols, zones humides, eaux de ruissellements) diminuant ainsi leur fluorescence (Morra et al., 1990 ; Fang et al., 1998). Concernant les PAHs, des études ont mis en évidence la complexation entre le pyrène, le phénanthrène, le naphtalène et des acides humiques synthétiques (Kumke et al., 1994 ;

Peuravuori, 2001), des acides fulviques synthétiques (Kumke et al., 1994), et de la matière organique extraite de tourbe (Peuravuori, 2001), de rivière (Jung et al., 2010) et de lac (Peuravuori, 2001). Dans ces études, les constantes de Stern-Volmer, qui définissent la spéciation entre un fluorophore et son quencheur, sont déterminées. Elles sont généralement différentes suivant le type de DOM. Il a été également démontré que le pH pouvait également jouer un rôle dans le phénomène de quenching. Le quenching permet de déterminer les forces de liaisons entre les substances humiques et des contaminants tels que les métaux, les biocides et les PAHs. Chaque contaminant qui va réagir avec un certain type de matière organique aura des affinités propres et donc des constantes de complexation différentes (Tableau I-1).

Tableau I-1. Contaminants et constantes de réaction de Stern-Volmer en fonction du type de DOM, du solvant et du pH.

Contaminants	Type de DOM	K_{sv} ($L\ kg^{-1}$)	pH	Solvant	Références
Carbaryl	Acide humique Aldrich	$0{,}96\ 10^4$	6	Eau	Fang et al., 1998
Carbofurane	Acide humique Aldrich	$8{,}75\ 10^4$	6	Eau	Fang et al., 1998
Aldicarbe	Acide humique Aldrich	$7{,}21\ 10^4$	6	Eau	Fang et al., 1998
Naphthol	Acide humique de loam limoneux	$0{,}04\ 10^4$	7	Eau	Morra et al., 1990
Naphtalène	Acide humique de loam limoneux	$0{,}02\ 10^4$	7	Eau	Morra et al., 1990
Phénanthrène	Aldrich humic acid	$13\ 10^4$	7,3	Eau	Doll et al., 1999
	NOM from lake Hohloh	$5{,}8\ 10^4$	7,3	Eau	Doll et al., 1999
Pyrène	Acide humique du lac Mekkojärvi, ultra filtration seuil de coupure des mollécules ≥ 1000000 Da	$3{,}21\ 10^4$	7	Acétate de sodium	Peuravuori, 2001
	Acide humique du lac Mekkojärvi, ultra filtration seuil de coupure des molécules 1000000-10000 Da	$3{,}93\ 10^4$	7	Acétate de sodium	Peuravuori, 2001

Acide humique de tourbe, extraction basique	$7{,}49\ 10^4$	7	Acétate de sodium	Peuravuori, 2001
Acide humique de la Moselle (rivière) extrait en été	$0{,}52\ 10^4$	8	Eau	Jung et al., 2010
Acide humique de la Moselle (rivière) extrait en automne	$0{,}31\ 10^4$	8	Eau	Jung et al., 2010
Acide humique Fluka	$11{,}30\ 10^4$	7	Acétate de sodium	Peuravuori, 2001
Acide humique Aldrich	$10\ 10^4$	11,5	Eau	Kumke et al., 1994
Acide humique Aldrich	$3\ 10^4$	2	Eau	Kumke et al., 1994
Acide fulvique du lac Mekkojärvi, ultra filtration seuil de coupure des mollécules ≥ 1000000	$2{,}66\ 10^4$	7	Acétate de sodium	Peuravuori, 2001
Acide fulvique du lac Mekkojärvi, ultra filtration seuil de coupure des mollécules 1000000-10000 Da	$3{,}00\ 10^4$	7	Acétate de sodium	Peuravuori, 2001
Acide fulvique du lac Mekkojärvi, ultra filtration seuil de coupure des molécules 10000-1000 Da	$1{,}87\ 10^4$	7	Acétate de sodium	Peuravuori, 2001
Acide fulvique du lac Mekkojärvi, ultra filtration seuil de coupure des molécules ≤ 1000 Da	$2{,}21\ 10^4$	7	Acétate de sodium	Peuravuori, 2001
Acide fulvique de tourbe, extraction basique	$2{,}28\ 10^4$	7	Acétate de sodium	Peuravuori, 2001
Matière organique de lac norvégien, osmose inverse	$2{,}32\ 10^4$	7	Acétate de sodium	Peuravuori, 2001

5.2.2. Le pH

Les variations de pH peuvent entraîner une modification de l'intensité de fluorescence des fluorophores. Elles peuvent être dues à la conformation des molécules, à de faibles pH, les molécules ont tendance à s'enrouler sur elles même alors qu'une augmentation du pH implique un déroulement de celles-ci (Hudson et Reynolds, 2007 ; Henderson et al., 2009). Cet enroulement aurait un impact sur les fonctions capables d'absorber de la lumière. Les variations du pH peuvent également affecter les électrons présents dans les orbitales moléculaires absorbant la lumière et donc avoir une influence sur l'intensité de fluorescence. Le passage d'un milieu basique ou neutre vers un milieu acide peut également impacter la fluorescence. La diminution déplacerait l'équilibre dans le sens de la dissolution de molécules composée des métaux en ions métalliques. L'augmentation de la concentration en ions métalliques permettrait de former des complexes organométalliques avec des fluorophores, ce qui, de ce fait modifierait l'intensité de fluorescence de l'échantillon (Patel-Sorrentino et al., 2002). La modification du pH peut également modifier la forme du spectre des fluorophores. Par exemple, le pic d'acide humique « C » subit un déplacement vers le rouge lorsque le pH augmente (Spencer et al., 2007). Les variations d'intensité fluorescence varient d'un fluorophore à un autre. Il a été observé que l'intensité de fluorescence des substances humiques avait tendance à augmenter pour des pH entre 4 et 5,5 et qu'au-delà de ces valeurs, l'effet sur la fluorescence perdurait mais de façon moins importante (Vodacek et Philpot, 1987). Pour les pics d'acides humiques « A » et « C », à des pH variant de 2 à 12 une augmentation d'intensité a été constatée, alors que pour des valeurs de pH supérieures, une légère diminution est observée (Patel-Sorrentino et al., 2002). D'autres études ont montré que l'intensité de certains pics « C » augmentait pour des pH croissant de 2 à 4 et restait stable pour des pH compris entre 4 et 10 avant de décroître pour des valeurs de pH supérieures (Spencer et al., 2007). Pour le pic d'acide humique « A » issu d'eaux usées et pour des acides fulviques standards, une diminution de 30 à 40% est observée pour des pH diminuant de 7 à 3 (Westerhoff et al., 2001). Pour le tryptophane, certains auteurs n'ont pas détecté d'influence du pH sur l'intensité de fluorescence (Spencer et al., 2007) alors que Reynolds (2003) a constaté une diminution de 15% de son intensité de fluorescence pour des pH inférieurs à 4,5 et une augmentation de 30% pour des pH supérieurs à 8. L'effet du changement de pH est par contre réversible entre les pH 2 et 12 car les structures des molécules ne sont pas impactées

(Henderson et al., 2009). Dans les eaux naturelles, le pH étant compris entre 5 et 9, les variations des intensités de fluorescence attendues seront d'environ 10% (Hudson et Reynolds, 2007).

5.2.3. La température

La température joue également un rôle significatif sur l'intensité de fluorescence de la DOM. Une augmentation de ce paramètre provoque une diminution de l'intensité de fluorescence. En effet, l'accroissement de température augmente la probabilité de collisions entre les molécules, ce qui provoque un retour de l'électron excité vers l'état fondamental sans émission de radiation (Valeur, 2001). Entre 45 et 10°C, l'intensité de fluorescence augmente en moyenne de 1% par degré Celsius. L'effet de la température est réversible et n'a aucun impact sur la structure de la FDOM d'où l'intérêt de réaliser des mesures de fluorescence dans un environnement à température contrôlée constante (Henderson et al., 2009).

5.2.4. Le solvant

Le solvant est également un paramètre important. En fonction de la polarité et de la viscosité, il pourra modifier les propriétés optique d'un composé en déplaçant la position des signatures de fluorescence et en augmentant ou réduisant la sensibilité des fluorophores (Ren, 1999 ; El-Rayyes et Htun, 2004). Lors de ces travaux de recherche, tous les échantillons ont de l'eau pour solvant.

5.2.5. L'effet d'écran

L'effet d'écran peut également impacter l'intensité de fluorescence des fluorophores. En effet, dans les milieux faiblement concentrés, la fluorescence dépend de la loi de Beer-Lambert. Cependant à partir d'un certain seuil de concentration, le modèle de Beer-Lambert n'est plus valable et les valeurs d'intensité de fluorescence ne suivent plus un modèle linéaire (Figure I-8).

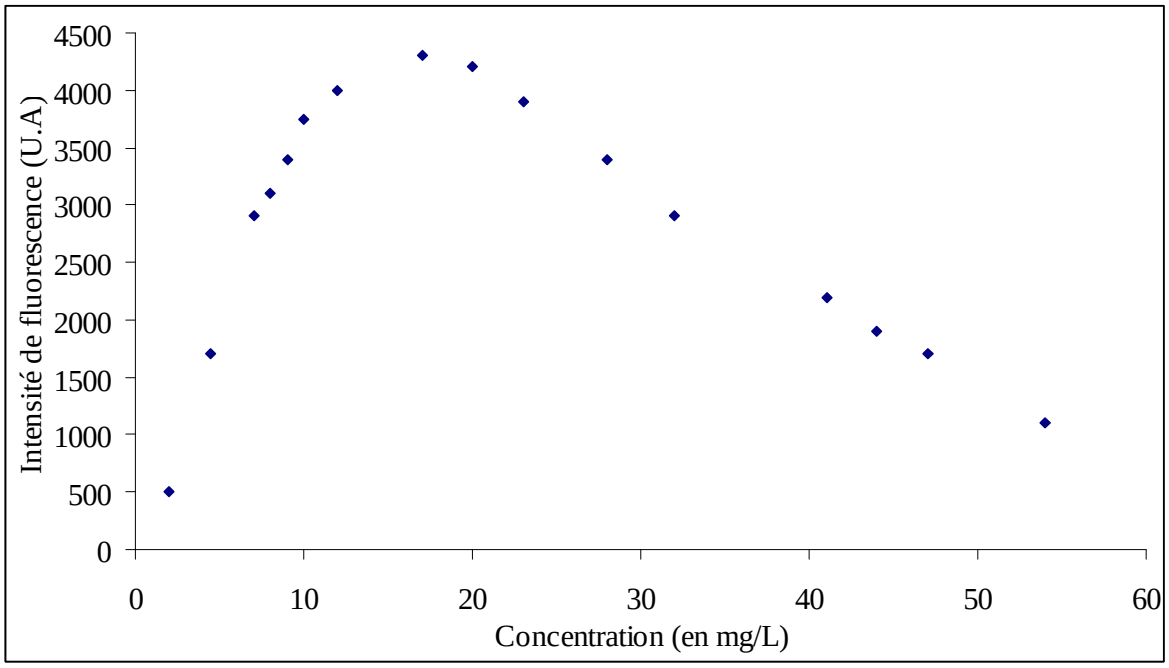

Figure I-8. Exemple de l'impact de l'effet d'écran sur la fluorescéine (modifié à partir de Luciani, 2007).

Il existe deux types d'effet d'écran, l'effet d'écran primaire qui est dû à l'absorption d'une partie de la lumière provenant de la source par un chromophore. Dans ce cas, seulement une partie de la lumière d'excitation atteindra le ou les fluorophores d'intérêts. L'effet d'écran secondaire est lié à l'absorption de la lumière d'émission provenant d'un fluorophore par un chromophore. Dans ce cas, seulement une partie de la lumière émise arrive vers le détecteur (Lakowicz, 2006).

Pour considérer l'impact que l'effet d'écran a sur l'échantillon, des mesures d'absorbances sont effectuées. Si à 250 nm, l'absorbance est supérieure à 0,05, l'influence qu'a l'effet d'écran sur l'intensité de fluorescence devient significatif (Hu et al., 2002 ; Larmagnat et Neuweiler, 2011) et des corrections doivent être apportées aux intensités de fluorescence. Pour corriger l'effet d'écran, deux solutions existent : 1) la mesure de fluorescence sur l'échantillon dilué, pour être dans le domaine de linéarité de la loi de Beer Lambert (Valeur, 2001) et 2) la mesure de fluorescence sur l'échantillon non dilué avec correction des intensités de fluorescence par les mesures d'absorbance (Ohno, 2002). Pour corriger les mesures de fluorescence à partir des mesures d'absorbance, il faut utiliser l'équation suivante (Ohno, 2002) :

$I(\lambda_{ex}, \lambda_{em}) = I_{0.(}\ \lambda_{ex,}\ \lambda_{em)}.10^{-b(Aex+Aem)}$

Où $I(\lambda_{ex}, \lambda_{em})$ représente l'intensité de fluorescence mesurée sur l'échantillon, $I_{0(}\lambda_{ex,}\ \lambda_{em)}$ correspond à l'intensité de fluorescence corrigée de l'effet d'écran, b correspond à la longueur de la cuve multipliée par 0,5 (il est considéré que l'effet d'écran primaire a lieu sur la première partie du trajet de la cuve et que l'effet d'écran secondaire a lieu sur la seconde partie), Aex et Aem correspondent respectivement à l'absorbance à la longueur d'onde d'excitation et à la longueur d'onde d'émission de fluorescence.

6. Composition de la FDOM

6.1. La matière organique dissoute naturelle fluorescente (FNDOM)

L'enregistrement et la compilation de spectres d'émissions pour plusieurs longueurs d'ondes d'excitation fixes permettent de constituer une matrice d'excitation et d'émission de fluorescence (MEEF) (Figure I-9 et I-10). Sur ces dernières apparaissent des pics de fluorescence correspondants à des fluorophores.

Les principaux fluorophores observés constitutifs de la FNDOM se divisent en deux groupes, les protéines représentées par les fluorophores de type tyrosine (B1, B2), tryptophane (T1, T2) et les substances humiques représentées par les fluorophores de type acide fulvique (A), acide humique (C) et acide humique marin (M1, M2) (Tableau. I-2 et Figure I-9). Ces fluorophores possèdent des pics (maximum de fluorescence) spécifiques caractérisés par des couples de longueurs d'onde d'excitation et d'émission (Hudson et Reynolds, 2007 ; Henderson et al., 2009 ; Fellman et al., 2010).

Les fluorophores de type protéine B et T (ou « protein-like ») sont généralement plus abondants que les fluorophores de type humique M, A et C (ou « humic-like ») dans les eaux marines (Figure I-10) (Hudson et Reynolds, 2007). Ils peuvent être d'origine autochtone (produit *in situ*) ou allochtone (transporté par les fleuves et les rivières) mais ils sont souvent liés à l'activité du phytoplancton (Parlanti et al., 2000 ; Cory et al., 2010 ; Lønborg et al., 2010 ; Romera-Castillo et al., 2010) ou à l'activité bactérienne pour le tryptophane (Determann et al., 1998 ; Stedmon et al., 2003 ; Cammack et al., 2004). Ce dernier est également utilisé comme indicateur de la présence d'eaux usées dans les eaux douces (Baker et Spencer, 2004 ; Baker et al., 2004) et dans les eaux

côtières (Tedetti et al., 2012). Les domaines fluorescence de chacun des fluorophores sont présentés dans la Figure I-9.

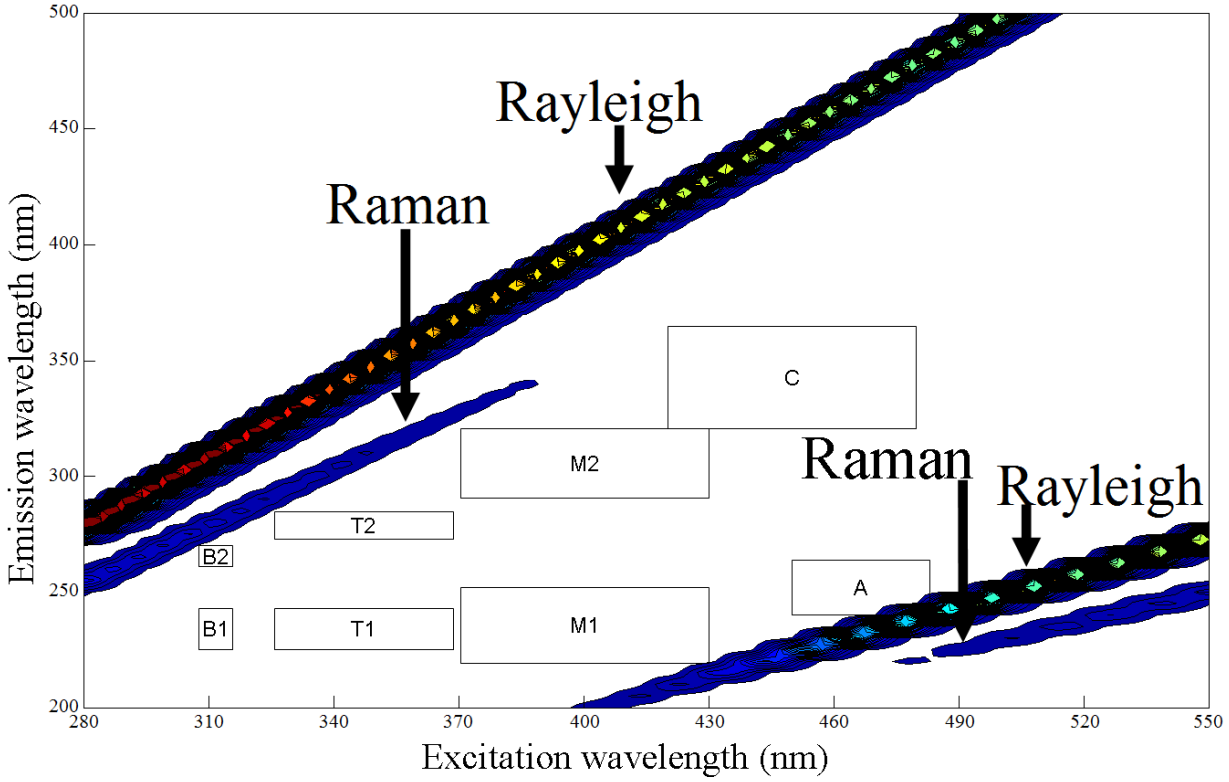

Figure I-9. Localisation des composés de la FNDOM, des zones permettant de déterminer les indices de fluorescence et des bandes de diffusion Raman et Rayleigh d'ordres 1 et 2.

Les fluorophores humiques A et C (Figure I-10) sont présents en grandes quantités dans les eaux douces (Hudson et Reynolds,, 2007). Ils proviennent de la dégradation des végétaux supérieurs et de la dissolution de la matière organique particulaire des sols (Katsuyama et Ohte, 2002 ; Hudson et al., 2008). Ce sont des composés de haut poids moléculaire ayant un degré d'aromaticité élevé. Dans les estuaires et dans le milieu marin, l'abondance de ces deux fluorophores décroît avec la salinité (Hudson et Reynolds, 2007). Le fluorophore humique marin M est bien plus ubiquiste. Il a déjà été détecté dans les eaux marines (Coble, 1996 ; Parlanti et al., 2000), dans les eaux douces (Stedmon et Markager, 2005 ; Murphy et al., 2008) et dans les sols (Balcarczyk et al., 2009). Son domaine de fluorescence est de plus courte longueur d'onde que celui des acides humiques A et C en raison de son degré d'aromaticité et de son plus poids moléculaire plus faibles (Fellman et

al., 2010). Sa présence est généralement attribuée à l'activité phytoplanctonique (Hudson et Reynolds, 2007).

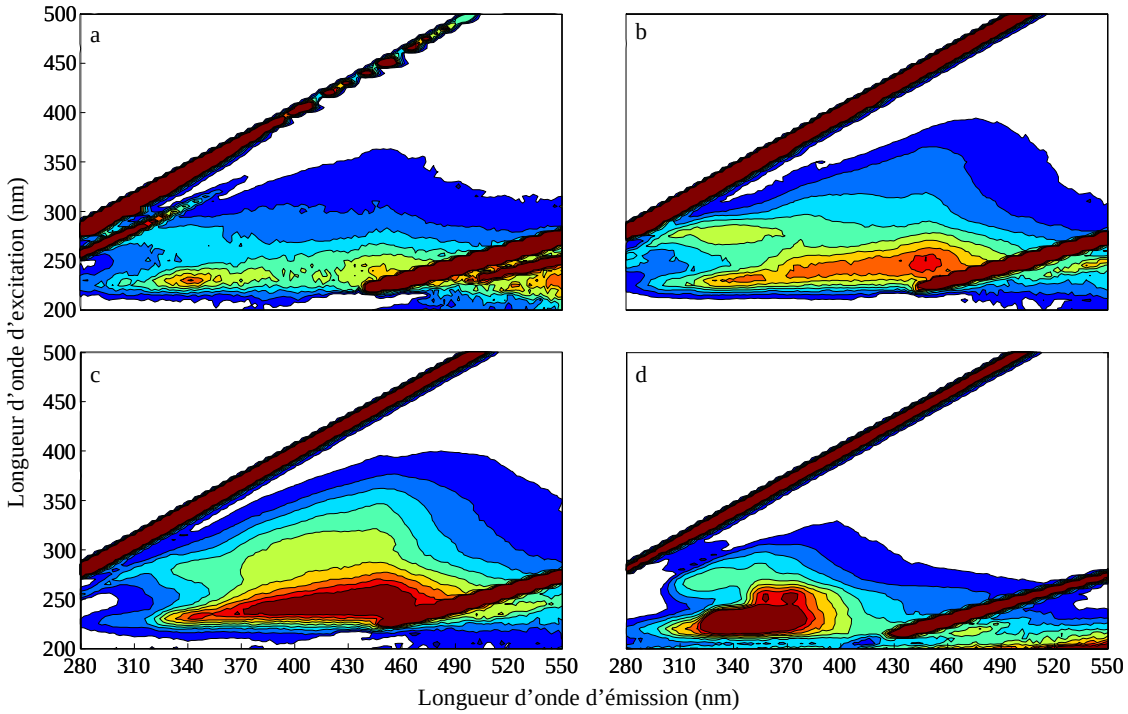

Figure I-10. Exemples de MEEFs obtenues dans des environnements aquatiques contrastés : eau marine (a), d'eau saumâtre (b), eau douce (c) et eau de port contaminée en hydrocarbures (d).

Tableau I-2. Fluorophores communs de la FNDOM observés dans l'environnement marin côtier (Hudson et Reynolds, 2007 ; Henderson et al., 2009).

Pic	λEx / λEm	Nom	Origines
A	260 < /448-480	Acide fulvique	Terrigène, dégradation des végétaux supérieurs
C	320-360 / 420-460	Acide humique	Terrigène, dégradation des végétaux supérieurs
M	250 < (290-325) / 370-430	Acide humique marin	Activité biologique, anthropique
B	225-237 (270-275) / 304-312	Tyrosine	Activité microbienne, production primaire
T	225-237 (270-280) / 330-368	Tryptophane	Anthropique, activité microbienne, Production primaire

En plus de l'identification des différents fluorophores présents, plusieurs indices de fluorescence sont utilisés pour obtenir des informations sur l'origine et le degré d'humification de la FDOM.

L'indice de fluorescence (FI) permet d'estimer l'origine principale de la FDOM ou d'évaluer le degré de dégradation de la DOM (DOM aromatique *versus* DOM non aromatique). Il se calcule en réalisant pour une longueur d'onde d'excitation de 370 nm, le rapport entre les intensités de fluorescence aux longueurs d'onde d'émission de 470 et de 520 nm :

$FI = I_{(370,470)} / I_{(370,520)}$

Une valeur du FI basse (1,2) traduit une origine terrestre de la DOM (fortement aromatique), tandis qu'une valeur de FI plus élevée (autour de 1,8) révèle une origine aquatique ou microbienne de la DOM (faiblement aromatique) (Fellman et al., 2010).

L'indice biologique (BIX) permet d'évaluer l'activité biologique autochtone ainsi que l'âge de la DOM. Il se calcule en effectuant pour une longueur d'onde d'excitation de 310 nm, le rapport entre les intensités de fluorescence aux longueurs d'onde d'émission de 380 nm (ce qui correspond à de la DOM fraîche) et de 430 nm (ce qui correspond au matériel humique) (Huguet et al., 2009) :

$BIX = I_{(310,380)} / I_{(310,430)}$

Dans les eaux naturelles, la valeur de BIX est relativement basse, entre 0,6 et 0,7. Des valeurs élevées (> 1) impliquent une prédominance de la DOM d'origine autochtone ainsi qu'une proportion importante de matière organique fraîche (Huguet et al., 2009).

L'indice d'humification (HIX) permet d'évaluer le degré d'humification de la DOM ainsi que son contenu. Il se calcule en effectuant pour une longueur d'onde d'excitation de 255 nm, le rapport de somme des intensités de fluorescence entre les longueurs d'onde d'émission allant de 434 à 480 nm sur la somme des intensités de fluorescence pour les longueurs d'onde d'émission allant de 300 à 344 nm (Zsolnay et al., 1999) :

$$HIX = \frac{\int_{i=434}^{i=480} I_{(255,i)}}{\int_{i=300}^{i=344} I_{(255,i)}}$$

Des valeurs de HIX élevées (entre 10 et 16) signifient que la DOM est fortement humifiée et d'origine terrestre alors que pour de faibles valeurs (< à 4), la DOM est principalement issue de la production autochtone (Fellman et al., 2010).

Sur les MEEFs présentées précédemment (Figure I-9 et I-10), apparaissent aussi les bandes de diffusion de Rayleigh et de Raman. Les bandes de Rayleigh sont observées à λex = λem (bande d'ordre 1) et à 2 λex = λem (bande d'ordre 2) et correspondent à la diffusion élastique (réflexion) du rayonnement incident sur la paroi de la cuve en quartz. Les bande de Raman (d'ordres 1 et 2) sont liées à la diffusion inélastique (i.e. diffusion avec changement de longueur d'onde) provoquée par la vibration de la liaison O-H des molécules d'eau (Hudson et Reynolds, 2007). Les fluorophores observés sur ces matrices ont chacun des caractéristiques différentes. Ils possèdent un couple d'excitation et d'émission et un rendement quantique qui leurs sont propres.

6.2. Composition de la FADOM

Parmi les composés anthropiques mentionnés précédemment certains d'entre eux ont des propriétés intrinsèques de fluorescence. C'est le cas de certains PAHs (Giamarchi et al., 2000 ; JiJi et Booksh, 2000 ; Christensen et al., 2005 ; Tedetti et al., 2010), qui ont un rendement de fluorescence élevé (Valeur, 2001), et de certains biocides (Fang et al., 1998 ; Jiji et al., 1999 ; Rodríguez-Cuesta et al., 2003 ; García Reyes et al., 2004) mais qui eux ont un rendement de fluorescence plus faible dû à la présence d'atomes lourds tels que le brome qui peuvent inhiber la fluorescence (Valeur, 2001). Les signatures de fluorescence de composés anthropiques sont relativement peu connues à ce jour malgré quelques études menées sur des composés standards. Le domaine de fluorescence de ces composés est similaire et se situe dans l'UV (220-390 nm) pour les longueurs d'onde d'excitation et dans l'UV et le visible pour les longueurs d'émission (305 et 406 nm) (Tableau I-3). Un exemple de MEEF présentant des fluorophores anthropiques est présenté Figure I-10.

Tableau I-3. Couple de longueurs d'onde d'excitation et d'émission et temps de vie de fluorescence (si calculé) de PAHs et de biocides dans leur solvant respectif.

PAHs et biocides	λEx / λEm (nm)	Temps de vie de fluoresecnce (ns)	Solvant	Références
Naphtalène	220(270) / 335		Eau	Tedetti et al., 2010
	224 / 340		Eau	Giamarchi et al., 2000
	225 / 330		Eau	Beltrán et al., 1998
	250 < (280) / 340		Dichlorométhane	Christensen et al., 2005
	270 / 330		Eau	Beltrán et al., 1998
	280 / 345		Ethanol	JiJi et Booksh, 2000
	- / 327, 337		Cyclohexane	Karcher et al., 1985
	266 / -	40,3	Eau désoxygénée	Meidinger et al., 1993
	302 (319) / 322	96	Cyclohexane désoxygéné	Kumke et al., 1995
1-méthyl naphtalène	266 / -	30,3	Eau désoxygénée	Meidinger et al., 1993
2-méthyl naphtalène	266 / -	24,6	Eau désoxygénée	Meidinger et al., 1993
Acenaphthene	300 (320) / 347	46	Cyclohexane désoxygéné	Kumke et al., 1995
Acenaphthylene	324 (456) / 541	0,9	Cyclohexane désoxygéné	Kumke et al., 1995
Fluorène	210(260)/310		Eau	Beltrán et al., 1998
	255/310		Eau	Giamarchi et al., 2000
	270 (290) / 305		Eau	JiJi et Booksh, 2000
	- / 306 (315)		Cyclohexane	Karcher et al., 1985
	260 / 310		Dichlorométhane	Christensen et al., 2005
	300 / 310	10	Cyclohexane désoxygéné	Kumke et al., 1995
Phénanthrene	245 / 360		Eau	Giamarchi et al., 2000
	245 / 360		Eau	Tedetti et al., 2010
	250 / 360		Eau	Beltrán et al., 1998
	270 / 355		Eau	JiJi et Booksh, 2000
	- / 346.5 (356) (364) (374)		Cyclohexane	Karcher et al., 1985

	250 / 375		Dichlorométhane	Christensen et al., 2005
	337 / -	16	Eau de mer	Rudnick et Chen, 1998
	330 (346) / 364	57,5	Cyclohexane désoxygéné	Kumke et al., 1995
Anthracène	245 / 380 (405)		Eau	Beltrán et al., 1998
	- / 378 (399) (423) (449)		Cyclohexane	Karcher et al., 1985
	337 / -	4	Eau de mer	Inman et al., 1990
	356 (374) / 399	4,9	Cyclohexane désoxygéné	Kumke et al., 1995
Pyrène	240 (275) (320) / 375 (395)		Eau	Beltrán et al., 1998
	332 / 372 (377) (382) (390) (395)		Ethanol	Jung et al., 2010
	332 / 372 (390)		Ethanol	Kalyanasundaram et Thomas, 1977
	- /372 (378) (383) (388) (392) (404)		Cyclohexane	Karcher et al., 1985
	337 / -	128	Eau de mer	Inman et al., 1990
	336 (372) / 383	450	Cyclohexane désoxygéné	Kumke et al., 1995
Fluoranthène	275 / 460		Eau	Giamarchi et al., 2000
	337 / -	32	Eau de mer	Inman et al., 1990
	359 / 462	53	Cyclohexane désoxygéné	Kumke et al., 1995
2,3 benzo-fluorène	260 / 350		Méthanol	Nahorniak et Booksh, 2006
	321 (362) / 381	44,7	Cyclohexane désoxygéné	Kumke et al., 1995
Benzanthracène	275 (290) / 390 (410)		Eau	Beltrán et al., 1998
	280 / 390		Eau	Kim et al., 2005
	300 (385) / 385	32,5	Cyclohexane désoxygéné	Kumke et al., 1995
Benzo(b)fluoranthène	302 (369) / 446	44,3	Cyclohexane désoxygéné	Kumke et al., 1995
Benzo(k)fluoranthène	304 / 420		Eau	Kim et al., 2005
	310 / 450		Méthanol	Nahorniak et Booksh, 2006
	308 (402) / 402	44,3	Cyclohexane désoxygéné	Kumke et al., 1995

Benzo(a)pyrène	263 / 410, 440		Eau	Giamarchi et al., 2000
	290 / 410		Méthanol	Nahorniak et Booksh, 2006
	392 / 406		Eau	Valero-Navarro et al., 2007
	385 (404) / 403	42,9	Cyclohexane désoxygéné	Kumke et al., 1995
Benz(e)pyrène	- / 387 (408) (434) (460)		Cyclohexane	Karcher et al., 1985
Benzo[g, *h*, i]perylene	- / 388 (398) (410) (420) (433)		Cyclohexane	Karcher et al., 1985
	300 (406) 419	54,3	Cyclohexane désoxygéné	Kumke et al., 1995
Dibenzo[*a*,*h*]anthracene	290 / 400		Eau	Kim et al., 2005
	322 (394) / 394	37,5	Cyclohexane désoxygéné	Kumke et al., 1995
Indeno[l,2,3-cd]pyrene	302 (460) / 503	7,2	Cyclohexane désoxygéné	Kumke et al., 1995
Naphtol	280 / 340		Méthanol	Jiji et al., 1999
	329 / 355		Méthanol	Jia et al., 2007
2-phényl-phénol	243 (267) / 350		Ethanol	García Reyes et al., 2004
Fuberidazole	312 / 356		Méthanol	García Reyes et al., 2004
Aldicarb	326 / 350-380		Methanol	Fang et al., 1998
Carbaryl	220 (280) / 330		Eau	Brahima et Richard, 2003
	279 / 330		Méthanol	Jiji et al., 1999
	270 / 320		Méthanol	Fang et al., 1998
	282 / 335		Méthanol	García Reyes et al., 2004
	295 / 335		Méthanol	Jia et al., 2007
Thiabendazole	250 (301) / 360		Ethanol	García Reyes et al., 2004
	300 / 340		Méthanol	Rodríguez-Cuesta et al., 2003

7. La FADOM dans l'environnement aquatique

Dans l'environnement aquatique, plusieurs fluorophores ont été suspectés d'être des contaminants organiques dans des milieux variés tels que des eaux douces (Carstea et al., 2010),

des eaux côtières (Tedetti et al., 2010 ; 2011), des eaux marines (Murphy et al., 2006 ; 2008) et dans des lixiviats de décharges (Baker et Curry, 2004 ; Lu et al., 2009). Cependant, ces études montrent qu'il existe un manque d'informations concernant les signatures de fluorescence des PAHs et des biocides. En effet, comme le suggère le Tableau I-3, peu de MEEFs ont été réalisées à ce jour sur des composés purs dilués dans de l'eau (Kim et al., 2005 ; Tedetti et al., 2010). De ce fait, il est délicat de pouvoir attribuer à une signature de fluorescence relevée sur une MEEF d'échantillon naturel, la présence d'un composé anthropique (il est difficile de comparer une signature de fluorescence d'un échantillon d'eau naturelle avec celles de composés standard dilués dans un solvant organique dans la mesure où ce dernier influe sur le domaine spectral de fluorescence dudit composé). Quelques travaux ont néanmoins attribué à des signatures de fluorescence « atypiques » la présence de contaminants organiques et en particulier de PAHs (Tableau I-4). Par exemple, Carstea et al. (2010) ont attribué des pics de fluorescence à λEx/λEm 225/340 et 280/340 nm respectivement à du naphtalène et du phénanthrène. Cependant, d'après le Tableau I-3, le second maximum de fluorescence (280/340 nm) pourrait plutôt correspondre au second pic du naphtalène. Aussi, dans les eaux côtières, Tedetti et al. (2010) ont montré une MEEF d'un échantillon d'eau collecté dans le port de Saumaty à Marseille contenant plusieurs signatures de fluorescence. Ces signatures, non identifiées, pourraient correspondre selon le Tableau I-3 au fluorène (λEx/λEm : 210/310-350 et 260/310 nm), au naphtalène (230/320-360 nm) et au phénanthrène (250/350 nm) (Tableau I-4). Dans l'écosystème récifo-lagonaire de La Réunion, Tedetti et al. (2011) ont reporté une signature de fluorescence à λEx/λEm : 240/340 et 300/340 nm présentant des intensités très élevées. Ces auteurs ont donc émis l'hypothèse d'une contamination pétrolière. Au regard du Tableau I-3, cette signature pourrait refléter la présence de naphtalène. De la même manière, les travaux de Murphy et al. (2006 ; 2008) suggèrent la présence de phénanthrène et de naphtalène dans les eaux de ballaste (Tableau I-4). Les signatures de fluorescence du phénanthrène et du naphtalène ont également été retrouvés dans des lixiviats issus de décharges (Baker et Curry, 2004). Enfin, Lu et al. (2009) estiment que les pics à λEx/λEm = 250 (310) (360)/460 nm pourraient traduire la présence de pyrène (Tableau I-4). Pourtant, cette signature de fluorescence est éloignée de celle du standard de pyrène (Tableau I-3). Dans cas particulier, cette signature de fluorescence pourrait en fait correspondre à celle de substances humqiues ou à un autre hydrocarbure.

Tableau I-4. Signatures de fluorescence anthropiques observées dans l'environnement aquatique et identification des composés potentiels en référence au Tableau I-3.

Etudes	Signatures	Identification selon les auteurs	Signature théorique du composé (Tableaux I-3)	Identification selon le Tableau I-3
Carstea et al., 2010	225 / 340	Naphtalène	220-225 (270-280) / 343-340	Naphtalène pic 1
	280 / 340	Phénanthrène	245-250 / 360	Naphtalène pic 2
Tedetti et al., 2010	230 / 320-360	-	-	Naphtalène pic 1
	260 / 310	-	-	Fluorène pic 1
	310 / 310-350	-	-	Fluorène pic 2
Tedetti et al., 2011	240 / 340	Hydrocarbure	-	Naphtalène pic 1
	300 / 340	Hydrocarbure	-	Naphtalène pic 2
Murphy et al., 2006, 2008	250 / 370	Phénanthrène ou pyrène	245-250 / 360 ou 240 (275) (320) / 375 (395)	Phénanthrène
	240 (300) / 338	Tryptophane	225-237 (270-280) / 330-368	Naphtalène
Baker et Curry, 2004	220-230 / 340-370	Naphtalène	225-237 (270-280) / 330-368	Naphtalène
Lu et al., 2009	250 (310) (360) / 460	Pyrène	240 (275) (320) / 375 (395)	Mélange d'humiques ou un autre composé anthropique

8. Manque de connaissances actuel sur la DOM

8.1. La FADOM

Même si certains PAHs et biocides ont été détectés par fluorescence dans les eaux naturelles (Tableau I-4), la spectrofluorimétrie n'a pas été réellement évaluée comme outils permettant la

détection « rapide » de polluants organiques d'intérêt dans des environnements anthropisés. Outre la caractérisation de certains fluorophores anthropiques, on ne connaît pas précisément les limites de détection de ces composés avec la spectrofluorimétrie. De plus, alors que les PAHs méthylés représentent plus de 80% de la concentration total en PAHs dans la phase dissoute des eaux de surface (Guigue et al., 2011), paradoxalement, les propriétés de fluorescence de ces dérivés méthylés ont été peu étudiées (Tableau I-3). Par exemple, on ne sait pas s'ils présentent les mêmes domaines de fluorescence, les mêmes rendements de fluorescence et donc les mêmes limites de détection que leurs homologues parents. Enfin, dans les eaux naturelles, les substances humiques sont ubiquistes et peuvent interagir avec les PAHs et les biocides pour former des complexes (Gauthier et al., 1986 ; Fang et al., 1998 ; Akkanen et al., 2012). Cependant, on ne sait pas si leur présence peut engendrer des difficultés au niveau de la caractérisation et de la quantification de ces polluants par spectrofluorimétrie, en raison des chevauchements de pics de fluorescence, de l'effet d'écran et des processus de quenching. Le problème des chevauchements de pics pourrait être résolu par l'utilisation de la méthode statistique multivariée PARAFAC, qui permet une séparation mathématique des fluorophores présents dans un mélange complexe. A notre connaissance, le PARAFAC n'a jamais été utilisé sur des mélanges de PAHs ou de biocides contenant des substances humiques (i.e sur des échantillons reflétant vraiment le milieu naturel). La séparation des fluorophores au sein d'un mélange complexe peut également être réalisée en exploitant les propriétés de temps de vie de fluorescence de chaque fluorophore. En effet, même si des fluorophores présentent le même domaine spectral de fluorescence, ils peuvent avoir des temps de vie de fluorescence très différents (de 2 à 150 ns). Des travaux ont déjà été conduits sur les temps de vie de fluorescence de certains composés anthropiques mais en se focalisant uniquement sur quelques PAHs (Rudnick et Chen, 1998 ; Chen, 1999). Peu d'études se sont intéressées aux biocides hormis le carbaryl (Burel, 2003).

8.2. L'ADOM

Même si de nombreux travaux ont déterminé les concentrations en hydrocarbures et en biocides dans les sédiments, les espèces biologiques (poissons) ou dans les particules de la colonne d'eau du delta du Rhône (Ribeiro et al., 2005 ; Buet et al., 2006 ; Comoretto et al., 2007 ; Chiron et al., 2009 ; Roche et al., 2009) et de Méditerranée nord-occidentale (Benlahcen et al., 1997 ; Dachs et al., 1997, 1999 ; Lipiatou et al., 1997 ; Pérez et al., 2003 ; Wafo et al., 2006 ; Borrell et al., 2007 ; Mille et al., 2007 ; Dierking et al., 2009 ; Berrojalbiz et al., 2011a, 2011b ; Munaron et al., 2012 ;

Salvadó et al., 2013), peu d'études se sont attachées à déterminer les concentrations en hydrocarbures ou en biocides dans la phase dissoute des eaux de surface du Rhône (Sicre et al., 2008), du delta du Rhône (Bouloubassi et Saliot, 1991 ; 1993) et de la baie de Marseille (Marty et Saliot, 1976 ; Siron et al., 1987 ; Guigue et al., 2011 ; Munaron et al., 2012). Ainsi très peu d'information est disponible concernant l'origine et la variabilité spatio-temporelle de ces polluants organiques dissous dans la zone côtière Méditerranéenne.

8.3. La FNDOM

Au cours de ces dernières années, la composition et la dynamique de la FNDOM ont été étudiées dans différents environnements aquatiques comme les rivières (Patel-Sorrentino et al., 2002 ; Carstea et al., 2010 ; Maie et al., 2010) les estuaires (Boyd et Osburn, 2004; Huguet et al., 2010 ; Singh et al., 2010) et les eaux marines (Luciani et al., 2008 ; Jørgensen et al., 2011 ; Stedmon et al., 2011). Cependant peu d'études se sont intéressées à la composition, aux sources et à la variabilité saisonnière de la FNDOM dans la baie de Marseille et dans les eaux continentales autour des côtes méditerranéennes (Para et al., 2010 ; Tedetti et al., 2010 ; 2012). Des intrusions d'eau du Rhône ont été observées récemment dans la baie de Marseille sous des conditions météorologiques particulières (Para et al., 2010 ; Pairaud et al., 2011). Cependant, l'influence des ces eaux du Rhône sur la dynamique de la FNDOM et la biogéochimie associée dans la baie de Marseille reste peu connue.

9. Objectifs de thèse

Le but général de cette thèse est d'améliorer les connaissances actuelles sur la composition et la dynamique de la matière organique dissoute fluorescente naturelle et anthropique en Méditerranée côtière nord-occidentale. Ce travail de thèse comporte trois objectifs principaux :

1) Le premier objectif vise à évaluer la pertinence de la spectroscopie de fluorescence (méthode MEEFs couplée à l'analyse multi-variée PARAFAC et méthode de spectroscopie de fluorescence résolue en temps) pour caractériser et quantifier les polluants organiques de type PAHs et biocides dans des mélanges complexes (en présence de substances humiques) et dans le milieu marin côtier anthropisé. La validation de cette méthode d'analyse sera réalisée à travers la comparaison de résultats obtenus sur des échantillons d'eau de mer par chromatographie (GC-MS) et par spectrofluorimétrie directe.

2) Le second objectif consiste à déterminer le degré de contamination en hydrocarbures et en biocides (carbaryl et bentazone) dissous dans les eaux de surface de systèmes continentaux (Rhône et étang de Vaccarès) et des eaux marines du littoral marseillais. L'influence du Rhône sur la distribution de ces polluants dans la baie de Marseille sera également étudiée.

3) Le troisième objectif concerne la caractérisation et la variabilité spatio-temporelle de la FNDOM dans les eaux de surface de systèmes continentaux (Rhône et étang de Vaccarès) et des eaux marines du littoral marseillais. La dynamique de la FNDOM sera mise en relation avec les paramètres environementaux. L'impact du Rhône sur l'étang de Vaccarès mais aussi sur plusieurs stations de la baie de Marseille sera évalué.

Ce travail de thèse s'inscrit dans le cadre du projet de recherche « IBISCUS » soutenu par l'Agence Nationale de la Recherche (ANR) - ECOTECH (projet ANR-09-ECOT-009-01 ; PI : M. Goutx ; 2010-2013) et contribue également à l'action « impact de l'urbanisation » (C3A) du Work Package 3 du projet CNRS-INSU-MISTRALS MERMEX. Cette thèse s'inscrit également dans des programmes de recherche internationaux tels que LOICZ qui vise notamment à mieux comprendre les interactions et les variations temporelles de flux de carbone entre les continents et le milieu marin côtier.

Chapitre II: Matériel et Méthodes

Cette thèse a fait l'objet dans un premier temps d'un travail expérimental au laboratoire sur des solutions standard complexes contenant des PAHs, des biocides et des substances humiques. Dans un second temps, des échantillons naturels ont été prélevés dans différents sites de la baie de Marseille ainsi que dans le Rhône et dans l'étang de Vaccarès dans le cadre d'un suivi saisonnier.

1. Choix des contaminants (PAHs et biocides) cibles et préparation des solutions standards

J'ai décidé de m'intéresser à des PAHs et des biocides qui répondaient à deux critères : 1) ils devaient être potentiellement présents ou connus pour être présents dans le milieu marin côtier et 2) ils devaient présenter des propriétés de fluorescence significatives. J'ai donc choisi neuf PAHs et quatre biocides d'intérêt. Pour les PAHs : le naphtalène, le 2,3 dimethyl naphtalène, le fluorène, le 1,8 dimethyl-9H-fluorène, le phénanthrène, l'anthracène, le pyrène, le benzo[a]anthracène et le benz(e)pyrène (Tableaux II-1). Pour les biocides : le carbaryl, le 2-phénylphénol, le thiabendazole et le bentazone. Le naphtalène, le phénanthrène, le fluorène, l'anthracène et le pyrène font partis des PAHs les plus répandus dans l'environnement marin (El Nemr et Abd-Allah, 2003). Les composés alkylés (2,3 dimethyl naphtalène, 1,8 dimethyl-9H-fluorène) et phénylés (benzo[a]anthracène, benz(e)pyrène) ont été sélectionnés car non seulement ils sont présents dans le milieu aquatique mais aussi pour comparer leurs propriétés de fluorescence avec celles de leurs homologues parents dont la structure est très proche. Le carbaryl est utilisé comme fongicide, molluscicide et insecticide en agriculture. Le 2-phénylphénol est utilisé comme nématicide, bactéricide et comme fongicide en agriculture pour empêcher la pourriture des cultures. Le bentazone est utilisé dans les champs agricoles en tant qu'herbicide. Ces quatre biocides ont déjà été détectés dans les eaux souterraines, en rivière et en mer (Marco et al., 1995 ; Dumbauld et al., 2001 ; Bocquené et Franco, 2005 ; Comoretto et al., 2007 ; Peng et al., 2008).

Tableau II-1. Liste des PAHs et des biocides sélectionnés pour étudier la caractérisation et quantification les polluants organiques dans des mélanges complexes. Le signe * désigne les molécules caractérisés par spectrofluorimétrie.

	Contaminants	Abbreviation	Structure	Formula, MW (g mol^{-1})
PAHs	Naphthalene*	Naph	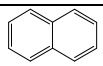	$C_{10}H_8$, 128
	Acénaphtylène	Acy	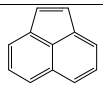	$C_{12}H_8$, 152
	Acénaphthène	Ace	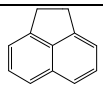	$C_{12}H_{10}$, 154
	Fluorène*	Flu	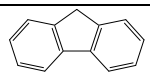	$C_{13}H_{10}$, 166
	Anthracène*	Ant	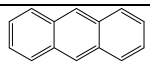	$C_{14}H_{10}$, 178
	Phénanthrène*	Phe	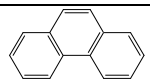	$C_{14}H_{10}$, 178
	Dibenzothiophène	DBT	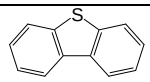	$C_{12}H_8S$, 184
	Pyrène*	Pyr	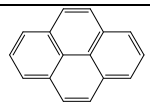	$C_{16}H_{10}$, 202
	Fluoranthène	Flt	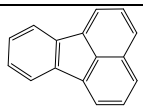	C_6H_{10}, 220
	Benzo[a]anthracène*	BaA	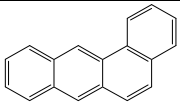	$C_{18}H_{12}$, 228
	Chrysène	Chr	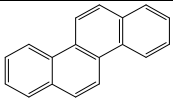	$C_{18}H_{12}$, 228
	Benzo[a]pyrène	BaP	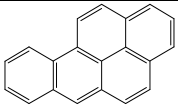	$C_{20}H_{12}$, 252

	Benzo[b]fluoranthène	BbF	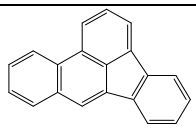	$C_{20}H_{12}$, 252
	Benzo[e]pyrène*	BeP	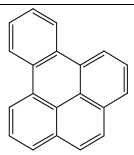	$C_{20}H_{12}$, 252
	Benzo[k]fluoranthène	BkF	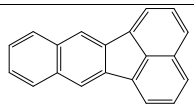	$C_{20}H_{12}$, 252
	Benzo[g,h,i]perylène	BP	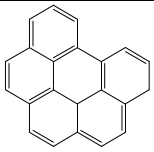	$C_{22}H_{12}$, 276
	Indeno[1,2,3-cd]pyrène	InDP	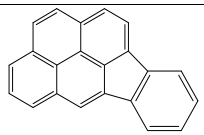	$C_{22}H_{12}$, 276
	Dibenz[a,h]anthracène	DBA	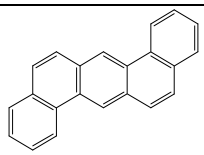	$C_{22}H_{14}$, 278
Biocides	2-phénylphénol*	Pho	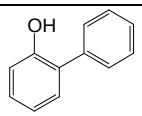	$C_{12}H_{10}O$, 170
	Carbaryl*	Car	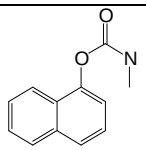	$C_{12}H_{11}NO_2$, 201
	Thiabendazole*	Thi	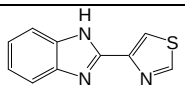	$C_{10}H_7N_3S$, 201
	Bentazone*	Ben	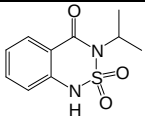	$C_{10}H_{12}\ N_2O_3S$, 240

Les neuf PAHs et les quatre biocides (Sigma-Aldrich, ≥ 98%) ont été utilisés sans purification préalable. Des solutions mères de chaque composé (50 mg L^{-1}) ont été préparées en solubilisant

le solide pur dans du méthanol (Rathburn HPLC grade). A partir de ces solutions mères, des solutions filles ayant des concentrations finales comprises entre 0,1 et 20 µg L^{-1} ont été préparées dans de l'eau ultra-pure (eau Milli-Q). Pour le bentazone, des solutions supplémentaires ont été réalisées jusqu'à 2000 µg L^{-1}. En plus des solutions individuelles, des solutions de mélange de PAHs et de biocides ont été préparées à partir des solutions mères. Les concentrations finales de chacun des composés dans ces mélanges étaient comprises entre 0,1 et 10 µg L^{-1}. Des acides humiques (HA, Suwannee River humique 2S101H) et des acides fulvique (FA, Suwannee River fulvique 2S101F) été obtenues auprès de l'International Humic Substances Society (IHSS). Les HA et FA ont été solubilisés respectivement dans de l'hydroxyde de sodium (≥ 30% RP Normapur Prolabo) et de l'eau ultra-pure pour obtenir des solutions mères de 250 mg L^{-1}. Ces deux solutions ont ensuite été mélangées pour obtenir une solution stock de substances humiques de 200 mg L^{-1} (100 mg L^{-1} de HA et 100 mg L^{-1} de FA). Cette solution mère a été ajoutée aux solutions de mélange de PAHs et de biocides pour obtenir des concentrations finales de substances humiques entre 0,2 et 20 mg L^{-1}. Le pH des solutions a été ajusté à 6 à l'aide d'hydroxyde de sodium. La composition ainsi que les concentrations des solutions standards (individuels et mélanges) sont indiquées dans le Tableau II-2. Les solutions ont été stockées dans des flacons en verre SCHOTT® dans le noir à 4°C pendant 48 heures maximum avant analyse.

2. Sites d'étude et échantillonnage en Méditerranée côtière nord-occidentale

Au cours de cette thèse, j'ai échantillonné plusieurs sites marins et continentaux en Méditerranée côtière nord-occidentale (Figure II-1). Les sites continentaux : le Rhône (site « Arles ») et l'étang de Vaccarès (site « Vaccarès ») sont des sites dans lesquels des contaminations aux hydrocarbures et aux biocides peuvent avoir lieu en lien avec des rejets industriels et agricoles. Les sites marins quant à eux ont été choisis en fonction de leur contamination potentielle en hydrocarbures. Les ports de Port de Bouc (entrée et intérieur du port) et de Saumaty pourraient être impactés par des rejets pétroliers. La station Couronne se trouve au sud du Golfe de Fos-sur-mer qui est une zone où le trafic maritime est important avec notamment la présence de pétroliers. C'est une station intermédiaire entre le Golfe de Fos-sur-mer et la baie de Marseille. La station Sofcom est située dans la baie de Marseille. Cette zone d'étude présente également un intérêt au niveau de l'étude de la dynamique de la NDOM. De plus, certaines de ces stations peuvent être soumises à des apports d'eau douce du Rhône (Pairaud et al., 2011) dont l'impact est encore inconnu sur la composition et sur les apports de NDOM.

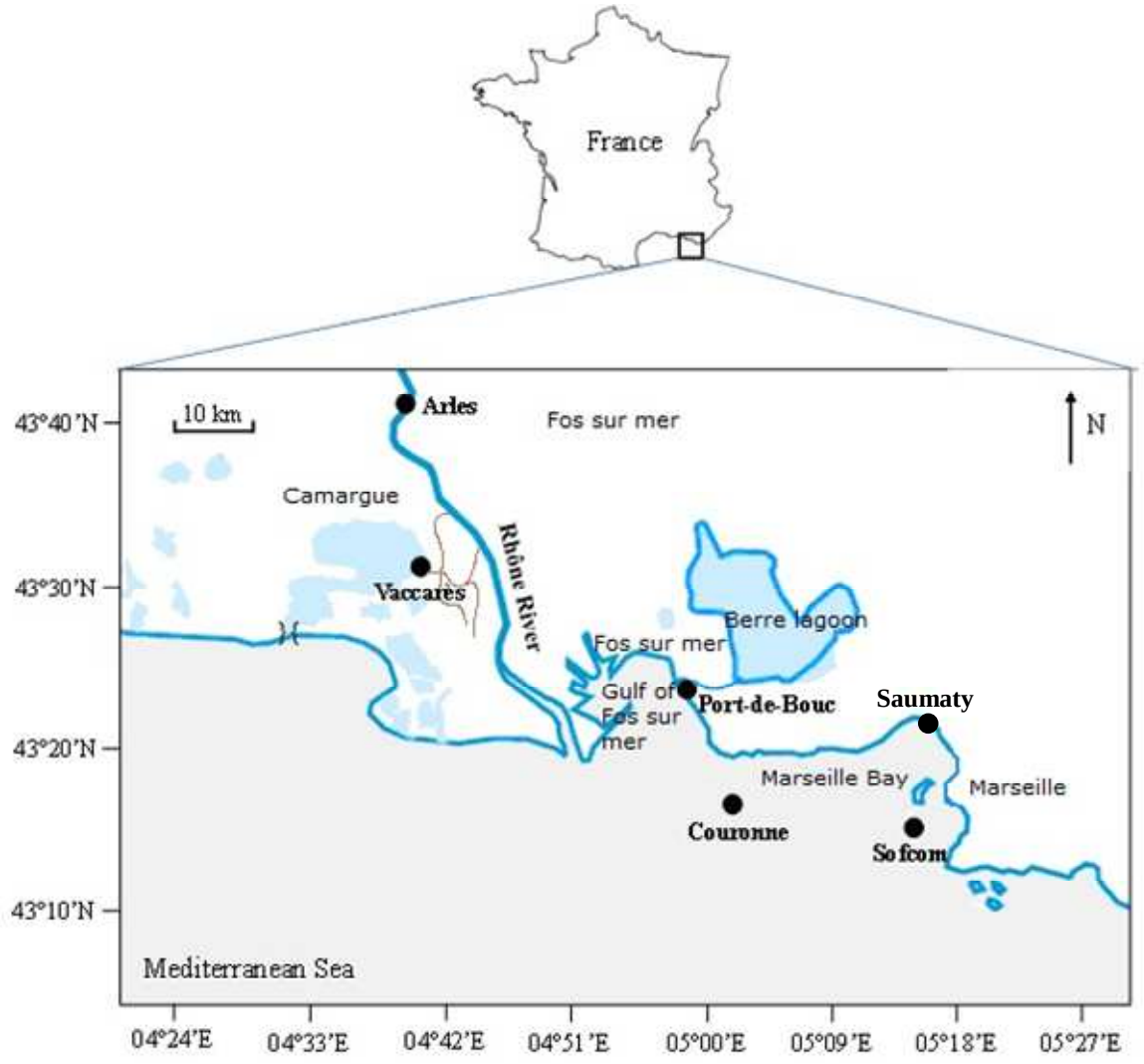

Figure II-1. Localisation des sites d'étude en Méditerranée côtière nord-occidentale.

Des prélèvements ont été effectués mensuellement ou bi-mensuellement entre février 2011 et janvier 2012 aux stations Arles, Vaccarès, Port-de-Bouc, Couronne et Sofcom. D'autre part, des prélèvements ont été réalisés selon un gradient de contamination à l'intérieur des ports de Saumaty et de Port de Bouc, respectivement en juillet 2011 et en juillet 2012. Tous les prélèvements ont été réalisés en subsurface (à 0,1 m de profondeur). Aux stations marines (Sofcom et Couronne), des échantillons ont aussi été collectés à 5 m de profondeur à l'aide d'une bouteille Niskin de 5 litres équipée d'un élastique et de joints en silicone pour éviter toute contamination organique. L'eau de la bouteille Niskin était transférée dans cinq flacons en verre SCHOTT® de 100 mL et une bouteille en polycarbonate Nalgene de 4 L pour les analyses de

fluorescence, les analyses des paramètres biogéochimiques [(nitrates (NO_3^-), nitrites (NO_2^-) phosphates (PO_4^{3-}), chlorophylle *a* (Chl *a*), carbone, azote, phosphore organique dissous (DOC, DON, DOP) et particulaire (POC, PON, POP)) et les analyses d'hydrocarbures et de biocides (uniquement aux stations Arles et Vaccarès)]. Tous les flacons et bouteilles ont été lavés 3 fois avec l'échantillon avant d'être remplis. Les échantillons ont été maintenus au frais à l'obscurité (dans des glacières) jusqu'au retour au laboratoire. En plus des prélèvements d'échantillons d'eau, des mesures *in situ* de pression, température, salinité, Chl *a*, FDOM et turbidité ont été réalisées le long de la colonne d'eau à Port-de-Bouc, Couronne et Sofcom avec un profileur vertical CTD 19plusV2 (SeaBird Electronics Inc., USA) équippé d'un fluorimètre WETStar Chl *a*, d'un fluorimètre Wetstar FDOM (WETLabs, Inc., USA) et d'un turbidimètre Seapoint.

De retour au laboratoire, les échantillons ont été immédiatement filtrés sous faible vide (< 50 mm Hg) à travers des filtres GF/F en microfibre de verre Whatman (0,7 µm de porosité, 25 ou 47 mm de diamètre) pré-brulés (500 °C pendant 4 h) avec des systèmes de filtration en polysulfone ou en verre. Les filtres et les systèmes de filtration ont été préalablement rincés avec de l'eau ultra-pure, puis avec l'échantillon. Le filtrat dédié aux mesures de fluorescence a été transféré dans des tubes en verre de 10 mL pré-brulés. Ces tubes ont été stockés à l'obscurité à 4 °C et ont été analysés dans les 24 h. Le filtrat pour l'analyse de paramètres biogéochimiques a été transféré dans des flacons Nalgene en polypropylène de 60 mL (NO_3^-, NO_2^-, PO_4^{3-}) et dans des flacons en verre SCHOTT® de 50 mL (DOC, DON, DOP). Ces flacons ont été stockés à -20 °C jusqu'à analyse. Les filtres pour l'analyse de la Chl *a* et du carbone particulaire (POC, PON, POP) ont été transférés dans des tubes en verre et congelés à -20 °C jusqu'à analyse. Le filtrat pour l'analyse des hydrocarbures a été transféré dans des flacons en verre SCHOTT® de 2 L, dans lesquels ont été ajoutés 50 mL de dichlorométhane. Ces flacons ont été conservés à l'obscurité à 4 °C pendant 48 h avant extraction des hydrocarbures. Le filtrat pour l'analyse des biocides a été transféré dans des flacons en verre SCHOTT® de 1 L, conservés à 4 °C à l'obscurité.

Le matériel utilisé lors de ce travail de thèse a été nettoyé avec l'acide chlorhydrique (HCl) 1 M, rincé à l'eau ultra-pure (i.e, eau Milli-Q provenant d'un système Millipore ayant une résistivité finale de 18,2 MΩ cm^{-1}) et brûlé à 500 °C pendant 5 h. Tout le matériel ne pouvant pas être brûlé à 500 °C a été lavé avec l'HCl 1 M, rincé à l'eau ultra-pure et séché à 50 °C. Les filtres en fibre de verre Whatman ont également été brûlés à 500 °C avant utilisation.

3. Traitement et analyse des échantillons

3.1. Analyse de la FDOM par fluorescence

3.1.1. Analyses spectrofluorimètriques (méthode des MEEFs)

Instrument et corrections spectrales. Les mesures de fluorescence ont été réalisées à l'aide d'un spectrofluorimètre Hitachi F-7000. Cet instrument permet de mesurer la fluorescence à des longueurs d'onde d'excitation (Ex) et d'émission (Em) de 200 à 700 nm. Il est équipé d'une lampe au xénon à arc court de 150 W avec un compartiment de la lampe auto désozonisé comme source de lumière. Il possède également deux réseaux de diffraction concaves stigmatiques avec 900 lignes mm^{-1} qui jouent le rôle de monochromateur, l'un pour l'Ex et l'autre pour l'Em. La précision de ces monochromateurs (± 0,4 nm) a était déterminée en mesurant la raie d'émission du mercure à 435,8 nm à l'aide d'un néon fluorescent. Cet instrument possède deux tubes photomultiplicateurs (PMT) Hamamatsu R3788 (185-750 nm), utilisés comme détecteur de référence (mesure de l'intensité du rayonnement émis par la lampe xénon) et comme détecteur de l'échantillon (mesure de l'intensité de fluorescence émise par l'échantillon). Les mesures de fluorescence sont donc réalisées en mode ratio (signal détecteur échantillon / signal détecteur de référence) ce qui permet de corriger en temps réel les mesures de fluorescence des variations de l'intensité de la lampe xénon (aux niveaux spectral et temporel). De plus, des corrections spectrales ont été également appliquées sur le domaine 200-600 nm pour corriger les mesures de fluorescence de la réponse instrumentale en Ex et en Em (car les différents composants optiques de l'instrument n'ont pas la même efficacité en fonction de la longueur d'onde). Dans un premier temps, les corrections spectrales ont été appliquées sur la partie Ex en plaçant dans le compartiment échantillon une cuve triangulaire en quartz contenant de la Rhodamine B (3 g L^{-1} dans de l'éthylène glycol) et un filtre rouge utilisé pour supprimer la lumière parasite < à 620 nm. Un spectre d'Ex a alors été réalisé de 200 à 600 nm pour une longueur d'onde d'Em de 640 nm (la Rhodamine présente la particularité d'émettre la fluorescence toujours à la même longueur d'onde quelque soit la longueur d'onde à laquelle elle est excitée). Le ratio du signal enregistré par le détecteur de référence sur celui enregistré par le détecteur de l'échantillon a fourni la courbe de correction pour l'Ex. Les corrections spectrales pour la partie Em ont été ensuite menées à l'aide d'une source de lumière calibrée, en l'occurrence la lampe xénon de l'instrument (calibrée lors des corrections spectrales sur la partie Ex). Un diffuseur en quartz a été placé dans

le compartiment échantillon et un spectre synchrone a alors été effectué de 200 à 600 nm avec $\Delta\lambda$ = 0 nm (i.e. mesure de fluorescence à Ex = Em). Le ratio du signal enregistré par le détecteur de l'échantillon sur celui enregistré précédemment par le détecteur de l'échantillon avec la Rhodamine B a fourni la courbe de correction pour l'Em. Les courbes de correction en Ex et en Em ont été appliquées directement par le logiciel du spectrofluorimètre (FL Solutions 2.1) pour corriger chaque mesure de fluorescence acquise.

L'importance d'appliquer les corrections spectrales aux mesures de fluorescence est illustrée en Figure II-2. La sulfate de quinine a une signature de fluorescence à Ex/Em = 250 (345)/450 nm. Lorsque l'on applique les corrections spectrales aux mesures de fluorescence de la quinine de sulfate à 10 µg L^{-1}, l'intensité de fluorescence est multipliée par 4,2 pour le premier pic (250/450 nm) et par 1,6 pour le second pic (345/450 nm) (Figure II-2).

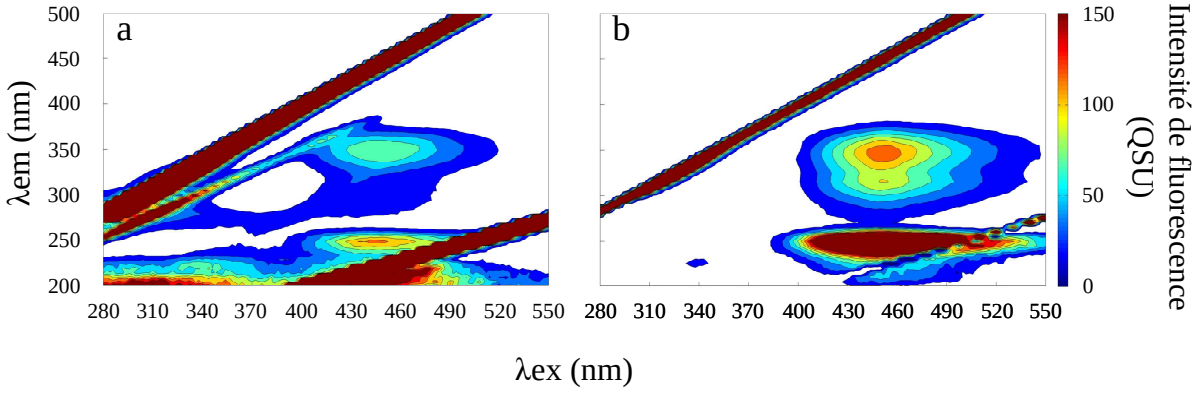

Figure II-2. MEEF de quinine de sulfate à 10 µg L^{-1} mesurée sans (a) et avec application des corrections spectrales en excitation et en émission (b).

Mesures. Toutes les mesures de fluorescence présentées dans ce travail de thèse ont été réalisées suivant le même protocole. Après retour à température ambiante à l'obscurité, les échantillons ont été transférés dans une cuve en quartz suprasil (170-2600 nm) ayant un trajet optique de 1 cm. Dans l'instrument, cette cuve était maintenue à la température constante de 20 °C grâce à un système de circulation d'eau autour du porte échantillon. Avant chaque analyse, la cuve était rincée au moins trois fois avec de l'eau ultra-pure et une fois avec l'échantillon. Les MEEFs ont été générées sur une gamme de longueurs d'onde d'Ex allant de 200 à 500 nm avec un intervalle

de 5 nm et sur une gamme de longueurs d'onde d'Em allant de 280 à 550 nm avec un intervalle de 2 nm. La vitesse de balayage utilisée était de 1200 nm min^{-1}, les largeurs de fentes pour l'Ex et l'Em étaient de 5 nm, le temps de réponse était de 0,5 s et la tension du PMT était de 700 V. Avec chaque série d'échantillons, des blancs (eau ultra-pure) et des solutions de quinine de sulfate (Fluka, purum for fluorescence) de 0,25 à 50 µg L^{-1} diluée dans l'acide sulfurique (H_2SO_4) 0,05 M ont été analysées. Le pH des échantillons naturels, qui variaient très peu (7,5-8,3), n'a pas nécessité d'ajustement de pH avant les analyses de fluorescence. Des mesures d'absorbance ont aussi été conduites de 200 à 550 nm dans une cuve en quartz de 1 cm de trajet optique avec un spectrophotomètre Shimadzu UV-Vis 2450. Ces mesures d'absorbance ont été faites avec une référence eau ultra-pure pour les échantillons continentaux (Arles, Vaccarès) et une référence salée (eau ultra-pure + NaCl calciné) pour les échantillons marins (Port-de-Bouc, Saumaty, Sofcom, Couronne).

Traitement des données de fluorescence. Les MEEFs acquises ont subi plusieurs étapes de traitement. 1) Toutes les données de fluorescence (échantillons, standards de quinine sulfate, eau ultra-pure) ont été normalisées par rapport à l'intensité du pic de diffusion de Raman de l'eau ultra-pure à Ex/Em = 275/303 nm, utilisé comme standard interne. 2) Les MEEFs ont ensuite été corrigées de l'effet d'écran en utilisant les mesures d'absorbance : chaque MEEF a été multipliée par une matrice de correction, calculée pour chaque couple de longueurs d'onde d'Ex et d'Em à partir de la valeur d'absorbance de l'échantillon (Ohno, 2002). 3) Les MEEFs ont été corrigées par le blanc en soustrayant à chaque MEEF d'échantillon, la MEEF moyenne de l'eau ultra-pure. 4) Les MEEFs ont été converties en unité quinine sulfate (QSU), où 1 QSU correspond à la fluorescence d'une solution de quinine de sulfate à 1 µg L^{-1} dans l'H_2SO_4 0,05 M à Ex/Em = 350/450 nm (largeurs de fentes : 5 nm). La conversion en QSU a été effectuée en divisant les valeurs de fluorescence par la pente moyenne de l'équation de la régression linéaire de la quinine de sulfate. Les limites de détection et de quantification des mesures de fluorescence étaient respectivement de 0,10 et 0,40 QSU.

3.1.2. L'analyse parallèle factorielle (PARAFAC)

Contexte. Avec les premières publications relatives à la caractérisation de la FDOM par méthode spectroscopique MEEF (Coble et al., 1990 ; Coble, 1996), il est rapidement apparu la nécessité de proposer des outils statistiques robustes pour le traitement qualitatif et quantitatif de ces données

de fluorescence multivariées. Stedmon et al. (2003) ont alors appliqué pour la première fois une analyse de type PARAFAC sur un grand nombre d'échantillons MEEF dans le but de tracer la DOM dans différents environnements aquatiques. Ce traitement PARAFAC a été proposé à la communauté travaillant sur la FDOM et détaillé sous forme de tutorial dans Stedmon et Bro (2008). Même si le PARAFAC n'est bien évidement pas la seule méthode multivariée permettant le traitement des données MEEF [Spencer et al. (2007) ayant par exemple exploité leurs résultats avec de l'analyse en composantes principales], l'analyse PARAFAC de C.A. Stedmon (NERI, Université de Aarhus, Danemark) est très largement employée à l'heure actuelle (conclusions de l'« International Training Workshop on Organic Matter Characterization Using Spectroscopic Techniques », mai 2010, Grenade). Dans ce contexte, j'ai décidé d'appliquer cette analyse PARAFAC sur mes échantillons MEEFs et de comparer les résultats obtenus avec ceux de la littérature.

Principe du PARAFAC. L'analyse PARAFAC est un traitement mathématique permettant de caractériser et de quantifier les fluorophores présents dans un jeu de données. C'est une méthode statistique multivariée basée sur un algorithme utilisant la méthode itérative des moindres carrés et qui est utilisée pour déconvoluer les signaux contenus dans des MEEF complexes dans lesquelles se trouvent des signaux de différents fluorophores ou composants (Bro, 1997). Chacune des matrices composant le jeu de données est empilée de façon à créer un cube (Figure II-3) où les longueurs d'onde d'Ex, les longueurs d'onde d'Em ainsi que le nombre de matrices représentent les 3 dimensions du cube.

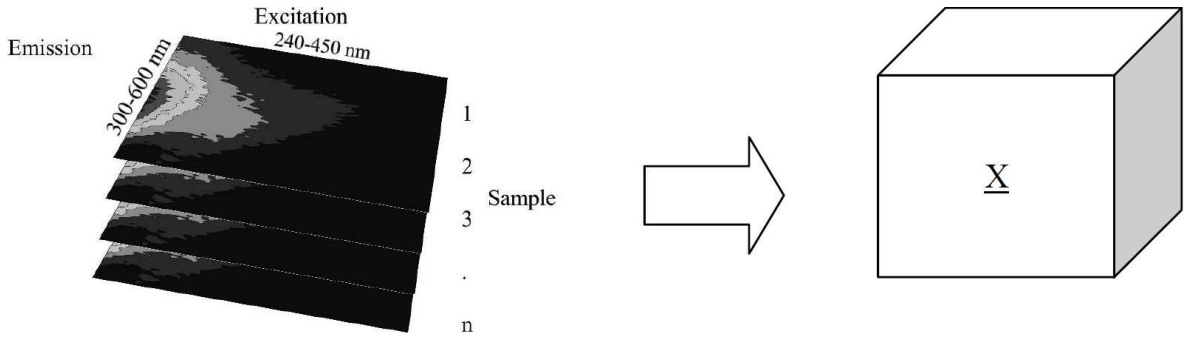

Figure II-3. Transformation d'un jeu de données de matrices MEEF en un cube X à trois dimensions (Stedmon et Bro, 2008).

L'analyse PARAFAC permet de décomposer mathématiquement ce cube en composant trilinéaires qui obéissent à l'équation suivante :

$$X_{i,j,k} = \sum_{f=1}^{F} a_{i,f} b_{j,f} c_{k,f} + \varepsilon_{i,j,k} \text{ avec } i = 1,..., I\ j = 1,\ldots, J \text{ et } k = 1,\ldots, K$$

$X_{i,j,k}$ représente l'intensité de fluorescence de l'échantillon i à la jième longueur d'onde d'Em et à la kième longueur d'onde d'Ex, F correspond au nombre de fluorophores présents dans chaque MEEF. $a_{i,f}$ est un facteur proportionnel à la concentration du fluorophore f dans l'échantillon i. $b_{j,f}$ est l'estimation du spectre d'Em du fluorophore f à la longueur d'onde j. $c_{k,f}$ est l'estimation du spectre d'Ex du fluorophore f à la longueur d'onde k et $\varepsilon_{i,j,k}$ représente la somme des résidus des matrices (la variabilité non expliquée par le modèle). Les sorties du modèle sont donc les matrices a, b, c, respectivement de dimensions KxF, JxF et IxF, représentant l'estimation de la contribution de chaque fluorophore dans chaque échantillon, l'estimation du spectre d'Em de chaque fluorophore et l'estimation du spectre d'Ex de chaque fluorophore. Pour résoudre l'équation précédente, la méthode itérative des moindres carrés est utilisée en définissant un nombre de fluorophores F et les itérations successives vont permettre d'estimer la structure de chaque fluorophores en minimisant l'erreur sur le résidu. La solution du modèle est trouvée quand l'algorithme atteint le minimum global. L'analyse PARAFAC va créer plusieurs modèles ayant différents nombres de fluorophores. Les bandes de diffusion Raman et Rayleigh, qui ne sont pas considérés comme des fluorophores, ne sont pas prises en compte lors de la création des modèles. Elles sont éliminées avant d'appliquer l'analyse et leurs valeurs d'intensité sont remplacées par la valeur 0. L'application du traitement PARAFAC prend en compte plusieurs hypothèses : 1) une variation de la concentration en fluorophore doit impliquer une modification de l'intensité de fluorescence mais pas un changement de l'allure des spectres d'Ex et d'Em, 2) les fluorophores ne doivent pas être affectés par l'effet d'écran et 3) la présence de fluorophores ne doit pas influencer l'allure des spectres des autres fluorophores. Pour réaliser un modèle PARAFAC robuste, un nombre d'au moins 20 MEEFs est requis. Les échantillons du jeu de données ne doivent pas être trop hétérogènes en terme de composition en fluorophores et d'intensités de fluorescence (Stedmon et Bro, 2008).

Validation des modèles PARAFAC. La première étape de l'analyse PARAFAC est la mise en évidence d' « outliers » contenu dans le jeu de données. Les outliers peuvent contenir un même

nombre de fluorophores mais avec des intensités de fluorescence vraiment différentes par rapport aux autres MEEFs. On peut par exemple avoir dans un jeu de données un échantillon qui peut contenir de l'eau contaminée par des hydrocarbures alors que les autres échantillons proviennent d'un milieu oligotrophe et pas contaminé. Dans ce cas là, l'échantillon contaminé pourra être considéré comme un outlier. La présence de ces outliers entraîne un biais sur les modèles PARAFAC générés et peuvent empêcher la validation de modèles ou rajouter un fluorophore existant uniquement sur un faible nombre d'échantillon. Il est donc préférable de les enlever du jeu de données. L'étape suivante est la première étape de la validation de modèles. Elle consiste en l'analyse de l'erreur sur le résidu. L'erreur sur ce dernier doit être minimale, la forme des données sur le résidu doit refléter un bruit de fond instrumental et non un fluorophore. Cette information permet de définir si la totalité des données des MEEF a été prise en compte ou pas. Une fois cette analyse réalisée, la « split-half analysis » est effectuée. Le jeu de données est alors divisé en quatre parties (Figure II-4).

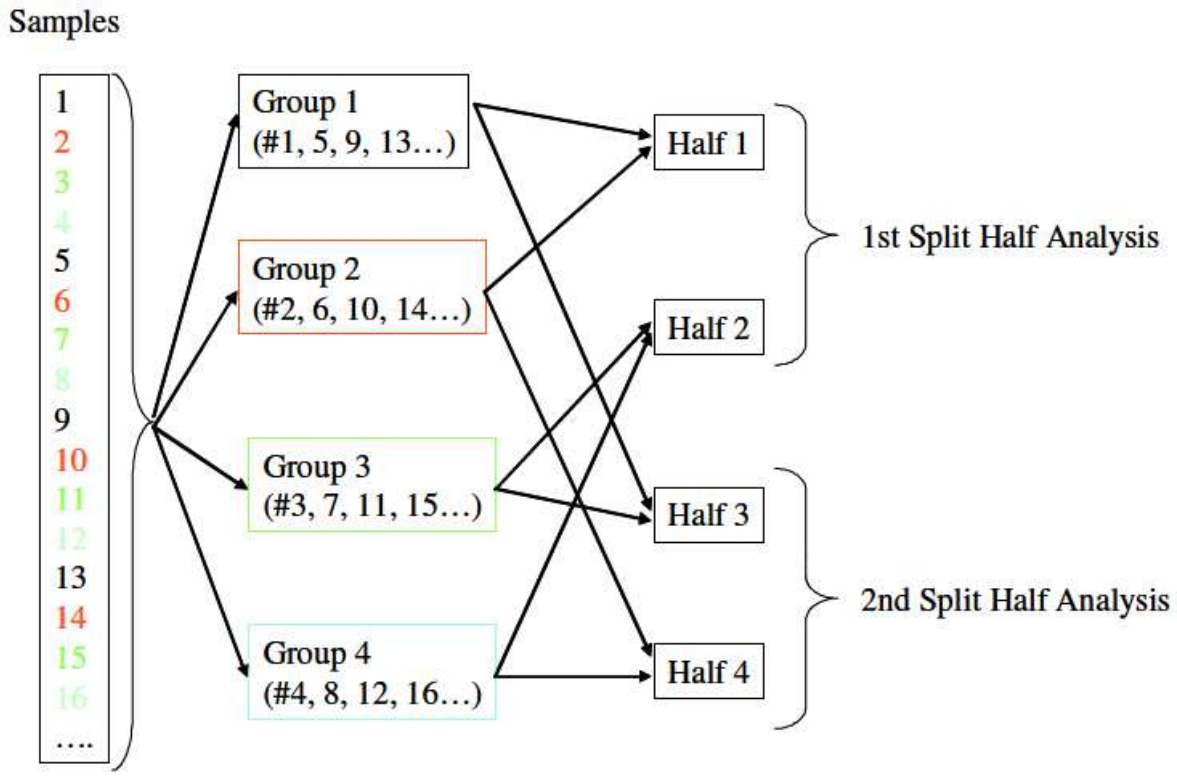

Figure II-4. Schéma explicatif de la division en chaque split du jeu de données de MEEFs, d'après Stedmon et Bro, 2008.

Sur chacun des groupes d'échantillons, des modèles ayant chacun un nombre différent de fluorophores sont créés indépendamment. La split-half analysis compare sur chacun des groupes, les spectres d'excitation et d'émission générés pour un modèle contenant F fluorophores. Si les résultats obtenus sont similaires alors le modèle est validé. A ce niveau là, plusieurs modèles peuvent être validés avec chacun un nombre différent de fluorophores. Il appartient à ce moment là à l'expérimentateur de choisir le modèle avec lequel les analyses seront poursuivies. Les modèles contenant des artefacts ou des composés qui ne correspondent pas à des fluorophores peuvent être éliminés. Une fois choisi, le modèle PARAFAC subit la « random initialisation ». Pour cela, dix modèles avec le même nombre de composant seront donc créés en utilisant l'ensemble des données et seront « fitté », ce qui va permettre d'affiner le résultat et ainsi d'obtenir le modèle avec plus faible nombre d'erreurs. La robustesse des résultats obtenus est ensuite vérifiée avec l'application du test « tucker core consistency » sur chacun des quatre groupes d'échantillons (Figure II-4). Ce test permet de comparer les spectres d'excitations et d'émissions obtenus à cette étape avec ceux précédemment trouvés avec la split-half analysis. Si ces derniers sont les mêmes, alors le test et validé et le modèle est considéré comme robuste.

J'ai réalisé mes analyses PARAFAC à l'aide de la DOMFluor toolbox v 1.6 proposé par C.A. Stedmon sur MATLAB® 7.10.0 (R2010a). Au cours de ma thèse j'ai validé plusieurs modèles PARAFAC. Pour l'étude sur les standards (chapitre III), cinq modèles ont été réalisés : 4 sur les échantillons synthétiques et un sur les échantillons naturels (Tableau II-2). Pour les échantillons synthétiques, deux modèles concernaient les PAHs, avec d'un côté les PAHs individuels plus les mélanges de PAHs (P^{T}_{PAHs}) et de l'autre côté, uniquement les mélanges de PAHs (P^{M}_{PAHs}). De la même manière, deux autres modèles concernaient les biocides : les biocides individuels plus les mélanges de biocides ($P^{T*}_{biocides}$ sans les échantillons de biocides à 20 $\mu g\ L^{-1}$) et les mélanges de biocides ($P^{M}_{biocides}$). Pour les échantillons naturels, le jeu de données était composé de tous les échantillons marins prélevés à Saumaty et à Port-de-Bouc.

Tableau II-2. Composition des jeux de données ayant subit les analyses PARAFAC pour l'étude sur les standard (Chapitre III). A, B et C représentent les différentes concentrations des solutions. Les analyses PARAFAC ont été réalisées sur les mélanges de contaminants avec et sans substances humiques (P^{M}_{PAHs} and $P^{M}_{biocides}$) et sur les mélanges de contaminants avec et sans substances humiques et avec les solutions individuelles de contaminants (P^{T}_{PAHs} and $P^{T}_{biocides}$).

	PAH_i	ΣPAH_i	$Biocides_i$	Σ $Biocides_i$	Port de Bouc	Saumaty
PAH_i	$9 \times A_9$ (81 MEEFs)					
ΣPAH_i		B_4 (4 MEEFs)				
$Biocides_i$			$3 \times A_9$ (27 MEEFs)			
Σ $Biocides_i$				B_4 (4 MEEFs)		
Substances Humiques (HA + FA)		$B_4 \times C_9$ (36 MEEFs)		$B_4 \times C_9$ (36 MEEFs)		
Port de Bouc					23 MEEFs	
Saumaty						9 MEEFs
Jeu de données PARAFAC		P^{M}_{PAHs} (40 MEEFs)		$P^{M}_{biocides}$ (40 MEEFs)		
	P^{T}_{PAHs} (121 MEEFs)		$P^{T}_{biocides}$ (67 MEEFs) $P^{T*}_{biocides}$ (64 MEEFs)		PARAFAC échantillons naturels (32 MEEFs)	

HA : acide humique; FA : acide fulvique.

A_9 : concentrations dans chacune des solutions contenant des contaminants individuels (0,1 ; 0,2 ; 0,5 ; 0,8 ; 1 ; 2 ; 5 ; 10 et 20 µg L^{-1}).

B_4 : Concentration finale en contaminants dans les solutions de mélanges (1 ; 2 ; 5 ; et 10 µg L^{-1}).

C_9 : concentration finale en substance humique (HA + FA) dans les solutions de mélange (0,2 ; 0,4 ; 1 ; 1,6 ; 2 ; 5 ; 10 ; 15 et 20 mg L^{-1}).

Pour l'étude du suivi saisonnier (Chapitre V), deux modèles PARAFAC ont été réalisés. Le premier modèle comportait un jeu d'échantillons exclusivement continentaux (Arles et Vaccarès) alors que le second était constituait uniquement d'échantillons marins (Sofcom, Couronne et Port-de-Bouc). Comme dit précédemment, le jeu de données d'un même modèle PARAFAC doit être homogène. Il n'est donc pas recommandé d'inclure dans un même modèle des échantillons marins et continentaux.

3.1.3. Analyses par spectroscopie de fluorescence résolue en temps (TRFS)

Certains des échantillons standards de PAHs et de biocide (bentazone) ont été aussi analysés par spectroscopie de fluorescence résolue en temps (TRFS) induite par laser. Le système TRFS (disponible au laboratoire PROTEE, université de Toulon) est composé de trois parties : la source lumineuse, le système de détection et l'ordinateur qui réceptionne les données.

La source lumineuse est un laser pompe qui fournit des pulses d'énergie espacés de 30 pico secondes (énergie maximum 50 mJ, fréquence 20 Hz) à un cristal de grenat d'yttrium-aluminium dopé au néodyme (Nd-YAG, EKSPLA PL2241A, Lituanie), qui, une fois excité émet des ondes électromagnétiques à 1064 nm. La source est couplée à un générateur harmonique qui permet de sélectionner la longueur d'onde d'Ex : 1064 (25 mJ), 532 (25 mJ), 355 (12 mJ) et 266 nm (7 mJ). La sélection de la longueur d'onde se réalise à l'aide d'un système de miroirs. Le système est également composé d'un oscillateur paramétrique optique qui permet de couvrir une large gamme de longueurs d'onde de 210-2300 nm. Ce système est cependant beaucoup moins énergétique que le générateur harmonique avec un maximum d'énergie de 1 mJ à 450 nm. La fluorescence est tout d'abord collectée au moyen d'un faisceau optique constitué de 16 fibres optiques de 200 µm et est dispersée à l'aide d'un spectromètre imageur (TRIAX 180, Horiba Jobin-Yvon, France). Ce dernier permet de choisir la longueur d'onde d'Em grâce à un réseau de diffraction. Une caméra ICCD (Horiba Jobin-Yvon, France, 1024x256) est couplée au spectromètre imageur. L'énergie lumineuse est convertie en données numériques qui représentent soit une accumulation de spectres d'Em pris à différents temps, soit une variation de l'intensité de fluorescence en fonction du temps. Afin d'obtenir des spectres d'Em résolue en temps, la connaissance du délai entre l'Ex et l'Em est nécessaire. Le dispositif de commande du laser produit un déclenchement électrique à l'instant t0 et l'impulsion laser arrive à un temps t0 + 500 ns.

Le déclenchement est également envoyé à un générateur d'impulsion DG535 (Stanford Research Systems) qui génère un champ électrique qui est défini par une largeur et un retard. La fluorescence résolue en temps est obtenue en augmentant le temps de retard entre le signal optique et le front montant du signal électrique. La gigue entre l'impulsion laser et la formation du champ électrique est approximativement égale à 100 ps. En scannant une porte de 35 ns de large, les spectres d'émission fluorescence peuvent être obtenus à différent temps de retard pour une excitation donnée. Afin d'augmenter la précision de la mesure de fluorescence, chaque impulsion laser est corrigée de la fluctuation d'énergie. Cette correction est réalisée en divisant le faisceau énergétique en deux, une partie va vers l'échantillon et l'autre est réfléchie et est enregistrée avec un détecteur pyroélectrique (PE10, Ophir Optronics). Pour une longueur d'onde d'Ex, les spectres d'Em sont suivis dans le temps avec un pas de retard défini en fonction de la réponse de l'échantillon. Les logiciels d'interface graphique développés en Labview (National Instruments) et Matlab (R2010a) sont utilisés pour contrôler l'ensemble du système, de l'acquisition au traitement des données et sont commandés à partir d'un PC.

Un exemple de séquence temporelle d'acquisition est donné en Figure II-5.

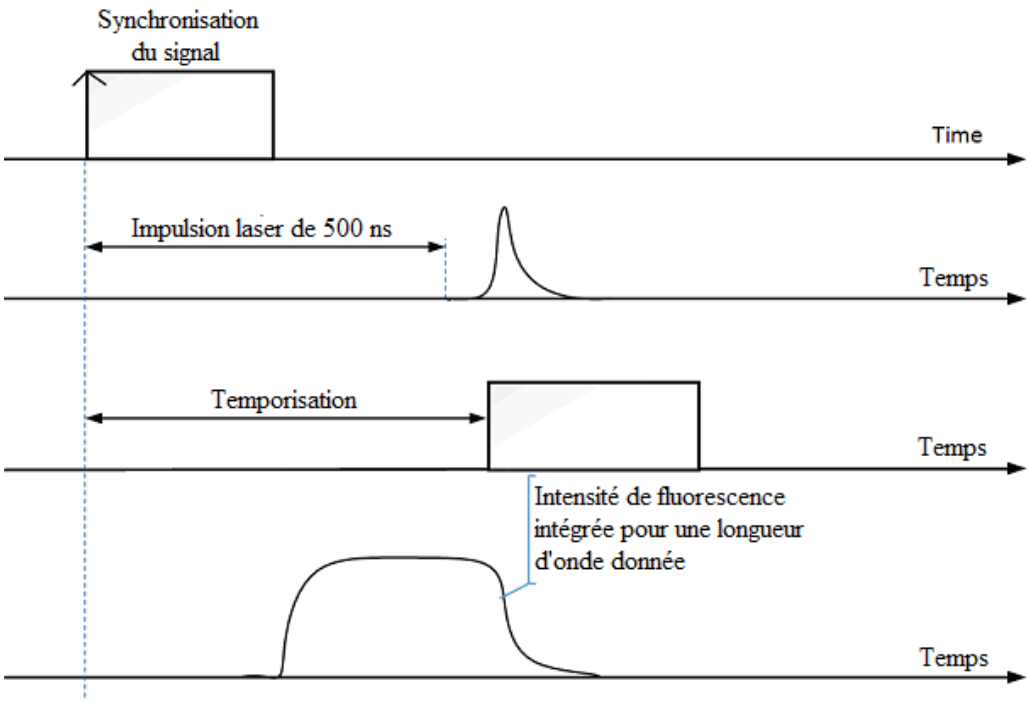

Figure II-5. Séquence temporelle d'acquisition avec le système de fluorescence laser.

Le signal obtenu est appelé réponse impulsionnelle. Il contient à la fois la réponse de l'échantillon mais également la réponse de l'appareil, c'est-à-dire l'impulsion laser (Figure II-6).

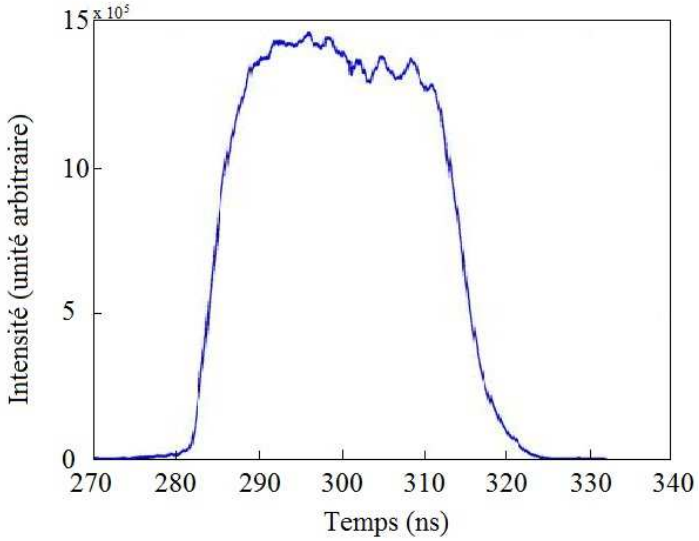

Figure II-6. Signal brut obtenu avec le système de fluorescence laser.

Afin d'éliminer la réponse instrumentale, une mesure sur l'eau ultra-pure est utilisée. On obtient alors un spectre de fluorescence correspondant uniquement aux signaux des fluorophores (Figure. II-7).

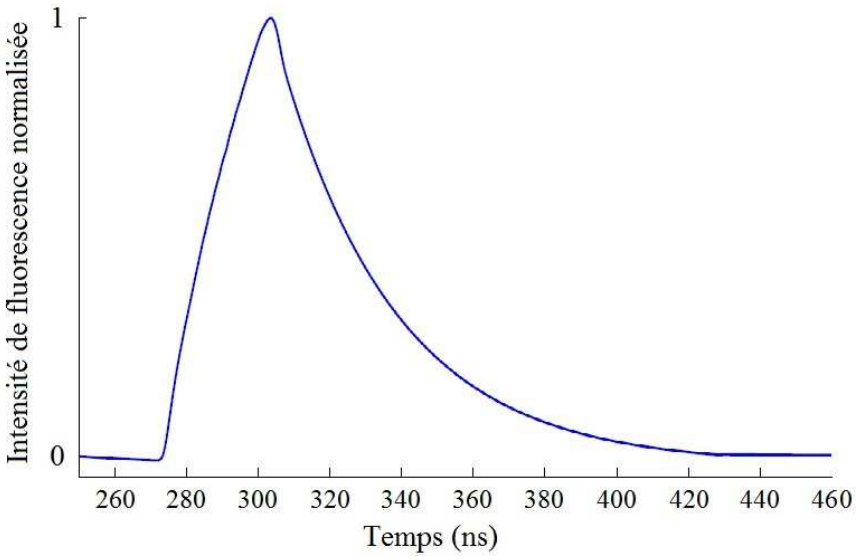

Figure II-7. Signal de la fluorescence totale pour une excitation à 355 nm obtenu après correction de la réponse instrumentale.

Ce signal peut contenir plusieurs fluorophores. Chacun d'entre eux aura une contribution propre au signal en fonction du temps. La valeur de l'intensité du signal peut être définie par l'équation suivante :

$$I(t) = \sum_{i=1}^{N} \alpha_i \exp(-t/\tau_i)$$

I représente l'intensité à un temps donné, α_i la contribution relative propre un fluorophore, t le temps et τ_i le temps de vie propre à un fluorophore.

Le signal mesuré est déconvolué de la réponse instrumentale et le traitement des données permet d'extraire le temps de vie de fluorescence (communication personnelle, C. Gadio, 2014). Pour retrouver le spectre d'émission du ou des fluorophores, la méthode utilisée est basée sur l'hypothèse qui prévoit une invariabilité du temps de vie de fluorescence pour chaque longueurs d'ondes d'émission. Le spectre d'émission est alors obtenu en réalisant une déconvolution du profil temporel associé à chaque longueur d'onde d'émission, permettant de déterminer la contribution relative propre associé à chaque longueur d'onde d'émission. Une fois déconvolué, on obtient plusieurs exponentielles définissant tous les fluorophores présents dans l'échantillon et leurs temps de vie pourront alors être déterminés (Figure II-7).

3.2. Analyse des contaminants par chromatographie

3.2.1. Extraction et analyses des hydrocarbures

Extraction. Les hydrocarbures dissous présents dans les échantillons ont été extraits par extraction liquide-liquide avec du dichlorométhane (2 x 80 mL par litre). La phase organique a été récupérée et évaporée à l'aide d'un évaporateur rotatif avant de réaliser un changement de solvant et de passer au *n*-hexane. L'extrait solubilisé dans le *n*-hexane a été purifié afin de séparer les hydrocarbures aliphatiques (fraction 1, F1) des PAHs (fraction 2, F2). L'extrait a été fractionné sur une colonne de 500 mg de silice. Le silica gel (extra pure, Merck) a été activé à 500 °C durant 4 h suivi d'une désactivation avec 4% d'eau. F1 a été éluée avec 2 mL de *n*-hexane et F2 avec 3 mL de *n*-hexane et de dichlorométhane (3:1 v/v). Des mélanges de standards deutérrés (C_{16}-d_{34}, C_{24}-d_{50}, C_{36}-d_{74} pour les hydrocarbures aliphatiques et Naph-d_8, Phe-d_{10}, Ant-

d_{10}, Per-d_{12} pour les PAHs) ont été introduits avant extraction ainsi qu'avant l'analyse. Ils ont été utilisés pour déterminer les taux de récupération et pour affiner la quantification. Tous les solvants organiques utilisés étaient de qualité trace analysis (Rathburn, Interchim).

Pour certains échantillons (Saumaty et Port-de-Bouc), les PAHs dissous ont été extraits par extraction sur phase solide (SPE) à l'aide de cartouches et de l'autotrace Dionex 280 SPE (Sunnyvale, California, USA). Les cartouches C_{18} (Envi-18, tube en verre de 6 mL) provenaient de Supelco (USA). Afin d'améliorer le rendement, du 2-propanol a été ajouté à l'échantillon (10% v/v). Les cartouches ont été au préalable conditionnées avec 10 mL de dichlorométhane, 10 mL de 2-propanol et 10 mL d'un mélange eau et de 2-propanol (9:1, v/v). L'échantillon a été alors passé à travers la cartouche. Les PAHs ont ensuite été élués avec deux fois 10 mL de dichlorométhane. Les phases organiques récupérées ont alors été additionnées et évaporées avec l'évaporateur rotatif.

Analyse par GC-MS. Les hydrocarbures ont été analysés par chromatographie gazeuse couplée à un spectrophotomètre de masse (GC-MS) (TraceISQ, ThermoElectron) fonctionnant avec une énergie d'ionisation de 70 eV pour un rapport m/z allant de 50 à 600 et utilisant l'hydrogène comme gaz vecteur avec un débit de 1,2 mL min^{-1}. Les températures de l'injecteur (utilisé en mode « splitless ») et du détecteur étaient respectivement de 250 et de 320 °C. La température initiale de la colonne était maintenue pendant 3 minutes à 70 °C avant d'augmenter de 15 °C min^{-1} jusqu'à 150 °C puis n'augmenter ensuite que de 7 °C min^{-1} pour atteindre une température finale de 320 °C qui était maintenue pendant 10 minutes. Les composés ont été identifiés à l'aide de mélanges de standards (47543-U, Supelco, USA). Des blancs de l'Autotrace SPE et des cartouches et des blancs de solvants ont été réalisés. Les valeurs des concentrations dans les échantillons ont été corrigées par les valeurs de blancs et par les taux de récupération.

3.2.2. Extraction et analyses des biocides

Le traitement et l'analyse des échantillons ont réalisés par le Centre d'analyses Méditerranée Pyrénées (CAMP).

Extraction. Les biocides dissous ont été concentrés en réalisant une extraction sur phase solide sur la base d'un volume de 500 mL (Oasis HLB 500 mg, Waters) après ajustement du pH à 7. Les cartouches ont été éluées successivement avec 3 mL d'acétate d'éthyle (Rathburn HPLC grade) et

10 mL de méthanol (Rathburn HPLC grade). L'éluat a été évaporé à 40 °C sous azote puis dissous dans 200 µl de méthanol.

Analyse par LC-MS-MS. Les biocides ont été analysés par LC-MS-MS. Le système était constitué d'une colonne C-18 150 x 2 mm avec une taille de particule de 3 µm (Varian, California) et d'un spectromètre de masse triple quadripole (Varian, California) équipé d'un électrospray d'interface. La détection en masse a été réalisée en mode ionisation négative pour le bentazone et en mode ionisation positive pour le carbaryl. La phase mobile pour l'ionisation négative était un mélange binaire de méthanol (éluant A) et d'une solution d'acide formique (éluant B) (Rathburn HPLC grade) à 0,07% alors que pour l'ionisation positive elle était constituée d'un mélange binaire d'acétonitrile contenant 0,01% d'acide formique (éluant C) et d'une solution d'acide formique à 0,01% (éluant D). Pour le mode ionisation négatif, un gradient du mélange allant de 40 à 100% en éluant A a été injecté durant 30 min. Par la suite, pendant 5 min, un mélange de 40% d'éluant A a été introduit dans l'appareil. En mode ionisation positive, l'éluant D a été introduit pendant 5 min. Pendant les 3 min suivantes, un 100% d'éluant D diminuait pour atteindre progressivement un mélange d'éluant D (70%) et C (30%). Pendant les 25 min suivantes, seulement de l'éluant C a été injecté puis pendant les 5 min le mélange d'éluant est passé progressivement d'une composition contenant uniquement l'éluant C à un éluant contenant uniquement de l'éluant D. Le débit était de 0,2 mL min^{-1}. La limite de détection de ces biocides était de 0,01 µg L^{-1}.

3.3. Analyse des paramètres biogéochimiques

Le traitement et l'analyse des échantillons ont été réalisés par le Plateau d'Analyse des Paramètres de Base du MIO.

3.3.1. Analyses des sels nutritifs

Les nutriments ont été analysés avec un AutoAnalyseur III Seal Bran Luebbe (Mequon, USA). Les échantillons ont été introduits dans une colonne de cadmium afin de réduire les NO_3^- en NO_2^- et 0,1 mL d'une solution de sulfamide à 10 g L^{-1} a été ensuite ajoutée. Cette solution a été préparée en mélangeant 1 g de sulfamide dans 10 mL d'acide chlorhydrique (37%), de l'eau ultra-pure a ensuite été ajoutée pour compléter le volume à 100 mL. Ce composé réagit avec les NO_2^- pour former un diazoïque en milieu acide (pH < 2). 0,1 mL d'une solution de N-naphtyl-

éthylènediamine à 1 g L^{-1} a été ensuite ajoutée. Cette dernière a été préparée en solubilisant 100 mg de N-naphtyl-éthylènediamine dans 100 mL d'eau ultra-pure. La solution obtenue se colore alors en rose. Le dosage colorimétrique a été réalisé à la longueur d'onde de 543 nm. On obtient dans ce cas la somme des concentrations de NO_2^- et de NO_3^-. La concentration en NO_2^- a été déterminée suivant le même protocole excepté la première étape de réduction. La concentration en NO_3^- a été déduite par soustraction des concentrations mesurées.

La quantification des PO_4^{3-} a été réalisée en complexant les phosphates avec du molybdate pour former un complexe phosphomolybdique en milieu acide. Cinq solutions ont été préparées pour faire la solution qui a été ajoutée à chaque échantillon. Dans la première solution, 85 mL d'acide sulfurique (18 mol L^{-1}) ont été mélangés avec de l'eau ultra-pure pour obtenir un volume final de 1 L. La deuxième solution contenait 12 g de molybdate d'ammonium dans 250 mL d'eau ultra-pure et enfin la troisième contenait 0,291 g de tartrate double d'antimoine et de potassium dans 100 mL d'acide sulfurique 4 N. Ces trois solutions ont ensuite été mélangées dans une fiole de 2 L qui a été complétée avec de l'eau ultra-pure. Dans 50 mL de cette solution, 1 g d'acide ascorbique a été dissout. Dans chaque échantillon, 1 mL de cette dernière solution a été ajouté. La formation de ce complexe qui colore la solution en bleu nécessite un temps de réaction de 15 minutes avant analyse de l'échantillon. Le dosage colorimétrique a été réalisé à une longueur d'onde de 820 nm.

Afin d'avoir des mesures reproductibles, des standards ont été utilisés et comparées à des produits commercialisés (OSIL) aux concentrations connues.

Les limites de détection des NO_3^-, NO_2^- et PO_4^{3-} étaient respectivement de 0,05, 0,05 et 0,02 µM.

3.3.2. Analyses de la chlorophylle *a*

La Chl *a* a été mesurée en utilisant la méthode de Raimbault et al. (2004). Afin d'extraire la Chl *a*, 5 mL de méthanol (RP prolabo) ont été ajoutés dans un tube en verre contenant le filtre GFF. Après 30 minutes d'extraction à l'obscurité à 4 °C, une mesure par fluorescence a été réalisée à l'aide d'un fluorimètre 10 Turner Designs (Sunnyvale, USA) à des longueurs d'onde d'Ex et d'Em de 450 et 660 nm. Le fluorimètre a été calibré avec des solutions de méthanol (RP prolabo) et de Chl *a* (Sigma C5753). La limite de détection de la Chl *a* était de 0,01 µg L^{-1}.

3.3.3. Analyses du carbone, de l'azote et du phosphore organique dissous

La quantification des concentrations en DOC, DON et DOP a été effectuée avec l'Autoanalyseur II Technicon (New York, USA). Avant oxydation de la matière organique, le carbone inorganique a été éliminé par ajout de 50 µL d'acide sulfurique 10 M afin de diminuer le pH jusqu'à environ 2,5. L'échantillon a alors été bullé pendant 5 minutes avec de l'O_2 afin d'éliminer le CO_2 formé par décomposition des carbonate. Après cette étape, 5 mL de réactif oxydant a été ajouté. Ce réactif était composé de 30 g de tetraborate de sodium (Merck 6308) dans 250 mL d'eau ultra-pure. 15 g de peroxodisulfate de potassium ont été également ajoutés dans l'échantillon et dissous rapidement par agitation. Les échantillons ont alors été fermés et placés dans un autoclave à 120 °C à 1 bar pendant 30 minutes. Le pH après oxydation de la matière organique atteignait des valeurs comprises entre 8,2 et 8,5, ce qui permettait au CO_2 formé de rester sous forme dissoute. Pour déterminer la quantité de carbone, la solution était directement pompée et la quantité de CO_2 formé était alors déterminée par colorimétrie. Une solution de phénolphtaléine était utilisée comme indicateur coloré. Cette solution était proportionnellement décolorée en fonction de la concentration en CO_2. L'échantillon était introduit dans un bain chauffant à 90 °C et acidifié avec un mélange d'acide sulfurique (28 mL L^{-1}) et du chlorure d'hydroxylammonium (70 g L^{-1}) afin d'éviter la formation de chlorides. Le CO_2 formé était pompé et injecté sur un réactif coloré préparé en diluant 0,4 mL de phénophtaléine à 1% dans 400 mL d'eau ultra-pure. 5 mL d'un mélange (0,25:1) de 0,1 M de Na_2CO_3 et de $NaHCO_3$. Pour réaliser des blancs, de l'eau ultra-pure acidifiée à pH 2,5 et bullée a été utilisée. Pour déterminer l'azote et le phosphore dissous, on reprend le protocole utilisé pour quantifier les nutriments. On obtient les concentrations en azote et phosphore total. Il suffit ensuite de retrancher la somme des concentrations nitrate + nitrite et la concentration en phosphate à respectivement la concentration azote et le phosphore total pour obtenir les valeurs de concentration de DON et DOP. La calibration a été réalisée avec des solutions standards en diluant dans de l'eau ultra-pure du biphthalate de potassium, du nitrate de potassium et du phosphate de potassium. Les limites de détection en DOC, DON et du DOP étaient respectivement de 3, 0,10 et 0,03 µM.

3.3.4. Analyses du carbone, de l'azote et du phosphore organique particulaire

La quantification des concentrations en POC, PON et POP a été effectuée avec l'Autoanalyseur II Technicon (New York, USA) sur le même échantillon, en utilisant une procédure d'oxydation par

voie sèche conformément aux travaux antérieurs (Raimbault et al., 1999a). Pour cela, les filtres sur lesquels ont été récupérées les particules, ont été introduits dans des flacons en verre de 50 mL SCHOTT®, 40 mL d'eau ultra-pure ont été ajoutés ainsi que 50 µL d'acide sulfurique 10 M afin d'éliminer le carbone inorganique en abaissant le pH à 2,5 environ, l'échantillon est alors filtré. Par la suite, pour l'analyse du POC, le protocole est le même que celui utiliser pour déterminer le DOC mais est repris à partir de l'étape de bullage. Pour l'analyse du PON et POP, le protocole est alors le même que celui utilisé précédemment pour l'analyse des nutriments. Le POC, le POP et le PON avaient respectivement des limites de détection de 0,50, 0,02 et 0,10 µM.

3.3.5. Analyses du pH

Le pH a été mesuré dans l'eau résiduelle contenue dans les flacons en verre avec un pH-mètre SG02-Secen GOTM Toledo (Schwerzenbach, Swizerland).

3.3.6. Analyses statistiques

Les analyses statistiques tels que les PCAs, régression, test de normalité, ANOVA, Man Whitney ont été réalisés avec XLSTAT 2013 5.01. Pour les régressions linéaires et les PCAs, la corrélation de Spearman a été préférée à celle de Pearson à cause des hautes amplitudes de certaines variables et de leur distribution non-normale. Pour chaque analyse et tests réalisés, le seuil de significativité a été fixé à $p < 0,05$.

3.3.7. Cartes représentant la salinité et la chlorophylle a dans les eaux de surfaces

Les images satellite de la concentration en Chl *a* ont été générées en appliquant l'algorithme OC5 les données provenant du spectrophotomètre d'images à résolution moyenne (MERIS) et le spectroradiomètre d'images à résolution modérées (MODIS) et sont fournie par l'IFREMER (Gohin, 2011). Les cartes de la salinité de surface ont été obtenues à partir d'un modèle hydrodynamique 3D appliqué à une échelle régionale (MARS3D, IFREMER) (Lazure et Dumas, 2008).

3.3.8. Profil de température, de salinité et de chlorophylle *a*

Les cartes représentant les profils CTD réalisés le long de la colonne d'eau sur les sites de Port de Bouc, Couronne et Sofcom durant la période d'étude ont été réalisées avec le logiciel Ocean Data View v4.

Chapitre III: Caractérisation de signatures de fluorescence d'hydrocarbures aromatiques polycycliques et de biocides dans des mélanges complexes à l'aide des matrices d'excitation-émission de fluorescence (MEEFs) et de l'analyse parallèle factorielle (PARAFAC)

Résumé

Dans ce chapitre, une étude a été réalisée sur des solutions contenant des standards de contaminants organiques tels que les hydrocarbures aromatiques polycycliques (PAHs) et les biocides. Les objectifs de cette étude étaient 1) de définir les signatures de fluorescence de ces composés, 2) d'évaluer la pertinence de la méthode MEEF/PARAFAC pour détecter et quantifier des fluorophores anthropiques en présence de DOM naturelle (substances humiques) et 3) d'utiliser cette méthode MEEF/PARAFAC dans des environnements côtiers naturels fortement anthropisés. Les signatures de fluorescence de 9 PAHs et de 3 biocides ont été caractérisées à partir de solutions standard. Ces contaminants présentaient des propriétés de fluorescence dans le domaine spectral UV (λ_{Ex} : 220-335 nm, λ_{Em} : 310-414 nm) ainsi que des limites de détection variant de 0,02 à 1,29 μg L^{-1}. Des MEEFs ont été réalisées sur des solutions contenant à la fois les contaminants mais aussi des substances humiques (0,2 à 20 mg L^{-1}) simulant ainsi des échantillons naturels. Deux analyses PARAFAC ont été réalisées : l'une sur un jeu de données correspondant à toutes les solutions contenant des PAHs (les solutions d'PAHs individuels ainsi que les mélanges) et l'autre sur toutes les solutions contenant des biocides (les solutions de biocides individuels ainsi que les mélanges). La méthode MEEF/PARAFAC appliquée sur le premier jeu de données a validé un modèle à sept composants qui comprenait un fluorophore de type substances humiques et six fluorophores de type PAHs. Sur le second jeu de données, cette méthode a validé un modèle à six composants comprenant un fluorophore de type substances humiques et trois fluorophores de type biocides. Je montre dans ce chapitre que la méthode MEEF/PARAFAC permet de quantifier précisément la plupart des contaminants pour les concentrations de substances humiques ne dépassant pas 2,5 mg C L^{-1}. Je démontre l'application de cette méthode dans le milieu naturel 1) en comparant les spectres d'excitation et d'émission des composants trouvés en mer avec ceux des standards de PAHs et 2) en corrélant les intensités de fluorescence des composants trouvés en mer avec les concentrations en hydrocarbures correspondants déterminées par GC-MS.

Identification and quantification of known polycyclic aromatic hydrocarbons and pesticides in complex mixtures using fluorescence excitation–emission matrices and parallel factor analysis

1. Introduction

Polycyclic aromatic hydrocarbons (PAHs) and biocides are among the most widespread organic contaminants in aquatic environments (Lepom et al., 2009 ; Roose et Brinkman, 2005). Due to their physico-chemical properties, PAHs and biocides are persistent and mobile, can strongly bioaccumulate in food chains and are harmful to living organisms through reprotoxic, carcinogenic, mutagenic or endocrine disrupting effects (Kennish, 1992; Landau-Ossondo et al., 2009; McKinlay et al., 2008). Thus, PAHs and biocides are recognised by various international organizations as priority contaminants: They are included in the list of 45 priority regulated substances by the European Union (Official Journal of the EU 24/08/2013, Directive 2013/39/EU), and in the list of priority regulated substances by the US Federal Water Pollution Control Act and the US Environmental Protection Agency (EPA). PAHs are introduced into marine and fresh waters from the direct discharges of crude oil or its derivatives during sea activities, or from industrial and urban wastes routed by surface runoffs, effluents or atmospheric particles (Dachs and Méjanelle, 2010; Wurl and Obbard, 2004). Biocides are particularly abundant near agriculture areas and enter marine and fresh waters mainly through surface runoffs (Bocquené and Franco, 2005; Jia et al., 2007). Gas or liquid chromatography coupled to mass spectrometry (GC-MS, LC-MS) is the reference analytical method to determine PAH and biocide concentrations at μg L^{-1} or ng L^{-1} levels in natural waters (Lepom et al., 2009). However, chromatographic analyses, which require large volumes of water (1-5 L) and several sample treatment steps, such as extraction, purification or concentration, are time-consuming and cannot be applied for a large number of samples.

Due to their aromatic structures, PAHs and (to a lesser extent) biocides have intrinsic fluorescence properties in the UV and blue spectral regions (Dabestani and Ivanov, 1999; JiJi and Booksh, 2000). Hence, fluorescence spectroscopy could be relevant for monitoring these contaminants in aquatic ecosystems. Currently, the state-of-the-art fluorescence spectroscopy technique that is used to characterise dissolved organic compounds in natural waters is fluorescence excitation-emission matrix (EEM), which involves a collection of sequential

fluorescence emission (Em) spectra at successively increasing excitation (Ex) wavelengths. EEM has two significant advantages over chromatographic methods: 1) it is quick since it does not entail any sample pretreatment and 2) it only requires very small volumes of water (~ 5 mL). Conversely, EEM has two main limits: 1) its sensitivity, with detection limits in the µg L^{-1} range and 2) its lack of selectivity, which is caused by overlapping fluorophore signatures. The overlapping in fluorescence signatures of individual compounds in multi-component mixtures, such as PAH- and biocide-contaminated natural waters, may be important and generate complex EEMs that are difficult to interpret. Therefore, advanced multivariate statistical techniques, such as parallel factor analysis (PARAFAC), were proposed recently to decompose the EEM complex fluorescence signal into underlying individual fluorescence spectra (Stedmon and Bro, 2008).

Humic substances, which represent a major component of dissolved organic matter (DOM) in natural waters (they are particularly abundant in freshwaters and coastal ecosystems), have a strong ability to absorb light and to fluoresce (Blough and Del Vecchio, 2002). Moreover, they are known to molecularly interact and bind with organic contaminants such as PAHs and biocides (Gauthier et al., 1986; Fang et al., 1998; Akkanen et al., 2012). Thus, the presence of humic substances in water samples containing PAHs or biocides may cause additional difficulties in the retrieval and quantification of these contaminants by the EEM/PARAFAC method because of fluorescence signature overlapping, but also of absorbance-induced inner filtering effects and fluorescence quenching processes.

Several studies have successfully used the EEM/PARAFAC method to characterise and quantify PAHs at the µg L^{-1} level from petroleum products such as gasoline, diesel, fuel, lubricating and crude oils (Christensen et al., 2005; Alostaz et al., 2008), from aqueous motor oil extract and asphalt leachate (Nahorniak and Booksh, 2006), from oceanic water enriched with gasoline (Booksh et al., 1996; Muroski et al., 1996), and from PAH mixtures in pure water (Beltrán et al., 1998; Yoon-chang Kim et al., 2005). Also, recent works have proposed the EEM/PARAFAC method to characterise and quantify some biocides at the µg L^{-1} level from biocide mixtures in pure water or methanol (Jiji et al., 1999; JiJi and Booksh, 2000; Rodríguez-Cuesta et al., 2003). However, to our knowledge, the EEM/PARAFAC method has never been applied on PAH or biocide mixtures in presence of humic substances, even though this would have allowed for better reflecting the content of natural waters.

In this context, the objectives of this study are 1) to characterise the fluorescence signatures of several PAHs and biocides of interest by using EEM spectroscopy, 2) to asses the relevancy of PARAFAC for discriminating contaminant fluorescence signatures in complex mixtures containing humic substances and 3) to apply the method on marine water samples and to compare the fluorescence intensities with concentrations of individual compounds determined by GC-MS.

2. Material and methods

2.1. Standard solutions

Nine PAHs and four biocides of interest were chosen to conduct our study. For the PAHs, we chose naphthalene (Naph), 2,3 dimethyl naphthalene (DNaph), fluorene (Flu), 1,8 dimethyl-9H-fluorene (DFlu), phenanthrene (Phe), anthracene (Ant), pyrene (Pyr), benzo[a]anthracene (BaA), and benz(e)pyrene (BeP). For the biocides, we selected 2-phenylphenol (Pho), carbaryl (Car), thiabendazole (Thi) and bentazone (Ben). Naph, DNaph, Flu, DFlu, Phe, Ant and Pyr are among the most abundant PAHs in the dissolved phase of natural waters (Guigue et al., 2014). Because of similarities in their structure (number of rings and π electrons), isomers (Phe and Ant), parents and their alkylated homologues (Naph and DNaph, Flu and DFlu) and phenylated PAHs (BaA and BeP) should have very close fluorescence signatures. Pho, Car and Thi are used as a fungicide, but also as molluscicide, insecticide (Car), nematicide, bactericide and antibiotic (Pho) and herbicide (Ben) in agriculture. These biocides have been detected in both freshwater and coastal marine environments (i.e., river of the Pearl River Delta, Vaccarès lagoon, coastline of Martinique, Willapa Bay)(Dumbauld et al., 2001; Bocquené and Franco, 2005; Comoretto et al., 2007;Peng et al., 2008).

The PAHs and biocides were purchased from Sigma-Aldrich ($\geq$ 98% and 99.9 % for Ben) and were used without further purification. Stock solutions of each individual compound (50 mg L^{-1}) were prepared by dissolving the pure solid or by diluting from initial stock solution for Ben in methanol (Rathburn HPLC grade). From the stock solutions, individual solutions with final concentrations of between 0.1 and 2000 $\mu g\ L^{-1}$ were prepared in ultrapure water (i.e., Milli-Q water). In addition, PAH and biocide mixtures were prepared from these stock solutions. The final concentrations of each compound in these mixtures were between 1 and 10 $\mu g\ L^{-1}$. Suwannee River humic (HA) (2S101H) and fulvic (FA) (2S101F) acids were purchased from the

International Humic Substances Society (IHSS). The HA and FA were dissolved in sodium hydroxide and ultrapure water, respectively, to obtain HA and FA solutions of 250 mg L^{-1}. These two solutions were then mixed together to obtain a stock solution of humic substances (HA + FA) in ultrapure water of 200 mg L^{-1}. This humic substance stock solution was added to the PAH and biocide mixtures to achieve final concentrations of HA + FA of between 0.2 and 20 mg L^{-1}, corresponding to concentrations of organic carbon of between 0.1 and 10 mg C L^{-1}. The Ben was not added to mixture solutions. All solutions were made in ultrapure water and their pH was adjusted to 6.0 with sodium hydroxide. Standard (individual and mixture) solutions were stored in SCHOTT® glass bottles and in the dark at 4 °C for 48 h prior to analysis.

2.2. Natural samples

Marine water samples were collected aboard the R/V Antédon II in the morning on 6 July 2011 in the Saumaty harbour (10 samples) and on 20 July 2012 in the Port-de-Bouc harbour (20 samples), located in the Marseilles Bay (northwestern Mediterranean Sea, France). Saumaty and Port-de-Bouc harbours are known to be heavily contaminated in hydrocarbons (Guigue et al., 2011). Saumaty is a dynamic fishing port that combines trawlers, tuna boats and wholesale trading centers, whereas Port-de-Bouc is surrounded by the Marseilles-Fos petrochemical complex, which includes several chemical, petroleum and steel-work plants. Samples were taken at ~ 0.1 m depth (subsurface water) with 4 L Nalgene polycarbonate bottles. The bottles were washed with 1 M HCl and ultrapure water before use, rinsed three times with the respective sample before filling and stored in the dark in the cold (4-8 °C). Back in the laboratory, samples were immediately filtered under a low vacuum (< 50 mm Hg) through precombusted (500 °C, 4 h) GF/F glass fiber filters (47 mm diameter, Whatman) using polysulfone filtering systems. For fluorescence measurements, filtered samples were stored in 10 mL glass tubes at 4 °C in the dark and were analysed within 24 h. For chromatographic (PAH) analyses, filtered samples were stored in 1 L SCHOTT® glass bottles at 4 °C in the dark before solvent extraction (within 48 h). All glassware was washed in 1 M HCl, rinsed with ultrapure water and heated to 500 °C for 4 h.

2.3. EEM fluorescence measurements

Fluorescence measurements were performed with a Hitachi F-7000 spectrofluorometer. The correction of spectra for instrumental response was conducted from 200 to 600 nm according to the procedure described in Tedetti et al. (2012). The samples were allowed to reach room

temperature in the dark before transferring into a far UV silica quartz cuvette with a 1 cm pathlength (170-2600 nm; LEADER LAB®). The temperature was maintained at 20 °C in the cell holder with an external circulating water bath. The EEMs were collected over Ex wavelength (λ_{Ex}) of between 200 and 500 nm with a 5 nm step, and over Em wavelength (λ_{Em}) of between 280 and 550 nm with a 2 nm step. Excitation and emission slit widths of 5 nm were used with a scan speed of 1200 nm min^{-1}, a time response of 0.5 s and a PMT voltage of 700 V. Blanks (ultrapure water) and quinine sulphate dihydrate solutions of between 0.5 and 50 µg L^{-1} (Fluka, purum for fluorescence) in 0.05 M H_2SO_4 were regularly measured during sample measurements. To account for inner filtering effects, absorbance measurements were performed with a Shimadzu UV-Vis 2450 spectrophotometer from 200 to 600 nm in a quartz cuvette with a 1 cm pathlength.

Each EEM was corrected for inner filtering effects by multiplying it by a correction matrix, which was calculated for each wavelength pair from the sample absorbance by assuming Ex and EM pathlengths of 0.5 cm in a 1 cm cuvette (Ohno, 2002). Next, the mean of the eleven ultrapure water EEMs was subtracted from each sample EEM. Finally, the fluorescence data were converted into quinine sulphate unit (QSU). One QSU corresponding to the fluorescence of 1 µg L^{-1} of quinine sulphate in 0.05 M H_2SO_4 at a λ_{Ex} /λ_{Em} of 350/450 nm (5 nm slit widths). The conversion to QSU was made by dividing the blank-corrected EEM fluorescence data by the mean slope of the quinine linear regressions (r^2 = 1.00, n = 8), i.e. 13 arbitrary fluorescence intensity units / QSU.

2.4. PARAFAC analysis

For standard solutions, PAH and biocide datasets were processed separately. For both contaminant types, PARAFAC was conducted first on the contaminant mixtures with and without humic substances (P^M_{PAHs} and $P^M_{biocides}$). Next, PARAFAC was performed on the contaminant mixtures with and without humic substances and with individual contaminant solutions (P^T_{PAHs} and $P^T_{biocides}$). These two types of datasets will provide information regarding whether the PARAFAC process is enhanced in the presence of individual EEMs. The EEM wavelength ranges that were used were 200-500 and 280-550 nm for Ex and Em, respectively. The EEMs were merged into a three-dimensional data array with the following formula: number of samples × 60 λ_{Ex} × 133 λ_{Em}. For the PAHs, the number of samples used for the PARAFAC analyses of the mixtures (P^M_{PAHs}) and of the mixtures plus the individual compounds (P^T_{PAHs}) was 40 and 121,

respectively. For the biocides, the number of samples for $P^{M}_{biocides}$ and $P^{T}_{biocides}$ was 40 and 67, respectively. For marine waters, 30 samples were used for PARAFAC.

PARAFAC was operated by the DOMFluor toolbox v1.6. in MATLAB® 7.10.0 (R2010a). The number of components tested ranged from 2 to 12 for standard solutions and from 2 to 6 for natural samples. For the PAH dataset, no outliers were detected. However, for the biocide dataset, three outliers were found. These outliers corresponded to samples that contained each individual biocide at 20 µg L^{-1}. These outliers were removed from the dataset to reduce the $P^{T}_{biocides}$ to $P^{T*}_{biocides}$ with 64 EEMs. The validation of the PARAFAC model (running with the non-negativity constraint) and the determination of the correct number of components were achieved through the examination of 1) the percentage of explained variance, 2) the shape of residuals, 3) the split half analysis and 4) the random initialization using the Tucker Congruence Coefficients (Stedmon and Bro, 2008).

2.5. PAH extraction and GC-MS analysis

Dissolved PAHs present in the fraction < 0.7 µm were extracted from marine water using solid phase extraction (SPE) on C_{18} cartridges (Envi-18, 6 mL glass tube, 500 mg of packing, Supelco). Cartridges were conditioned with 10 mL of CH_2Cl_2, followed by 10 mL of 2-propanol and 10 mL of water-2-propanol (9:1, v/v). Then the samples were sucked through the cartridges. PAHs were eluted with 2 × 10 mL of CH_2Cl_2. Organic phases were combined and evaporated on a rotary evaporator. Deuterated standard mixtures (Naph-d_8, Phe-d_{10} and Per-d_{12}) were introduced prior to extraction, as well as a supplementary deuterated standard before injection, and used as surrogates to assess the recoveries of analytical procedures and to perform quantitation accuracy. PAHs were concentrated under a gentle stream of nitrogen and analyzed by gas chromatograph-mass spectrometer (GC-MS) (TraceISQ, ThermoElectron) operating at an ionization energy of 70 eV for a m/z range of 50-600, using hydrogen as carrier gas at a flow rate of 1.2 mL min^{-1}. Compounds were identified by reference to the analysis of a standard mixture (47543-U, Supelco, USA). All concentration values were blank and recovery corrected (Guigue et al., 2011, 2014).

3. Results and discussion

3.1. Fluorescence signatures of the individual PAHs and biocides

The EEMs of the individual PAHs and biocides (excepted for Ben) in ultrapure water are depicted in the Figure III-1. Table III-1 shows the spectral position (λ_{Ex} /λ_{Em}) and the Stokes shift ($\lambda_{Em} - \lambda_{Ex}$) of the fluorescence maxima of the individual PAHs and biocides in ultrapure water that were obtained from EEMs and peak picking technique. The linear regression parameters between the contaminant concentration and fluorescence peak intensity are also presented: slope, y intercept, coefficient of determination (r^2), and detection and quantification limits (DL and QL). The PAHs with the lowest λ_{Ex} were Naph and DNaph (λ_{Ex} /λ_{Em}: ~ 220/334 nm), while the PAH with the highest λ_{Ex} was Pyr (λ_{Ex} /λ_{Em}: 335/392 nm). Among PAHs, Flu and DFlu had the lowest λ_{Em} (λ_{Ex} /λ_{Em}: 260/310 nm) and BaA had the highest λ_{Em} (λ_{Ex} /λ_{Em}: 285/410 nm). Among biocides, Car was the more blue-shifted (λ_{Ex} /λ_{Em} : 220/334 nm). In contrast, Ben had peak at longer wavelengths (λ_{Ex}: 330 nm, λ_{Em}: 466 nm). The number of fluorescence maxima ranged from 1 (Flu, DFlu, Phe) to 8 (Pyr) whereas the other compounds exhibited two fluorescence peaks (Table III-1). The positions of the fluorescence maxima of the parent and alkylated PAHs (Naph and DNaph, and Flu and DFlu) were analogous. However, the fluorescence maxima of the parent and phenylated PAHs (Ant and BaA, and Pyr and BeP) had different spectral positions and peak numbers. Phe and Ant, which are isomers, had similar λ_{Ex} values but different λ_{Em} values (the λ_{Em} of Ant was red-shifted). BeP and BaA had similar fluorescence maxima. Car, which is a naphthalene-derived chemical, had a fluorescence maximum that was similar to those of Naph and DNaph. The Stokes shift varied from 39 (Pyr) to 169 nm (Pho) (Table III-1).

For each fluorescence maximum, a significant positive linear relationship was observed between the compound concentration and the fluorescence intensity over the range of 0.1-2000 µg L^{-1} (r^2 = 0.98-1.00, n = 9, $p < 0.01$) (Table III-1). The DL of the PAHs was between 0.02 (BeP at λ_{Ex} /λ_{Em}: 275/398 nm) and 1.29 µg L^{-1} (Naph at λ_{Ex} /λ_{Em}: 225/334 nm). The QL value was between 0.07 and 4.30 µg L^{-1} for the same PAHs. Regarding biocides, the DL was between 0.10 (Car at λ_{Ex} /λ_{Em}: 220/334 nm) and 86.30 µg L^{-1} (Ben at λ_{Ex} /λ_{Em}: 245/458 nm), with corresponding QL values of 0.35 and 284.20 µg L^{-1} (Table 1). The studied contaminants displayed a diversity of fluorescence signatures regarding spectral position, number of peaks, Stokes shift and the

DL/QL. However, similarities were found between the parent and alkylated PAHs and between some of the PAHs and biocides (Naph and Car) (Table III-1).

The fluorescence signature of a given fluorophore is largely influenced by its conjugated π-electron system. When the number of conjugated π-electrons increases within a fluorophore, its intrinsic fluorescence capacity tends to expand through an increase in both its molar absorption coefficient (ε) and fluorescence quantum yield (Φ). In addition, an increasing number of conjugated π-electrons causes a red-shift in the absorbance wavelength as the energy decreases between the ground and excited states (Valeur, 2001). Here, we observed a significant positive linear relationship between the number of conjugated π-electrons and the λ_{Em} ($r^2 = 0.47$, n = 29, $p < 0.01$). Interestingly, when excluding alkylated PAHs and biocides (i.e., the compounds that present heteroatoms, methyl, phenolic hydroxyl or carbamic acid functions), the linear correlations between the number of conjugated π-electrons and the DL, and between the number of conjugated π-electrons and λ_{Em} reached $r^2 = 0.73$ and $r^2 = 0.65$ (n = 20, $p < 0.01$), respectively. This result emphasises the major role of conjugated π-electron systems in controlling the magnitude and spectral domain of fluorescence for contaminants composed of only aromatic rings, such as the parent PAHs.

As mentioned above, parent and alkylated PAHs had the same fluorescence maxima positions. Nevertheless, their slopes, DL and QL were significantly different (Table III-1). The number of conjugated π-electrons of these compounds (which remained unchanged) did not explain the discrepancies in fluorescence intensity. Indeed, besides the conjugated π-electron system, other parameters potentially modify Φ, including the introduction of methyl groups into the aromatic structure (Nijegorodov et al., 2003). For naphthalene, the addition of methyl groups increased its sensitivity (DL of DNaph < DL of Naph; Table III-1) because the molecule symmetry was diminished and the fluorescence rate constant increased (Nijegorodov et al., 2009). In contrast, the addition of methyl groups to fluorene reduced the Φ (DL of DFLu > DL of Flu; Table III-1) by increasing the intersystem crossing rate constant and by decreasing the fluorescence rate constant. These changes were attributed to the stability of the molecular symmetry (Nijegorodov et al., 2009).

The fluorescence maxima of the PAHs and biocides found in this study were very similar to those reported in previous studies that used ultrapure water as a solvent, with differences in λ_{Ex} and λ_{Em}

≤ 5 nm (Beltrán et al., 1998; Fang et al., 1998; Tedetti et al., 2010). Nevertheless, when the fluorescence spectra of the contaminants were measured in methanol, ethanol or hexane, blue shifts in λ_{Em} and red shifts in λ_{Ex} and λ_{Em} occurred (Table III-1). Indeed, solvent polarity is known to modify the fluorescence maxima. When the solvent polarity decreased, blue shifts are observed in λ_{Em} and Φ increased due to changes in the non-radiative decay rate or in the conformational structure of the fluorophore (Valeur, 2001).

3.2. Discrimination of fluorescence signatures in complex mixtures

The analysis on mixtures sample show like expected overlaps between the fluorophores (Figure III-2). It is difficult to bring out the components present in the sample with peak picking method and a PARAFAC analysis is required for each contaminant type, the results obtained from the two PARAFAC models (i.e., P^M and P^T) were analogous. Thus, only the PARAFAC model results from the mixtures and individual solutions are presented below (i.e., P^T_{PAHs} and $P^{T*}_{biocides}$).

P^T_{PAHs} validated a seven-component model, which included one humic-like fluorophore (humic-like 1) and six PAH-like fluorophores (Figure III-3). To identify these fluorophores, the Ex and Em spectra of the components that were modelled by PARAFAC were compared with the Ex and Em spectra of the individual compounds acquired from the EEM measurements (Figure III-4). These comparisons showed that the six PAH-like components that were revealed by PARAFAC included DNaph, Flu, Phe, Ant, Pyr and BaA. On the other hand, Naph, DFlu and BeP did not have the corresponding components identified in the PARAFAC model. Indeed, the EEM spectra of DNaph and Flu fitted the Naph-like and Flu-like components better than the EEM spectra of Naph and DFlu (Figure III-4). Hence, the PARAFAC analysis applied on PAH mixtures was not able to separate the parent and alkylated compounds (i.e., the fluorophores that had the same fluorescence maxima). The compounds that had the highest fluorescence were “selected” by the PARAFAC: DNaph and Flu (Table III-1). As previously mentioned, BaA and BeP had similarities in their fluorescence domains. Likewise, the PARAFAC model selected BaA (Figure III-3; III-4), which was more fluorescent than BeP according to the linear regression parameters (Table III-1).

$P^{T*}_{biocides}$ validated a six-component model that included one humic-like fluorophore (humic-like 2), three biocide-like fluorophores and two fluorophores considered as artifacts (Figure III-5). The three biocides, Pho, Car and Thi, were identified by comparing the measured EEM spectra

with the modelled PARAFAC spectra (Figure III-4). The greatest discrepancies between the measured and modelled spectra were observed for Thi, which presented the lowest fluorescence (Table III-1). Figure III-4 also show the good correspondence between the spectra of the two humic-like components ("humic-like 1" for the PAH model and "humic-like 2" for the biocide model) and the spectra of the pure humic substance solution. By opposition, the spectra of the two artifacts derived from the biocide model did not fit at all with the spectra of the pure humic substance.

The contaminant concentrations in the mixtures that were determined from peak picking and PARAFAC techniques were compared to the true contaminant concentrations, with regard to the humic substance concentrations (Figure III-6). For peak picking method, the contaminant concentrations in the mixtures were calculated using linear regression parameters between the individual contaminant concentrations (0.1-20 µg L^{-1} for PAHs and biocides) and their corresponding EEM fluorescence intensities (data reported in Table III-1). For PARAFAC method, the contaminant concentrations in the mixtures were calculated using linear regression parameters between the individual contaminant concentrations (0.1-20 µg L^{-1} for PAHs, 0.1-10 µg L^{-1} for biocides) and their corresponding PARAFAC component intensities (data not shown). Whatever the true contaminant concentration in the mixtures (1, 2, 5 or 10 µg L^{-1}), the trends of retrieved concentrations were similar. Thus, only the results relating to the 5 µg L^{-1} concentration are presented here (Figure III-6). When considering all humic substance concentrations, the mean contaminant concentration that was derived from PARAFAC analysis (4.7 ± 0.7 µg L^{-1}) was much closer to the true contaminant concentration than that derived from peak picking (7.1 ± 1.7 µg L^{-1}). Clearly, concentrations were overestimated with the peak picking method due to overlapping fluorescence signatures. As shown in Figure III-6, this overestimation increased with increasing humic substance concentrations. The Pho concentration was the most overestimated because its fluorescence signature was very close to that of humic substances (Table III-1; Figure III-4).

In contrast, the PARAFAC-derived concentrations tended to decrease with increasing humic substance concentration (Figure III-6). Taken into account that samples were corrected for inner filtering effects, this decrease in PARAFAC-derived concentrations may be explained by fluorescence quenching processes induced by the presence of humic substances (Fang et al.,

1998; Kumke et al., 1994; Peuravuori, 2001; Lee et al., 2003; Jung et al., 2010). Pyr and BaA, which were always underestimated (Figure III-6), would be particularly sensitive to these quenching processes. Other compounds such as Phe, Ant and Car are also known to be affected by quenching (Fang et al., 1998; Kumke et al., 1994; Peuravuori, 2001; Lee et al., 2003; Jung et al., 2010). On the contrary, regardless of the humic substance concentration, the PARAFAC-derived Flu and DNaph concentrations were always overestimated. PARAFAC was unable to discriminate the fluorescence signatures of the parent and alkylated PAHs. Therefore, the fluorescence intensities of DFlu and Naph were very likely superimposed on those of Flu and DNaph. Consequently, these results show that the EEM/PARAFAC identification and quantification of PAHs and biocides at the µg L^{-1} level is efficient but, due to organic matter quenching processes, its efficiency is limited to aquatic systems containing humic substance amount not exceeding 2.5 mg C L^{-1} (Figure III-6).

3.3. Application to marine samples

Three components were validated by the PARAFAC model applied to 30 marine samples collected in two harbours in the Marseilles Bay (northwestern Mediterranean Sea, France) (Figure III-7). We found that the fluorescence maxima of C1 (λ_{Ex} /λ_{Em}: 225, 285/340 nm), C2 (λ_{Ex} /λ_{Em}: 250/356, 372 nm) and C3 (λ_{Ex} /λ_{Em}: 265/324 nm) were very close to fluorescence maxima of Naph, Phe and Flu or of their alkylated compounds, respectively (Table III-1; Figure III-3). Interestingly, these components were very similar to the three oil-related components ascertained by Zhou et al. (2013) in the water column of the Gulf of Mexico during the Deepwater Horizon oil spill: C1 (λ_{Ex} /λ_{Em}: 226/340 nm), C2 (λ_{Ex} /λ_{Em}: 236/360 nm) and C6 (λ_{Ex} /λ_{Em}: 252/311 nm). These components would be derived from crude and weathered oil (Zhou et al., 2013). The concentration in dissolved organic carbon of our marine samples ranged from 0.85 to 2.3 mg C L^{-1}. Thus, their organic carbon content was not high enough to induce significant fluorescence quenching effects.

On the same marine samples, individual parent and alkylated (methyl, dimethyl and trimethyl) PAH concentrations were determined by chromatographic analysis (GC-MS). Total (parent + alkylated) PAH concentrations ranged from 0.2 to 18 µg L^{-1}. Major (parent + alkylated) compounds were Phe, comprising 20-60% of total PAHs, followed by Naph (12-54% of total PAHs) and Flu (6-29% of total PAHs). The fluorescence intensities of PARAFAC components

C1, C2 and C3 were thus compared to the concentrations of parent Naph, Phe and Flu and to the concentrations of parent + alkylated Naph, Phe and Flu (Figure III-8). We observed that the fluorescence intensities were much better correlated to parent + alkylated concentrations (r^2 = 0.92, 0.93, 0.90 for respectively Naph, Phe and Flu) than to parent concentrations (r^2 = 0.06, 0.90, 0.71 for respectively Naph, Phe and Flu). The good correlations between these two techniques implied that the EEM/PARAFAC method could substitute chromatographic analysis for predominant PAHs in highly contaminated aquatic environments. Our study confirms the importance of alkylated (methyl, dimethyl and trimethyl) compounds in the pool of dissolved PAHs (Guigue et al., 2011, 2014) and highlights their strong contribution to the PAH fluorescence signal in marine coastal waters.

4. Conclusion

In this study, we combined the EEM and PARAFAC methods to discriminate and quantify PAHs (DNaph, Flu, Phe, Ant, Pyr, BaA) and biocides (Pho, Car) at the µg L^{-1} level in the presence of humic substances (at relevant freshwater concentrations). We underlined the quenching effect on PAHs and biocides for humic substance concentrations exceeding 2.5 mg C L^{-1}. The application of this method to natural (marine) samples was demonstrated through the highlight of fluorescence signatures of PAH and the good linear correlations between spectrofluorimetry and GC-MS results. The PAH fluorescence signal in marine coastal waters was mainly due to alkylated compounds. Although this combined fluorescence spectroscopy/multi-way analysis method cannot replace standard chromatographic techniques to measure organic contamination at trace levels (ng L^{-1}), it may be useful as low cost, efficient screening method to monitor PAH and biocide concentrations in the µg L^{-1} range in chronically or sporadically contaminated natural waters.

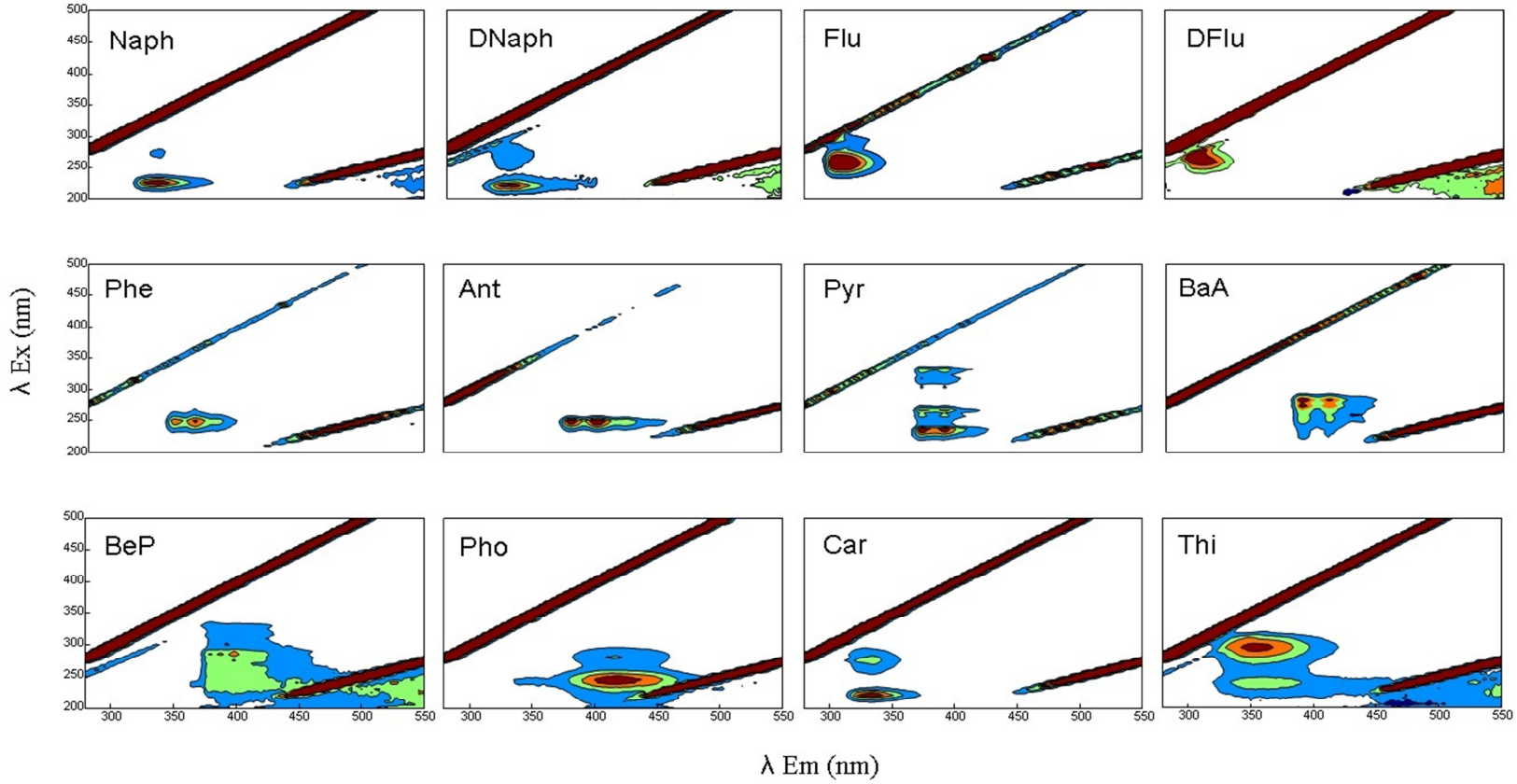

Figure III-1. Excitation-emission matrix (EEM) contour plots of individual PAHs at 2 µg L^{-1} and biocides at 10 µg L^{-1} in ultrapure water excepted the Ben. Each EEM are at different scales.

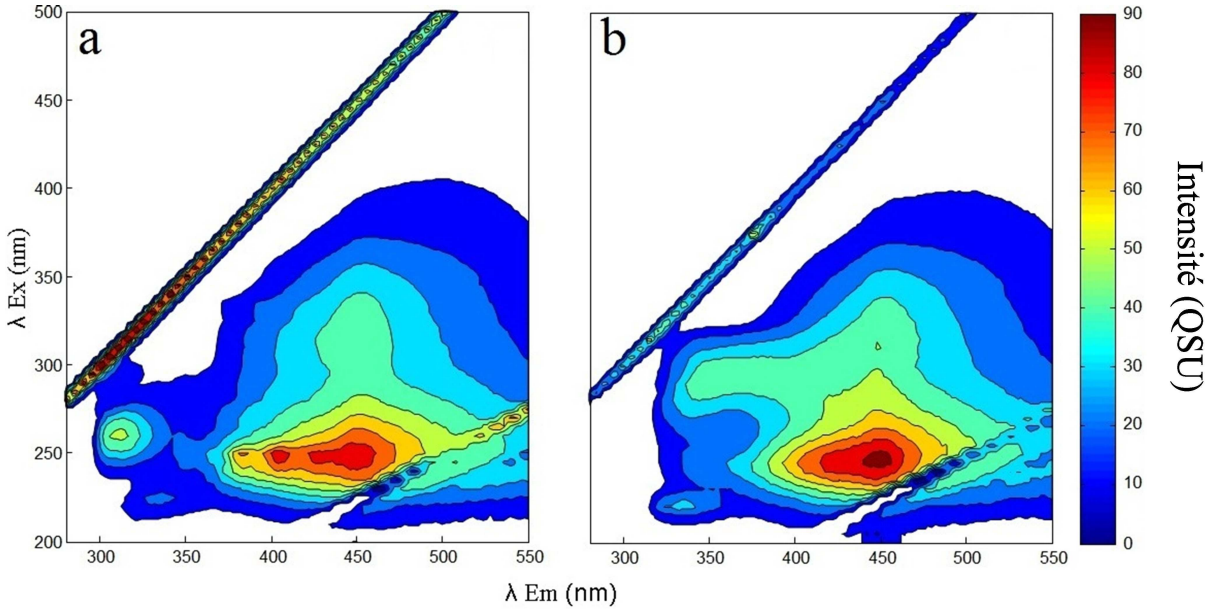

Figure III-2. Examples of excitation-emission matrix (EEM) in quinine sulphate unity, contour plots of standard mixtures in ultra pure water: A mixture of PAHs (9 compounds, each at 2 µg L^{-1}) and humics substances (humic and fulvic acids, each at 5 mg L^{-1}), and B mixture of biocides (3 compounds, each at 10 µg L^{-1}) and humics substances (humic and fulvic acids, each at 5 mg L^{-1}). Clearly, the fluorescence signatures of contaminants are totally or partially masked by those of humic substances.

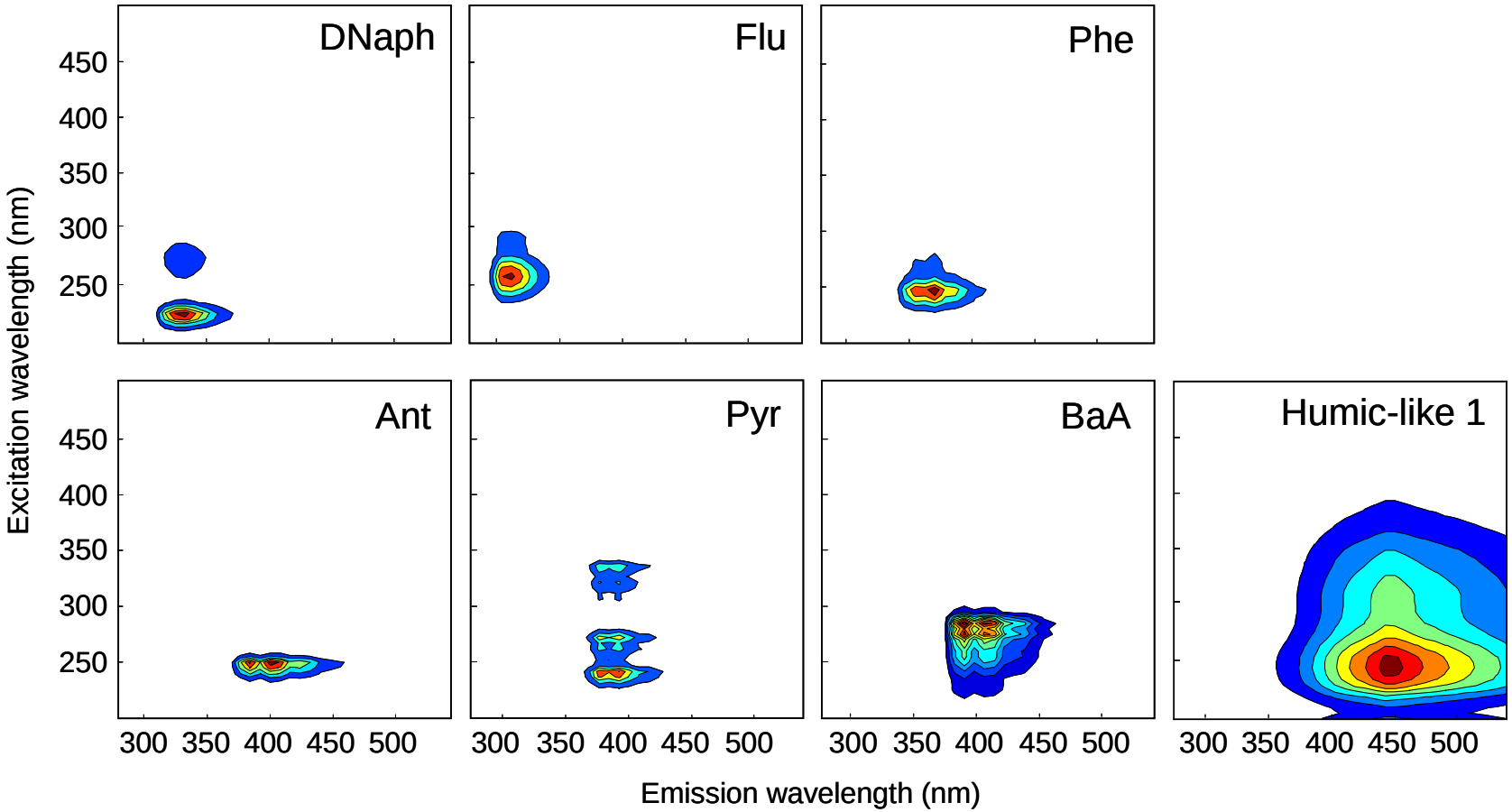

Figure III-3. Contour plots of the seven components that were validated by the PARAFAC model applied to PAH mixtures with and without humic substances plus the individual PAHs in ultrapure water (P^{T}_{PAHs}, 121 samples).

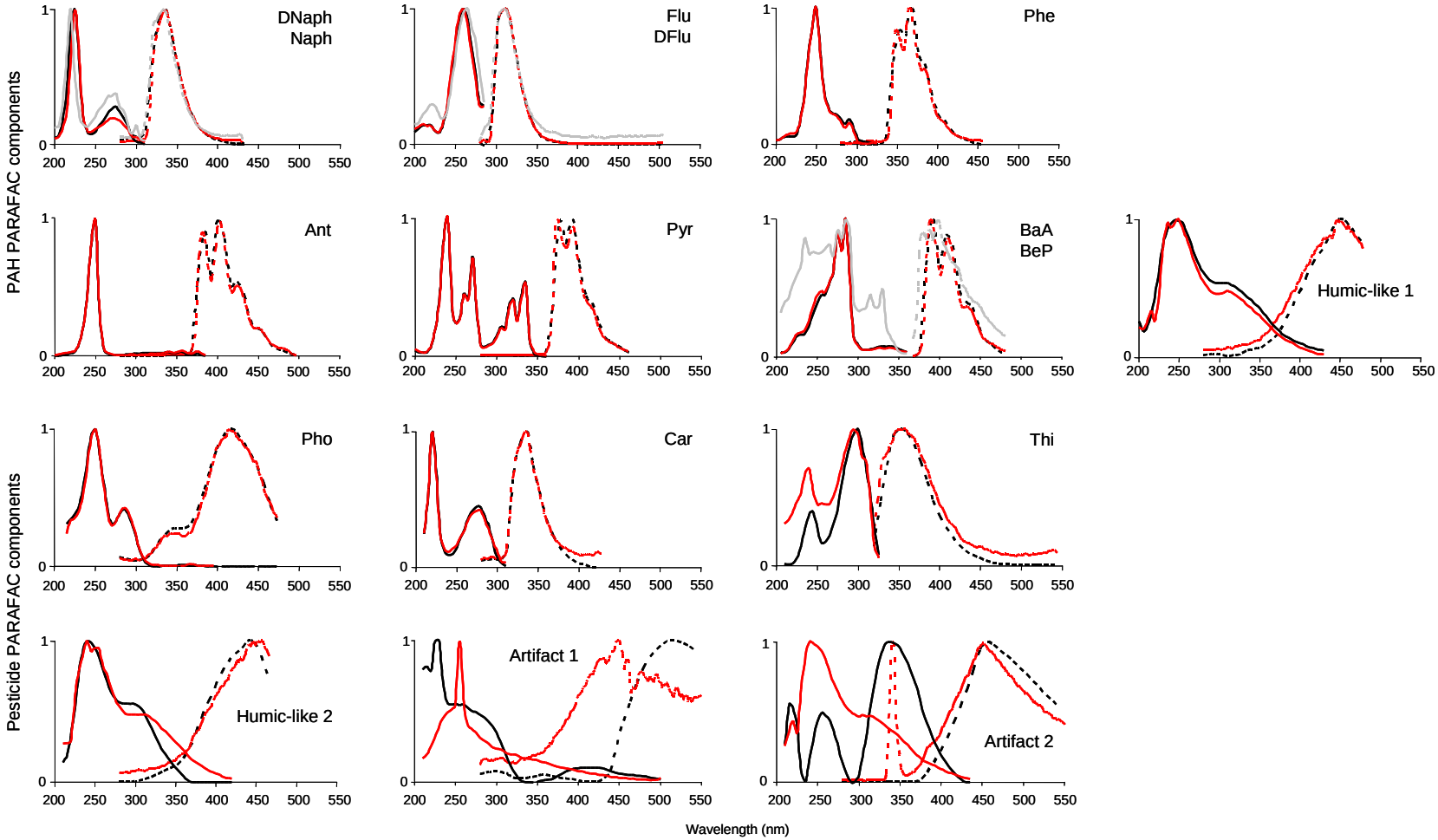

Figure III-4. Comparison between the excitation (solid line) and emission (dotted line) spectra of the PAH-, biocide- and humic-like components that were validated by the PARAFAC models (in black) and of the individual compounds that were obtained from the EEM measurements (in red) at PAH and biocide concentrations of 5 µg L^{-1} and at humic substance concentration of 1 mg C L^{-1}. The individual spectra of Naph, DFlu and BeP were also added (in grey). All spectra were normalised to their maximal intensities.

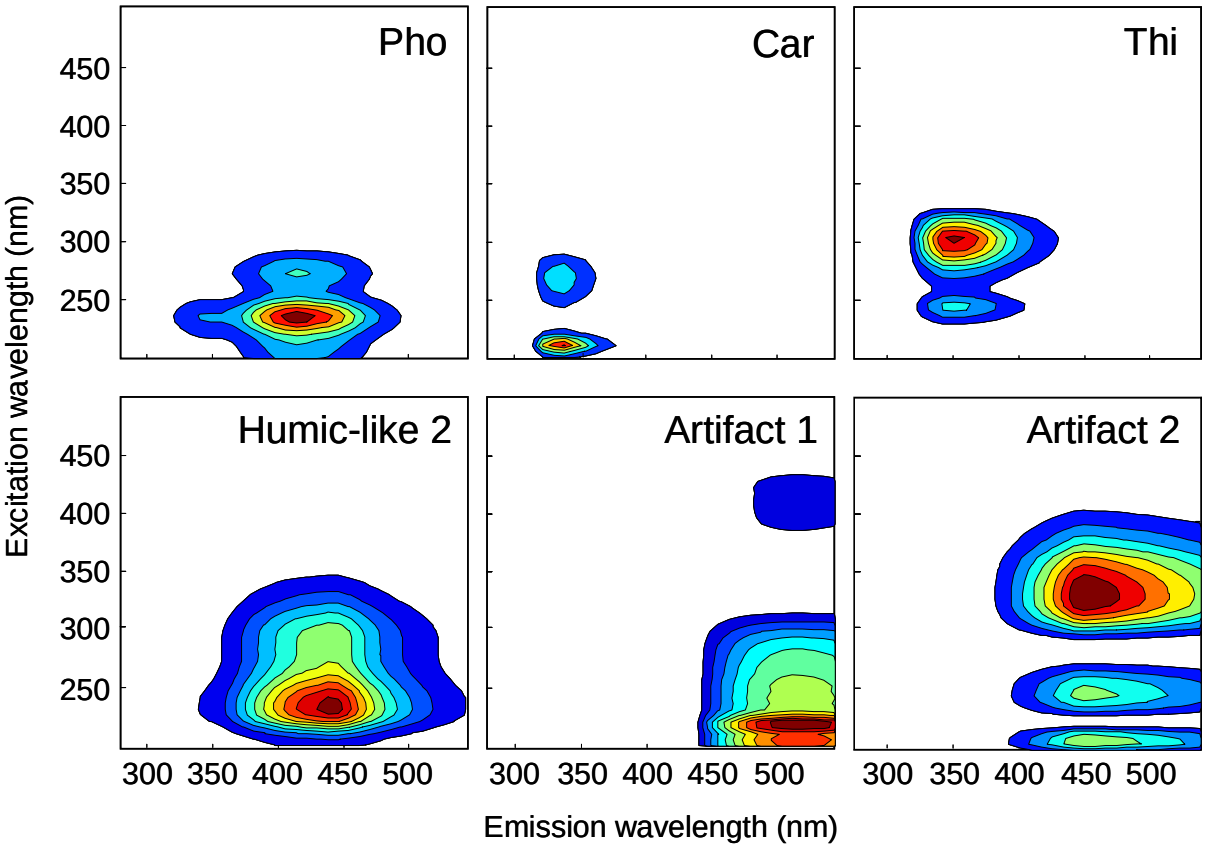

Figure III-5. Contour plots of the six components that were validated by the PARAFAC model applied to the biocide mixtures with and without humic substances plus individual biocides in ultrapure water ($P^{T*}_{biocides}$, 64 samples).

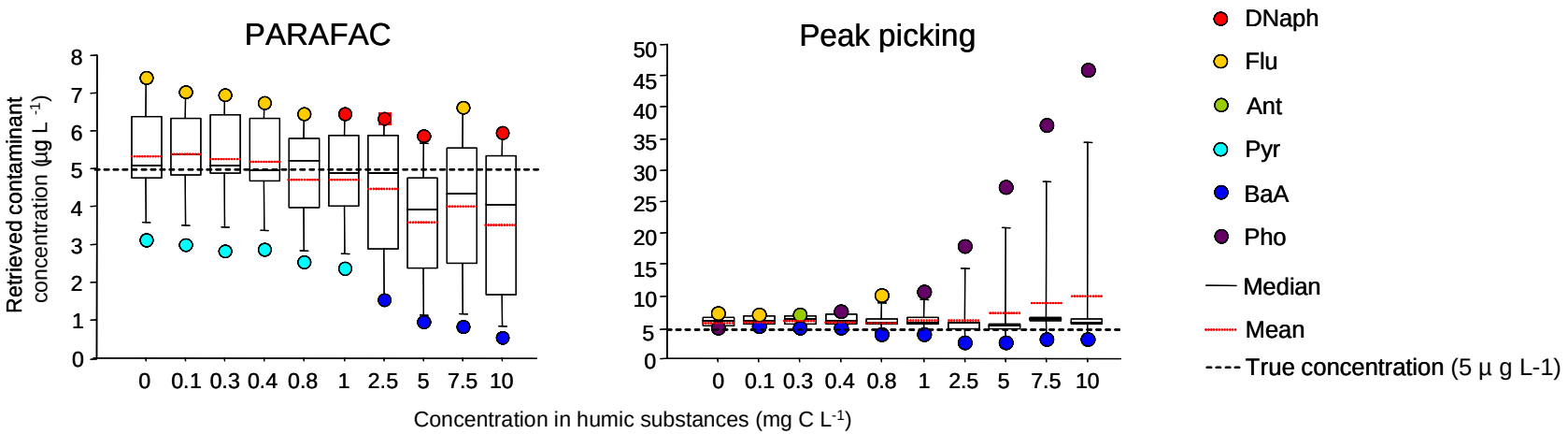

Figure III-6. Box-and-whisker plots of the PAH (DNaph, Flu, Phe, Ant, Pyr, BaA) and biocide (Pho, Car) concentrations obtained from PARAFAC and peak picking methods, with regard to the humic substance concentrations (from 0 to 10 mg C L^{-1}). These individual contaminant concentrations were retrieved from mixtures containing true contaminant concentrations of 5 µg L^{-1}. The Thi concentrations, which were greater than the other compound concentrations, are not included in this figure.

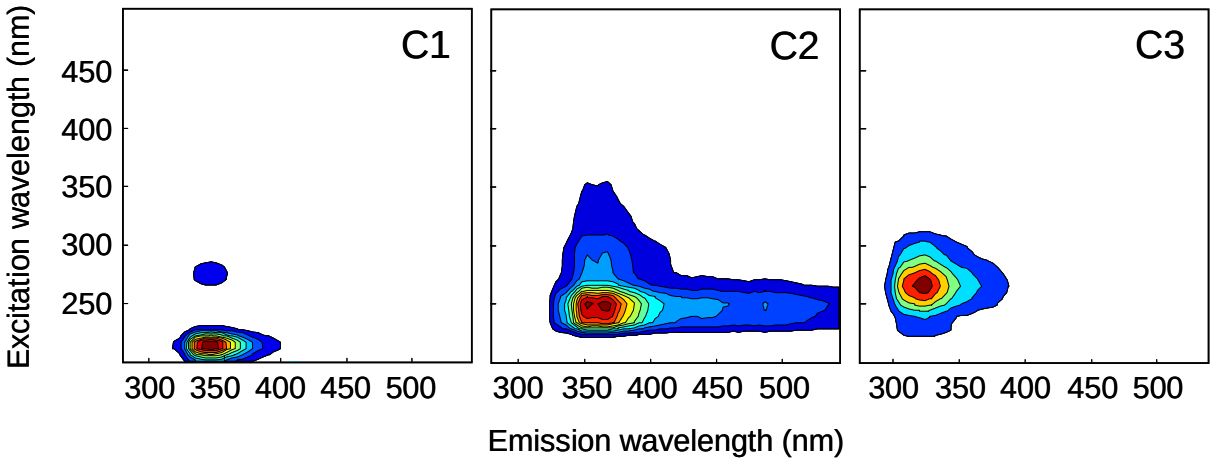

Figure III-7. Contour plots of the three components that were validated by the PARAFAC model applied to 30 marine samples collected in two harbours in the Marseilles Bay (northwestern Mediterranean Sea, France).

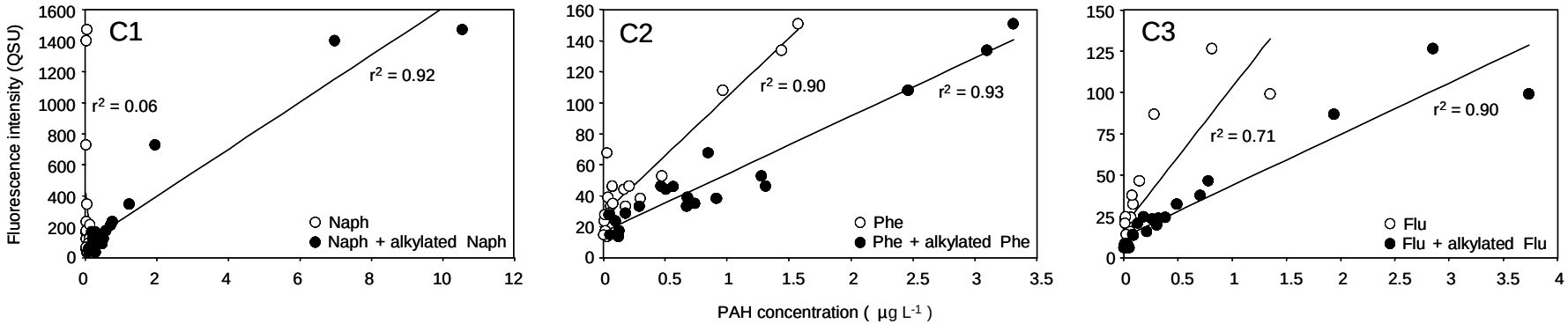

Figure III-8. Comparison between the fluorescence intensities of PARAFAC components and the concentrations of PAHs determined by GC-MS (parent Naph, Phe and Flu in white or sum of parent + alkyltated Naph, Phe and Flu in black) for marine samples collected in two harbours in the Marseilles Bay (northwestern Mediterranean Sea, France).

Table III-1. Spectral position (λ_{Ex} /λ_{Em}) and Stokes shift (λ_{Em} – λ_{Ex}) of the fluorescence maxima of the individual PAHs and biocides [*i.e*: naphthalene (Naph), 2,3 dimethyl naphthalene (DNaph), fluorene (Flu), 1,8 dimethyl-9H-fluorene (DFlu), phenanthrene (Phe), anthracene (Ant), pyrene (Pyr), benzo[a]anthracene (BaA), and benz(e)pyrene (BeP), 2-phenylphenol (Pho), carbaryl (Car), thiabendazole (Thi) and bentazone (Ben)] in ultrapure water that were obtained from the EEM measurements and peak picking technique. The linear regression parameters between the contaminant concentration (0.1-20 µg L^{-1}) and fluorescence peak intensity (QSU) are presented: slope, y-intercept, determination coefficient (r^2), detection limit (DL) and quantification limit (QL). The results from previous studies are included for comparison.

	This work							Previous studies			
PAHs and biocides	λ_{Ex} /λ_{Em} (nm)	Stokes shift (nm)	Slope (QSU L µg^{-1})	y-intercept (µg L^{-1})	r^2	DL (µg L^{-1})	QL (µg L^{-1})	λ_{Ex} /λ_{Em} (nm)	Stokes shift (nm)	Solvent	Reference
Naph	220/334	114	4.0 ± 0.1	2.4 ± 0.5	0.98	1.29	4.30	220/335	115	Water	Tedetti et al., 2010
								225/330	105	Water	Beltrán et al., 1998
	275/334	59	1.6 ± 0.0	0.9 ± 0.1	0.98	1.23	4.10	270/330	60	Water	Beltrán et al., 1998
								270/335	65	Water	Tedetti et al., 2010
								280/345	65	Water	Jiji et al., 2000
								-/327, 337	-	Cyclohexane	Karcher et al., 1985
DNaph	225/336	111	9.8 ± 0.2	3.3 ± 1.6	1.00	0.50	1.68				
	275/336	61	1.9 ± 0.0	0.8 ± 0.3	1.00	0.49	1.63				
Flu	260/310	50	26.5 ± 0.2	1.5 ± 1.8	1.00	0.20	0.68	260/310	50	Water	Beltrán et al., 1998
								270/305	35	Water	Jiji et al., 2000
								290/305	15	Water	Jiji et al., 2000
								-/306, 315	-	Cyclohexane	Karcher et al., 1985
DFlu	260/310	50	4.0 ± 0.1	0.4 ± 0.6	1.00	0.41	1.38				
Phe	250/366	116	11.5 ± 0.1	1.3 ± 0.6	1.00	0.16	0.52	245/360	115	Water	Tedetti et al., 2010

								250/360	110	Water	Beltrán et al., 1998
								270/355	85	Water	Jiji et al., 2000
								-/346.5, 356, 364, 374	-	Cyclohexane	Karcher et al., 1985
Ant	245/382	137	25.2 ± 0.5	-3.5 ± 4.0	1.00	0.53	1.75	245/380	135	Water	Beltrán et al., 1998
	245/402	157	27.1 ± 0.5	-6.3 ± 4.2	1.00	0.54	1.79	245/405	60	Water	Beltrán et al., 1998
								-/378, 399, 423, 449	-	Cyclohexane	Karcher et al., 1985
Pyr	240/374	134	22.7 ± 0.6	8.7 ± 4.7	1.00	0.62	2.06	240/375	135	Water	Beltrán et al., 1998
	240/392	152	22.0 ± 0.5	7.2 ± 4.0	1.00	0.54	1.80	240/395	155	Water	Beltrán et al., 1998
	270/374	104	16.9 ± 0.4	4.7 ± 2.8	1.00	0.50	1.67	275/375	100	Water	Beltrán et al., 1998
	270/392	122	16.2 ± 0.4	4.6 ± 2.6	1.00	0.51	1.69	275/395	120	Water	Beltrán et al., 1998
	320/374	54	9.5 ± 0.2	2.6 ± 1.5	1.00	0.47	1.57	320/375	55	Water	Beltrán et al., 1998
	320/392	72	9.3 ± 0.2	2.4 ± 1.4	1.00	0.46	1.54	320/395	75	Water	Beltrán et al., 1998
	335/374	39	12.3 ± 0.3	3.2 ± 2.0	1.00	0.48	1.60	332/372	40	Ethanol	Kalyanasundaram and Thomas, 1977
	335/392	57	12.1 ± 0.2	3.2 ± 1.9	1.00	0.47	1.56	332/390	58	Ethanol	Kalyanasundaram and Thomas, 1977
								-/371.5, 378, 383, 387.5, 392, 404	-	Cyclohexane	Karcher et al., 1985
BaA	275/390	115	14.1 ± 0.0	0.3 ± 0.2	1.00	0.06	0.19	275/390	115	Water	Beltrán et al., 1998
	275/410	135	12.1 ± 0.0	0.2 ± 0.2	1.00	0.06	0.21	275/410	135	Water	Beltrán et al., 1998
	285/390	105	15.8 ± 0.0	0.3 ± 0.3	1.00	0.06	0.20	290/390	100	Water	Beltrán et al., 1998
	285/410	125	13.4 ± 0.1	0.4 ± 0.8	1.00	0.07	0.23	290/410	120	Water	Beltrán et al., 1998
								-/387, 407.5, 433.5, 460	-	Cyclohexane	Karcher et al., 1985

BeP	275/398	123	3.3 ± 0.0	-0.02 ± 0.01	1.00	0.02	0.07	-/388, 397.5, 409.5, 420, 433	-	Cyclohexane	Karcher et al., 1985
	285/398	113	3.4 ± 0.0	-0.08 ± 0.02	1.00	0.04	0.14				
Pho	245/414	169	2.5 ± 0.0	1.1 ± 0.3	1.00	0.31	1.04	243/350	107	Ethanol	García Reyes et al., 2004
	280/414	134	1.1 ± 0.0	0.3 ± 0.1	1.00	0.15	0.50	267/350	83	Ethanol	García Reyes et al., 2004
Car	220/334	114	4.2 ± 0.0	0.6 ± 0.1	1.00	0.10	0.35	279/330	59	Methanol	Jiji et al., 1999
	275/334	59	2.1 ± 0.0	-0.2 ± 0.2	0.99	0.36	1.20	270/320	50	Methanol	Fang et al., 1998
								282/335	53	Methanol	García Reyes et al., 2004
								295/335	40	Methanol	Jia et al., 2007
Thi	240/352	112	0.7 ± 0.0	0.8 ± 0.2	0.99	0.66	2.21	250/360	110	Ethanol	García Reyes et al., 2004
	295/354	59	1.4 ± 0.0	0.2 ± 0.3	0.99	0.71	2.37	300/340	40	Methanol	Rodríguez-Cuesta et al., 2003
								301/360	59	Ethanol	García Reyes et al., 2004
Ben	245/458	204	0.02 ± 0.00	1.90 ± 0.50	100	86.30	284.20				
	330/466	136	0.01 ± 0.00	0.08 ± 0.10	1.00	36.60	121.90				

DL and QL of contaminants were calculated from the slope (*a*) and the standard deviation of the y-intercept (σ) of the equation of the linear regression between the contaminant concentration and the fluorescence peak intensity as following: $\mathrm{DL} = \frac{3\,\sigma}{a}$ and $\mathrm{QL} = \frac{10\,\sigma}{a}$.

σ was calculated according to the formula $\sigma = \sqrt{\frac{\sum (y_i - y'_i)^2}{n-2}} \times \sqrt{\frac{\sum x_i^{\,2}}{n\sum (x_i - \bar{x})^2}}$ where n is the number of samples, x_i and y_i are the contaminant concentrations and the measured fluorescence intensities, respectively, y'_i are the fluorescence intensities calculated from the linear regression equation, and $\bar{x}$ is the mean contaminant concentration.

Chapitre IV: Variabilités spatiale et saisonnière des hydrocarbures et des biocides dissous dans les eaux de surface de la mer Méditerranée Nord-occidentale

Résumé

Dans ce chapitre, une étude saisonnière de 12 mois sur la dynamique des concentrations en hydrocarbures et en biocides a été réalisée dans les eaux continentales du Rhône, de l'étang de Vaccarès, ainsi qu'en Méditerranée nord-occidentale. L'objectif était d'évaluer la distribution spatio-temporelle des hydrocarbures dissous et de deux biocides (le carbaryl et le bentazone). Les concentrations en hydrocarbures aliphatiques (HA) variaient de 0,04 à 0,53 μg L^{-1} et les concentrations en PAHs totaux variaient de 8,1 à 405 ng L^{-1}. La grande majorité des PAHs présent dans l'ensemble des échantillons sont des composés légers (2 à 3 cycles aromatiques) avec principalement les naphtalènes (parents + dérivés méthylés) qui correspondent à 49 ± 20%, les phénanthrènes (15 ± 7%) et les fluorènes (11 ± 4%). On obtient donc au maximum pour la somme des concentrations en naphtalène, phénanthrène et fluorène des valeurs respectives de 280, 60 et 10 ng L^{-1}. Les PAHs étaient plus abondants en hiver avec une augmentation qui serait liée à la combustion de composés fossiles alors que les concentrations en HAs augmentaient en été et semblaient liées à des apports atmosphériques et à des apports du Rhône. Une source pétrogénique a été identifiée dans le site de Port-de- Bouc en raison du fort trafic maritime et des activités industrielles.

Concernant les biocides, seul le bentazone a été détecté au cours de la période d'échantillonnage, et uniquement dans l'étang de Vaccarès, avec des concentrations allant de 0,046 à 0,97 μg L^{-1}. Les maximums de concentration en bentazone étaient observés au début de l'été et coïncidaient avec l'épandage des biocides pour les cultures de riz.

Spatial and seasonal variabilities of dissolved hydrocarbons and biocides in surface waters from the Northwestern Mediterranean Sea: Results from one year intensive sampling

1. Introduction

Hydrocarbons, including aliphatic hydrocarbons (AHs), polycyclic aromatic hydrocarbons (PAHs) and peticides, are among the most widespread organic contaminants found in the marine environment. Some of them are harmful to living organisms with reprotoxic, carcinogenic, mutagenic or endocrine disrupting effects (Kennish, 1992; Landau-Ossondo et al., 2009; McKinlay et al., 2008).

Hydrocarbons are introduced in the coastal marine waters mainly through atmospheric depositions, rivers, municipal/industrial effluents and surface runoffs (Tolosa et al., 1996; Lipiatou et al., 1997; Castro-Jiménez et al., 2012). Biocides have only anthropogenic origin. Inputs occurred mostly by runoff waters (Richards and Baker, 1993) but also through accidental contaminations, lixiviats and by the washing of equipment used for spreading (Konstantinou et al., 2006). They could be also introduced in aquatic environments by wet and dry depositions (Albanis et al., 1998; Charizopoulos and Papadopoulou-Mourkidou, 1999). Accumulation of these contaminants is linked to rainfall amounts, the season and to soil properties (Konstantinou et al., 2006). Biocides tend to be accumulated in surface waters and mostly in the surface microlayer (Wu et al., 1980). Reversely to biocides, hyrocarbons could have several origins. Indeed, AHs and PAHs may be both of biogenic or anthropogenic origin, although PAHs, especially in the highly urbanized and industrialized areas, are almost exclusively considered of anthropogenic origin. Moreover PAHs are sensitive indicators of petrogenic (uncombusted petroleum) and pyrogenic (incomplete combustion of fossil fuels) sources (see reviews by Wang et al., 1999; Wurl and Obbard, 2004). The uncoupling of the sources, transport and removing processes affecting these two hydrocarbon classes has already been evoked (Bouloubassi and Saliot, 1993; Wakeham, 1996). Thus, the simultaneous analysis of AHs and PAHs constitutes a powerful and indispensable approach, for the comprehensive assessment of various inputs, as well as for the determination of their environmental behaviour, especially in estuarine and coastal regions.

Because of their low water solubility, AHs and PAHs are considered to be preferentially associated with particles in the coastal marine waters. This is highlighted by the large number of studies dealing with hydrocarbons in coastal sediments and particles while hydrocarbons in

the dissolved phase of the water column have been much less investigated. However, in some systems with a low suspended matter load, the concentrations of PAHs in the dissolved phase were similar or even higher than those recorded in the particulate phase (Bouloubassi and Saliot, 1991; Guigue et al., 2011). In addition, dissolved hydrocarbons in the marine coastal environment are subjected to various transformation processes including evaporation, interactions with dissolved organic matter, biodegradation and photodegradation (Jordan and Payne, 1980; Schwarzenbach et al., 1993; Eisenreich, 2006). A better knowledge of the distribution and fate of hydrocarbons in the dissolved phase of the water column is essential for a more accurate estimation of their fluxes and budgets within marine ecosystems.

Dissolved hydrocarbons, their degradation products and pesticides could be bioconcentrated into organisms by passive diffusion and respiration (Berrojalbiz et al., 2009; 2011a, 2011b). For small organisms at the basis of many marine trophic chains, dissolved hydrocarbons are much more bioavailable and therefore more likely to have toxic effects on the biota than hydrocarbons present in particles, which are bioaccumulated through ingestion (Tilseth et al., 1984 and Akkanen et al., 2012). Documenting dissolved hydrocarbon concentrations, which data are presently scare in marine waters, is relevant for assessments of toxicological effects within coastal marine ecosystems.

Marseilles (Southern France) is the first Mediterranean harbour for goods traffic and the Marseilles-Fos petrochemical complex is the world's third oil port. Marseilles is also the second most populated city in France, and thus generates important industrial, shipping, nautical and tourism activities. Hence, the Marseilles coastal area (Northwestern Mediterranean Sea) is exposed to numerous sources of contamination such as urban and industrial wastes, petroleum inputs and atmospheric depositions from transports, pyrogenic residues, and industrial and harbour activities. Moreover, the Marseilles coastal area is highly influenced by the Rhône River, which is the most significant source of freshwater in the Mediterranean Sea (Durrieu de Madron et al., 2003; Pairaud et al., 2011). Indeed, the Rhône River is the largest French river in terms of water discharge, and represents a considerable transport pathway for contaminants to the marine environment (Olivier et al., 2009). Before to reach the sea, the Rhône River forms a delta where intensive agricilture occurs. Hence, Rhône waters may be deviated to irrigate rice cultures. By means of a channel system, fields are irrigated and the ultimate receptacle is the Vaccarès Pond, which is connected to the sea. This area may be subjected to pesticides and hydrocarbons released from nearby agricultural and industrial activities (Hélène Roche et al., 2002; Comoretto et al., 2007; Chiron et al., 2009; H.

Roche et al., 2009). Numerous works have reported the concentrations of hydrocarbons and pesticides in waters, fishes and sediments from the Northwestern Mediterranean Sea (Benlahcen et al., 1997; Borrell et al., 2007; Dachs et al., 1997, 1999; Lipiatou et al., 1997; Pérez et al., 2003; Wafo et al., 2006; Mille et al., 2007; Dierking et al., 2009; Berrojalbiz et al., 2011a, 2011b; Munaron et al., 2012; Salvadó et al., 2013) and in fishes, waters of the Rhône delta for pesticides (Ribeiro et al., 2005; Buet et al., 2006; Comoretto et al., 2007; Chiron et al., 2009; Roche et al., 2009). However little is known about the concentrations of dissolved AHs and PAHs in surface water of the Rhône River (Sicre et al., 2008), the Rhône Delta (Bouloubassi et Saliot, 1991, 1993) and the Bay of Marseilles (Marty et Saliot, 1976; Siron et al., 1987, Guigue et al., 2011). Concerning the biocides few informations are available on concentration (Munaron et al., 2012) and nothing about their seasonal trend in north-Mediterranean Sea. The main objectives of the present work are (i) to assess the spatial and temporal variabilities of dissolved contaminants in the surface water of the Marseilles coastal area in term of concentration, molecular composition, origin and fate and (ii) to better understand the influence of the Rhône River on their distribution.

2. Material and methods

2.1. Study sites

Two continental (Arles and Vaccarès) and three marine (Port-de-Bouc, Couronne and Sofcom) sites were studied in the Marseilles coastal area neighbouring according to their different potential levels and sources of contamination (Figure IV-1; Table IV-1). Arles station (AR) is located in the Rhône River, which is 812 km long and has a drainage basin of approximately 97,800 km^2. The Rhône delta has a surface area of ~1750 km^2 and is composed mainly of wetlands, ponds and salt marshes. The central part of the delta, known as the 'Camargue' (~ 750 km^2), comprises farmlands and salted ponds. The Vaccarès pond (VA, 12 km long, 6,500 km^2, < 2 m depth) is the largest pond of Camargue. It is the main element of the control system of the Rhône delta waters. VA is thus directly under the influence of the Rhône River. It is also subjected to pesticides and hydrocarbons from agricultural operation and nearby industrial areas such as the Marseilles-Fos petrochemical complex through atmospheric transport.

Port-de-Bouc (PB) is a harbour situated in the Gulf of Fos-sur-mer and surrounded by the Marseilles-Fos petrochemical complex, which includes several chemical, petroleum and steel-work plants. The Gulf of Fos-sur-mer receives some freshwater inputs coming from the

Rhône River and the Berre Lagoon (Ulses et al., 2005). In addition, PB is positioned on the route of oil cargo ships going to the Berre Lagoon through the Caronte channel. Couronne (CO) is a nearshore site off PB. CO is located close to the Rhône River plume whose extent depends on Rhône water discharges and wind conditions (Pairaud et al., 2011). Sofcom (SO), situated in the Bay of Marseilles near the Frioul Islands (~ 7 km off Marseilles), is a nearshore observation site of the national Service d'Observation en Milieu LITtoral (SOMLIT; http://www.domino.u-bordeaux.fr/somlit_national/). It is located much farther from the Rhône River and was selected as marine reference by comparison to the other anthropogenically impacted sites.

2.2. Sampling strategy

All sites were sampled around bi-monthly from February 2011 to February 2012 in the morning between 8:00 and 12:00 am (Table IV-1). Freshwater samples (AR and VP) were taken directly from the edge while marine samples (PB, CO and SO) were collected from the R/V Antédon II. AR, VA and PB were sampled only at 0.1 m depth (subsurface water, SSW) whereas offshore marine sites were sampled at 0.1 (CO s and SO s) and 5 m depths (CO 5 m and SO 5 m). SSW samples were collected directly in 4 L Nalgene® polycarbonate bottles. The bottles were opened below the water surface to avoid the sampling of the surface microlayer. Five m depth samples were taken by means of a 5 L Niskin bottle equipped with silicon ribbons and Viton o-rings. They were then transferred into Nalgene® bottles. The bottles were washed with 1 M hydrochloric acid (HCl) and ultrapure water (i.e. Milli-Q water from Millipore system, final resistivity: 18.2 MΩ cm^{-1}) before use, rinsed three times with the respective sample before filling and stored in the dark in the cold (4-8 °C).

2.3. Filtration of samples

Back in the laboratory, samples were immediately filtered under a low vacuum (< 50 mm Hg) through precombusted (500 °C, 4 h) GF/F (~ 0.7 µm) glass fiber filters (47 mm diameter, Whatman) using polysulfone filtering systems for hydrocarbons (AHs and PAHs) and all-glassware systems for biogeochemical parameters, i.e. nitrates (NO_3^-), chlorophyll *a* (Chl *a*) and particulate organic carbon (POC). The hydrocarbons present in the particulate matter, which was retained on the filters, are not presented here. The material that passes through GF/F filters consists in truly dissolved and colloidal matters which can be each subjected to specific processes (Gustafsson and Gschwend, 1997). However, as it is difficult to separate operationally these two fractions and despite of the bias, most of the environmental studies

(including the present one) consider the material presents in GF/F filtered water simply as the 'dissolved matter'. It is worth noting that hydrocarbon concentrations in the truly dissolved phase would be lower than those reported afterward. Filtered samples for dissolved hydrocarbon analyses were stored in 2 L SCHOTT® glass bottles with 50 mL dichloromethane (CH_2Cl_2) at 4 °C in the dark before solvent extraction (within 48 h). Filtered samples for NO_3^- and filters for Chl *a* and POC were stored frozen until analysis. During the experiments and analyses, gloves were worn and care was taken to avoid contaminations. All the glassware was washed with 1 M HCl and ultrapure water and combusted at 500 °C during 4 h. All the materials that could not be baked were washed with 1 M HCl and ultrapure water and dried at room temperature.

2.4 Biocide extraction

Dissolved biocides present in the fraction < 0.7 µm were extracted from water by solid phase extraction (Oasis HLB 500 mg, Waters). pH was adjusted to 7. Cartridges were eluated successively with 3 mL of acetate ethyl (Rathburn HPLC grade) and 10 mL of methanol (Rathburn HPLC grade). The eluate was evaporated at 40 °C under nitrogen and dissolved in 200 µl of methanol.

2.5. Hydrocarbon extraction and purification

Dissolved hydrocarbons present in the fraction < 0.7 µm were extracted from water by liquid-liquid extraction with CH_2Cl_2 (2 x 80 mL per litter). Organic phases were combined and evaporated on a rotary evaporator. Prior to purification, solvent was change to *n*-hexane. Hexane solubilised extracts were then purified to separate AHs (fraction 1, F1) from PAHs (fraction 2, F2). Extracts were fractionated on a 500 mg silica column. Silica gel (extra pure, Merck) was activated at 500 °C for 4 h followed by partially deactivation with 4% water by weight. F1 was eluted with 2 mL *n*-hexane while F2 was eluted with 3 mL *n*-hexane/CH_2Cl_2 (3:1 v/v). All solvents were of organic trace analysis quality (Rathburn, Interchim).

2.6. Analysis of biocides by LC-MS-MS

Biocides were analysed by LC-MS-MS. The system included one column C-18 150 x 2 mm with a particle size of 3 µm (Varian, California) and a mass spectrum triple quadripole (Varian, California) equipped with an interface electrospray. Mass detection was conducted in negative ionisation mode for bentazone and in positive ionisation mode for carbaryl. The mobile phase for negative ionisation was a binary mixture of methanol (eluent A) and with a solution of formic acid (eluent B) (Rathburn HPLC grade) at 0.07%. For the positive

ionisation, the mobile phase was a binar mixture of acetonitril with 0.01% of formic acid (eluent C) and a solution of formic acid at 0.01% (eluent D). For the negative ionisation mode, a gradient of mixture from 400 to 100% of the eluent A was injected during 30 minutes. Next, a mixture of the eluent A at 40% was introduced during 5 minutes. For the positive ionisation, the eluent D was introduced during 5 minutes. During the next 3 minutes, a mixture of both eluent containing eluent D at 100 % decreased to 70% during 3 minutes. During the next 25 minutes, only the eluent C was injected. The next step consisted of adding during 5 minutes a mixture of eluent C and D from a composition of 100 to 0% of the eluent C. The flow rate was 0.2 mL min^{-1}. The detection limit was 0.01 μg L^{-1} for both biocides.

2.7. Analysis of hydrocarbons by gas chromatography (GC-MS)

Both F1 and F2 fractions were concentrated under a gentle stream of nitrogen and analyzed by gas chromatograph-mass spectrometer (GC-MS) (TraceISQ, ThermoElectron) operating at an ionization energy of 70 eV for a m/z range of 50-600, using hydrogen as carrier gas at a flow rate of 1.2 mL min^{-1}. The injector (used in splitless mode) and detector temperatures were 250 and 320 °C, respectively. The initial column temperature was held for 3 min at 70 °C, then ramped at 15 °C min^{-1} (ramp 1) to 150 °C and then at 7 °C min^{-1} (ramp 2) to a final temperature of 320 °C, which was held for 10 min. Data were carried out using selected ion monitoring (SIM) mode.

2.8. Determination of hydrocarbon indices and ratios

For AHs, we determined R, which corresponds to the sum of the concentrations of the resolved *n*-alkane series from *n*-C_{15} to *n*-C_{36} with two isoprenoids, pristane (Pr) and phytane (Phy). We also determined the UCM concentrations by integrating the hump (when present) using the mean response factor of the resolved compounds (relationship between the area of the peak and the mass of each AH). The UCM hump corresponds to a mixture of many structurally complex isomers and homologues of branched and cyclic hydrocarbons that cannot be resolved by capillary GC columns (Bouloubassi and Saliot, 1993). Its relative importance, expressed as the ratio of unresolved to resolved compounds (UCM/R), is commonly used as diagnostic criteria of pollutant inputs (Mazurek and Simoneit, 1984).

Concerning PAHs, we determined the concentrations of 17 parent PAHs (PAHs-$_P$), namely naphthalene (Naph), acenaphthylene (Acy), acenaphtene (Ace), fluorene (Flu), dibenzothiophene (DBT), phenanthrene (Phe), anthracene (Ant), fluoranthene (Flt), pyrene (Pyr), benz[*a*]anthracene (BaA), chrysene (Chr), benzo[*b*]fluoranthene (BbF),

benzo[*k*]fluoranthene (BkF), benzo[*a*]pyrene (BaP), dibenz[*a,h*]anthracene (DBA), benzo[*g,h,i*]perylene (BP), indeno[1,2,3-*cd*]pyrene (IndP), as well as the concentrations of alkylated homologues (methyl = C_1, dimethyl = C_2, trimethyl = C_3) of the five target compounds Naph, Flu, Phe, Pyr and Chr, which lead to a total of 32 PAHs (PAHs-$_{P+A}$). Naph, Acy, Ace, Flu, DBT, Phe and Ant are low molecular weight (LMW) compounds (2-3 rings) while Flt, Pyr, BaA, Chr, BbF, BkF, BaP, DBA, BP and IndP are high molecular weight (HMW) compounds (4-6 rings). In order to assess the contamination sources (petrogenic or pyrogenic), we determined the isomer ratios Phe/Ant and Flt/Pyr but also Alk/Par ratio (Azimi et al., 2005; Budzinski et al., 1997; Mille et al., 2007; Readman et al., 2002).

2.9. Quality assurance/Quality control

Deuterated standard mixtures (C_{16}-d_{34}, C_{24}-d_{50}, C_{36}-d_{74} for AHs, and Naph-d_8, Phe-d_{10}, Per-d_{12} for PAHs) were introduced prior to extraction, as well as a supplementary deuterated standard before injection, and used as surrogates to assess the recoveries of analytical procedures and to perform quantitation accuracy. The C_{16}-d_{34}, C_{24}-d_{50} and C_{36}-d_{74} average recoveries were of 30, 63 and 85%, respectively, while Naph-d_8, Phe-d_{10}, Per-d_{12} average recoveries were of 38, 74 and 88%, respectively. Cautions were taken during the evaporation under nitrogen because dryness could lead to the total loss of the more volatile compounds. In addition, blanks were run for the whole procedure including extraction, solvent concentration and purification. They ranged from 0.02 to 0.03 µg L^{-1} and from 3.3 to 4.1 ng L^{-1} for AHs and PAHs, respectively. All concentration values were blank and recovery corrected. Detection limits for individual compounds varied from 1 to 30 pg.

Compounds were identified and quantified by reference to the analysis of standard mixtures (04071, Fluka and 47543-U, Supelco among others). Calibration curves were constructed for all target compounds analysed except for the alkylated homologues that were quantified with their parent compound calibration curves. The calibration was performed in SIM mode. The correlation coefficients were > 0.99 for all the compounds studied.

Samples were treated and analysed as the sampling was performed. Variations in calibration curves over one year study were not significant (including after maintenance operations, i.e essentially consumable changes). However, at the end of the study, a few samples from each sites and seasons were injected again under exactly the same conditions to confirm the spatial and temporal variabilities of the results.

2.10. Ancillary data

For marine sites, profiles of temperature and salinity were obtained from a 19*plus* conductivity temperature depth (CTD) profiler (Seabird Electronics Inc., USA). Because the deployment of the CTD profiler was not possible in shallow freshwaters, salinity at AR and VA was measured on 0.1 m depth discrete samples using a refractometer (MASTER-S/Millα, Atago, Tokyo).

Concerning biogeochemical parameters, NO_3^- were analyzed using an automated colourimetric method (Aminot and Kérouel, 2007). The detection limit was 0.05 µM. Chl *a* was analyzed by fluorescence method following a methanol extraction (Raimbault et al., 2004). POC was determined using wet-oxidation procedure of Raimbault et al. (1999a).

2.11. Statistics

A one-way analyse of variance (ANOVA) performed with StatView 5.0 was used to compare the means of independent data groups (normally distributed). The significance threshold was set at $p < 0.05$.

3. Results

3.1. Hydrological and biogeochemical description of the study sites

Hydrological and biogeochemical data are reported in Table IV-2. The lowest salinities were found in the continental sites. They were stable at AR (0) and ranged from 0 to 15 at VA. These latter values confirmed the (natural or anthropogenically constrained) mixing between the Rhône River waters and the Mediterranean marine waters. At PB, CO s and CO 5 m, salinity ranged 24.8-36.8, 34.7-38.1 and 37.3-38.0, respectively, which pointed out Rhône water intrusions in these sites. On the contrary, at SO salinity values (37.7-38.2, except on 12/12/2011) were typical of Mediterranean marine waters.

POC concentrations ranged from 6.0 to 125 µM (flood) and from 12 to 278 µM at AR and VA, respectively. For marine waters, POC concentrations ranged from 6.0 to 39 µM at PB, from 2.1 to 83 µM at CO s, from 1.9 to 33 µM at CO 5 m, from 1.4 to 12.5 µM at SO s and from 1.2 to 9.0 µM at SO 5 m.

NO_3^- concentrations ranged from 69 to 125 µM and from 0.75 to 34 µM at AR and VA, respectively. For marine waters, NO_3^- concentrations ranged from 0.04 to 13 µM at PB, from

0.0 to 13 µM at CO s, from 0.0 to 3.7 µM at CO 5 m, from 0.0 to 2.1 µM at SO s and from 0.0 to 2.4 µM at SO 5 m.

Chl *a* concentrations ranged from 0.41 to 16 µg L^{-1} and from 0.51 to 26 µg L^{-1} at AR and VA, respectively. For marine waters, Chl *a* concentrations ranged from 0.62 to 5.7 µg L^{-1} at PB, from 0.20 to 3.2 µg L^{-1} at CO s, from 0.29 to 1.3 µg L^{-1} at CO 5 m, from 0.16 to 2.2 µg L^{-1} at SO s and from 0.21 to 1.8 µg L^{-1} at SO 5 m.

With regard to these hydrological and biogeochemical characteristics, it appears that the study sites were quite different one from another, except CO and SO. Salinity was negatively correlated to POC, NO_3^- and Chl *a* ($r = -0.49 – -0.74$, $p < 0.0001$, $n = 117$), while Chl *a* was positively correlated to POC and NO_3^- ($r = 0.20\text{-}0.66$, $p < 0.001\text{-}0.03$, $n = 117$). These results confirmed that the Rhône River is a source of nutrients and drains large amounts of material (both dissolved and particulate) and that hydrological and biogeochemical parameters may be used as tracers of the Rhône River plume, either by direct inputs (lower salinities associated with increases in POC, $NO_3^-$and/or Chl *a* concentrations), or by inducing *in situ* primary production (Pujo-Pay et al., 2006). Because of the geomorphology of the drainage basin, VA and PB were intensively impacted by the Rhône River (Ulses et al., 2005). CO, located off PB, and SO were impacted occasionally (salinity < 37.8) under specific wind conditions (Pairaud et al., 2011) and quite weakly (Para et al., 2010), respectively, by the Rhône River plume.

3.2. Spatial and seasonal variations of dissolved biocides

Throughout the sampling period, in each of the investigated sites, carbaryl concentrations were lower than the detection limit (<0.01 µg L^{-1}), reflecting the law use of this biocide in the studied area. The bentazone was only brought out in VA with concentrations ranging from 0.022 à 0.97 µg L^{-1} with a mean value of 0.20 ± 0.29 µg L^{-1} (Figure. IV-2). This contaminant was detected throughout the year with a peak of contamination at the begining of the summer between the 27 June and the 18 July (0.71-0.97 µg L^{-1}) where the contamination in biocides generally increased in the environment (Chiron et al., 2009; Comoretto et al., 2007; Griffini et al., 1997). This concentration level at this period was in agreement with results obtained in a previous study with an increase of the bentazone abundance between the 1st and the 30 June (1.8-0.69 µg L^{-1})(Comoretto et al., 2007). Considering the concentration threshold of 1 µg L^{-1} defined by the European Council for drinking water (98/83/CE), bentazone concentrations measured in this site suggest that VA lagoon was sporadicaly contaminated by this biocide

which could impact the biota. The absence of correlation between this contaminant and others biogeochemical parameters affirmed that bentazone come from the spreading of pesticides and eliminated other source like particles desorption linked to sediment resuspension.

3.3. Spatial and seasonal variations of dissolved AHs

3.3.1. Concentration levels

At all sites, the concentrations of resolved alkanes (R) ranged from 0.04 to 0.58 µg L^{-1} (mostly < 0.30 µg L^{-1}; Table IV-3). No significant differences were found for R concentrations, neither between 0.1 and 5 m depths at CO and SO ($p = 0.52$, $n = 14$), nor within the five sites ($p = 0.07$-0.95, $n = 13$-29). R concentrations were not correlated to hydrological and biogeochemical parameters ($r = -0.10$-0.10, $p = 0.31$-0.69, $n = 105$) during the sampling period. However, they were significantly lower in summer compared to the other 3 seasons ($p = 0.0013$-0.05, $n = 24$-30), which exhibited comparable values ($p = 0.17$-0.69, $n = 24$-30), suggesting less inputs and/or more removing processes during the warmer months.

3.3.2. Composition patterns and ratios

AH composition patterns are presented in Figure IV-3. They displayed bimodal distributions showing spatial and seasonal alternations. For the lighter compounds (< *n*-C_{20}), patterns exhibited very variable maximum alternating between *n*-C_{16}-*n*-C_{17}+Pr (from spring to fall) and *n*-C_{19} (fall and winter) as well as a general depletion in *n*-C_{18}. For the heavier compounds (≥ *n*-C_{20}), patterns were centred on *n*-C_{28}-*n*-C_{30}. In spring and winter, all sites exhibited predominance (more or less marked) of even over odd carbon numbered *n*-alkanes in the range *n*-C_{20}-*n*-C_{36} especially at offshore sites (CO and SO). This predominance tended to reduce/disappear in summer and fall at AR, VA and PB but remained visible at CO and SO. Thus, even *n*-alkane predominance was related to season and affected riverine waters as well as marine sites with no river influence. Besides, one can notice the dominance of *n*-C27, *n*-C29, *n*-C31 typically originating from epicuticular waxes of higher plants in fall at VA (Douglas and Eglinton, 1966). Finally UCM was noticeable in the range 0.13-1.6 µg L^{-1} with UCM/R ratios varying from 0.51 to 5.7. UCM occurrences were too scarce to perform statistical tests.

3.4. Spatial and seasonal variations of dissolved PAHs

PAHs-$_P$ (sum of 17 parent PAHs) and PAHs-$_{P+A}$ (sum of PAHs-$_P$ + alkylated homologues of 5 target PAHs) concentrations are reported Table IV-4. Although PAHs-$_P$ represent essential data to assess a preliminary level of hydrocarbon contamination in the environment and to establish comparisons with literature data, PAHs-$_{P+A}$ are more relevant to investigate more deeply the distribution and dynamics of hydrocarbons (Wang and Fingas, 1995) as well as to assess their toxicological effects on marine ecosystems. While both PAHs-$_P$ and PAHs-$_{P+A}$ concentrations are described, statistical tests and distribution patterns were performed only on the PAHs-$_{P+A}$ dataset.

3.4.1. Concentration levels

The potential enrichment in aromatic compounds due to alkylated homologues (PAHs-$_{P+A}$/PAHs-$_P$) varied from 1.3 to 3.9. PAHs-$_P$ and PAHs-$_{P+A}$ concentrations ranged from 6.1 to 101 ng L^{-1} and from 12 to 241 ng L^{-1}, respectively at AR, while they varied from 9.4 to 115 and from 15 to 360 ng L^{-1}, respectively at VA. At marine sites, PAHs-$_P$ and PAHs-$_{P+A}$ concentrations ranged from 6.3 to 135 ng L^{-1} and from 13 to 364 ng L^{-1}, respectively at PB, while they varied from 4.8 to 151 ng L^{-1} and from 8.1 to 324 ng L^{-1}, respectively at COU (both depth) and from 4.7 to 80 ng L^{-1} and from 8.9 to 217 ng L^{-1}, respectively at SO (both depth). It is worth noting that on 07/07/2012, sporadic high values were recorded at PB and CO showing a specific contamination. Correspondingly to AHs, no significant differences were recorded for PAHs-$_{P+A}$ concentrations between 0.1 and 5 m depths at CO and SO ($p = 0.80$, $n = 36$) but, contrary to AHs, significant differences were found among sites. PAHs-$_{P+A}$ concentrations were higher at PB than at the other 4 sites ($p = 0.0012$-0.03, $n = 17$-38) while AR, VA, CO and SO depicted no difference from each other ($p = 0.08$-0.96, $n = 17$-38). In addition, PAHs-$_{P+A}$ concentrations were higher in winter than during the other 3 seasons ($p = < 0.001$-0.003, $n = 26$-44) while no significant differences were found between spring, summer and fall ($p = 0.26$-0.76, $n = 26$-44). PAHs-$_{P+A}$ concentrations were not correlated to hydrological and biogeochemical parameters ($r = -0.37$-0.03, $p = 0.65$-0.99, $n = 17$-38).

3.4.2. Composition patterns and ratios

Spatial and seasonal variations of the PAHs-$_{P+A}$ composition patterns are presented in Figure IV-4. These patterns were highly dominated by light compounds (2-3 rings). On the whole dataset, 2-3 ring compounds represented 90 ± 5% of PAHs-$_{P+A}$, for which naphtalenes (sum of Naph, C_1-Naph, C_2-Naph and C_3-Naph) were the major components (49 ± 20%) followed by

phenanthrenes and fluorenes (15 ± 7 and 11 ± 4%, respectively). Moreover, heavy compounds like C_2- and C_3-Pyr, C_1-, C_2- and C_3-Chr, BbF, BkF, BaP, DBA, BP and IndP were almost never detected. Interestingly, spatial and seasonal variation patterns were due mainly to the distribution within naphtalenes. The similar seasonal evolution in the PAHs-$_{P+A}$ composition at AR, VA, CO and SO suggested a common dynamics at these sites. On the contrary, at PB, the composition patterns were different from the other sites and between seasons (alternating dominance between Naph and its alkylated homologues). This pointed out more local and various sources. Besides, on 07/07/2011, the PAHs-$_{P+A}$ composition exhibited unusual profiles at PB, CO s and CO 5 m with Naph reaching 49, 52 and 61% of PAHs-$_{P+A}$, respectively, followed by C_1-Naph, C_2-Naph, C_3-Naph in a decreasing order (sum of naphtalenes = 82-91%). These latter patterns associated with the high concentration levels, can be explained by a sporadic spillage from industrial activities and/or the use of light oil (e.g. gasoline) shortly before.

At all sites, Phe/Ant ratios ranged from 3.9 to 19 and were lower in winter than in spring and summer ($p = 0.0002$-0.004, $n = 26$-44) while Flt/Pyr ratios ranged from 0.1 to 1.3 and were higher in winter than in fall ($p = 0.007$, $n = 30$-44). In addition, at all sites, Alk/Par ratios were 1.2 ± 0.6 and were higher in winter ($p < 0.0001$-0.0203, $n = 26$-44). Figure IV-5 presents the cross plot between Phe/Ant and Flt/Pyr ratios. From April to November 2011 (spring to fall), when PAH concentrations were the lowest, hydrocarbons were rather of strictly petrogenic origin. In February-March 2011 and from December 2011 to February 2012 (late fall and winter), when PAH concentrations were the highest, mixed origin PAHs dominated.

3.5. Relationship between dissolved AHs and PAHs-$_{P+A}$

When considering the whole data set, AH and PAHs-$_{P+A}$ concentrations were not correlated ($r = -0.1$, $p = 0.33$, $n = 105$). In addition, sporadic increases in concentrations of one hydrocarbon class were not associated with fluctuations from the other class. For instance, the higher AH values at offshore sites (both depth) on 21/09/2011, along with low $CPI_{21\text{-}33}$ values especially at CO, were not associated with an increase in PAHs-$_{P+A}$ concentrations. In the same way, the PAHs-$_{P+A}$ contamination observed on 07/07/2011 as well as the higher PAHs-$_{P+A}$ values recorded in winter were not combined with a rise in AH concentrations.

4. Discussion

4.1. Significance of AH and PAH concentrations

Due to their hydrophobic properties, it is considered that AHs are preferentially adsorbed onto particles, thus dissolved *n*-alkane concentrations are less widespread than dissolved PAH concentrations in the literature (Cincinelli et al., 2001; Stortini et al., 2009). Comparison with the literature must be used with caution because the number of studied compounds as well as the segregation between the particulate and the dissolved phases may vary between authors. Considering this, the concentrations reported in this study for a series of resolved C_{15}-C_{36} *n*-alkanes and 2 isoprenoids (0.04-0.53 µg L^{-1}) are in the same range than those recorded in Antarctic surface waters (0.11 to 0.30 µg L^{-1}; Stortini et al., 2009), in the coastal Tyrrhenian Sea (0.14-0.82 µg L^{-1}; Cincinelli et al., 2001) and in the Marseilles coastal waters (0.04-0.41 µg L^{-1}; Guigue et al., 2011). It appears surprising to record levels comparable to those from Antarctic surface waters for which there are no major local anthropogenic sources. However, the authors of this study explain that slightly higher AH concentrations in the Gerlache Inlet Sea may originate from phytoplankton as well as research station activities and shipping. In addition, long range atmospheric transport and subsequent depositions associated with a sequestration by low water temperatures and degradation processes of lower magnitude, as it has been highlighted for the Arctic (Macdonald et al., 2000), may be an additional explanation. In addition, dissolved AH concentrations of the present study were one order of magnitude higher than those reported for the Northwestern Black Sea (0.012- 0.05 µg L^{-1}, Maldonado et al., 1999) but they were one order of magnitude lower than those measured by Marty and Saliot, (1976) for the Northwestern Mediterranean Sea (0.70-2.4 µg L^{-1}). One can assume that this decrease in AH concentrations might be linked to the MARPOL 73/78 convention, adopted in 1973 and modified several times so far, which deals with the prevention of the hydrocarbon pollution from tankers. Indeed, over the last 40 years, accidental spills of hydrocarbons from ships have been reduced by a factor four in the world ocean. Moreover, since 1987, the Marseilles sewage treatment plant treats wastewaters and run-offs from low rain waters (diverting rivers, such as the Huveaune River that previously flowed into the coastal waters, Figure IV-1) from Marseilles and 15 surrounding municipalities. The effluent, after several treatment levels including oil removing, flows into the Cortiou creek in the South Bay of Marseilles.

The dissolved PAH concentrations (PAHs-$_P$: 4.7-151 ng L^{-1}; PAHs-$_{P+A}$: 8.1-405 ng L^{-1}) from these Northwestern Mediterranean surface waters were of the same order of magnitude than those previously recorded in this area (Bouloubassi and Saliot, 1991; Tedetti et al., 2010; Guigue et al., 2011) and in other Mediterranean coastal waters (El Nemr and Abd-Allah, 2003; Manodori et al., 2006; Valavanidis et al., 2008). Moreover, a previous study focused on the Rhône River reported the same range of concentrations (PAHs-$_P$: 3.1-89 ng L^{-1}; Sicre et al., 2008). For Barcelona (Spain) and Banyuls-sur-mer (France), Guitart et al. (2007) observed lower values (PAHs-$_P$: 4.3-31 ng L^{-1}), but consistent with the present work during the warmer months (April -November 2011). On the other hand, our PAH concentrations remained far below the concentrations recorded by Zhou et al. (2000) and Guo et al. (2007) from the Xiamen harbour (from 106 to 945 ng L^{-1}) and the Daliao River watershed (from 946 to 13448 ng L^{-1}), respectively (China). According to these comparisons, Marseilles coastal area may be considered as moderately contaminated in PAHs. Nevertheless, several months after the *Prestige* oil spillage, Gonzalez et al. (2006) measured dissolved PAHs-$_{P+A}$ in surface waters from 350 to 580 ng L^{-1} and, 3 years after the *Prestige* wrecks had been sealed for leaks, Elordui-Zapatarietxe et al. (2010) still measured dissolved PAHs-$_{P+A}$ from 31 to 188 ng L^{-1}. With regard to these latter information, dissolved PAH concentrations we recorded in the Marseilles coastal area (up to 405 ng L^{-1} for PAHs-$_{P+A}$), especially during the colder months, reflected an anthropogenic forcing of the same order as that still observed several months after a tanker oil spill.

Despite some similarities observed between these two hydrocarbon classes such as the seasonal alternations and some contribution from anthropogenic sources (detailed below), AH and PAHs-$_{P+A}$ concentrations were not correlated. Since the concentration levels and molecular composition reflect the balance between the source, transport and removing processes, the miscorrelation between these two classes in the dissolved phase, extended to hydrological and biogeochemical parameters (unfortunately dissolved organic carbon values were not available), mirrored the uncoupling of their own dynamics, as already mentioned in sediments (Bouloubassi and Saliot, 1993; Wakeham, 1996). Thus, the simultaneous analysis of dissolved AHs and PAHs is supposed to reveal complementary information for a better comprehensive assessment of various natural and anthropogenic inputs as well as for the determination of their environmental behaviour.

4.2. Sources of hydrocarbons

4.2.1. Biogenic sources

Spatial and seasonal alternations in AH molecular distributions displayed wide and various biogenic signatures (planktonic, bacterial and terrigeneous). Indeed, according to lighter AH molecular distributions, at all sites except PB, remarkable increase in *n*-C_{17}+Pr (from spring to fall) and *n*-C_{19} (winter) were observed. The emergence of short odd carbon chain (*n*-C_{15}- *n*-C_{19}) is indicative of planktonic contributions (Wakeham, 1996). In addition, Pr, which is present in crude oil, may also be of natural origin (Didyk et al., 1978). Furthermore, the predominance of odd or even *n*-alkanes reflected rather a biogenic origin, while its absence is a sign of an anthropogenic origin. The predominance of even compounds which is much less common than the odd one, was especially marked at CO and SO in spring and has already been reported for dissolved water (passing through 1.2 µm porosity filter) in the range *n*-C_{16}-*n*-C_{31}. Even *n*-alkanes come from direct microorganism contribution (bacteria, fungi, yeast) and from their action on algal detritus (Elias et al., 1997 and reference therein). Microorganism signatures were more marked at offshore sites where the inputs of HMW petroleum residues carried by the Rhône River are not (or little) significant and less likely masked the even *n*-alkanes.

Finally, the characteristic molecular distribution pattern at VA in fall underscored that VA was the most terrigeneous impacted site. Terrigeneous signatures were scarcely recorded from the dissolved phase and previous studies (Mille et al., 2007; Guigue et al., 2011) found that they were only recovered in sediments and particles in this area. One reason for this is that hydrophobic long chain *n*-alkane molecular markers from higher plants, such as *n*-C_{27}, *n*-C_{29} and *n*-C_{31}, have very high affinity for particles/sediments, and even in the case of turbulence they are not easily transferred to the dissolved phase.

It is worth noting that a few PAHs (especially Naph and Phe) may be biogically produced in plants, soils and sediments which could have some influence on the waters affected by riverine inputs, however we did no evidence significant differences in their distribution between continental and offshore marine sites. In addition, it is well admitted that PAHs in temperate area soils are mainly from anthropogenic origin (Wilcke, 2007 and references therein).

4.2.2. Anthropogenic sources

In summer and fall, chronic petroleum inputs of AHs affected all studied sites, especially in the Rhône and adjacent waters at AR, VA and PB (molecular composition patterns without even or odd *n*-alkane predominance). Additional fingerprint of degraded petroleum, like UCM, (UCM/R > 4; Mazurek and Simoneit, 1984) was occasionally evidenced only in the Rhône River with UCM/R values of 5.5 and 5.7 on July and September 2011, respectively. However, this tended to confirm that the Rhône River drains significant amounts of anthropogenic contaminants (Sicre et al., 2008).

The PAH composition patterns (Figure IV-4) revealed unburned fossil fuel inputs (predominance of 2-3 ring compounds with a high proportion of alkylated homologues; Cripps, 1989) whatever the site and the season. The dominance of the petrogenic nature of dissolved compounds in surface waters was in line with the knowledge of dissolved-particulate PAH distribution and with the results from Manoli et al. (2000) for the Southeastern Mediterranean. However, due to the partitioning of LMW and HMW PAHs between the dissolved and particulate phases which is directly related to their difference of solubility in water (K_{ow}), focusing only on the dissolved PAHs-$_{P+A}$ molecular distribution would not be very relevant to identify the origin of the contamination in our study sites. Hence, to identify the contamination sources of PAHs, it seems more appropriate to use indices that are not affected by the dissolved/particulate partitioning, such as the ratios between isomer compounds (Phe/Ant and Flt/Pyr), albeit one should be careful when interpreting these ratios, especially for samples collected far from defined sources because it has been demonstrated that they could be affected by removing processes such as biodegradation (Wang et al., 1999; Katsoyiannis et al., 2011). We believe that in the present study, plots of isomer ratios clearly show petrogenic and mixed origins of PAHs-$_{P+A}$ over the year. The mixed origin of PAHs is the surperimposition of both petrogenic and pyrogenic sources. A larger number of winter samples show this signature in comparison to samples from the other seasons. This suggests an increase of pyrogenic inputs in winter. However, the values of Alk/Par ratios indicated meanwhile an increase in petrogenic signatures during the colder months. These conflicting results did reflect the increase in both origin inputs since it is well known that unburned and incompletely combusted petroleum PAHs originating from traffic and industrial/domestic heating increase in winter (Palm et al., 2004). The petrogenic and mixed origins of PAHs were also reported by Manodori et al. (2006) for the Venice lagoon and consistent with a highly urbanized and industrialized area.

Even though isomer ratios did not distinguish PB from the others, composition patterns and significant higher PAHs-$_{P+A}$ concentrations indicated recent petroleum sources, especially in winter (Gonzalez et al., 2006). This information confirmed the contamination of PB site from rather petrogenic additional sources suspected to be industrial activities/wastes and shipping traffic.

Overall, the overlap of signatures from various sources made difficult the unambiguous identification of the hydrocarbon origins in the dissolved phase.

4.3. Fate of dissolved hydrocarbons in surface waters

Identifying explicitly the fate of hydrocarbons is difficult in the marine environment because a wide variety of processes including evaporation, bio- and photo-degradation, adsorption onto suspended particles, integration into the food web are interacting during transport (Jordan and Payne, 1980; Tsapakis et al., 2006). The hydrocarbon pattern that we observed over the year in the surface continental and marine waters close to Marseilles suggested some major transport pathways (including the Rhône River and the atmospheric circulation) and several removing processes (see below).

4.3.1. Major transport pathways

According to hydrological and biogeochemical parameters, VA and PB were highly impacted by the Rhône River inputs (characterized at AR), while CO and SO were impacted occasionally and weakly, respectively. In addition, AH molecular patterns (Figure IV-3) at AR, VA and PB were close from each other and differed from CO and SO. This suggests that the Rhône River inputs impacted dissolved AH composition at the three former sites while the patterns at CO and SO evoked different sources and transport pathway. Besides the PAH concentrations increased in winter over the whole study area and PAH composition patterns were quite homogeneous between continental and offshore marine sites, the Rhône River could not be the only transport pathway involved in hydrocarbon distribution. Actually, PAH patterns suggested that the atmosphere might be another major transport and entering pathway for the introduction of dissolved hydrocarbon in surface coastal waters.

Indeed, it is very well admitted that a major source of dissolved hydrocarbons, such as LMW *n*-alkanes (< *n*-C_{24}) and 2-3 ring PAHs in the surface marine waters are gaseous atmospheric depositions and especially in coastal area of highly urbanized and industrialized city (Mandalakis et al., 2002; Tsapakis et al., 2006; Castro-Jiménez et al., 2012). Most

inputs/outputs (with highest fluxes for LMW compounds) from the atmosphere are due to diffusive exchanges with surface waters and were subjected to strong seasonal variations (Jurado et al., 2007). In winter, at low temperature, the air-water partitioning favors higher PAH concentrations in surface waters (Palm et al., 2004).

Finally, an additional source of dissolved hydrocarbons can be the sediment remobilization (resuspension, refocus). The influence of sediment is very likely more important in shallow sites such as AR, VA and PB (Table IV-1). Indeed, the stronger anthropogenic fingerprint from AH composition patterns (no predominance) recorded at these three sites compared to offshore sites may reveal sediment inputs. Moreover, at PB, the AH distribution in the dissolved phase is very similar to that recorded in the sediments (Mille et al., 2007). However, the influence of sediment is more difficult to highlight for PAHs whose composition over this area is characterized by an enrichment in $\geq$ 3-ring compounds which hardly partition to dissolved water (Benlahcen et al., 1997; Mille et al., 2007).

4.3.2. Hydrocarbon removing from surface waters

Several studies showed that weathering processes (i.e. evaporation, biodegradation and photodegradation) induced a preferential loss of LMW hydrocarbons (Wang and Fingas, 1995; Dachs et al., 1999; 2002; Yamada et al., 2003; Tsapakis et al., 2006). Evaporation to the atmosphere is the most important process that hydrocarbons undergo after their introduction /deposition to surface waters and it affects both AHs and PAHs with regard to their vapor pressure (Yamada et al., 2003). Degradation by marine bacteria and photodegradation lead to synergetic reactions that enhance the degradation (Watkinson and Griffiths, 1987; Literathy et al., 1989). Seasonal variations of removing processes have also been widely described. In summer, with the temperature increase, there is a net volatilization of LMW hydrocarbons (Fingas, 1995; Dachs et al., 2002; Palm et al., 2004). Moreover, lower concentrations of LMW hydrocarbons in summer have been often ascribed to higher rates of photo- and bio-degradations (Yamada et al., 2003; Palm et al., 2004). In our study area (the Mediterranean Sea), the differences in the sea surface temperature and in the solar irradiance received at the surface between winter and summer (13 and 26 °C, and 144 and 540 W m^{-2}, respectively) are very likely great enough to promote more intense weathering processes of dissolved hydrocarbons from surface waters in summer. Indeed, we found that, along with lower concentrations, 2-ring PAHs-$_{P+A}$ proportions were lower in spring, summer and fall (51 ± 9%) compared to winter (60 ± 8%) (ANOVA, $p < 0.0001$, $n = 26$-44), highlighting an

increase in weathering effects during the warmer months. In a previous study, Albinet et al. (2007) recorded PAHs derivatives associated with photochemical processes (nitrated and oxygenated PAHs) originating mainly from gasoline and diesel engines in the ambient air of Marseilles.

Hydrocarbons can also be removed from surface waters by sorption onto biogenic and/or atmospherically deposited particles (Dachs et al., 1996; 2002; Ko et al., 2003; Berrojalbiz et al., 2009). This process is likely to concern HMW compounds and follow the (organic) particle seasonal cycle. Although biogeochemical parameters pointed out significantly higher POC concentrations in spring relative to winter due to biological activity (Table IV-2; $p = 0.019$, $n = 26$), we found no relationship between the dissolved AH, PAHs-$_{P+A}$ and POC concentrations throughout the year. Thus adsorption onto particles was not the main driver of the decrease in dissolved LMW PAHs-$_{P+A}$ (and AHs) we observed during the warmer months.

5. Conclusions

This one year study highlights the Marseilles coastal area are not contaminated in carbaryl and bentazone excepted in VA. In this site, only sporadic contaminations in bentazone occurred in summer. The results on hydrocarbons showed that the study area is moderately contaminated in hydrocarbons compared to other coastal environments, except Port-de-Bouc harbour which, subjected to an intense shipping traffic and industrial activities/wastes, may reach PAHs-$_{P+A}$ levels encountered several months after oil spillages. Our results underline various natural and anthropogenic sources of hydrocarbons along with different transport pathway and removing processes. The major entering pathways for allochtonous dissolved hydrocarbons in this coastal area seemed to be the atmosphere and the Rhône River (limited to the plume extent) while some autochthonous biogenic hydrocarbon were also evidenced. We show a seasonal alternation of inputs and removing processes, with higher inputs from unburned petroleum/incompletely combusted emissions and higher surface run-offs and less weathering processes in winter, whereas the opposite pattern was observed in summer (less inputs and more evaporation/degradation). Interestingly, no differences were found between 0.1 and 5 m depth, neither for biogeochemical and hydrological parameters, nor for hydrocarbon concentrations. This study demonstrates the complexity and the pertinence of investigating the dynamics of organic pollutants in the dissolved phase of the water column since it provides access to complementary information that is not available when studying settling/sinking particles and sediments. Dissolved organic pollutants may interact with

natural organic matter (especially humic substances) to form different complexes. These complexes are known to modify their bioavailability/toxicity and their transport in the coastal environment. Hence, further investigations taking into account the complexation between pollutants and organic matter are necessary to get a global picture of the dynamics of dissolved organic pollutants in marine coastal waters.

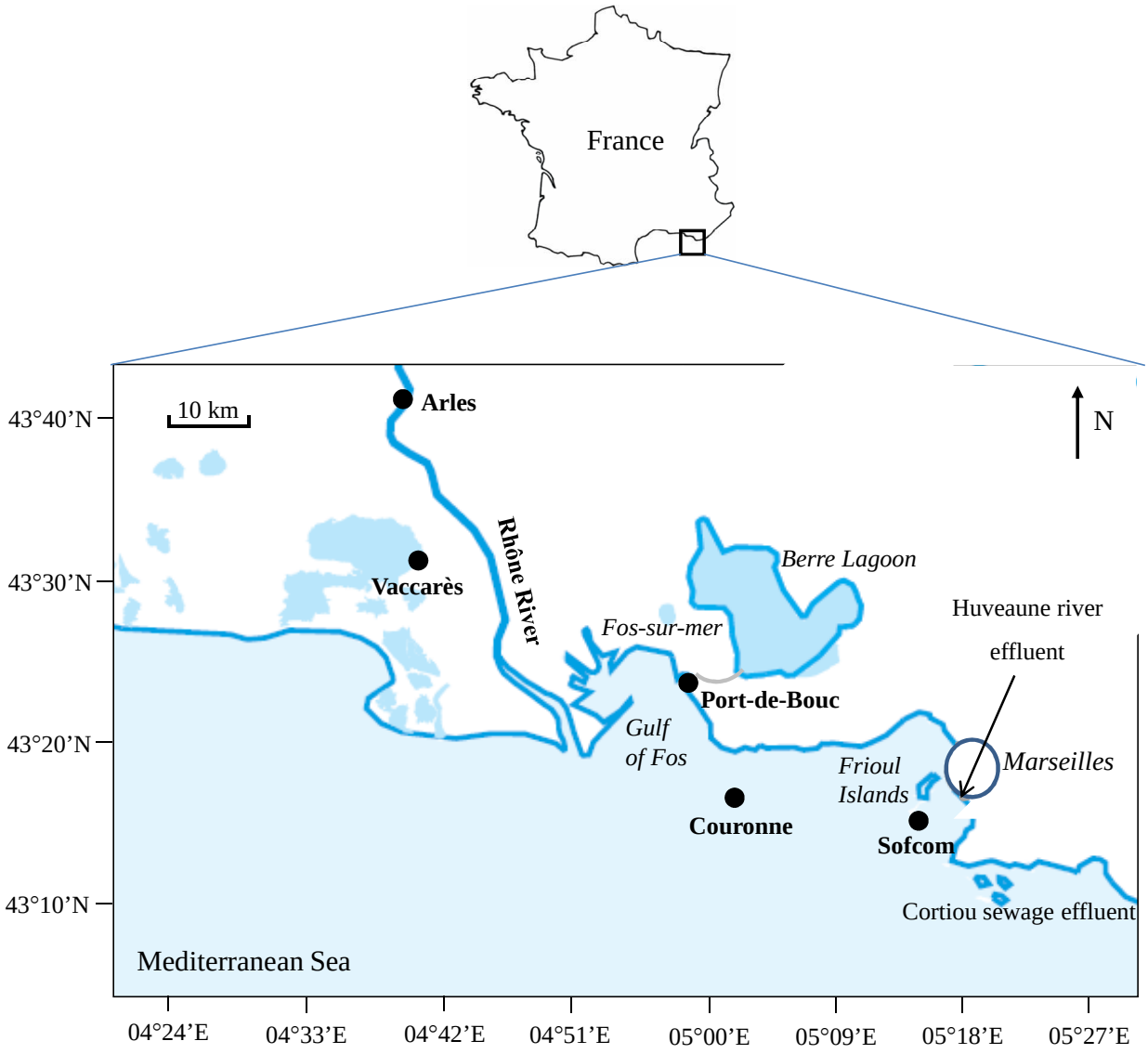

Figure IV-1. Location of the five study sites in the Marseilles coastal area (Northwestern Mediterranean Sea, France): Arles (AR), Vaccarès (VA), Port-de-Bouc (PB), Couronne (CO) and Sofcom (SO). The detailed characteristics of these sites are provided in Table IV-1.

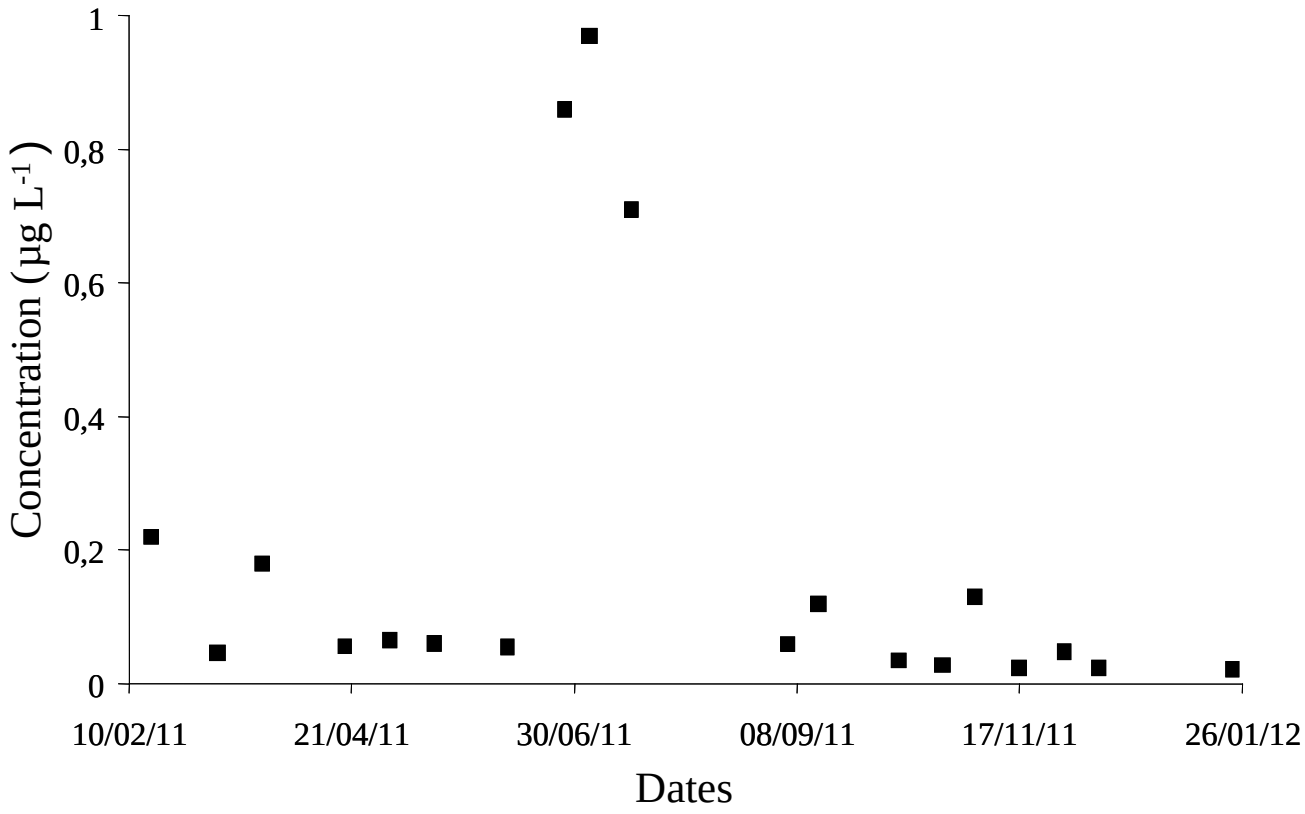

Figure IV-2. Concentrations in bentazone in Vaccarès Pond during the study period.

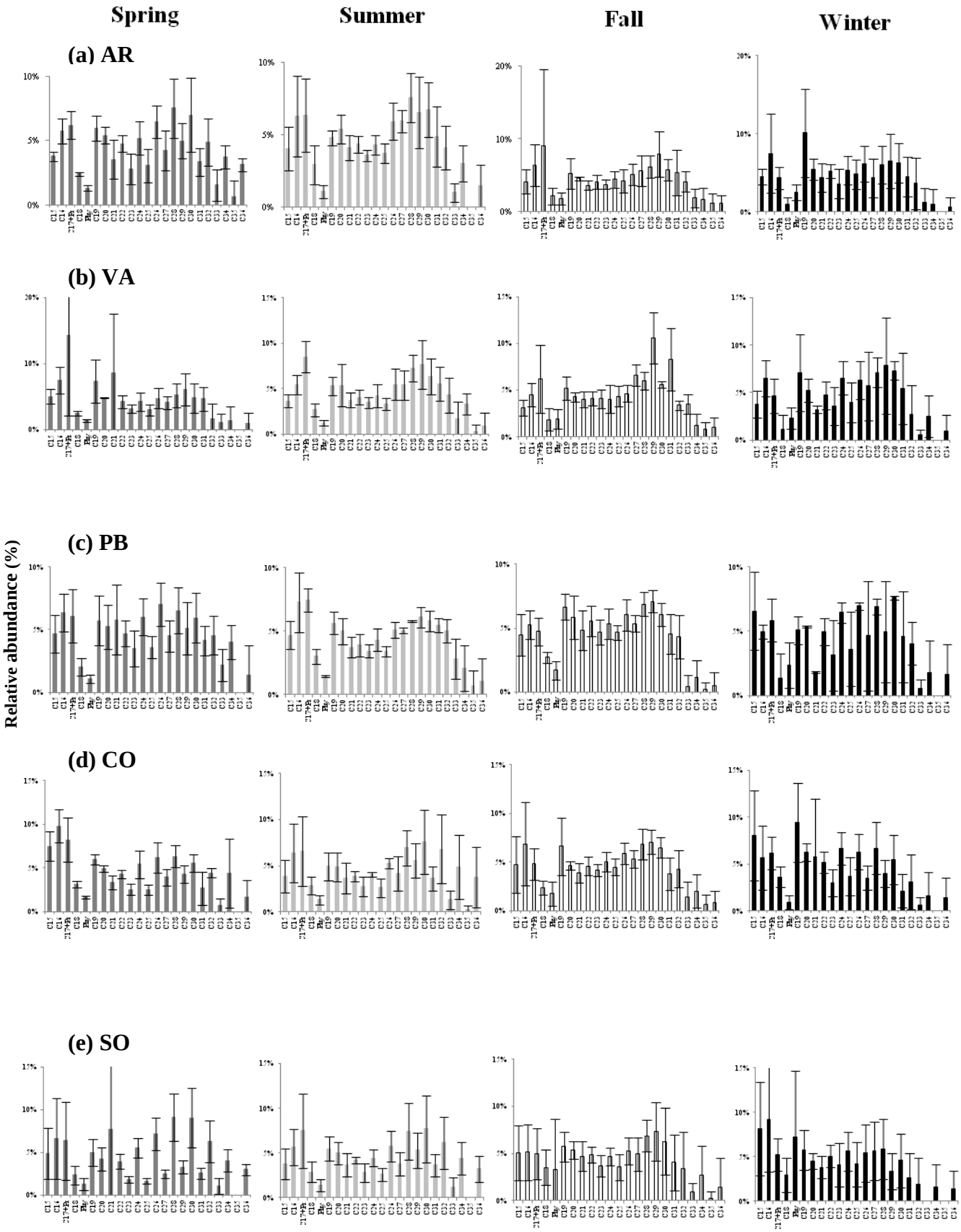

Figure IV-3. Composition patterns of dissolved AHs (in %) at AR (a), VA (b), PB (c), CO (d) and SO sites (e). Pr = Pristane; Phy = Phytane.

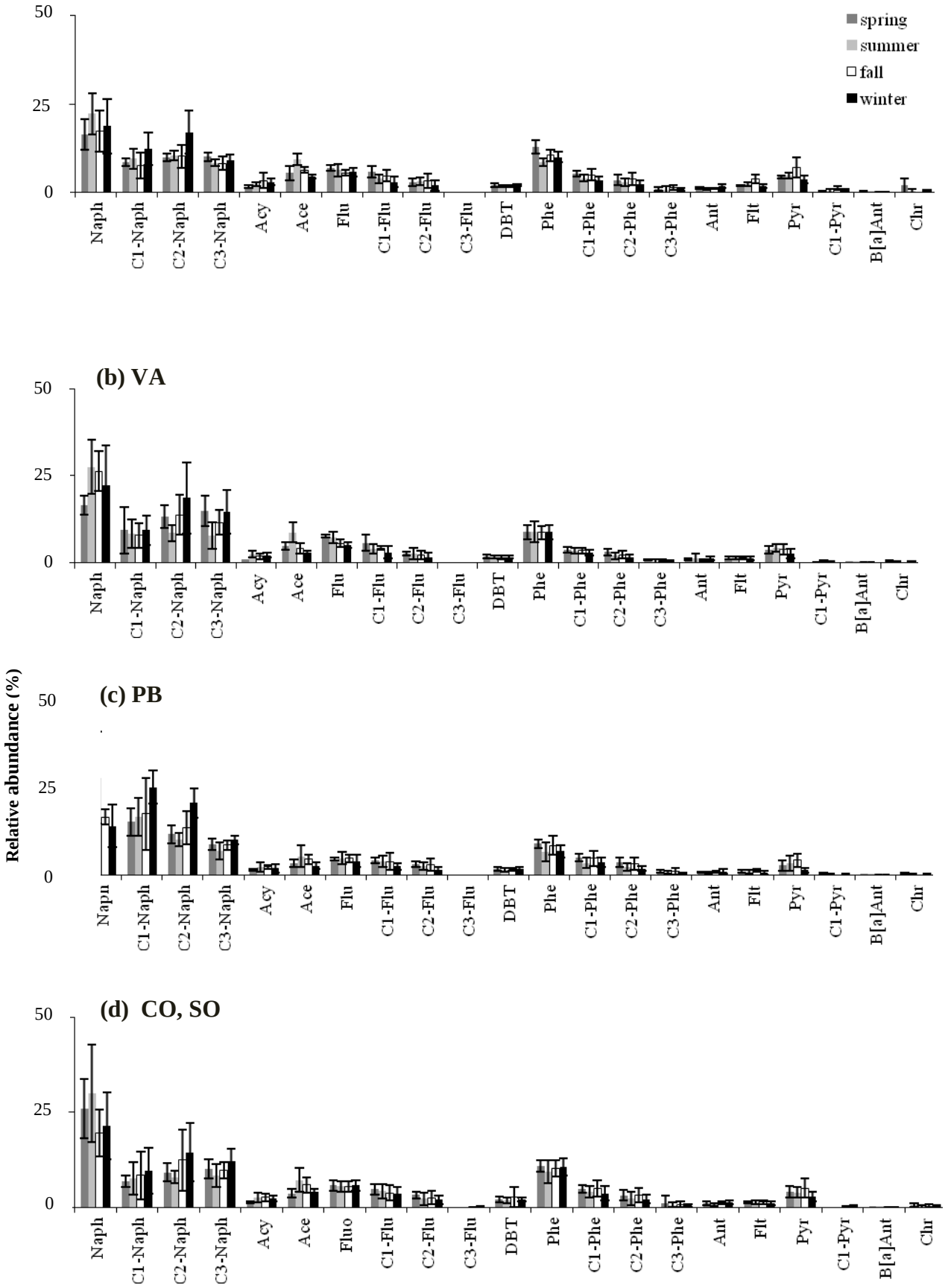

Figure IV-4. Composition patterns of dissolved PAHs (in %) at AR (a), VA (b), PB (c), CO and SO sites (d). Naph: naphtalene; C_1-Naph: methylnaphtalenes; C_2-Naph: dimethylnaphtalenes; C_3-Naph: trimethylnaphtalenes; Acy: Acenaphthylene; Ace: Acenaphtene; Flu: Fluorene; C_1-Flu: methylfluorenes; C_2-Flu: dimethylfluorenes; C_3-Flu: trimethylfluorenes; DBT: dibenzothiophene; Phe: phenanthrene; C_1-Phe:

methylphenanthrenes; C_2-Phe: dimethylphenanthrenes; C_3-Phe: trimethylphenanthrenes; Ant: anthracene; Flt: fluoranthene; Pyr: pyrene; C_1-Pyr: methylpyrene; B[a]Ant: benz[a]anthracene; Chr: chrysene.

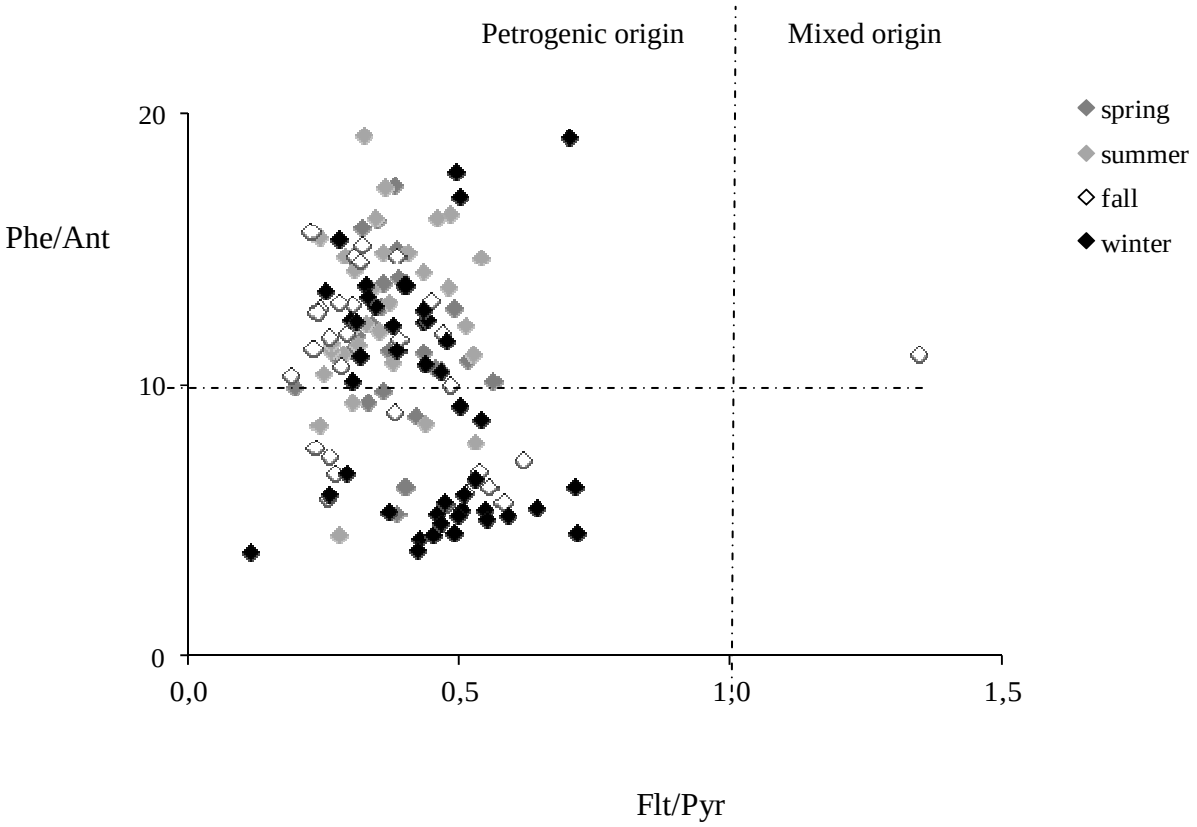

Figure IV-5. Cross plot of Phe/Ant *versus* Flt/Pyr ratios for all sites.

Table IV-1. Characteristics of the study sites, located in the Marseilles coastal area (Northwestern Mediterranean Sea, France) and sampled from February 2011 to February 2012.

Name	Abbreviation	Water type	Position	Depth of the water column	Sampling depth
Arles	AR	Freshwater	43°40.7'N, 04°37.3'E	2 m	0.1 m
Vaccarès	VA	Freshwater	43°31.4'N, 04°38.1'E	0.5 m	0.1 m
Port-de-Bouc	PB	Harbour water	43°24.1'N, 04°59.0'E	5 m	0.1 m
Couronne	CO	Marine coastal water	43°16.5'N, 05°02.1'E	90 m	0.1 and 5 m
Sofcom	SO	Marine coastal water	43°14.3'N, 05°17.3'E	60 m	0.1 and 5 m

Table IV-2. Hydrological and biogeochemical parameters.

		2011																	2012				
		17/02	24/02	10/03	24/03	18/04	03/05	17/05	09/06	27/06	05/07	18/07	05/09	15/09	10/10	24/10	03/11	17/11	01/12	12/12	09/01	23/01	06/02
AR	Salinity	0	0	0	0	0	0	0	0	0	0	0	0	0	0	0	0	0	0	0	0	0	0
	POC (µM)	14	11	7.3	21	18	36	28	27	10	14	10	8.1	8.1	10	6.0	8.1	12	8.1	24	125	32	24
	NO_3^- (µM)	115	122	125	104	106	86	87	84	69	69	70	70	76	77	81	83	81	90	100	111	120	111
	Chl *a* (µg L^{-1})	2.3	16	9.7	1.9	2.3	11	3.7	4.9	15	2.9	2.5	1.7	1.8	NA	NA	NA	0.49	0.41	1.1	3.0	1.3	1.1
VA	Salinity	7	7	15	4	4	1	2	4	1	0	0	2	2	14	14	3	0	0	8	5	13	
	POC (µM)	18	17	12	132	236	158	70	278	143	78	89	58	50	97	30	137	78	72	48	62	66	
	NO_3^- (µM)	2.4	2.1	1.6	4.0	34	28	20	0.75	9.6	20	16	12	9.4	2.0	2.1	6.4	4.0	1.8	3.0	9.1	11	
	Chl *a* (µg L^{-1})	21	10	4.5	20	11	19	10	26	0.51	8.6	7.5	4.9	9.6	NA	NA	NA	6.9	7.4	2.8	6.4	6.0	
		10/02	15/02	17/03	28/03	08/04	09/05	01/05	07/06	28/06	07/07	19/07	07/09	21/09	14/10	21/10		22/11	09/12	12/12	11/01	25/01	
PB	Salinity (1m)	24.8	32.3	33.4		29.1	28.2	34.8	NA NA	35.8	36.0		30.0	29.9	32.0	26.7		34.6	36.8		31.0	33.6	
	POC (µM)	6.1	9.0	16		21	17	17	29	32	23		39	24	17	21		12	18		16	6.0	
	NO_3^- (µM)	13	7.6	5.9		1.3	0.4	0.67	0.29	0.06	0.04		0.42	0.75	2.5	2.3		3.5	1.5		8.1	9.3	
	Chl *a* (µg L^{-1})	0.75	1.0	1.6		0.82	0.78	1.9	4.7	NA	2.7		5.7	3.0	NA	NA		2.4	2.1		0.95	0.62	
COs	Salinity	38.0	NA	37.9	37.6	37.8	37.7	36.8		36.2	37.6		37.5	36.1	38.1	37.8		38.0	34.7		37.8	37.6	
	POC (µM)	3.0	3.8	4.4	11.5	9.8	7.4	26		83	29 2		6.8	9.0	3.5	3.5		2.4	7.1		2.1	2.6	
	NO_3^- (µM)	0.83	1.13	0.77	0.44	0.0	0.04	0.14		0.05	1.2		0.0	4.9	0.04	0.72		0.37	13		3.7	3.1	
	Chl *a* (µg L^{-1})	0.54	0.58	0.66	1.1	0.20	0.32	2.0		0.66	3.2		0.39	1.0	NA	NA		0.33	0.66		0.33	0.31	

	Salinity	38.0	NA	37.9	37.6	37.9	37.8	38.0		37.7	37.0		37.7	37.7	38.1	37.8		38.0	37.3		37.8	37.6	
CO	POC (µM)	3.0	3.1	4.5	11	8.5	8.1	12		33	19		6.4	5.4	3.8	3.3		2.1	5.0		1.9	2.1	
5 m	NO_3^- (µM)	0.85	1.2	0.76	0.59	0.00	0.05	0.02		0.05	0.01		0.0	0.60	0.05	0.76		0.42	2.4		3.7	2.7	
	Chl *a* (µg L^{-1})	0.50	0.78	0.73	0.75	0.46	0.37	1.1		3.5	0.47		0.29	0.50	NA	NA		0.34	1.3		0.31	0.31	
	Salinity	38.0	38.0	38.0	NA	37.9	37.8	38.0	37.8	37.9	37.7	NA	NA	38.1	38.1	38.2		38.0	37.8	37.1	38.2	38.2	
SO	POC (µM)	3.2	3.3	4.1	5.7	8.4	7.8	4.4	7.7	4.5	3.5	9.0	4.2	2.6	5.0	3.1		2.4	4.5	12.5	1.7	1.4	
s	NO_3^- (µM)	0.93	1.1	1.3	0.40	0.00	0.20	0.19	0.38	0.5	0.02	0.01	0.0	0.0	0.05	0.07		0.33	0.31	1.15	2.1	1.4	
	Chl *a* (µg L^{-1})	0.55	0.64	0.49	0.40	0.59	0.50	0.30	0.78	0.25	0.16	0.53	0.18	0.12	NA	NA		0.33	1.0	2.20	0.34	0.37	
	Salinity	38.0	38.0	37.9	NA	37.9	37.8	38.0	37.9	38.1	37.8	NA	NA	38.0	38.1	38.2		38.0	37.8		38.1	38.2	
SO	POC (µM)	2.6	4.2	4.0	6.1	8.2	7.1	3.9	7.6	4.0	4.5	9.0	4.5	2.6	4.7	3.5		2.6	5.0		1.4	1.2	
5 m	NO_3^- (µM)	1.0	1.1	0.82	0.41	0.00	0.17	0.13	0.40	0.43	0.32	0.00	0.00	0.00	0.04	0.08		0.38	0.53		2.4	1.7	
	Chl *a* (µg L^{-1})	0.69	0.56	0.57	0.78	0.19	0.57	0.30	0.82	1.8	0.27	0.66	0.21	0.25	NA	NA		0.34	0.50		0.37	0.28	

POC: particulate organic carbon; NO_3^-: nitrates; Chl *a*: chlorophyll *a*.

NA: not available.

Table IV-3. Concentrations of AHs and UCM (µg L^{-1}), and UCM/R ratio.

		2011															2012		
	10/03	24/03	18/04	03/05	09/06	27/06	05/07	18/07	05/09	15/09		24/10	03/11	17/11	01/12	12/12	09/01	23/01	06/02
AR	R (µg L^{-1})	0.28	0.28	0.19	0.12	0.13	0.15	0.18	0.15	0.10	0.22		0.16	0.11	0.16	0.17	0.17	0.18	0.16
	UCM (µg L^{-1})							0.62	0.87		1.6			0.38	0.27				
	UCM/R							3.5	5.5		5.7			2.9	1.8				
VA	R (µg L^{-1})	0.39	0.29	0.15	0.14	0.19	0.24	0.13	0.06	0.09	0.16		0.15	0.10	0.31	0.53	0.15	0.16	0.13
	UCM (µg L^{-1})							0.29							0.49				
	UCM/R							2.3							1.6				
		17/03	28/03	08/04	09/05	07/06	28/06	07/07	19/07	07/09	21/09	14/10	21/10		22/11	09/12		11/01	25/01
PB	R (µg L^{-1})	0.21		0.20	0.12	0.12	0.07	0.08		0.09		0.19	0.15		0.24	0.20		0.10	
	UCM (µg L^{-1})														0.25				
	UCM/R														1.0				
CO s	R (µg L^{-1})	0.20	0.08	0.13	0.23		0.13	0.04		0.11	0.58	0.07	0.17		0.10	0.18		0.10	0.10
	UCM (µg L^{-1})										0.76								
	UCM/R										1.2								
CO 5 m	R (µg L^{-1})	0.20	0.07	0.13	0.17		0.10	0.05		0.07	0.29	0.04	0.17		0.13	0.21		0.09	0.16
	UCM (µg L^{-1})										0.29								

	UCM/R										1.0								
SOs	R (µg L^{-1})	0.22	0.13	0.25	0.28		0.22	0.06	0.08	0.08	0.29		0.08		0.14	0.15		0.11	0.12
	UCM (µg L^{-1})										0.30		0.18		0.13				
	UCM/R										0.91		2.4		0.98				
SO 5 m	R (µg L^{-1})	0.25	0.13	0.24	0.24		0.22	0.09	0.09	0.09	0.26	0.45	0.11		0.11	0.22		0.19	0.09
	UCM (µg L^{-1})											0.23	0.28						
	UCM/R											0.51	2.7						

R: resolved aliphatic hydrocarbons (sum of *n*-alkanes from C_{15} to C_{36} with two isoprenoids, pristane and phytane); UCM: unresolved complex mixture; UCM/R: unresolved complex mixture over resolved aliphatic hydrocarbon concentration ratio.

Table IV-4. Concentrations of 17 parent PAHs (PAHs-$_P$) and 32 parents + alkylated PAHs (PAHs-$_{P+A}$) (ng L^{-1}), and Phe/Ant, Flt/Pyr and Alk/Par ratios.

		2011																	2012				
		17/02	24/02	10/03	24/03	18/04	03/05	17/05	09/06	27/06	05/07	18/07	05/09	15/09	10/10	24/10	03/11	17/11	01/12	12/12	09/01	23/01	06/02
AR	PAHs-$_P$	53	38	23	18	16	13	11	10	16	19	19	17	13	6.1	23	10	13	40	101	93	33	40
	PAHs-$_{P+A}$	91	63	40	37	28	23	20	20	30	33	35	27	23	12	36	20	22	70	241	223	66	84
	Phe/Ant	5.4	11	13	8.8	11	11	11	14	14	15	11	8.7	8.0	10	11	12	9.1	6.9	4.4	4.0	5.1	5.4
	Flt/Pyr	0.4	0.4	0.4	0.5	0.5	0.5	0.4	0.4	0.5	0.5	0.5	0.4	0.5	0.5	1.3	0.5	0.4	0.5	0.4	0.4	0.5	0.5
	Alk/Par	1.1	0.8	1.0	1.4	1.0	1.1	1.2	1.2	1.2	1.0	1.3	0.9	1.2	1.5	0.8	1.3	0.9	1.1	2.0	2.0	1.5	1.5
	POC (µM)	18	17	12	132	236	158	70	278	143	78	89	58	50	97	30	137	78	72	48	62	66	
	NO_3^- (µM)	2.4	2.1	1.6	4.0	34	28	20	0.75	9.6	20	16	12	9.4	2.0	2.1	6.4	4.0	1.8	3.0	9.1	11	
VA	PAHs-$_P$	75	41	25	27	19	12	9.4	11	12	27	12	14	15	10	25	13	18	52	115	114	30	
	PAHs-$_{P+A}$	136	76	43	45	43	25	15	22	24	36	19	22	25	17	44	24	31	116	352	360	73	
	Phe/Ant	6.8	12	19	9.3	9.0	9.4	6.3	16	17	4.5	11	14	12	15	15	15	12	5.7	5.4	6.6	4.6	
	Flt/Pyr	0.3	0.3	0.7	0.5	0.4	0.3	0.4	0.3	0.4	0.3	0.4	0.4	0.3	0.4	0.3	0.3	0.4	0.5	0.5	0.5	0.7	
	Alk/Par	1.0	1.0	0.8	0.8	1.6	1.5	0.7	1.3	1.3	0.5	0.9	0.8	0.8	0.9	0.9	1.1	0.8	1.6	2.8	2.9	2.1	
	10/02	15/02	17/03	28/03	08/04	09/05	01/05	07/06	28/06	07/07	19/07	07/09	21/09	14/10	21/10		22/11	09/12	12/12	11/01	25/01		
PB	PAHs-$_P$	105	73	56		28	26	19	9.6	21	62		11	7.0	6.3	16		18	82		135	27	
	PAHs-$_{P+A}$	405	192	221		58	60	37	22	47	106		20	18	13	32		41	225		364	63	
	Phe/Ant	14	11	18		10	15	12	11	19	11		12	8.6	12	15		7.8	5.7		4.5	5.5	
	Flt/Pyr	0.3	0.3	0.5		0.6	0.4	0.3	0.3	0.3	0.3		0.3	0.2	0.3	0.3		0.2	0.6		0.4	0.6	
	Alk/Par	3.7	1.9	3.6		1.3	1.6	1.1	1.7	1.4	0.7		1.0	1.8	1.4	1.3		1.6	2.3		2.3	2.0	
	POC	3.0	3.1	4.5	11	8.5	8.1	12		33	19		6.4	5.4	3.8	3.3		2.1	5.0		1.9	2.1	

	(µM)																					
COs	PAHs-$_P$	31	20	9.8	10	16	12	10		8.8	41		10	7.6	5.3	7.2		7.3	65		119	61	
	PAHs-$_{P+A}$	49	39	18	16	25	21	18		14	64		16	13	8.8	12		13	154		324	127	
	Phe/Ant	13	16	17	13	13	5.3	14		16	16		13	12	13	11		5.9	7.3		4.9	6.3	
	Flt/Pyr	0.3	0.3	0.5	0.4	0.5	0.4	0.4		0.3	0.5		0.4	0.3	0.2	0.3		0.2	0.6		0.5	0.7	
	Alk/Par	0.7	1.1	1.0	0.7	0.7	1.1	1.0		0.9	0.6		0.8	0.9	0.9	0.8		1.0	1.9		2.4	1.6	
	Chl *a* ($\mu g\ L^{-1}$)	0.55	0.64	0.49	0.40	0.59	0.50	0.30	0.78	0.25	0.16	0.53	0.18	0.12	NA	NA		0.33	1.0	2.20	0.34	0.37	
CO 5 m	PAHs-$_P$	22	17	8.5	10	15	11	12		9.1	151		10	4.8	5.6	8.6		5.4	49		106	61	
	PAHs-$_{P+A}$	38	32	15	16	24	19	22		15	221		16	8.1	11	13		8.8	123		269	180	
	Phe/Ant	10	13	12	11	12	10	13		15	16		14	9.5	10	11		6.8	6.3		4.6	5.3	
	Flt/Pyr	0.3	0.3	0.5	0.5	0.5	0.2	0.4		0.4	0.5		0.3	0.3	0.2	0.2		0.3	0.6		0.5	0.5	
	Alk/Par	0.9	1.1	0.8	0.7	0.7	0.9	1.0		0.9	0.5		0.8	0.9	1.2	0.7		0.8	2.0		2.2	2.8	
SOs	PAHs-$_P$	26	25	12	9.1	13	10	8.5	8.9	8.0	7.8	8.0	7.6	6.0	6.7	8.0		5.3	37		54	36	
	PAHs-$_{P+A}$	53	43	21	16	20	19	16	18	15	13	13	13	9.8	12	13		9.2	95		136	87	
	Phe/Ant	6.0	13	12	14	10	11	11	15	15	11	12	12	14	16	13		12	13		5.7	6.0	
	Flt/Pyr	0.3	0.3	0.4	0.4	0.4	0.4	0.3	0.3	0.3	0.2	0.5	0.3	0.3	0.2	0.3		0.3	0.4		0.5	0.5	
	Alk/Par	1.2	0.8	0.9	0.9	0.5	1.1	1.1	1.2	1.1	0.7	0.8	1.1	0.8	1.2	0.9		0.9	1.3		2.1	2.1	
SO 5 m	PAHs-$_P$	5.9	22	12	8.8	12	7.3	9.8	7.9	7.0	18	8.5	7.7	6.4	6.6	7.2		4.7	55		80	46	
	PAHs-$_{P+A}$	12	45	19	15	19	13	17	16	15	23	13	12	11	12	13		8.9	145		217	112	
	Phe/Ant	3.9	14	11	12	11	12	16	17	15	11	15	12	16	13	7.5		13	6.1		5.2	5.2	
	Flt/Pyr	0.1	0.2	0.4	0.4	0.5	0.3	0.3	0.4	0.3	0.3	0.4	0.3	0.2	0.3	0.3		0.2	0.5		0.5	0.6	

	Alk/Par	1.4	1.3	0.8	0.8	0.6	0.9	1.0	1.3	1.4	0.4	0.7	0.8	0.8	1.2	1.1		1.1	2.3		2.5	2.1	

PAHs-$_P$: 17 parent polycyclic aromatic hydrocarbons (PAHs); PAHs-$_{P+A}$: sum of 17 parents and 15 alkylated homologues PAHs; Phe/Ant: phenanthrene (Phe) over anthracene (Ant) concentration ratio. Flt/Pyr: fluoranthene (Flt) over pyrene (Pyr) concentration ratio; Alk/Par: alkylated homologues over parent PAH concentration ratio.

Chapitre V: Caractérisation et évolution saisonnière de la matière organique dissoute fluorescente dans des environnements contrastés dans le bassin du Rhône et en Méditerranée nord-occidentale

Résumé

Dans ce chapitre, une étude de 12 mois a été réalisée sur les mêmes échantillons que ceux du chapitre précédent. Les objectifs de cette étude était 1) d'évaluer la qualité de la FDOM en baie de Marseille ainsi que dans les eaux continentales du bassin du Rhône, 2) de déterminer la variabilité saisonnière de la FDOM dans ces différents sites en rapport avec les paramètres environnementaux et 3) de déterminer l'impact du Rhône dans l'étang de Vaccarès et en baie de Marseille.

Afin de caractériser la FDOM, des MEEFs ont été générées et deux analyses PARAFAC ont été réalisées, l'une sur le jeu de données contenant uniquement les eaux continentales et l'autre sur le jeu de données contenant les échantillons marins. Dans les eaux continentales, 2 fluorophores de type substances humiques, C1 (λ_{Ex} /λ_{Em}: 250 (330)/394 nm) et C3 (λ_{Ex} /λ_{Em}: 250 (350)/454) et un fluorophore de type tryptophane, C2 (λ_{Ex} /λ_{Em}: 230 (380)/340 nm) ont été mis en évidence. En revanche, dans les eaux marines, un seul fluorophore de type humique, C6 (λ_{Ex} /λ_{Em}: 245 (300)/450 nm) a été détecté, associé à 2 fluorophores de type protéine, C4 (λ_{Ex} /λ_{Em}: < 220 (275)/< 300 nm) et C5 (λ_{Ex} /λ_{Em}: 230 (280)/342 nm), qui correspondent respectivement à la tyrosine et au tryptophane. Dans les eaux continentales, les substances humiques dominaient et traduisaient la forte proportion de matériel organique terrigène. Dans les eaux marines, ce sont au contraire les protéines qui dominaient. La série temporelle d'échantillonnage montre que la présence du fluorophore de type tyrosine était liée à la production de matière autochtone tandis que les fluorophores de type tryptophane et de type humique avaient une origine principalement allochtone. En mer, les intrusions d'eau du Rhône montraient un impact sur la biogéochimie locale en augmentant la quantité de fluorophores (jusqu'à + 63 % pour C5 et + 163 % pour C6), soit par un apport direct de FDOM terrestre, soit indirectement *via* une stimulation de l'activité biologique (production primaire) (jusqu'à + 63 % pour C4) et probablement une fraction de C5 en lien avec l'apport de sels nutritifs. Dans ce chapitre aucun fluorophore d'origine anthropique de type hydrocarbures aromatiques polycycliques (*i.e.*, naphtalène, phénanthrène, fluorène) ou biocide (le bentazone) n'a pu être identifié malgré la présence de ces composés dans le milieu (voir Chapitre IV). La limite de détection trop élevée de la specrofluorimétrie pour ces composés anthropiques (chapitre III) et leur faible concentration dans le milieu (chapitre IV) en sont la cause. Malgré l'impact que peut avoir la présence de groupes méthyles sur la limite de détection du composé parent (*i.e* : division par 2,6 de la limite de détection du 2,3 diméthyle naphtalène par rapport à celle du naphtalène) (Chapitre III), les concentrations des dérivés

méthyles présents dans les échantillons n'étaient pas suffisantes pour permettre de les identifier et de les quantifier par spectrofluorimétrie. De plus, les concentrations particulièrement élevées en substances humiques dans les milieux tels que l'étang de Vaccarès ont pu interférer avec la mesure et ne pas permettre la séparation des fluorophores contaminants par analyse PARAFAC.

Seuls les quelques échantillons prélevés plus tôt à la sortie de la zone industrielle du Golf de Fos (voir chapitre III) présentaient des signatures anthropiques.

Cette étude confirme que l'analyse en spectrofluorimétrie est adaptée à la recherche de contaminants (notamment HAPs) en mer, mais ne convient pas pour le monitoring de zones faiblement contaminées.

Characterization and seasonal pattern of fluorescent dissolved organic matter in contrasted environments of the Rhone basin and the north-western Mediterranean Sea (southern France)

1. Introduction

Marine dissolved organic matter (DOM) is one of the greatest reactive organic carbon pool on Earth (~ 700 Gt), composed of a heterogeneous mixing of organic molecules (Hedges, 2002; Battin et al., 2009). Marine DOM originates from varied sources including dissolution of terrigenous particles, phytoplankton excretion, zooplankton grazing, cellular lysis, degradation/exudation of macrophytes and dissolution from resuspended sediment (Nagata, 2000; Bertilsson and Jones Jr., 2003). Terrestrial organic matter is transported in coastal and offshore marine waters through rivers. However, these terrestrial inputs represent only a low contribution (2-3%) to the oceanic DOM pool (Opsahl and Benner, 1997), the major contribution coming mainly from the autochthonous biological activity (Myklestad, 2000).

In recent years, fluorescence was used to characterize the dynamics and composition of DOM in rivers (Patel-Sorrentino et al., 2002; Carstea et al., 2010; Yamashita et al., 2011), lakes (Liu et al., 2007; Gondar et al., 2008; Borisover et al., 2009), estuaries (Boyd and Osburn, 2004; Huguet et al., 2010; Singh et al., 2010) and marine waters (Luciani et al., 2008; Jørgensen et al., 2011; Stedmon et al., 2011). However, so far, only few studies have investigated the composition and seasonal variability of fluorescent DOM (FDOM) in the Mediterranean Sea and in freshwaters around the Mediterranean coasts (Para et al., 2010; Tedetti et al., 2010; 2012).

The Mediterranean Sea is composed of two basins with an oligotrophic gradient from western to eastern. The water of this semi-enclosed sea has a short residence time (~70 years) and a specific thermohaline circulation. The main water exchanges occur with the Atlantic Ocean and the Black Sea *via* respectively the Gibraltar and Bosphore strait (The MerMex group, 2011). Because of the weak cloud cover, the Mediterranean Sea is subjected to high levels of solar radiation compared to other temperate oceanic areas of same latitude (Bishop and Rossow, 1991).

The Rhône River is the main source of freshwaters to the Mediterranean Sea (around 50%). Its presence induces a large transfer of particulate and dissolved materials and enhances the primary production because of nutrient and carbon inputs (Moutin et al., 1998; Sempéré et al., 2000). Before reaching the sea, the Rhône River forms a delta in which intensive rice

agriculture occurs. Hence, Rhône waters may be deviated to irrigate rice cultures. By means of a channel system, fields are irrigated and the ultimate receptacle is the Vaccarès Pond, which is connected to the sea. The Rhône plume entering the Mediterranean Sea moves generally to the west under the influence of the North Current. However, sometimes, the Rhône plume can move towards the east under particular meteorological conditions, i.e. northwest wind condition and after flooding events (Para et al., 2010; Pairaud et al., 2011). Little is known about FDOM, carbon cycle and the impact of Rhône River waters in the Vaccarès Pond and the Marseilles Bay.

This study has three objectives: 1) to characterize the FDOM composition in contrasted environments of the Rhône basin and the north-western Mediterranean Sea, 2) to assess the FDOM temporal variability over the course of one year in relation with environmental parameters, and 3) to determine the influence of the Rhône River on the Vaccarès Pond and the Marseilles Bay.

2. Material and methods

2.1. Study sites

Five sites were sampled in the Rhône River basin and the north-western Mediterranean Sea (southern France): two inland stations (Arles and Vaccarès) and three marine stations (Port-de-Bouc, Couronne and Sofcom) (Figure V-1; Table V-1). Arles station (AR, 1-3 m depth) is located in the Rhône River, which is the largest French river in term of water discharge (interannual average discharge: ~ 1700 $m^3 s^{-1}$). It is 812 km long and has a drainage basin of approximately 97,800 km^2. Its delta has a surface area of ~ 1750 km^2, composed mainly of wetlands, ponds and salt marshes. The central part of the delta, known as the "Camargue" (~ 750 km^2), is composed of two parts: farmlands in the northern part and salted ponds where particular ecosystems are developed in the southern part. Camargue is an area of horse and bull breeding, rice cultivation and salt exploitation. Because of its ecological importance to wildlife and fisheries, Camargue is protected for decades (Figure V-1; Table V-1).

The Vaccarès Pond (VA) is the largest pond of Camargue and covers 66 km^2 with a mean water depth of 1.4 m and a maximum depth of 2.1 m. It is the main element of the control system of the Rhône delta waters. Inter-annual water level fluctuations are generally limited to ± 0.3 m (Chauvelon, 1996). VA is connected to the Mediterranean Sea and is directly under the influence of the Rhône River through a 6 km channel system used to irrigate rice cultivations from April to September. The bottom sediments of the pond are covered with a

35 to 300 mm layer of unconsolidated fine particles (Vaquer and Heurteaux, 1989). Although Camargue is a national wildlife park, VA may be subjected to pesticides and hydrocarbons released from nearby agricultural and industrial activities (Figure V-1; Table V-1) (Roche et al., 2002, 2009; Comoretto et al., 2007; Chiron et al., 2009).

Port-de-Bouc (PB, 12 m depth) is a harbour situated in the Gulf of Fos-sur-mer and surrounded by the Marseilles-Fos petrochemical complex, which includes several chemical, petroleum and steel-work plants. PB continuously receives freshwaters from the Berre Lagoon through the Caronte channel (Ulses et al., 2005) and may receive episodically freshwaters from the Rhône River. Thus, at PB, salinity is always lower than that of Mediterranean waters. Furthermore, PB is positioned on the route of oil cargo ships going to the Berre Lagoon (Figure V-1; Table V-1).

Couronne (CO, 90 m depth) is a marine nearshore site located at 6 km off PB, between the Rhône River mouth and the Marseilles Bay. Sofcom (SO, 60 m depth), situated in the Marseilles Bay (7 km off Marseilles), is the nearshore observation station of the Mediterranean Institute of Oceanography (SOMLIT; http://www.domino.u-bordeaux.fr/somlit_national/) and is sampled bi-monthly since 1995 for the measurement of hydrological and biogeochemical parameters. CO and SO may receive freshwaters from the Rhône River depending on the Rhône discharge and wind conditions (Para et al., 2010; Pairaud et al., 2011) (Figure V-1; Table V-1).

2.2. Sampling, *in situ* measurements and filtration

Each site was sampled ca bi-monthly from February 2011 to February 2012 in the morning between 8:00 and 12:00 am. Inland water samples (AR and VA) were taken directly from the edge, while marine samples (PB, CO, SO) were collected from the R/V Antédon 2. AR, VA and PB were sampled only at 0.1 m depth (subsurface water), whereas nearshore marine sites (CO and SO) were sampled at 0.1 m depth ("CO s" and "SO s") and 5 m depth ("CO 5 m" and "SO 5 m") (Table V-1). Inland water samples were taken directly with 4 L Nalgene® polycarbonate bottles. Marine samples were collected with a 5 L Niskin bottle equipped with silicon ribbons and Vitton o-ring (to avoid organic contaminations), and then transferred to Nalgene® bottles. The bottles were washed with 1 M hydrochloric acid (HCl) and pure water (i.e. Milli-Q water, final resistivity: 18.2 MΩ cm^{-1}) before use, rinsed three times with the respective sample before filling and stored in the dark in the cold (4-8 °C).

During the collection of marine samples (PB, CO, SO), *in situ* measurements of temperature, salinity, chlorophyll *a* (Chl *a*) concentration, FDOM intensity (at $\lambda_{Ex}/\lambda_{Em}$ of 370/460 nm) and turbidity along the water column were performed with a 19*plus* conductivity temperature depth (CTD) profiler (SeaBird Electronics Inc., USA) equipped with a WETStar Chl *a* fluorometer, a WETStar FDOM fluorometer (WETLabs, Inc., USA) and a Seapoint turbidity meter (Seapoint Sensors, Inc., USA). Because the deployment of the CTD profiler was not possible in shallow inland waters, salinity at AR and VA was measured on the 0.1 m depth discrete samples using a refractometer (MASTER-S/Millα, Atago, Tokyo).

Back in the laboratory, samples were immediately filtered under a low vacuum (< 50 mm Hg) through pre-combusted (500 °C, 4 h) glass fiber GF/F filters (25 mm diameter, Whatman) using all-glass filtration systems. The latter were washed twice with 100 mL of pure water and once with 50 mL of the sample of interest. GF/F filtered water was transferred into pre-combusted glass bottles for FDOM, dissolved organic carbon (DOC), dissolved organic phosphorus (DOP) and dissolved organic nitrogen (DON) analyses, and in polypropylene Nalgene® bottles for nitrates (NO_3^-), nitrites (NO_2^-) and phosphates (PO_4^{3-}) analyses. FDOM samples were stored at 4 °C in the dark and were analyzed within 24 h. Samples for DOC, DOP, DON, NO_3^-, NO_2^- and PO_4^{3-} were stored at -20 °C before analysis. Between 0.5 to 2 l of water were filtered for Chl *a*, particulate organic carbon (POC), particulate organic phosphorus (POP) and particulate organic nitrogen (PON). GF/F filters were stored in glass tubes at -20 °C before analysis.

2.3. FDOM analysis and data processing

FDOM analyses were performed with a Hitachi F-7000 spectrofluorometer (Tokyo, Japan), which measures fluorescence from 200 to 750 nm for both excitation (Ex) and emission (Em) sides. This instrument is equipped with a 150 W xenon short-arc lamp with a self-deozonating compartment, two stigmatic concave diffraction grating with 900 lines/mm brazed at 300 (Ex side) and 400 nm (Em side) as single monochromators, and Hamamatsu R3788 (185-750 nm) photomultiplier tubes (PMTs) as reference and sample detectors (fluorescence measurements acquired in signal over reference ratio mode). Spectral corrections for Ex and Em were executed according to Hitachi (Hitachi F-7000 Instruction Manual). They are fully described elsewhere (Tedetti et al., 2012).

One hour before fluorescence analyses, samples were allowed to reach room temperature in the dark. They were then transferred into a 1 cm pathlength far UV silica quartz cuvette (170-

2600 nm; LEADER LAB®), thermostated at 20 °C in the cell holder by an external circulating water bath. Excitation-emission matrices (EEMs) were generated for Ex wavelengths (λ_{Ex}) between 200 and 500 nm in 5 nm intervals and for Em wavelengths (λ_{Em}) between 280 and 550 nm in 2 nm intervals, with 5 nm slit widths on both Ex and Em sides, a scan speed of 1200 nm min^{-1}, a time response of 0.5 s, and a PMT voltage of 700 V. Blanks (pure water) and solutions of quinine sulphate dihydrate (Fluka, purum for fluorescence) in 0.05 M sulphuric acid (H_2SO_4) from 0.5 to 50 µg L^{-1} were run with each set of samples. For each sample, 5 successive analyses (i.e. 5 EEMs) were carried out, from which an average EEM was determined and further processed (see below).

To correct the average EEMs for inner filtering effects, absorbance measurements were performed between 200 to 550 nm in a 1 cm pathlength quartz cuvette with a Shimadzu UV-Vis 2450 spectrophotometer. The reference used was pure water for continental waters and a salt solution (pure water with pre-combusted NaCl; Sigma-Aldrich) for marine waters. Each EEM was multiplied by a correction matrix calculated for each wavelength pair from the sample absorbance, assuming a 0.5 cm pathlength of Ex and Em light in a 1 cm cuvette (Ohno, 2002). EEMs were then blank corrected by subtracting the pure water EEM (i.e. the average of ten filtered pure water EEMs). Finally, EEMs were converted into quinine sulphate unit (QSU), 1 QSU corresponding to the fluorescence of 1 µg L^{-1} quinine sulphate in 0.05 M H_2SO_4 at $\lambda_{Ex}/\lambda_{Em}$ of 350/450 nm (5 nm slit widths). The conversion into QSU was made by dividing the EEM fluorescence data by the slope of the quinine linear regression. The detection and quantification limits of the fluorescence measurement were 0.10 and 0.40 QSU, respectively. The Raman scatter peak of pure water was monitored at $\lambda_{Ex}/\lambda_{Em}$ of 275/303 nm during the whole study period. Because its variability was very low (coefficient of variation = 6%, n = 65), normalization of fluorescence intensities was not applied to our dataset. The Raman scatter peak was integrated from λ_{Em} 380 to 426 nm at λ_{Ex} of 350 nm for ten pure water samples. The average value was used to establish the conversion factor between QSU and Raman units (RU, nm^{-1}), based on the Raman-area normalized slope of the quinine linear regression (Murphy et al., 2010). The conversion factor was 0.012 RU per QSU.

2.4. PARAFAC analysis

PARAFAC is a multi-way statistical method based on an alternating least square algorithm and used to decompose the complex EEM signal measured into its underlying individual fluorescent profiles (components) (Bro, 1997). Here, PARAFAC models were created and validated according to the method by Stedmon and Bro (2008). PARAFAC application

requires the following assumptions: 1) the fluorophore concentration variations must only modify the fluorescence intensity but not the shape of Ex and Em spectra, 2) fluorophores must not be affected by inner filtering effects, 3) the presence of a fluorophore does not influence the spectral shape of the other fluorophores.

Inland and marine water datasets were processed separately to have the best representation of fluorophores within samples. Indeed, according to Stedmon and Bro (2008), it is not suitable to apply a unique PARAFAC analysis onto two group of samples which show great differences in term of salinity and fluorescence intensity. As a matter of fact, when we took into account all inland and marine water samples, we were able to validate a unique PARAFAC model with 6 components. However, one of these components, which displayed fluorescence peaks at λ_{Ex1} (λ_{Ex2})/λ_{Em} of 270 (400)/500 nm), was actually not present within samples, as examined from the peak picking technique.

For inland water samples, the EEM wavelength ranges used for PARAFAC analysis were 210-500 nm (Ex) and 280-520 nm (Em). For marine samples, the EEM wavelength ranges used were 220-500 nm (Ex) and 300-550 nm (Em). EEMs were thus merged into a three-dimensional data array of the form: 42 samples × 58 λ_{Ex} × 120 λ_{Em} for inland waters and 94 samples × 56 λ_{Ex} × 125 λ_{Em} for marine waters.

PARAFAC was operated using the DOMFluor toolbox v1.6. running under MATLAB® 7.10.0 (R2010a). For the two EEM datasets (inland and marine water samples), we tested models from two to six components. With regard to sample and wavelength leverages, no outlier was initially present in the datasets. The validation of the two PARAFAC models (running with the non negativity constraint) and the determination of the correct number of components were achieved through the examination of 1) the percentage of explained variance, 2) the shape of residuals, 3) the split half analysis and 4) the random initialization using the Tucker Congruence Coefficients (Stedmon and Bro, 2008).

2.5. Physico-chemical and biogeochemical analyses

pH was measured in unfiltered samples with a pH meter SG02-SevenGO™ pH Mettler-Toledo (Schwerzenbach, Switzerland). pH may modify FDOM fluorescence in term of intensity and spectral position (Patel-Sorrentino et al., 2002). In this work, no pH adjustment was carried out for FDOM measurements because the pH variation was very low within samples (7.6-8.2).

Nutrient concentrations were measured with a AutoAnalyseur III Seal Bran Luebbe (Mequon, USA) using the method described in previous study (Tréguer and LeCorre, 1975). To have reproducible nutrient measurements, standard were used and compared to commercially products (OSIL). The detection limits of NO_3^-, NO_2^- and PO_4^{3-} were respectively 0.05, 0.05 and 0.02 µM.

Chl *a* concentration was measured according to previous work (Raimbault et al., 2004). To extract Chl *a*, 5 mL of methanol (RP prolabo) was added to the glass tube. After 30 minutes of extraction in the dark at 4 °C, a fluorescence measurement was performed with a fluorometer model 10 Turner Designs (Sunnyvale, USA) at $\lambda_{Ex}/\lambda_{Em}$ of 450/660 nm. Fluorometer was calibrated with solutions of methanol (96%) and Chl *a* (Sigma C5753). This method allows measuring the total Chl *a* (divinyl Chl *a* and Chl *a*) and the detection limit was of 0.01 µg L^{-1}.

POC, POP and PON quantification were performed simultaneously with a AutoAnalyseur II Technicon (New York, USA) on the same sample, using the wet-oxidation procedure according to the literature (Raimbault et al., 1999a). POC, POP and PON had a detection limit of 0.50, 0.02 and 0.10 µM, respectively. DOC, DOP, DON were measured with the same instrument used for POC, POP and PON. To quantify these parameters, samples were acidified with 100 µl H_2SO_4 0.5 N and bubbled with a high purity oxygen/nitrogen gas stream for 15 minutes. Persulfate wet-oxidation was used to digest the organic matter in these samples (Raimbault et al., 1999b). All reagents and sample blanks were prepared using fresh Millipore Mili-Q plus® water.

2.6. Statistical analysis

Normality test, Mann-Whitney non-parametric test (U-test), linear regressions and principal component analysis (PCA) were performed with XLSTAT 2013.5.01 (Microsoft Excel add-in program). For linear regressions and PCA, spearman's (rank) correlations were preferred to Pearson's correlations because of the high amplitudes of some variables and their non-normal distribution (Jolliffe, 1986). For the different analyses and tests, the significance threshold was set at $p < 0.05$. Means are given ± SD.

2.7. Maps of surface salinity and chlorophyll *a*

Remotely sensed images of surface Chl *a* concentration were purchased from PREVIMER (http://www.previmer.org/). They were generated by applying the OC5 algorithm to water-leaving radiances derived from the Medium Resolution Imaging Spectrometer (MERIS) and

the Moderate Resolution Imaging Spectroradiometer (MODIS) sensors (Gohin, 2011). Maps of surface salinity were obtained from the 3D hydrodynamical model for applications at regional scale (MARS3D, IFREMER) (Lazure and Dumas, 2008).

3. Results

3.1. Meteorology

In the study area during the sampling period (February 2011-Feburay 2012), the atmospheric pressure ranged from ~ 1000 (February 2011) to 1035 hPa (April 2011) (Figure V-2a), while air temperature ranged from 7 (December 2011) to 28 °C (August 2011) (Figure V-2b). The dominant winds were north-northwest winds ("Mistral") that favor upwelling formation, and in a lesser extent, south-southeast winds inducing downwelling processes (Figure V-2c). After southeast winds, low salinity waters thought to result from an eastward extension of the Rhône River plume may be observed up in the Marseilles Bay (Pairaud et al., 2011). Throughout the year, gusts of wind characterized the pattern of wind intensity, with higher frequency in winter (Figure V-2d).

Rain cumulative intensity per month was also higher in winter with exception of July 2011 that exhibited unusual high recordings of rainfall. Recordings of rain fall showed a strong rain event at the beginning of November 2011, characterized by high rains up to 60 mm (Figure V-3a). This November rain was accompanied by bursts of wind above 25 m s^{-1} and a peak in the Rhône River flood. Unfortunately, the November sampling could not be carried out before 22 November. At this time, rain, wind and flood were at their lowest values.

Peaks of rain higher than 20 mm were observed throughout the year (February, end of April, end of July and September 2011) (Figure V-3a).

The average daily Rhône discharges were measured at AR and provided by the Compagnie Nationale du Rhône (Figure V-3b). The discharge for 2011-2012 was on average 1450 $m^3 s^{-1}$, with higher values in winter (1488 ± 580 $m^3 s^{-1}$) than in summer (839 ± 251 $m^3 s^{-1}$). In general, strong and persistent gusts of wind accompanied the high discharge of the Rhône River during the autumn/winter period, and shorter wind blows accompanied lower Rhône discharges during the spring/summer period. Peaks of floods (> 3000 $m^3 s^{-1}$) were observed in November, December 2011 and January 2012. In addition, burst of water flows occurred throughout the year (February: > 1400 $m^3 s^{-1}$; beginning of March: > 1800 $m^3 s^{-1}$; June: >1400

m^3 s^{-1}; July: 1624 m^3 s^{-1}). Background minimal values were observed in May, August, September and October 2011.

3.2. Hydrology

The CTD profiles of temperature, salinity and Chl *a* concentration (Figure V-4) acquired at the shallow PB site suggested that the water column was mixed most of the year with exception of a weak stratification noticeable in winter and late spring. In addition, we observed an increase in summer temperature with a subsequent increase in Chl *a* biomass. Superimposed on this seasonal pattern, low salinity events (S < 30 PSU) occurred several times during the year 2011 (10 February, 8 April, 9 May, 7 September and 21 October) with salinity in the range 24.8 to 30 PSU, and a drop down from 36.8 to 31 PSU in January 2012. During periods of high flows (February and November 2011), the Rhône plume was likely to spread over a large part of Marseilles Bay and may have induced these low salinity events. As the Rhône River is a source of nutrients for phytoplankton, its plume can be associated with an increase in Chl *a* concentration.

This is illustrated by maps of surface salinity and Chl *a* concentration (Figure V-5) that confirmed the Rhône River intrusions in the Marseilles Bay (at least up to CO site) in February and December 2011. On the contrary, the low salinity event on 8 April at PB could be neither related to a high Rhône River flow, nor to an exceptional rain event. Indeed, maps clearly showed no relationship between the extension of the Rhône River plume and the low salinity event in April (Figure V-5). Thus, the hypothesis of freshwaters coming from the Berre Lagoon and influencing the hydrology at PB in April may be put forward.

At CO and SO, the seasonal hydrological patterns were different from PB. Waters were warmer and stratified from May to October, and mixed and cooler from November to April (Figure V-4). The spring bloom occurred mostly beyond 10 m depth by the end of March. At CO, increases in Chl *a* concentrations occurred when freshening events were noted (31 May, 28 June, 7 July only at 5 m, 21 September and 9 December in surface and at 5 m). These freshening events were characterized by a drop down of salinity below 37.5 PSU at these sites. As they related to increases in the Rhône discharge, most of these events (except that of May and September) were attributed to the Rhône River intrusion in the Marseilles Bay according to Auger et al. (2011). The subsequent Chl *a* increase was particularly significant in December and extended to SO site (Figure V-5).

3.3. Variability and seasonal patterns of hydrological and biogeochemical parameters

The range of variations of all parameters is depicted in Figure V-6. For describing the seasonal pattern of hydrological and biogeochemical parameters in each site, we grouped the spring and the summer samples collected from April to September, and the autumn and the winter samples collected from October to March (Figure V-7). This choice was motivated by the fact that (1) our number of samples for each season was too low for statistical comparisons, (2) the repartition of samples within these two periods was homogenous and (3) the meteorological and hydrological conditions presented clear patterns between these two periods (see sections 3.1 and 3.2).

3.3.1. Temperature and salinity

CO and SO marine sites displayed lower temperature variations (mean T: 16.6 ± 2.6 °C for CO and 16.2 ± 2.2 °C for SO) than inland waters (AR and VA) and PB (mean T: 15.6 ± 4.2 °C for AR, 14.9 ± 4.5 °C for VA, 15.8 ± 3.8 °C for PB), for which the shallower water column was more sensitive to air temperature variations (Figure V-6, V-7). Salinity 0 dominated at AR throughout the year (Figure V-6). Salinity ranged from fresh to brackish water (0-14) at VA (mean S: 5.1 ± 4.9) as a result of hydraulic exchanges between the Camargue hydrosystem and the Mediterranean Sea (Figure V-6). Salinity at VA showed a seasonal trend with a decrease in spring and summer compared to autumn and winter ($p < 0.05$) (Figure V-7). At PB, CO s and CO 5 m, salinity was 31.5 ± 3.3, 37.4 ± 0.9 and 37.8 ± 0.3 PSU, respectively (Figure V-6), which pointed out the freshwater intrusions from the Rhône River at these sites and/or from the Berre Lagoon at PB. On the contrary, at SO, salinity values (38.0 ± 0.1 PSU for both depths) (Figure V-6) were typical of the Mediterranean marine waters, with exception on 12 December 2011 (data not shown).

3.3.2. pH

All sites displayed pH values around 8 during the sampling period. In VA waters, we observed a significant decrease in pH values below 8 during the spring-summer period ($p < 0.05$). In all other sites no seasonal trends were observed ($p > 0.05$).

3.3.3. $NO_3^- + NO_2^-$

$NO_3^- + NO_2^-$ were more abundant in inland waters (92.8 ± 18.5 µM at AR and 10.7 ± 9.8 µM at VA) than in marine waters (3.6 ± 4.0 µM at PB, 1.8 ± 3.1 µM at CO s, 0.8 ± 1.1 µM at CO 5 m, 0.6 ± 0.6 µM at SO s and SO 5 m) (Figure V-6). In inland waters, at VA, $NO_3^- + NO_2^-$

abundance increased during the spring-summer period ($p < 0.05$) whereas in the Rhône River (AR), concentrations were higher in winter ($p < 0.05$). In marine waters, at PB and CO (all depths), the NO_3^- + NO_2^- seasonal pattern was similar to that of the Rhône River with higher concentrations in the autumn-winter period than in the spring-summer period ($p < 0.05$). At SO no significant differences were observed ($p < 0.05$) (Figure V-6, V-7).

3.3.4. PO_4^{3-}

PO_4^{3-} concentrations increased from marine waters to inland waters with values ranging from 0 to 2.67 µM (0.8 ± 0.3 µM at AR, 0.5 ± 0.6 µM at VA, 0.2 ± 0.2 µM at PB, 0.0 ± 0.1 µM at CO s, 0.0 ± 0.0 µM at CO 5 m, SO s and SO 5 m). PB and SO 5 m exhibited a significant seasonal trend with higher concentrations during the autumn-winter period ($p < 0.05$). In inland waters and in other marine sites no statistical differences were brought out ($p = 0.94$, 0.38, 0.16, 0.72 and 0.38 for AR, VA, CO s, CO 5 m and SO s) (Figure V-6, V-7).

3.3.5. Chl *a*

Chl *a* concentration was higher at AR (4.6 ± 4.8 µg L^{-1}) and VA (10.2 ± 6.8 µg L^{-1}) than in marine sites (2.0 ± 1.5 µg L^{-1} at PB, 0.8 ± 0.8 µg L^{-1} at CO s and CO 5 m, 0.4 ± 0.2 µg L^{-1} at SO s and 0.5 ± 0.4 µg L^{-1} at SO 5 m) and showed no marked seasonal cycle ($p > 0.05$) (Figure V-6, V-7).

3.3.6. DOC, DON and DOP

In contrast to inorganic nutrients, DOC, DON and DOP concentrations were one order of magnitude higher at VA (873.0 ± 394.8 µM, 67.0 ± 26.2 µM and 1.0 ± 0.5 µM, respectively) than at AR (137.2 ± 47.3, 20.3 ± 2.9 and 0.8 ± 0.2 µM, respectively) and at the other marine sites. In inland waters, DOC accumulated during the autumn-winter period ($p < 0.05$) but no seasonal trends were observed for DON and DOP (Figure V-6, V-7). In marine waters, DOC (78 ± 11.9 µM, CO s; 76.3 ± 16.1 µM, CO 5 m; 80.0 ± 11.6 µM, SO s; 83.0 ± 11.6 µM, SO 5 m), DON (6.2 ± 1.7 µM, CO s; 5.8 ± 0.7 µM, CO 5 m; 5.8 ± 0.7 µM, SO s; 6.2 ± 1.7 µM, SO 5 m) and DOP (0.2 ± 0.1 µM for CO s and CO 5 m, 0.2 ± 0.0 µM for SO s and SO 5 m) concentrations were not much different at these sites and increased at PB (DOC: 150.8 ± 34.3 µM, DON: 17.9 ± 6.3 µM, DOP: 0.32 ± 0.2 µM). DOC, DON and DOP seasonal pattern were not significant ($p > 0.05$), with exception of DON and DOP at PB and DOP at CO 5 m that accumulated during the autumn-winter period ($p < 0.05$) (Figure V-6, V-7).

3.3.7. POC, PON and POP

POC, PON and POP concentrations were also higher at VA (92.0 ± 67.2 µM, 14.1 ± 9.5 µM, 1.9 ± 1.2 µM, respectively) than at AR (20.9 ± 24.8 µM, 3.4 ± 2.5 µM, 0.5 ± 0.5 µM, respectively) and at the other marine sites (Figure V-6). The highest concentrations were related to floods. In marine waters, POC (18.7 ± 8.4 µM, PB; 12.5 ± 18.6 µM, CO s; 7.8 ± 7.5 µM, CO 5 m; 4.5 ± 2.2 µM, SO s; 4.6 ± 2.1 µM, SO 5 m), PON (3.8 ± 2.7 µM, PB; 1.5 ± 1.6 µM, CO s; 1 ± 0.5 µM, CO 5 m; 0.8 ± 0.3 µM, SO s; 0.8 ± 0.3 µM, SO 5 m) and POP (0.3 ± 0.1 µM, PB; 0.1 ± 0.1 µM, CO s; trace to 0.1 µM at CO 5 m, SO s and SO 5 m) concentrations decreased from the near shore coastal sites to the central bay. During the spring-summer period, POC and PON concentrations exhibited high variations at VA, CO and SO. At PB and at CO s, respectively, POC and POP were accumulated during the warmest seasons ($p < 0.05$) (Figure V-7). The abundance of particulate organic matter during these seasons corresponded to the period of field irrigation at VA which could transport organic matter from channels.

3.4. Spectral characteristics and identification of PARAFAC components

Spectrofluorimetry coupled to PARAFAC analysis of the samples led to validate two PARAFAC models at three components: components C1-C3 for the inland sample dataset (Figure V-8) and components C4-C6 for the marine sample dataset (Figure V-9). The fluorescence maxima of each component are summarized in Table V-2. These fluorophores have been already detected in the aquatic environment and belong to the humic-like (C1, C3 and C6) and protein-like (C2, C4, and C5) types. C1 exhibits two fluorescence maxima at $\lambda_{Ex}/\lambda_{Em}$ of 250(330)/394 nm and corresponds to a humic-like fluorophore (peaks A + M) (Coble, 1996; Ishii and Boyer, 2012). It has been found that this fluorophore originated from biological or anthropogenic activities (Borisover et al., 2009; Zhang et al., 2010; Jørgensen et al., 2011; Ishii and Boyer, 2012) (Table V-2). C2 and C5 have very close fluorescence signatures with $\lambda_{Ex}/\lambda_{Em}$ of 230(280)/340 nm and 230(280)/342 nm, respectively, and correspond to tryptophan-like fluorophore (peak T1 + T2) (Coble, 1996; Hudson et al., 2007). This fluorophore is associated to autochthonous production or anthropogenic activity (Stedmon et al., 2007; Jørgensen et al., 2011; Osburn and Stedmon, 2011; Yao et al., 2011) (Table V-2). In the same way, C3 and C6 have quite similar fluorescence signatures with $\lambda_{Ex}/\lambda_{Em}$ of 250 (350)/454 nm and 245 (300)/450 nm, respectively (peaks A+C). This humic-like fluorophore is mainly present in the euphotic zone and shallow waters and was linked to terrestrial origin (Chen et al., 2010; Ishii and Boyer, 2012; Stedmon et al., 2003) (Table V-2).

C4 displays two fluorescence maxima with $\lambda_{Ex}/\lambda_{Em}$ of < 220(275)/< 300 nm. It corresponds to tyrosine-like fluorophore (peaks B1 + B2) (Coble, 1996; Hudson et al., 2007) and is derived from autochthonous processes (Stedmon and Markager, 2005a) (Table V-2).

3.5. Spatio-temporal variations of FDOM

In inland sites, the fluorescence intensities of humic-like C1, tryptophan-like C2 and marine humic-like C3 components were higher at VA (C1: 60.8 ± 23.8 QSU; C2: 23.5 ± 5.9 QSU; C3: 62.3 ± 29.6 QSU) than at AR (C1: 14.4 ± 4.6 QSU; C2: 8.8 ± 1.8 QSU; C3: 14.0 ± 5.8 QSU) (Figure V-10). The seasonal patterns of fluorescence intensities of humic-like materials were characterized by a re-increase of C1 and C3 at VA during the autumn-winter period ($p < 0.05$). At AR, C1 and C3 did not vary significantly with the season ($p > 0.05$). Similarly, tryptophan-like C2 component exhibited higher intensities during the autumn-winter period at VA ($p < 0.05$), while it had no significant seasonal pattern at AR. The other protein-like component, tyrosine-like C4, was only present in marine waters. C4 fluorescence intensity decreased from PB (6.5 ± 2.6 QSU) to CO s (4.3 ± 1.8 QSU), CO 5 m (3.9 ± 1.3 QSU), SO s (3.6 ± 1.3 QSU) and SO 5 m (2.9 ± 1.9 QSU) (Figure V-10, V-11). Only CO s showed a seasonal pattern with maximal values in spring and summer months ($p < 0.05$) (Figure V-11). In marine waters, the fluorescence intensity of the tryptophan-like fluorophore (C5 component) was higher at PB (9.3 ± 3.5 QSU) than at the other marine sites CO s (2.8 ± 1.0 QSU), CO 5 m (2.4 ± 0.7 QSU), SO s (2.3 ± 0.6 QSU) and SO 5 m (1.8 ± 0.7 QSU) (Figure V-10, V-11). At CO for both depth and at SO 5 m, C5 fluorescence intensities were higher in spring and summer ($p < 0.05$). At PB and SO s, no seasonal trends were observed. The humic C6 (marine waters) and C3 (inland waters) components had similar fluorescence signatures (Figure V-8, V-9). In marine waters, C6 component displayed the highest intensities at PB (8.9 ± 3.5 QSU) (Figure V-10, V-11). Its fluorescence intensity ranged from 1.1 to 11.4 QSU (2.2 ± 0.8 QSU), from 0.9 to 2.6 QSU (1.8 ± 0.5 QSU), from 1.3 to 2.4 QSU (1.7 ± 0.3 QSU) and from 0.7 to 1.9 QSU (1.2 ± 0.4 QSU) at CO s, CO 5 m, SO s and SO 5 m, respectively. At CO, the values obtained in spring and summer were higher than during the other seasons ($p < 0.05$). In other sites, no trend was observed ($p > 0.05$) (Figure V-10, V-11).

3.6. PCA classification of samples

To discriminate the inland and the marine samples according to their biogeochemical and hydrological characteristics, PCA was conducted with the PARAFAC component fluorescence intensities, and the hydrological and biogeochemical parameters acquired during

the whole sampling period (February 2011-February 2012) (Figure V-12a). For inland water dataset (AR and VA), F1 explained 51% of the total variability within samples. It was positively related to organic material (C1, C2 and C3 components, POP, PON, POC, DOC and DON; Table V-3). F1 was negatively related to NO_3^-, NO_2^- and pH. F2 explained 14% of the total variability and was positively related to temperature, PO_4^{3-} and DOP, and negatively weakly to Chl *a* and salinity. Hence, F1 discriminated VA waters from AR waters, while F2 achieved discrimination between the warmer season (spring-summer) and the cooler season (autumn-winter) (Figure V-12a).

For marine dataset (PB, CO, SO), F1 explained 44% of the total variability and was positively related to particulate organic matter descriptors POC, PON and POP and to fluorophores C5, C6 and C4 to a lesser extent (Table V-4). It was negatively correlated to salinity indicating the strong impact of freshwaters on the biogeochemistry of this marine area. F2 explained 15% of total variability and was positively related to temperature and C4 component, and negatively correlated to NO_3^- and NO_2^- (Table V-4). Therefore, F1 allows the discrimination of sites with regard to their salinity values and thus to the occurrence of freshening events. F2 achieved discrimination between the warmer and the cooler season (Figure V-12b).

4. Discussion

4.1. General observations

The observations made during our study were driven by the meteorological conditions that prevailed during the period investigated. The wind blow, rain falls and air temperature were of moderate intensity. Consequently, the Rhône River discharge remained under critical values typical of this area. The plume extension in Marseilles Bay was weak, reflecting these conditions. Nevertheless, the hydrological and biogeochemical features in the Rhône basin and Marseilles Bay confirmed that the Rhône River was a major source of nutrients and carries dissolved and particulate material. Thus, correlation and PCA analyses of the hydrological, biogeochemical and FDOM data set collected during one year period allowed deciphering the major factors affecting FDOM composition in the Rhône River basin and the Marseilles Bay waters (Figure V-12).

4.2. Impact of environmental conditions on the FDOM composition of inland and marine waters

FDOM content in inland waters was much higher than in marine waters in relation to higher amount of organic matter and nutrients (Figure V-6, V-10). Inland waters (AR, VA) displayed a much higher proportion of humic-like fluorophores (C1, C3) relative to tryptophan-like material (C2) (Figure V-10, V-12a). This FDOM composition is typical of aquatic systems strongly influenced by terrestrial organic matter. Indeed, humic-like material present in inland waters is issued from the microbial degradation of higher plants and soil organic matter (Hudson and Reynolds, 2007; Henderson et al., 2009; Fellman et al., 2010). It has been shown that C1 fluorophore was abundant in lake and was linked to agriculture activities, whereas C3 was related to terrestrial inputs (Ishii and Boyer, 2012). In agricultural catchments, C1 component was often dominant compared to other fluorophores (Bieroza et al., 2009). In several studies, tryptophan-like component has been attributed to primary production and phytoplankton activity (Parlanti et al., 2000; Lønborg et al., 2010; Romera-Castillo et al., 2010; Yamashita et al., 2010). Hence, in inland waters, tryptophan-like material may be derived from autochthonous biological activity, which could explain the correlation of C2 with the Chl *a*. However, the high correlations of C2 with the humics C1 and C3 ($r = 0.86$ and 0.79) (Table V-4) could also implied that a part of C2 may had an allochthonous origin. The fact that C1 was strongly correlated to C3 ($r = 0.97$) while the correlations between humic and tryptophan fluorophores were slightly lower ($r = 0.86$ for C1 and C2; $r = 0.79$ for C3 and C2) (Table V-3; Figure V-12a) reinforces the hypothesis of an allochthonous (terrestrial) origin for C1 and C3 humic components in AR and VA waters.

FDOM amount was noticeably more important at VA than at AR (Figure V-10, V-12a). The higher proportion of tryptophan material at VA may be due to a higher primary production/phytoplankton activity as suggested by the higher Chl *a* concentrations found in this site compared to AR (Figure V-6). The Vaccarès Pond is characterized as highly turbid. DOM comes from field drainage by irrigation and rain waters and is transported through channels to the pond. Resuspension of bottom particles and dissolution in the water column may also contribute to the enrichment in humic material. Previous studies highlighted the dominant role of wind velocity in controlling the concentrations of suspended matter in this shallow pond (Banas et al., 2005) and suggested that phytoplankton productivity could represent only a minor source of autochthonous suspended matter (De Groot and Golterman, 1999).Contrary to inland waters, FDOM in marine waters was dominated by protein-like

material (Figure V-10). Protein-like fluorophores (tyrosine and tryptophan) in marine coastal waters have be shown to be originated from autochthonous biological activities, either phytoplankton or bacterial activities (Determann et al., 1998; Parlanti et al., 2000; Stedmon et al., 2003; Cammack et al., 2004; Lønborg et al., 2010; Romera-Castillo et al., 2010; Yamashita et al., 2010). The origin of humic-like fluorophore in marine waters is less evident because some works demonstrated that it had a terrestrial source (Fellman et al., 2010; Ishii and Boyer, 2012), while other studies found it was derived from the degradation of organic matter by marine bacteria (Yamashita and Tanoue, 2004; Lønborg et al., 2009; Yamashita et al., 2010). FDOM was higher at PB than at CO and SO. Indeed, due to the influence of the Berre Lagoon, which is considered as an eutrophic system with Chl *a* concentrations reaching up to 33 µg L^{-1} (Delpy et al., 2012), PB presented higher amounts of nutrients and organic material compared to CO and SO sites. Typically, the nutrient concentrations in the Mediterranean Sea surface waters range 2-3 and 0.15-0.20 µM for NO_3^- and PO_4^{3-}, respectively (Marty et al., 2002). At PB, NO_3^- and PO_4^{3-} concentrations ranged 0.04-13.30 and 0.01-0.90 µM, respectively. FDOM in CO and SO were typical of oceanic environments in term of composition and quantity (Para et al., 2010; Yamashita et al., 2011; Tedetti et al., 2012). Interestingly, higher correlations were observed between tryptophan (C5) component and humic (C6) component (r = 0.87) than between tryptophan and tyrosine (C4) components (r = 0.72) (Table V-4; Figure V-12b). These results showed that tryptophan and humic fluorophores may have a common origin. This hypothesis was enhanced by negative correlations with each of them and the salinity (r = -0.66 and -0.68 with C5 and C6, respectively) (Table V-4; Figure V-12b) which implies that these fluorophores may be of allochthonous origin (Rhône River). The weaker correlation between salinity and C4 (r = -0.42) and the correlation between C4 and temperature (r = 0.52) (Table V-4; Figure V-12b) suggested that this fluorophore was rather linked to *in situ* marine production. It should be noticed that tryptophan C5 could also be produced *in situ* and could be linked to bacteria activity (Determann et al., 1998; Stedmon et al., 2003; Cammack et al., 2004). The input of organic matter during freshening events could stimulate bacteria activity and release C5 compound (Paoli, 2005) explaining the absence of correlation with the temperature. Even though humic C6 has generally has an allochthonous (terrestrial) origin and display a conservative behaviour from freshwater to seawater (Yamashita and Jaffe, 2008; Osburn and Stedmon, 2011), it may be produced *in situ* in marine waters from bacterial degradation of organic matter (Hudson et al., 2008).

4.3. Effect of seasonality on biogeochemical and FDOM properties

The humic-like material (C1 and C3) at AR exhibited peaks of abundances during the coldest months because of terrestrial inputs such as degraded material from higher plants (Fellman et al., 2010). At VA, the coldest season was marked mostly by high salinity (Figure V-7, 12a) and an increase in C1 and C3 intensities that was much more pronounced than at AR. This showed that irrigation was not the major source of C1 and C3 increase in the Vaccarès pond in winter but reinforces the hypothesis of a dominant role of wind velocity and sediment particle resuspension in controlling the concentrations of DOM in this shallow pond. The seasonal variability of tryptophan material (C2) was different between AR and VA sites. C2 was slightly more important in spring-summer at AR whereas at VA, C2 was more abundant during the coldest seasons and showed the opposite classic seasonal trend for tryptophan linked to primary production (Fellman et al., 2010). This observation suggests that C2 sources in VA may be sought in the release of terrigeneous DOM through rain and wind events that dominated the winter period. This interpretation could also explain the good correlation between this component and both humic C1 and C3 ($r = 0.86$ and 0.79, respectively) (Table V-4). The seasonal trend of C2 at AR (higher in spring-summer) may reflect the seasonal cycle of biological activity (tryptophan released by phytoplankton activity) and also implies that VA was stronger impacted by rain events than AR.

At the marine site, negative correlations between temperature and $NO_3^- + NO_2^-$ concentrations ($r = -0.50$, $p < 0.05$; Table V-4) reflected the release of inorganic nutrients in the water column during the coldest seasons by organic matter mineralization at depth and re-introduction of nutrients at the surface through mixing (Packard et al., 1988; Minas et al., 1991). The negative correlation between salinity and nutrients ($r = -0.26$, $p < 0.05$; Table V-4) showed that there was also probably a terrestrial origin of nutrients *via* freshwater inputs (Rhône River or Berre Lagoon). Chl *a* concentration was not dependant of the season (Figure V-7) and was negatively correlated to salinity ($r = -0.44$, $p < 0.05$; Table V-4). Hence, Chl *a* concentrations could be stimulated by freshening events (inputs of riverine water with high amount of nutrients) leading to an increase in phytoplankton activity. The strongest seasonality was observed at the CO site for the tryptophan-like C4 that considerably increased during the warmest months and to a lesser extent the tyrosine-like C5 and the humic-like C6 fluorophores (Figure V-11). This pattern at CO confirmed the autochthonous origin of C4 proposed above. Indeed, light and temperature increase during the spring-summer period may likely results in higher biological production induced by freshwater inputs and subsequent

enrichment of the water in C4 fluorophore at CO (Para et al., 2010; Tedetti et al., 2012). C5 and C6 fluorophores at CO were less affected by the seasonality, which re enforces the hypothesis of a major contribution of allochthonous sources at these fluorophores.

4.4. Impact of the Rhône River on the Vaccarès pond and on the Marseille Bay

Rhône River inputs in Vaccarès lagoon and in marine sites influenced the water biogeochemistry. In the Vaccarès pond, rice field irrigation with the Rhône waters occurred from the beginning of April to the end of September (spring and summer). The first impact was observed on the salinity values. During the irrigation period, the salinity tended to decrease whereas marine water intrusions led to higher salinity values during the rest of the year (Figure V-12). The irrigation water pumped from the Rhône River transported a high quantity of organic material and nutrients (due to the use of fertilizers) to VA after crossing fields. As a consequence, at VA, the concentrations in POC, PON, POP and NO_3^- + NO_2^- were clearly higher in spring-summer (Figure V-7). This continuous seasonal process likely created the enrichment of the pond in humic substances (C1 and C3) through direct inputs or indirect biomass production.

At CO, Rhône River intrusion events were observed and visible onto PCA (Figure V-12b) through samples located close to PB samples and displaying high abundance of tyrosine, humic and particulate C/N/P materials. After each event, biogeochemical parameters such as Chl *a*, NO_3^- + NO_2^-, POC, PON and POP concentrations increased at both depths. These Rhône River intrusions had two consequences. The first was an enrichment in all FDOM fluorophores (Figure V-10) and the second was a stimulation of the primary production (Figure V-3) like observed in a previous study (Para et al., 2010). The Rhône River intrusions at CO induced a clear increase in the intensity of humic-like material (14-163%). C4 and C5 components (tyrosine and tryptophan-like fluorophores) were less impacted with an increase between 12 and 63%, except in June.

At SO, no significant salinity decrease was observed during the sampling period. However, on 12 December, the plume of the Rhône extended up to the CO site and could also impact the SO area like reported in a Para et al. (2010). With a salinity of 37.8 PSU, we could not consider clearly that the Rhône plume impacted SO. However at this date, we observed a drastic increase in Chl *a*, NO_3^- + NO_2^-, POC, NOP and POP. Simultaneously, C5 and C6 fluorophores increased by 23 and 53%. These observations strongly suggested a triggering effect of marine autochthonous production by the Rhône waters in the Marseilles Bay (at

Sofcom), although the signature of the plume was not noticeable when measuring salinity at this site.

5. Conclusions

This study highlights the FDOM composition and seasonal variability in inland and marine waters under the influence of the Rhône River. Inland waters were dominated by terrestrial humic-like material whereas marine waters were dominated by protein-like fluorophores. In inland waters, humic substances dominated, and reflected the high proportion of terrestrial organic material. On the contrary, in marine waters, protein-like fluorophores dominated. The fluorophore tyrosine was linked to the production of autochtonous material while the tryptophan and the humic-type fluorophore had a predominantly allochtonous origin. In marine coastal sites, intrusions of the Rhone River have an impact on the local biogeochemistry by increasing the amount of all fluorophores, or by direct input of terrestrial FDOM or indirectly via stimulation of biological activity (primary production) related to addition of nutrients.

Table V-1. Characteristics of the study sites located in the Rhône basin (Arles, Vaccarès) and the north-western Mediterranean Sea (Port-de-Bouc, Couronne, Sofcom) in southern France and sampled from February 2011 to February 2012.

Station	Abbreviation	Water type	Position	Site depth (m)	Sampling depth (m)
Arles	AR	Freshwaters (Rhône River)	43°40.72’ N, 4°37.27’ E	1-3	0.1
Vaccarès	VA	Brackish waters (Vaccarès Pond); Under the influence of the Rhône River and the Mediterranean Sea	43°31.44’ N, 4°38.14’ E	0.5-1.5	0.1
Port-de-Bouc	PB	Harbour marine waters (Gulf of Fos-sur-mer); Under the influence of the Berre Lagoon and potentially under the influence of the Rhône River	43°23.75’ N, 4°59.20’ E	12	0.1
Couronne	CO	Marine waters (between Rhône mouth and Marseilles Bay); Potentially under the influence of the Rhône River	43°16.50’ N, 5°02.04’ E	90	0.1 and 5
Sofcom	SO	Marine waters (Marseilles Bay); Potentially under the influence of the Rhône River	43°14.50’ N, 5°17.50’ E	60	0.1 and 5

Table V-2. Excitation and emission maxima (λ_{Ex} and λ_{Em} max) of the six components validated by the PARAFAC models applied on inland (C1-C3) and marine (C4-C6) samples, and identification (type/nature and possible origins) of these components by comparison with the literature data.

Components	λ_{Ex}[a] and λ_{Em} max (nm)	Type/Nature	Possible origin	Previous studies
C1	250 (330) / 394	Humic-like	Anthropogenic, biological or terrestrial	C4; 250 (330) / 400 (Ref.1) C3; < 240-260 (295-380) / 374-450 (Ref. 2) C4: < 240 (310) / 400 (Ref. 3) C3; 250 (310) / 400 (Ref. 4) C4; 250 (330) / 410 (Ref. 6) C2; < 250 (300) / 400 (Ref. 8) C2; 235 (300) / 404 (Ref. 12) C2; 235 (290) / 397 (Ref. 13) C1; < 230 (290) / 410 (Ref. 14)
C2	230 (280) / 340	Tryptophan-like	Autochthonous (microbial or plankton) or anthropogenic	C5; < 240 (280) / 360 (Ref. 6) C7; 280 / 344 (Ref. 7) C4; < 240 / 300 / 360 (Ref. 8) C2; < 230 (270) / 346 (Ref. 9) C1; 230 (280) / 344 (Ref. 12) C4; < 240 (260-280) / 330-350 (Ref. 13)
C3	250 (350) / 454	Humic-like	Terrestrial, photoproduct	C2; < 250 / 450 (Ref. 1) C1; < 230-260 / 400-500 (Ref. 2) C3; 240 / 424 (Ref. 5) C1; < 240 / 436 (Ref. 6) C1; < 248 / 450 (Ref. 7)

C4	< 220 (275) / < 300	Tyrosine-like	Autochthonous (microbial or plankton)	C5; < 250 (280) / 310 (Ref. 8) C1; < 230 (275) / 306 (Ref. 9) C4; 230 (270) / 380 (Ref. 12) C3; < 225 (275) / 322 (Ref. 13)
C5	230 (280) / 342	Tryptophan-like	Autochthonous (microbial or plankton) or anthropogenic	C5; < 240 / 280 / 360 (Ref. 6) C7; 280 / 344 (Ref. 7) C4; < 240 / 300 / 360 (Ref. 8) C2; < 230 (270) / 346 (Ref. 9) C1; 230 (280) / 344 (Ref. 12) C4; < 240 (260-280) / 330-350 (Ref. 13)
C6	245 (300) / 450	Humic-like	Terrestrial, photoproduct	C2; < 250 / 450 (Ref. 1) C1; < 230-260 / 400-500 (Ref. 2) C3; 240 / 424 (Ref. 5) C1; < 240 / 436 (Ref. 6) C1; < 248 / 450 (Ref. 7)

[a] The secondary Ex maximum is given in brackets.

References (Ref): 1. Chen et al., 2010; 2. Ishii and Boyer, 2012; 3. Jørgensen et al., 2011; 4. Kowalczuk et al., 2009; 5. Osburn and Stedmon, 2011; 6. Stedmon et al., 2003; 7. Stedmon and Markager, 2005a; 8. Stedmon et al., 2007; 9. Tedetti et al., 2012; 10. Yamashita et al., 2010b; 11. Yamashita et al., 2010c; 12. Yao et al., 2011; 13. Zhang et al., 2010; 14. Zhang et al., 2011; 15. Stedmon and Markager, 2005b.

Table V-3. Spearman correlation coefficients between physico-chemical, biogeochemical parameters and PARAFAC components for inland sites (Arles, Vaccarès). Coefficients in bold are significant for $\alpha = 0.05$.

	C1	C2	C3	$NO_3^- + NO_2^-$	PO_4^{3-}	Chl *a*	DOC	DON	DOP	POC	PON	POP	T	S	pH
C1	**1**	**0.86**	**0.97**	**-0.76**	**-0.36**	0.25	**0.76**	**0.83**	0.24	**0.67**	**0.65**	**0.61**	-0.24	**0.66**	-0.27
C2		**1**	**0.79**	**-0.87**	**-0.40**	**0.40**	**0.71**	**0.79**	0.19	**0.61**	**0.62**	**0.54**	-0.03	**0.76**	**-0.34**
C3			**1**	**-0.68**	**-0.39**	0.28	**0.73**	**0.80**	0.18	**0.73**	**0.69**	**0.67**	-0.20	**0.59**	**-0.34**
$NO_3^- + NO_2^-$				**1**	**0.46**	**-0.39**	**-0.70**	**-0.68**	-0.09	**-0.46**	**-0.45**	**-0.37**	0.01	**-0.80**	**0.38**
PO_4^{3-}					**1**	**-0.48**	**-0.50**	**-0.38**	**0.53**	**-0.43**	-0.28	-0.17	0.13	**-0.73**	0.29
Chl a						**1**	**0.33**	0.22	-0.25	**0.31**	0.25	0.20	0.09	**0.35**	**-0.34**
DOC							**1**	**0.77**	0.11	**0.58**	**0.49**	**0.35**	**-0.33**	**0.70**	-0.02
DON								**1**	**0.36**	**0.67**	**0.64**	**0.53**	-0.14	**0.64**	-0.24
DOP									**1**	0.03	0.16	0.15	0.07	-0.12	0.08
POC										**1**	**0.96**	**0.90**	0.10	**0.48**	-0.29
PON											**1**	**0.94**	0.24	**0.40**	-0.28
POP												**1**	0.27	0.28	**-0.36**
T													**1**	-0.21	-0.12
S														**1**	-0.26
pH															**1**

Table V-4. Spearman correlation coefficients between physico-chemical, biogeochemical parameters and PARAFAC components for marine sites (Port-de-Bouc, Couronne, Sofcom). Coefficients in bold are significant for $\alpha = 0.05$.

	C4	C5	C6	$NO_3^- + NO_2^-$	PO_4^{3-}	Chl *a*	DOC	DON	DOP	POC	PON	POP	T	S	pH
C4	**1**	**0.72**	**0.67**	-0.11	0.17	**0.32**	**0.47**	0.20	0.18	**0.56**	**0.57**	**0.37**	**0.52**	**-0.42**	**0.31**
C5		**1**	**0.87**	0.11	**0.27**	**0.41**	**0.49**	**0.52**	**0.34**	**0.73**	**0.71**	**0.64**	0.13	**-0.66**	0.01
C6			**1**	**0.23**	**0.32**	**0.50**	**0.46**	**0.46**	**0.38**	**0.67**	**0.66**	**0.66**	0.09	**-0.68**	0.11
$NO_3^- + NO_2^-$				**1**	**0.56**	**0.25**	0.12	**0.26**	**0.23**	-0.14	-0.11	**0.26**	**-0.50**	**-0.26**	-0.06
PO_4^{3-}					**1**	**0.23**	**0.28**	**0.21**	-0.05	0.06	0.09	**0.24**	-0.17	**-0.27**	**0.21**
Chl a						**1**	**0.46**	**0.40**	**0.30**	**0.57**	**0.59**	**0.57**	0.11	**-0.44**	0.12
DOC							**1**	**0.27**	0.03	**0.49**	**0.50**	**0.42**	0.16	**-0.42**	0.13
DON								**1**	**0.51**	**0.58**	**0.61**	**0.75**	-0.15	**-0.60**	-0.15
DOP									**1**	**0.33**	**0.37**	**0.48**	-0.12	**-0.39**	-0.06
POC										**1**	**0.98**	**0.82**	**0.25**	**-0.70**	-0.01
PON											**1**	**0.85**	**0.28**	**-0.70**	0.02
POP												**1**	-0.00	**-0.70**	-0.08
T													**1**	-0.03	**0.38**
S														**1**	-0.01
pH															**1**

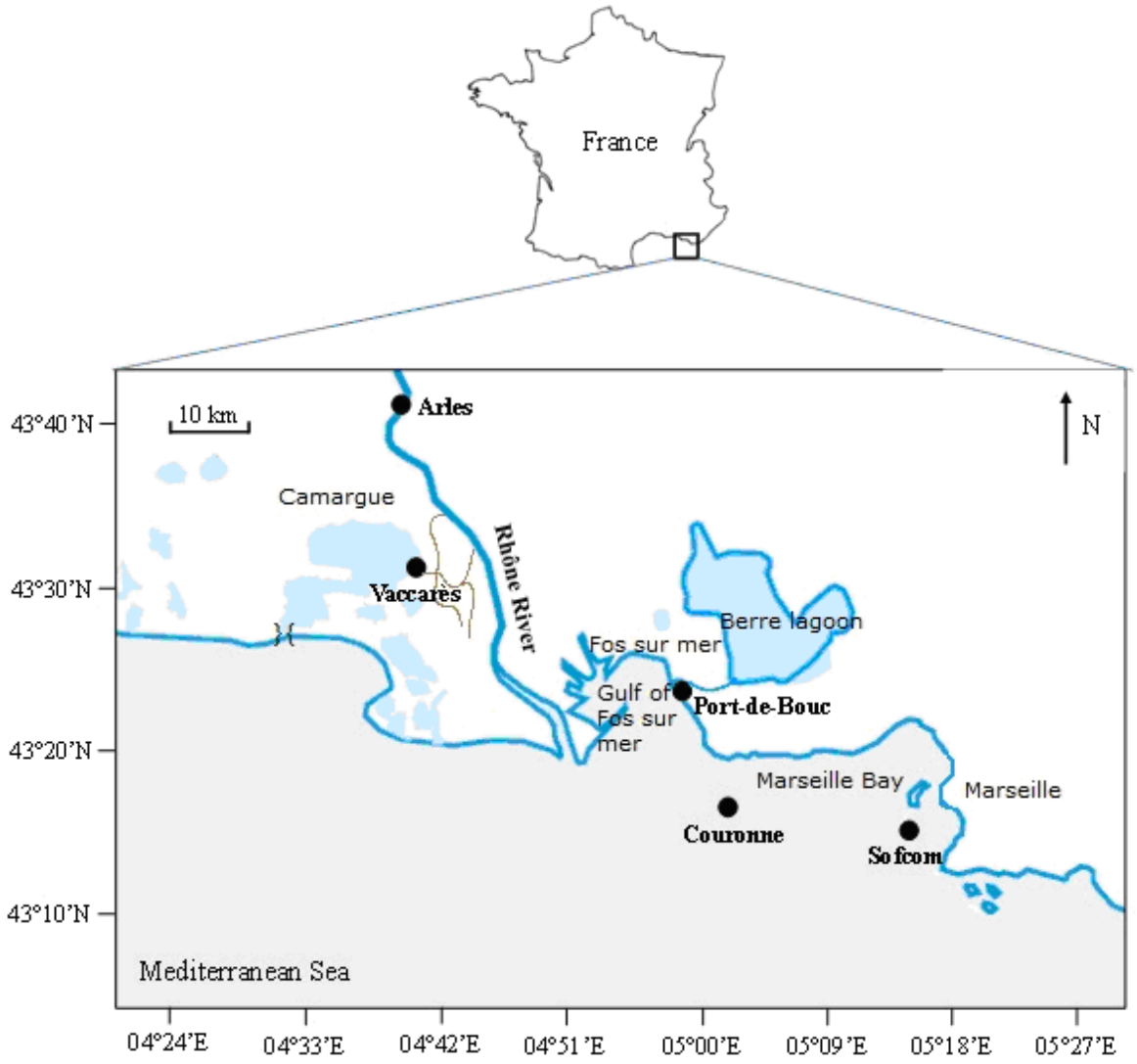

Figure V-1. Location of the five study sites in the Rhône basin (Arles, Vaccarès) and the north-western Mediterranean Sea (Port-de-Bouc, Couronne, Sofcom), southern France. The distance between the Rhône mouth and Port-de-Bouc, Couronne and Sofcom is 13, 16 and 37 km, respectively. The Rhône River is connected to the Vaccarès Pond through a 6 km channel system. The detailed characteristics of these sites are provided in Table 1.

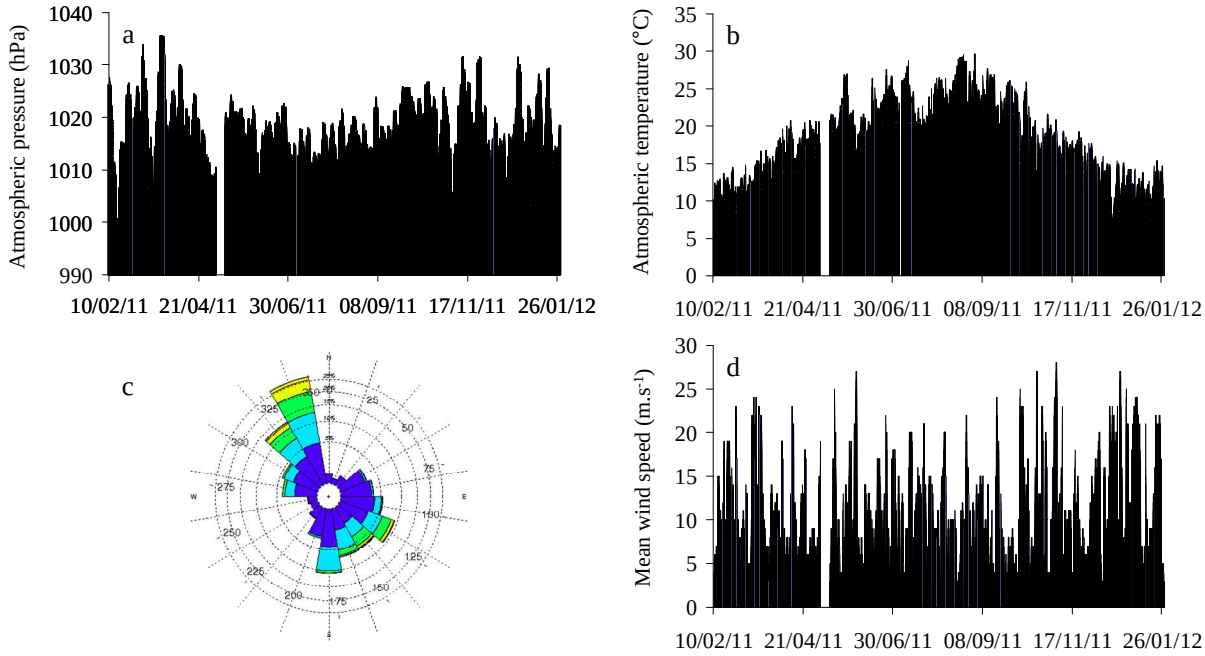

Figure V-2. Atmospheric pressure (a) and temperature (b), wind direction (c) and mean wind speed (d) in the study area during the sampling period (February 2011-February 2012).

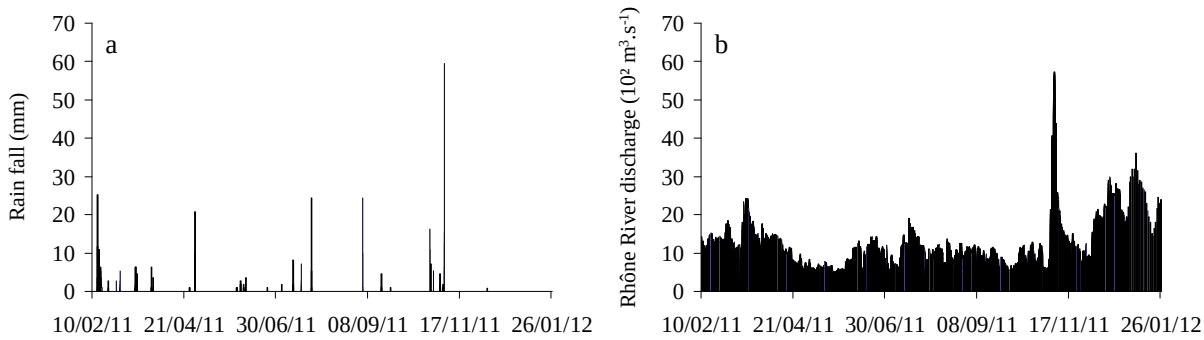

Figure V-3. Rain fall in the study area (a) and Rhône River discharge (b) during the sampling period (February 2011-February 2012).

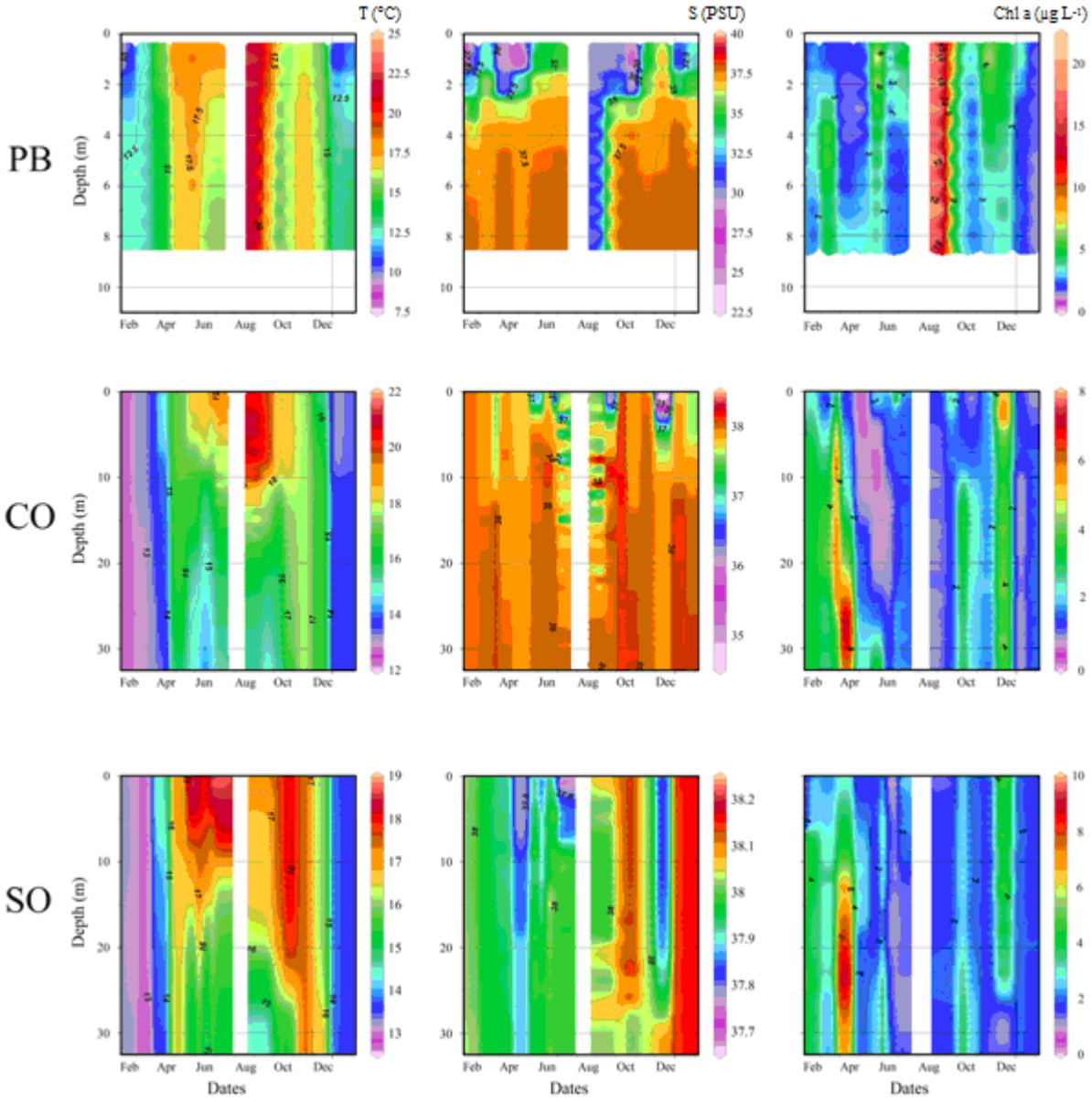

Figure V-4. CTD profiles of temperature, salinity and Chl *a* concentration in the water column of Port-de-Bouc (PB), Couronne (CO) and Sofcom (SO) stations during the sampling period (February 2011-February 2012). Maps made with Ocean Data View v4.

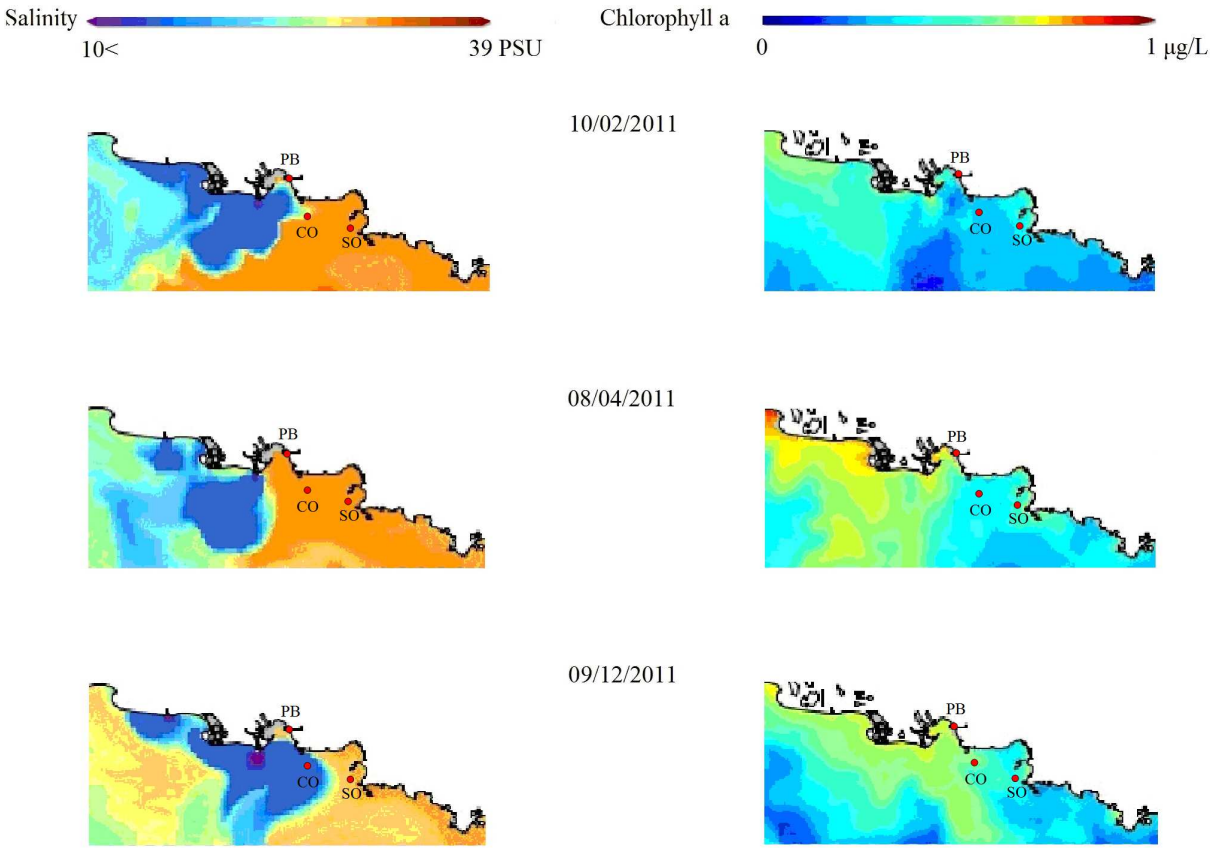

Figure V-5. Surface maps of salinity and Chl *a* concentration in the Marseilles Bay at three different dates: 10 February, presence of the Rhône River plume at Port-de-Bouc (PB); 8 April, absence of the Rhône River plume at PB; 9 December, presence of the Rhône River plume at Couronne (CO) and Sofcom (SO).

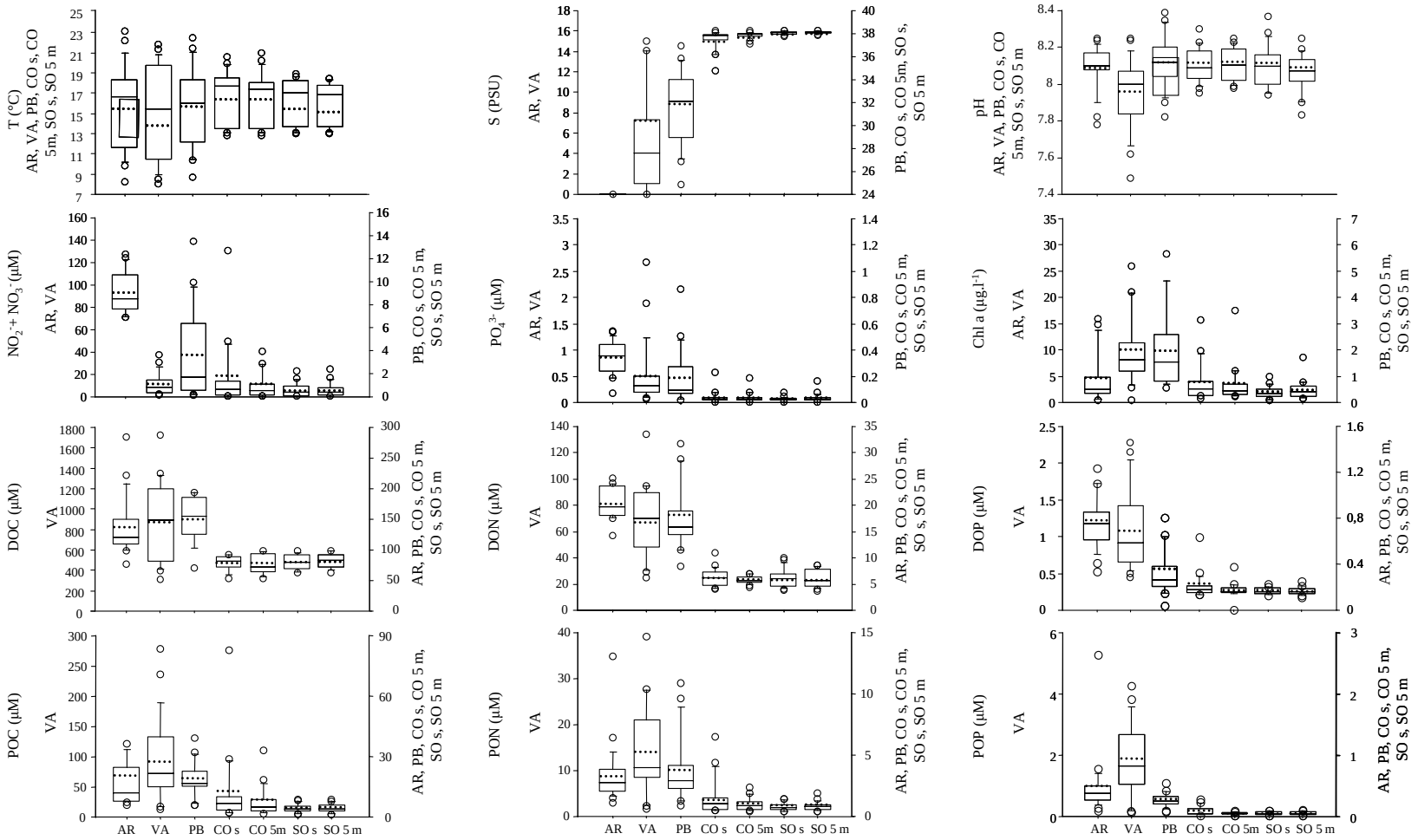

Figure V-6. Box-and-whisker plots of temperature (T, in °C), salinity (S, in PSU), pH, nitrates plus nitrites (NO_3^- + NO_2^-, in µM), phosphates (PO_4^{3-}, in µM), chlorophyll *a* (Chl *a*, in µg L^{-1}), dissolved organic carbon, nitrogen, phosphorus (DOC/N/P, in µM), particular organic carbon, nitrogen, phosphorus (POC/N/P, in µM) for inland (AR, VA) and marine waters (PB, CO, SO) during the whole study period (February 2011-February 2012). For CO and SO, both depths are presented: subsurface (s) and 5 m. The bottom and top of boxes are the 25th and 75th percentiles,

respectively. In dotted and solid lines are represented the mean and the median (the 50^{th} percentile), respectively. The ends of the error bars correspond to the 10^{th} percentile (bottom) and to the 90^{th} percentile (top). The dots in color represent the observations < 10^{th} percentile and the observations > 90^{th} percentile.

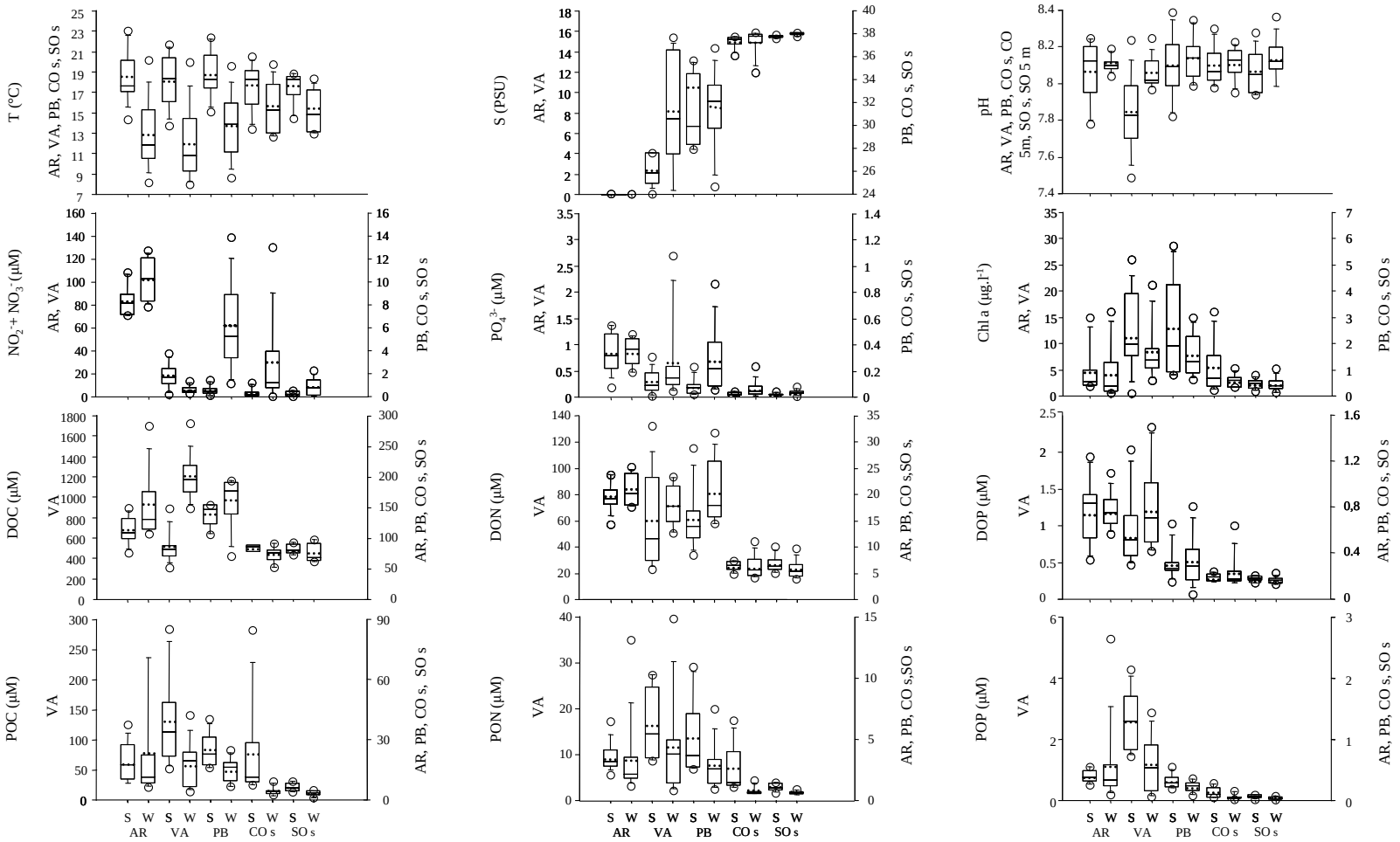

Figure V-7. Box-and-whisker plots of temperature (T, in °C), salinity (S, in PSU), pH, nitrates plus nitrites (NO_3^- + NO_2^-, in µM), phosphates (PO_4^{3-}, in µM), chlorophyll *a* (Chl *a*, in µg L^{-1}), dissolved organic carbon, nitrogen, phosphorus (DOC/N/P, in µM), particular organic carbon, nitrogen, phosphorus (POC/N/P, in µM) for inland (AR, VA) and marine waters (PB, CO, SO) for two periods: Spring + Summer (S) and Autumn + Winter (W). For CO and SO, only subsurface data (s) are presented. The bottom and top of boxes are the 25th and 75th percentiles,

respectively. In dotted and solid lines are represented the mean and the median (the 50^{th} percentile), respectively. The ends of the error bars correspond to the 10^{th} percentile (bottom) and to the 90^{th} percentile (top). The dots represent the observations < 10^{th} percentile and the observations > 90^{th} percentile.

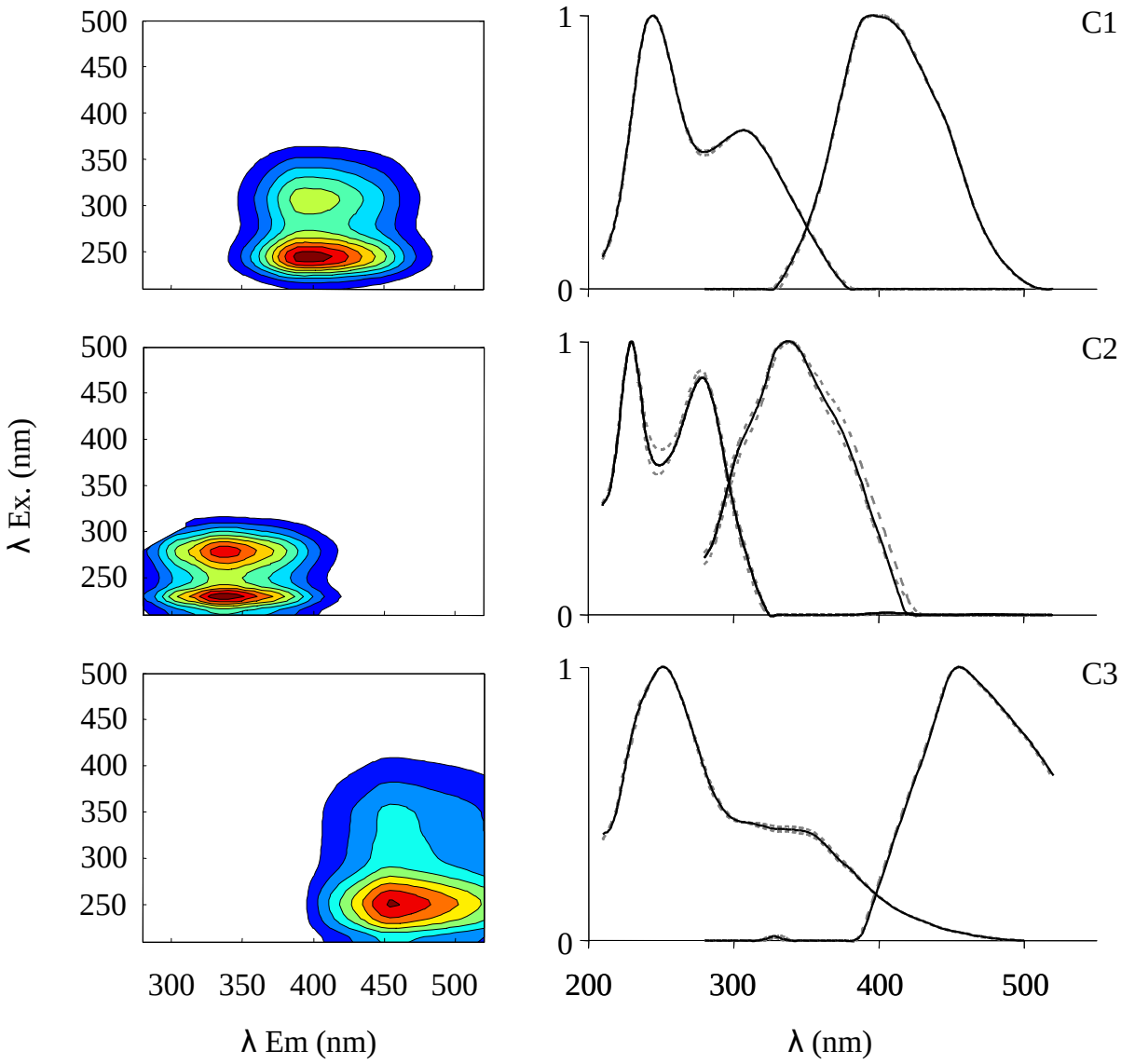

Figure V-8. Spectral characteristics of the 3 components (C1-C3) validated by the PARAFAC analysis for 42 inland samples collected in the Rhône River (Arles) and the Vaccarès Pond (Vaccarès). Both contour (left column) and line (right column) plots are depicted. The line plots show the excitation (left side) and emission (right side) fluorescence spectra. The grey dotted lines correspond to the split half analysis results.

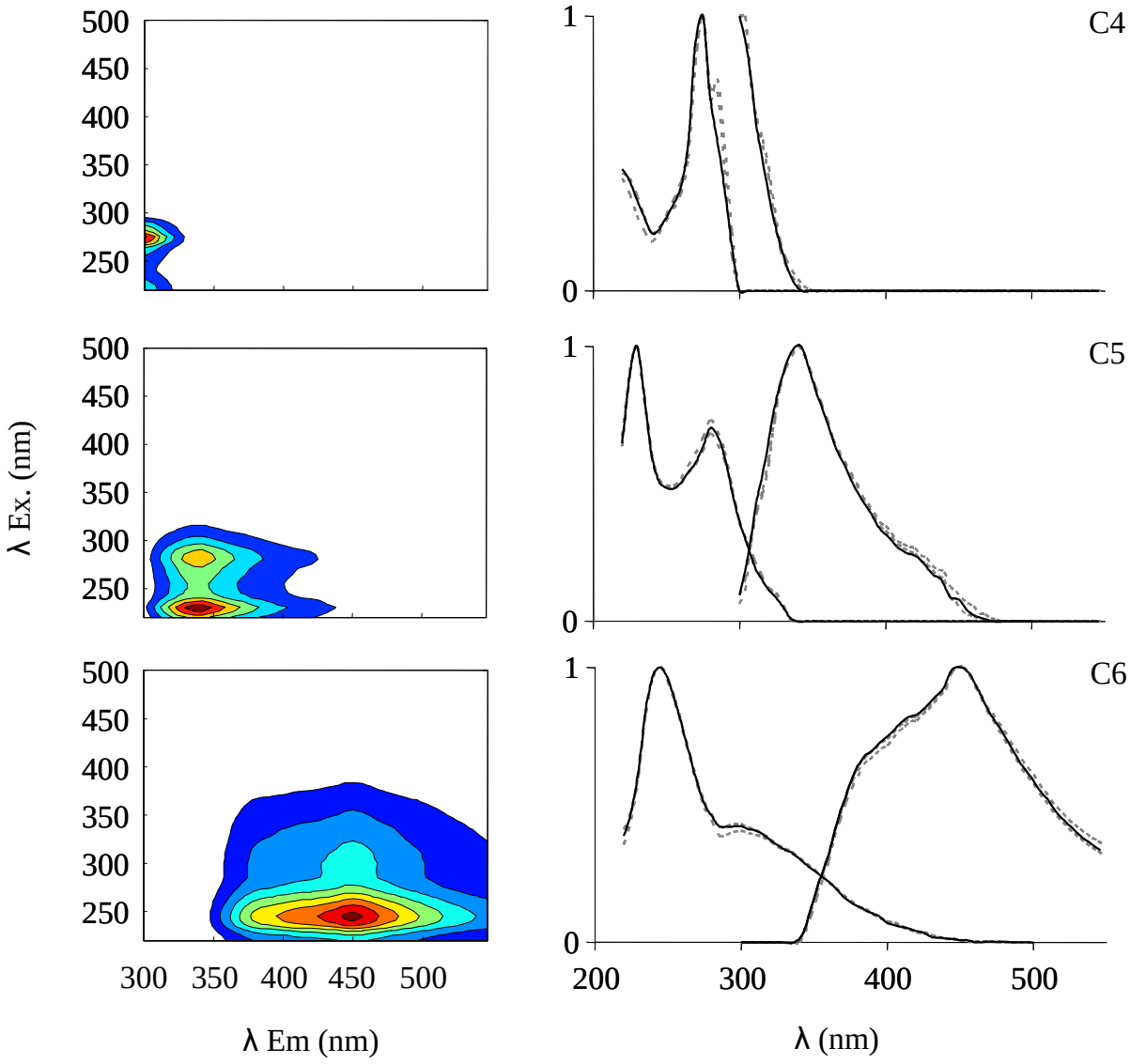

Figure V-9. Spectral characteristics of the 3 components (C4-C6) validated by the PARAFAC analysis for 94 marine samples (Port-de-Bouc, Couronne, Sofcom). Both contour (left column) and line (right column) plots are depicted. The line plots show the excitation (left side) and emission (right side) fluorescence spectra. The grey dotted lines correspond to the split half analysis results.

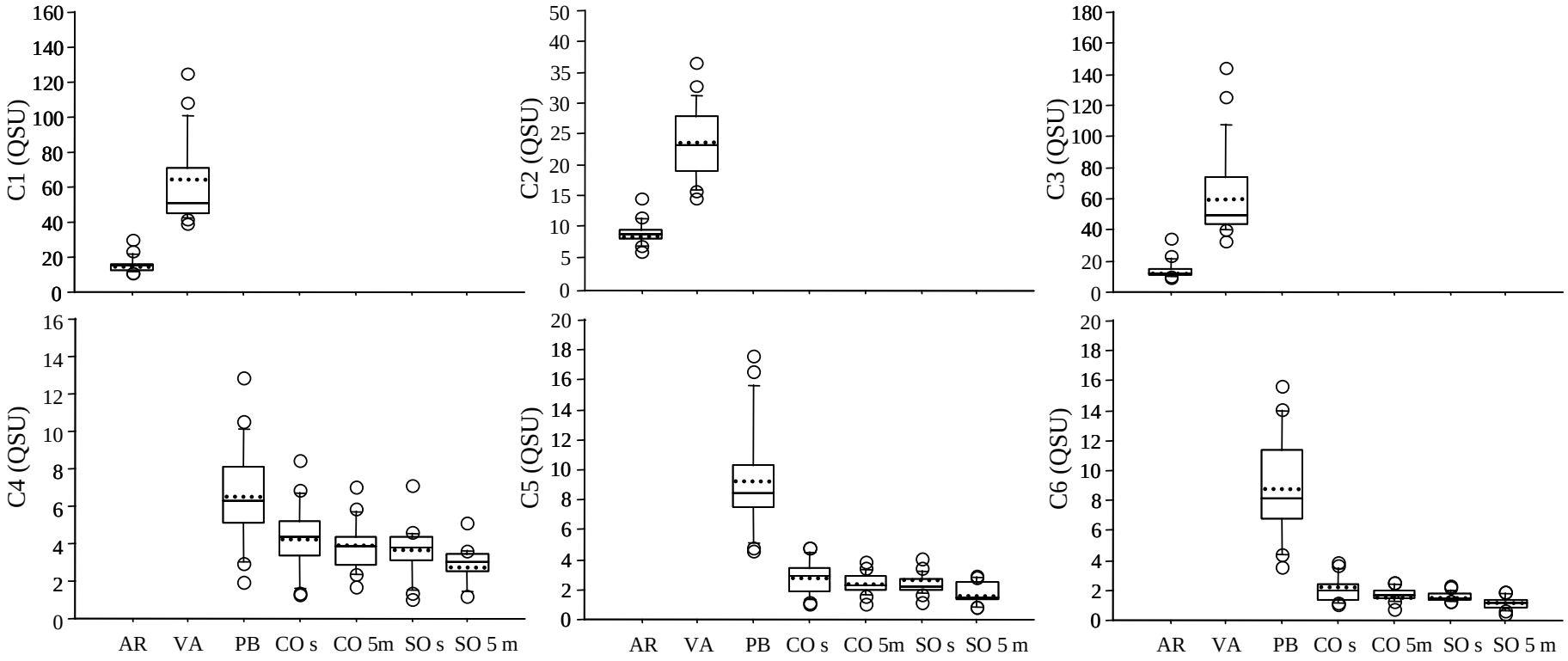

Figure V-10. Box-and-whisker plots of PARAFAC components (fluorescence intensity in QSU) for inland (AR, VA) and marine waters (PB, CO, SO) during the whole study period (February 2011-February 2012). Components C1-C3 for AR and VA, components C4-C6 for PB, CO and SO. For CO and SO, both depths are presented: subsurface (s) and 5 m. The bottom and top of boxes are the 25th and 75th percentiles, respectively. In dotted and solid lines are represented the mean and the median (the 50th percentile), respectively. The ends of the error bars correspond to the 10th percentile (bottom) and to the 90th percentile (top). The dots represent the observations < 10th percentile and the observations > 90th percentile.

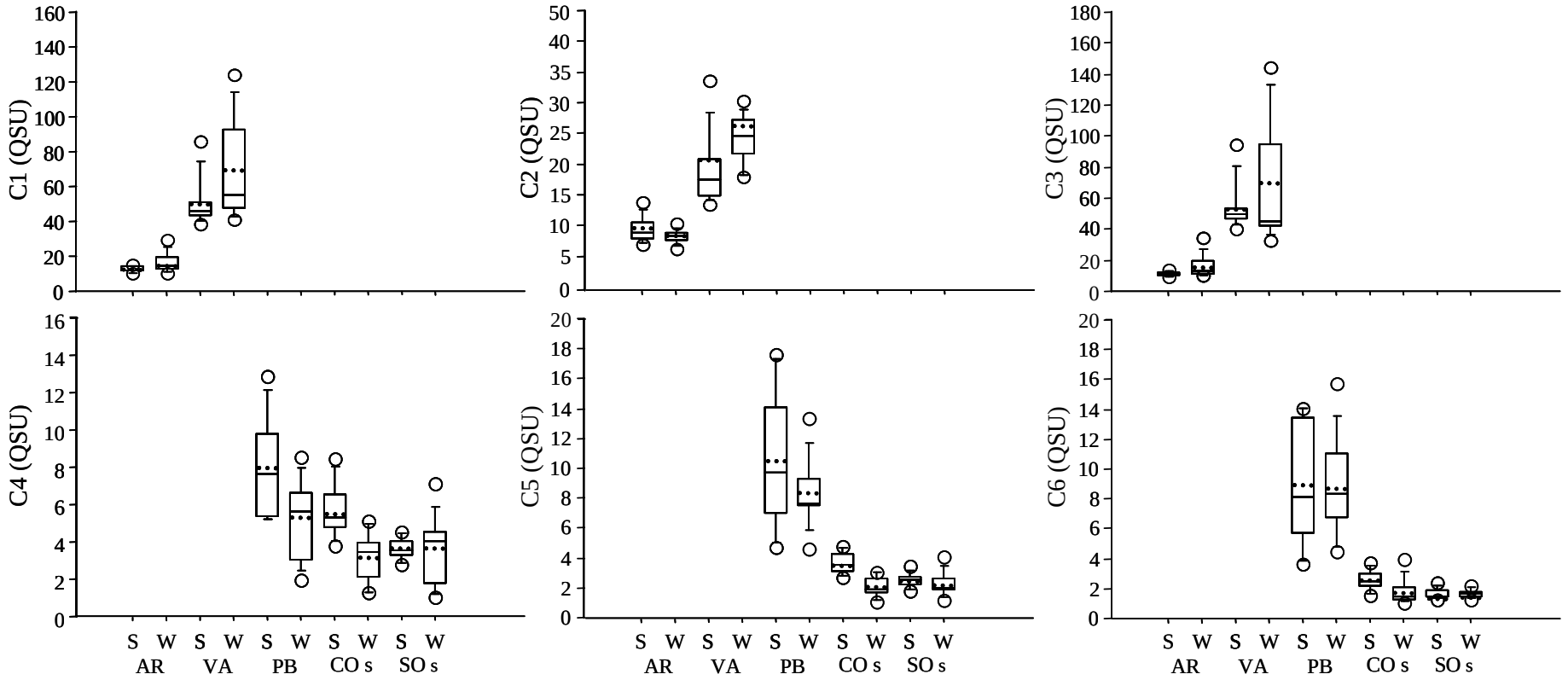

Figure V-**11.** Box-and-whisker plots of PARAFAC components (fluorescence intensity in QSU) for inland (AR, VA) and marine waters (PB, CO, SO) for two periods: Spring + Summer (S) and Autumn + Winter (W). Components C1-C3 for AR and VA, components C4-C6 for PB, CO and SO. For CO and SO, only subsurface data (s) are presented. The bottom and top of boxes are the 25th and 75th percentiles, respectively. In dotted and solid lines are represented the mean and the median (the 50th percentile), respectively. The ends of the error bars correspond to the 10th percentile (bottom) and to the 90th percentile (top). The dots represent the observations < 10th percentile and the observations > 90th percentile.

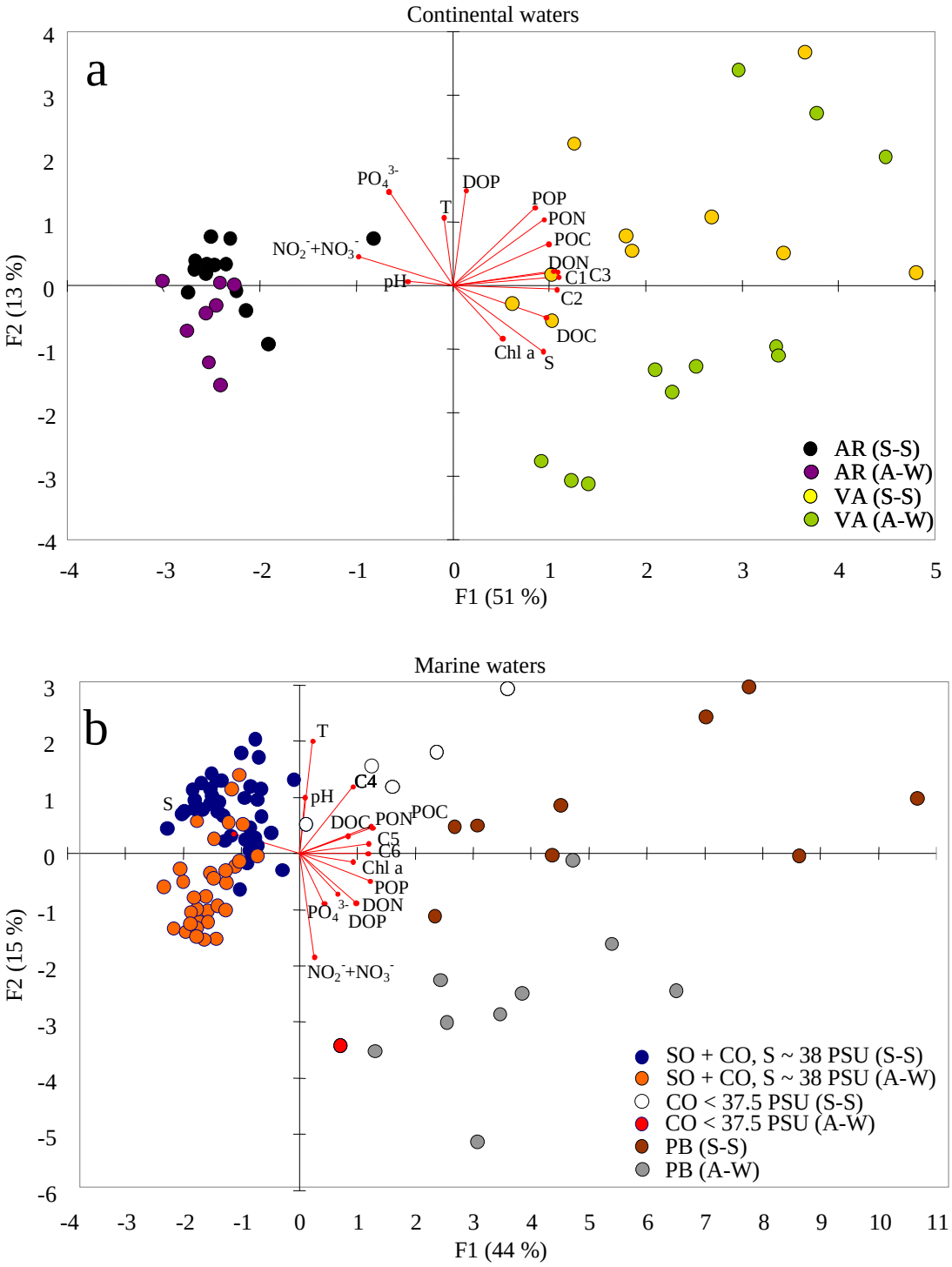

Figure V-12. Principal component analysis (PCA) based on Spearman's rank-order correlation matrix computed on the hydrological, biogeochemical and FDOM parameters, applied on inland waters (a) and marine waters (b). Correlation circle is displayed along with the projection of samples on the first factorial plane (F1 *versus* F2). Seasons are represented by either S-S for spring and summer or by A-W for autumn and winter.

Chapitre VI: Caractérisation d’hydrocarbures aromatiques polycycliques et de bentazone par fluorescence induite par laser résolue en temps

Résumé

Afin de résoudre le problème de chevauchement de pics et de sensibilité, la spectrofluorimétrie résolue en temps a été utilisée. Cette dernière permet de séparer physiquement des fluorophores à l'aide de leur temps de vie de fluorescence si bien sûr ces derniers sont différents. Les objectifs de ce chapitre était de comparer la sensibilité vis-à-vis de contaminants (naphtalène, fluorène, phénanthrène, pyrène et bentazone) de l'analyse par fluorescence induite par laser résolue en temps (TRFS)et de la méthode classique de mesure de fluorescence à l'aide de EEMs, de déterminer le temps de vie de fluorescence de ces contaminants, et enfin, d'utiliser ce paramètre pour pouvoir les séparer physiquement dans des mélanges contenant à la fois un contaminant et des substances humiques. Les limites de détection de ces contaminants par les deux techniques d'analyses étaient du même ordre de grandeur (0.23-90.30 μg L^{-1} pour la méthode EEM et 0.26-58.15 μg L^{-1} pour la méthode TRFS) excepté pour le phénanthrène qui a une limite de détection plus basse de deux ordres de grandeur pour la TRFS (0.11 contre 0.002 μg L^{-1}). Les mesures de temps de vie variaient de 4.4 à 126.3 ns pour chacun des contaminants ciblés et étaient différents de ceux des substances humiques (1.1 et 7 ns). La faible limite de détection du phénanthrène permet d'affirmer que la TRFS est un outil intéressant pour monitorer les contaminations pétrogéniques et ce dans différents types d'environnements, si la perspectives de séparer ce contaminants des substances humiques est réalisable.

Characterisation of polycyclic aromatic hydrocarbons and bentazone by time–resolved laser–induced fluorescence

1. Introduction

Polycyclic aromatic hydrocarbons (PAHs) and pesticides are among the most widespread organic contaminants in aquatic environments (Booksh et al., 1996; Fang et al., 1998). These contaminants can bioaccumulate in food chain and have an impact on living organism causing reprotoxic, carcinogenic, mutagenic or endocrine disrupting effects (Kennish, 1992; Hélène Roche et al., 2002; McKinlay et al., 2008; Landau-Ossondo et al., 2009). Thus, PAHs and pesticides are recognized by various international organizations as priority contaminants and are included in the list of 33 priority regulated substances by the European Parliament and Council of the European Union (Official Journal of the EU 24/08/2013, Directive 2013/39/EU). Hydrocarbons have various sources like by direct dischargers of crude oil and its derivatives, industrial and urban wastes transported by runoff waters or by atmospheric deposition (Wang et al., 1997; Dabestani and Ivanov, 1999; Dachs et al., 2002; Zhendi Wurl and Obbard, 2004). Pesticides are particularly abundant near agriculture areas and enter in marine and fresh waters mainly through surface runoff (Jia et al., 2007). Most of time, these molecules were brought out and quantified with gas or liquid chromatography coupled to a mass spectrometry (GC-MS, LC-MS) at µg and ng L^{-1} level (Comoretto et al., 2007; Guigue et al., 2011). However, these analyses require large volumes of water (several litters) and several sample treatment steps which increase contamination opportunities and analytical time.

Fortunately, some these contaminants have fluorescence properties linked to their aromatic structure (Renee D. Jiji et al., 1999; Mastral et al., 2003). Spectrofluorimetry could be then an alternative technique to characterise organic contaminations in natural waters. This technique was quicker than classic analytical tools because it required only quick pre-treatment step like filtration and nitrogen bubbling of few minutes. Generally excitation-emission matrix (EEM) were used to characterise contaminant signatures in field or in standard samples (Booksh et al., 1996; Jiji et al., 1999; Jiji et al., 2000; García Reyes et al., 2004a; García Reyes et al., 2004b; Kim et al., 2005; Nahorniak and Booksh, 2006; Tedetti et al., 2010). However natural fluorophores like tryptophan, tyrosine or humic acids had signatures close to some of such pollutants like naphthalene, fluorene or pyrene (Fellman et al., 2010; Ferretto et al., 2014). When two fluorophores had the same fluorescence signatures or if overlaps with others fluorophores were too important, PARAFAC analysis was not able to separate the

components (Ferretto et al., 2014). Time Resolved Fluorescence Spectroscopy (TRFS) was able to include one dimension more using the fluorescence lifetime of a fluorophore. This fourth dimension allows separating fluorophore physically. Some studies already focus on contaminants and on oil type identification with TRFS (Berlman, 1971; Inman et al., 1990; Meidinger et al., 1993; Rudnick and Chen, 1998; Baszanowska et al., 2011). Moreover, to our knowledge only one pesticide was studied (Burel, 2003). In this study, we propose to study most abundant PAHs in the environment and another pesticide, the bentazone which was never studied in fluorescence spectroscopy to our knowledge. The objectives of this study were to evaluate the relevance to use TRFS to characterise and to quantify contaminants, to compare TRFS with EEM method and to characterise the fluorescence lifetimes of selected contaminants.

2. Material and methods

2.1. Standard solution preparation

Four PAHs, naphthalene (Naph), fluorene (Flu), phenanthrene (Phe), pyrene (Pyr) and one biocide, the bentazone (Ben) were selected for this study. Naph, Flu, Phe and Pyr are among the most abundant PAHs in aquatic environments (El Nemr and Abd-Allah, 2003). The Ben was an herbicide and was used already found in river and lagoon (Comoretto et al., 2007; Bach et al., 2010). The PAHs and Ben were purchased from Sigma-Aldrich (≥ 98%) and (99.9%) respectively for PAHs and Ben. Theses contaminants were used without further purification. Stock solutions of each individual compound (50 mg L^{-1}) were prepared by dissolving the pure solid for PAH or by dilution of the stock solution for the Ben in methanol (Rathburn HPLC grade). From these solutions, individual solutions with final concentrations of between 0 to 10 μg L^{-1} for the PAHs and from 0 to 2000 μg L^{-1} for the bentazone. Solution of a mixture of Suwannee River humic (HA) (2S101H) and fulvic (FA) (2S101F) acids were purchased from the International Humic Substances Society (IHSS). The HA and FA were dissolved in sodium hydroxide and ultrapure water, respectively, to obtain HA and FA solutions of 250 mg L^{-1}. These two solutions were then mixed together to obtain a stock solution of humic substances (HS) in ultrapure water of 200 mg L^{-1}. Solution containing 2 mg L^{-1} of humic substances was prepared. All solutions were prepared in ultrapure water (i.e., Milli-Q water from a Millipore system, the final resistivity was 18.2 MΩ cm^{-1}) and their pH was adjusted to 6.0 with sodium hydroxide. The compositions and concentrations of the

standard solutions are shown in Table VI-1. Standard solutions were stored in SCHOTT® glass bottles and in the dark at 4 °C prior to analysis.

2.2. Fluorescence measurement

The fluorescence measurements were made at a constant temperature of 20 °C. The samples were allowed to reach room temperature in the dark before transferring into a far UV silica quartz cell with a 1 cm path-length (170-2600 nm; LEADER LAB®). Analyses were performed with on two different spectrofluorimeter. The Hitachi F-7000 is a tool allowing to send a continuous photon flow on a sample and was described in a previous paper (Tedetti et al., 2012). Fluorescence measurements were carried from 200 to 500 nm in λ_{ex} and from 280 to 500 nm in λ_{em} with both excitation and emission slits at 5 nm and a scan speed of 1200 $nm.min^{-1}$. The second spectrofluorimeter sends pulse of photons on the sample with monochromatic excitation wavelengths (1064, 512, 355, 266 nm). The system consists of three main parts: the excitation light source, the detection and a computer workstation. Following the beam path, the sample receives the excitation light pulse. The emitted fluorescence collected at 90° from the incident pulse is directed into the entrance slit of the spectrophotometer.

The output is connected to an intensified charge-coupled device (ICCD) which digitizes the received spectra and sends informations to controller CCD-3000V (Horiba, Jobin-Yvon). The excitation system is composed of a picosecond laser pump (Nd-YAG EKSPLA PL2241A, Lithuania) combined with a harmonic module. The Nd-YAG source provides excitation pulse with a width of 30 ps (maximum pulse energy: 50 mJ, repetition rate: 20 Hz), and the harmonic module allows the selection of excitation wavelengths (1064 nm, 532 nm: 25 mJ, 355 nm: 12 mJ, 266 nm: 7 mJ) and the selection of harmonic output is carried out via a system of flipping mirrors.

A part of the fluorescence emission is collected through an optical bundle made of 16 optical fibers of 200 µm diameter and dispersed with an imaging spectrograph (TRIAX 180, Horiba Jobin-Yvon, France). The spectrograph has a focal length of 190 mm (aperture f/3.9) and possesses three UV-VIS gratings (300 grooves/mm, 900 grooves/mm and 2400 grooves/mm) allows obtaining three different spectral resolutions (0.27 nm/pixel, 0.09 nm/pixel and 0.034 nm/pixel, respectively). The ICCD (Horiba Jobin-Yvon, France, 1024x256 pixel array) is coupled to the spectrograph output. In order to obtain the time-resolved emission spectra, prior knowledge about the timing between excitation, emission and electronic detection are

required. The laser controller produces an electric trigger (TTL signal-like) at the time t_0 and the laser pulse arrives at the time t_0+500 ns. The trigger is also sent to a DG535 pulse generator (Stanford Research Systems) which generates an electric gate defined by a width and a delay. Time-resolved fluorescence is acquired by increasing the time-delay between the optical signal and the rising edge of TTL. The jitter between the laser pulse and the gate is approximately equal to 100 ps. By scanning the ICCD gate defined by the user, generally 35 ns wide, fluorescence emission spectra can be acquired at different time-delays with respect to excitation light. For a given set of parameters, each emission spectrum is recorded in an accumulation mode of several emission spectra. In order to increase the accuracy of the measurements, each laser pulse is corrected in energy fluctuation by splitting the laser beam and recording the reflected energy with a pyroelectric sensor (PE10, Ophir Optronics). For each excitation wavelength λ_{ex}, fluorescence emission spectra are monitored over time, separated by a constant incremental time-delay depending on the sample fluorescence response. The acquisition software is fully automated. Those devices are controlled via a computer workstation. Measurements were made at λ_{ex} of 266 because this wavelength allowed to measure fluorescence of all contaminants and of humic substances. The λ_{em} ranged from 275 to 620 nm and depends of the sample in order to avoid the two Rayleigh peaks on the spectra. The samples were bubbled with N_2 to avoid photo-oxidation.

2.3. Determination of fluorescence lifetime in solution

Estimation of the intrinsic fluorescence decay curve I(t) was done through a deconvolution process (Lakowicz, 2006) in order to find the lifetimes and the relative contributions of each fluorophore in the mixtures. I(t) can be modelled in a multi-exponential form:

$$I(t_i) = \sum_{p=1}^{Nc} H(t_i)\, C_p \exp(-t/\tau_p)$$

where C_p, τ_p, Nc and $H(t_i)$ are respectively the pre-exponential actors, the lifetimes, the number of fluorescent compounds and the Heaviside function at time t_i. The measured signal is deconvolved from the instrumental response (C. Gadio, personal communication, 2014) and a data treatment allows the extraction the lifetime, associated to the emission spectra of the fluorophore present in the solution (C. Gadio, personal communication, 2014). To recover, emission spectra, the method was based on the invariability of the fluorescence lifetime for each emission wavelength. The emission spectrum is obtained through a deconvolution of the

temporal profile associated to each emission wavelength, allowing to find the pre-exponential actors associated to each emission wavelength.

3. Results and discussion

3.1. Calibration curves with both time resolved fluorescence (TRFS) and EEM methods

The Figure VI-1 exhibits the fluorescence signature of each fluorophore acquired with the EEM method and their fluorescence maxima were summarised in the Table VI-2. Maximum λ_{ex} were located in the UV region and ranged from 245 (Ben) to 275 (Naph). Maximum of λ_{em} maxima ranged from 310 (Flu) to 458 nm (Ben). Signatures of PAHs were closed to those found in a previous study (Ferretto et al., 2014). Fluorescence peaks range from 1 (Phe) to 8 (Pyr). Linear regression curves were built with peak picking method at maxima $\lambda_{ex}/\lambda_{em}$. Good correlations were found for all contaminants (R^2 = 0.99-1.00, n = 6-8, $p < 0.01$), the curve parameters (slope, Y-intercep and R^2) were showed in the Table VI-2. For PAHs, the detection limit (DL) ranged between 0.11 (Phe) and 0.45 µg L^{-1} (Naph) and the quantification limit (QL) were between 0.36 and 1.50 µg L^{-1}. For the bentazone, the DL and QL were respectively of 90.3 and 301 µg L^{-1}. In the environments, the sum of the total concentration of PAHs ranged from ng L^{-1} to µg L^{-1} in highly contaminated waters (Valero-Navarro et al., 2007; Men et al., 2009; Guigue et al., 2011) and Ben concentration ranged from 0.01 to 6.1 µg L^{-1} (Laganà et al., 2002; Comoretto et al., 2007; Loos et al., 2010). Comparing to the environment concentration values, detection limits were too high to monitor contaminants in all environments. With such detection limits, steady state fluorescence allow then to measure contaminants only in highly contaminated environments.

With TRFS method, calibration curves were calculated by integrating spectra on all the temporal range. The spectral band was own to the contaminant considered to avoid the presence of the Raman peak (Table VI-2) and the same concentrations were used than with EEM method. Good linear regression relationships (r^2 = 0.99-1, n = 8-9, $p < 0.01$) (Table VI-2) were obtained for all contaminants excepted for the Phe due to inner filter effect. In these case, to successfully implement a calibration curve, a linearization using a logarithm function (r^2 = 0.98, n = 6, $p < 0.01$) was made (Table VI-2). The DL ranged from 3.10^{-3} to 58.15 µg L^{-1} and the QL ranged from 8.10^{-3} to 193.8 µg L^{-1} which correspond respectively the Phe and the Ben. The detection limit calculated with both methods were not very different excepted for the Phe and the Ben where DL was divided by respectively 1.55 and 55. One can note that, reversely to the EEM measure, for TRFS experiment the used wavelength excitation was not

those of the higher fluorescence signal. Even this, TRFS succeed to have at least similar performances than the EEM method. This highlighted the potential performance of TRFS to reach such better detection limits. With a system which sends photons at the corresponding wavelength, the detection could be enhanced. For most of contaminants, the DL and QL values exhibited that this technique is suited to analyse contaminants in polluted environments excepted for phenanthrene. For this last compound, DL reached a very low value which implied this contaminant could be monitored as petroleum fingerprint in environment weakly impacted.

3.2. Fluorescence life time in individual standard solutions

In individual solutions, we determined the fluorescence lifetimes of each contaminant and of the humic substances. Values ranged from 1 (HS) to 126.3 (Pyr) ns and were summarised in the Table VI-3. These values were closed to the values found in previously study which worked with water as solvent (Inman et al., 1990; Meidinger et al., 1993; Kumke et al., 1995; Clark et al., 2002). Fluorescence lifetimes obtained in cyclohexane exhibited different results than in water and were longer. The fluorescence lifetime (τ) is linked to the fluorescence quantum yield (ϕ_f) and to the rate constant of radiative de-excitation (k_R) and follow the equation:

$\phi_f / k_R = \tau$ (Lakowicz, 2006)

The solvent polarity is known to impact both the fluorescence spectra and the fluorescence quantum yield. When the polarity decreased, the fluorescence quantum yield increased and then increased the fluorescence lifetime (Valeur, 2001) which explained differences between the two solvent mentioned above.

In this work, the humic substances solution exhibited two fluorescence lifetimes, one at 1 ns (τ_1) and another at 7 ns (τ_2). Maximum λ_{em} were observed at 450 nm for the first compound and at 400 nm for the second which corresponded respectively to the FA and to the HA (Henderson et al., 2009). The fluorescence lifetimes of the HS were closed to those found in a previous study (Clark et al., 2002).

4. Conclusion

In this work, we compared TRFS and EEM methods to characterise PAHs (Naph, Phe, Flu, Pyr) and one pesticide, the bentazone in standards solutions at $\mu g\ L^{-1}$ and $ng\ L^{-1}$. Because of the low DL of the phenanthrene, one of the main PAHs present in fuel, TRFS was the better

method comparing to EEM measurements to monitor contamination. Although TRFS cannot replace chromatography that can characterise various contaminants at ng L^{-1} level, this technique is rapid and does not need large amount of sample. In this work, we did not apply TRFS on mixture sample containing humic substances and contaminants or on field samples. In the future, it would be necessary to use TRFS on these kind of samples to demonstrate whether or not this technique is able to separate physically signals of contaminants and may be consider as an alternative to EEM-PARAFAC method.

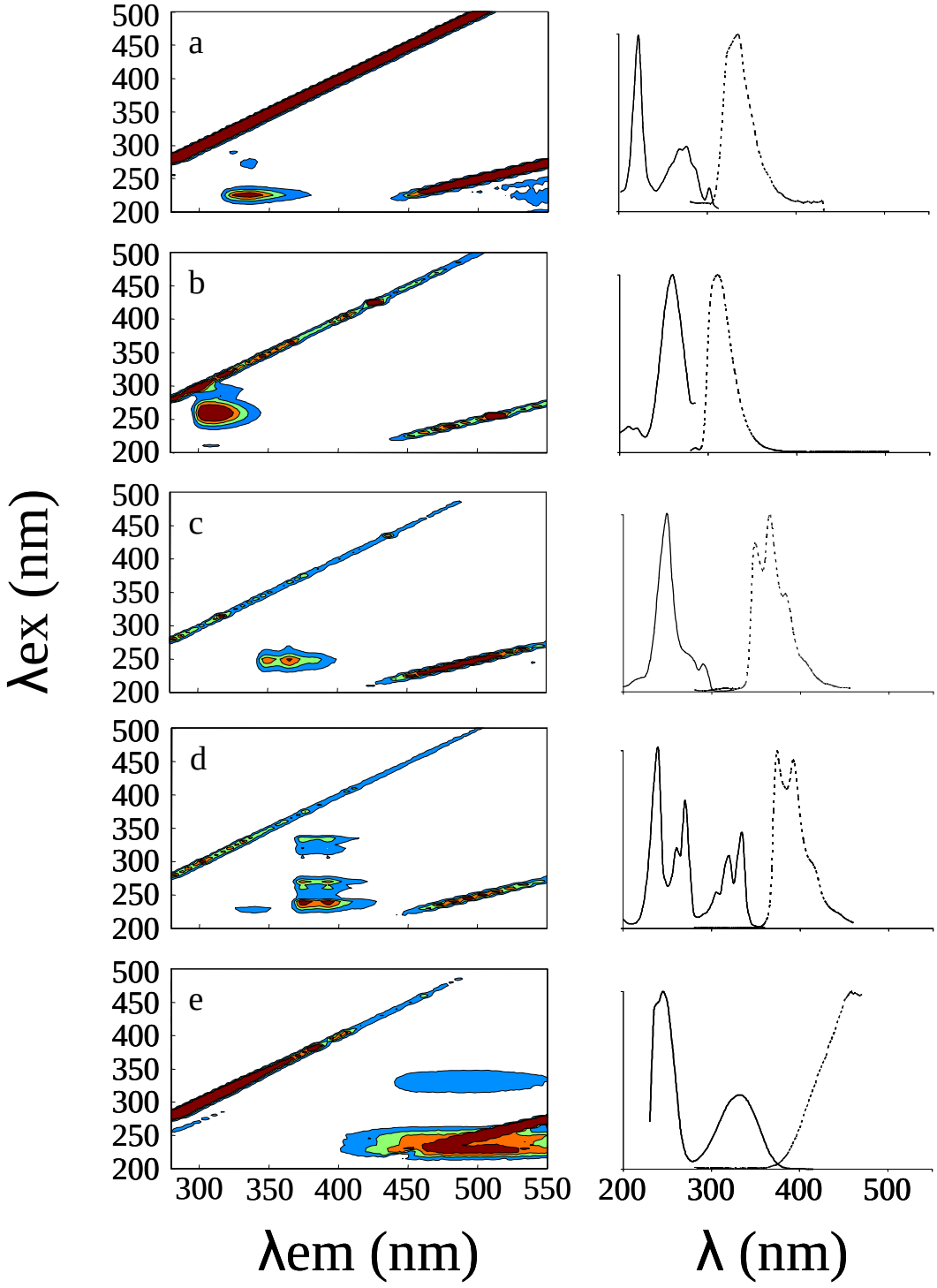

Figure VI-1. EEM, Ex and Em fluorescence spectra of Naph (a), Flu (b), Phe(c), Ant (d), Pyr (e) and Ben (f). The λ_{ex} and λ_{em} fixed to plot excitation and emission spectra corresponded to the wavelength couple with the maximum fluorescence intensity.

Table VI-1. Composition and concentrations of the standard solutions (individual solutions).

A, B and C represent the different solution concentrations of contaminants.

A_9: contaminant concentrations of the individual solutions (0, 0.1, 0.2, 0.5, 0.8, 1, 2, 5 and 10 µg L^{-1}).

B_8: contaminant concentrations of the individual solutions (0, 0.1, 0.2, 0.5, 0.8, 1, 2 and 5 µg.l^{-1}).

C_9: contaminant concentrations of the individual solutions (0, 0.5, 1, 5, 20, 50, 100, 200 and 2000 µg.l^{-1}).

D_1: Final humic substance concentrations (HS) in the mixture solutions (2 mg L^{-1}).

	Naph	Flu	Phe	Pyr	Ben	HS
Naph	A_9					
Flu		B_8				
Phe			B_8			
Pyr				B_8		
Ben					C_9	
HS						D_1

Table VI-2. Fluorescence maxima obtained from EEM, excitation and spectral band integrated to calculate linear regression for TRFS method, parameters of linear regression curves, detection and quantification limit for each fluorescence maxima of each contaminant for both methods. For Phe in TRFS method, the parameters of regression indicated are those obtain after linearization and were then without unity.

	EEM method						TRFS method (integration for λ_{Ex} = 266 nm)					
Contaminants	$\lambda_{Ex}/\lambda_{Em}$ (nm)	Slope (UA.L.µg^{-1})	Y-intercept (µg L^{-1})	DL (µg L^{-1})	QL (µg L^{-1})	r²	Range λ_{Em} (nm)	Slope (UA.L.µg^{-1})	Y-intercept (µg L^{-1})	DL (µg L^{1})	QL (µg L^{-1})	r²
Naph	220/334	4.00 ± 0.06	0.81 ± 0.26	0.40	1.33	0.99	296-384	12.33 ± 0.11	2.73 ± 0.43	0.26	0.86	1.00
	275/334	1.55 ± 0.03	0.30 ± 0.11	0.45	1.50	0.99						
Flu	260/310	26.50 ± 0.20	1.50 ± 1.80	0.20	0.68	1.00	275-363	20.01 ± 0.46	0.23 ± 0.86	0.31	1.04	1.00
Phe	250/366	12.06 ± 0.10	0.43 ± 0.22	0.11	0.36	1.00	316-404	0.47 ± 0.03	-0.38 ± 0.21	2 10^{-3}	8 10^{-3}	0.98
Pyr	240/374	23.19 ± 0.76	3.16 ± 1.70	0.41	1.37	1.00	356-443	11.27 ± 0.59	5.18 ± 1.42	0.71	2.40	0.99
	240/392	21.82 ± 0.55	3.15 ± 1.22	0.31	1.05	1.00						

	270/374	16.84 ± 0.40	1.67 ± 0.88	0.30	0.99	1.00						
	270/392	16.21 ± 0.36	1.52 ± 0.80	0.28	0.93	1.00						
	320/374	9.51 ± 0.18	0.98 ± 0.40	0.23	0.78	1.00						
	320/392	9.26 ± 0.17	0.89 ± 0.37	0.23	0.75	1.00						
	335/374	12.26 ± 0.27	1.13 ± 0.60	0.26	0.92	1.00						
	335/392	12.09 ± 0.25	1.07 ± 0.57	0.26	0.88	1.00						
Ben	245/458	0.02 ± 0.00	1.16 ± 0.62	201.30	671.00	1.00	387-474	0.08 ± 0.00	1.27 ± 0.52	58,15	193,82	1
	330/466	0.01 ± 0.00	-0.11 ± 0.11	90.30	301.00	1..00						

Table VI-3. Fluorescence life time found for each fluorophore. Results from previous study second the solvent were included.

	This study	Previous studies		
Contaminants	Life time (ns)	Life time (ns)	Solvent	Ref
Naph	29.5	40,3	Water deoxygenated	Meidinger et al., 1993
		96	Cyclohexane deoxygenated	Berlman, 1971
Flu	4.4	10	Cyclohexane deoxygenated	Berlman, 1971
Phe	14.8	16	Sea water	Rudnick and Chen, 1998
		57,5	Cyclohexane deoxygenated	Berlman, 1971
Pyr	126.3	128	Sea water	Inman et al., 1990
		450	Cyclohexane deoxygenated	Berlman, 1971
Ben	8.9			
HS	1.1 and 7	0.5, 3 and 6-9	Estuary waters	Clark et al., 2002

Chapitre VII: Conclusion et perspectives

1. Conclusion

Ce travail de thèse avait pour objectif de combler un manque de connaissances concernant la composition et la distribution de la DOM naturelle et anthropique en Méditerranée côtière nord-occidentale. Dans le chapitre III, nous avons pu mettre en évidence les signatures de fluorescence de plusieurs PAHs et de pesticides d'intérêt. Les limites de détection obtenues avec la technique de fluorescence étaient de l'ordre de la centaine de ng L^{-1} ou de quelques µg L^{-1} pour le naphtalène et le bentazone. De telles valeurs montrent très clairement que le suivi de la dynamique spatiale et temporelle de ces contaminants par mesure de fluorescence ne peut s'effectuer que dans des milieux fortement contaminés de manière chronique ou lors de contaminations accidentelles. Aussi, dans ce chapitre nous avons mis en exergue que les signatures de fluorescence des PAHs parents étaient très proches, voir superposées, à celles de leur homologues méthylés. Ceci implique donc que la méthode fluorescence/PARAFAC ne permet pas de discriminer les composés parents des composés méthylés alor que, nous l'avons vu dans le chapitre IV, les PAHs méthylés constituent une part très significative de l'ensemble du pool de PAHs dissous dans les eaux côtières. Par ailleurs, nous avons montré que la quantification des contaminants par la méthode fluorescence/PARAFAC était influencée par la concentration en substances humiques. En effet, il apparaît qu'une concentration en substances humiques égale ou supérieure à 2,5 mg C L^{-1} engendre un phénomène de quenching (extinction) de fluorescence due à la formation de complexes entre la matière humique et les contaminants, réduisant la fluorescence et sous estimant ainsi la concentration de ces derniers. D'après nos résultats, ce phénomène de quenching est « composé dépendant ». Le corollaire que l'on peut bien sûr mentionner est que le quenching de fluorescence peut-être utilisé pour évaluer le degrès de complexation entre la DOM naturelle et certains contaminants organiques. Dans le milieu marin côtier, les seules signatures de fluorescence de contaminants organiques que nous avons observées et clairement identifiées (par comparaison aux signatures de composés standard et par comparaion aux mesures chromatographiques) en utilisant la technique fluorescence /PARAFAC étaient celles de trois PAHs (+ leurs homoloques méthylés) : le naphtalène, le fluorène et le phénanthrène. La détection par fluorescence de ces HAPs, qui sont d'origine pétrogénique (i.e. issus du pétrole brut ou de ses dérivés), s'explique par le fait que 1) ce sont les PAHs parmi les plus abondants dans le milieu côtier (ceci a été confirmé par nos analyses chromatographiques) et 2) ils sont hautement fluorescents, en particulier le diméthyl naphtalène, le phénanthrène et le fluorène, comme nous l'avons démontré grâce à l'étude sur

les composés standards. Par conséquent, même si cette technique fluorescence/PARAFAC a certaines limites comme nous l'avons vu, elle pourrait se révéler très pertinente pour détecter et tracer des contaminations pétrogéniques dans l'environnement marin en ciblant ces trois PAHs.

Dans le chapitre IV, nous avons montré que seul le delta du Rhône était impacté par les biocides, avec la présence de bentazone à des concentrations allant de 20 à 970 ng L^{-1}. Le pic de bentazone était observé en début d'été et correspondait à la période d'épandage de pesticides pour la culture du riz. Les hydrocarbures étaient présents dans chaque site avec des concentrations en PAHs totaux allant de 8,1 à 405 ng L^{-1}. Les concentrations les plus élévées étaient enregistrées à Port de Bouc en raison de l'important trafic maritime et de la proximité du complexe industriel de Fos-sur-mer. D'autre part, notre étude a mis en avant une tendance saisonnière assez marquée concernant les hydrocarbures avec des concentrations nettement plus élevées en hiver, en lien très vraisemblablement avec des dépôts atmosphériques et des apports du Rhône plus importants à cette saison. En outre, en été, les processus de dégradation (photodégradation, évaporation) seraient plus accentués renforçant d'autant cette différence saisonnière. Cette étude confirme et renforce donc les travaux antérieurs qui soulignent l'importance du pool de contaminants à l'état dissous dans la dynamique et le budget global de contaminants organiques dans les eaux marines côtières.

Dans le chapitre V, nous avons déterminé la composition et les variations saisonnières de la FNDOM dans des eaux continentales et marines sous influence du Rhône. Les eaux continentales étaient dominées par les substances humiques alors que les fluorophores de type protéines dominaient dans les eaux marines de la baie de Marseille. Dans l'étang de Vaccarès, l'augmentation de l'abondance des substances humiques en hiver paraissait liée au drainage des sols par les pluies et à la forte remise en suspension du sédiment par le vent. La station marine de Port de Bouc était sous l'influence des apports d'eaux dessalées de l'étang de Berre. Lors de fortes dessalures ($S < 30$) imputées à ce dernier, on y observait une augmentation de l'abondance de tous les fluorophores. Dans les eaux purement marines, la présence du Rhône était caractérisée par une salinité infèrieure à 37,5 et se traduisait par une augmentation de la quantité de fluorophores issus soit d'un transport direct *via* le fleuve (substances humiques et tryptophane) et/ou soit d'un apport indirect résultant de la stimulation de la production primaire par les nutriments véhiculés par le fleuve (production de fluorophores de type tyrosin-like par la biomasse).

Dans le chapitre VI, nous avons montré que la spectroscopie de fluorescence résolue en temps (TRFS) pouvait être une technique d'analyse pertinente pour la mise en évidence de contaminations pétrogéniques. En effet, cette technique permettait d'atteindre une limite de détection de 2 ng L^{-1} pour le phénanthrène, soit une limite de détection environ 100 fois plus faible que celle obtenue avec la fluorescence statique (voir chapitre III). Nous pouvons donc en conclure que cette technique serait très efficace pour détecter des contaminations pétrogéniques dans l'environnement marin.

2. Perspectives

Ce travail de thèse a permis de répondre à un certain nombre de questions concernant la matière organique dissoute naturelle et antrhopique. Cependant, d'autres interrogations subsistent. Dans le chapitre III, nous avons utilisé des mélanges de contaminants organiques et de substances humiques dans le but de simuler des échantillons naturels. Or, les fluorophores de type protéine (tryptophane et tyrosine), au même titre que les substances humiques, font parti des fluorophores naturels ubiquistes de la FDOM dont les signatures de fluorescence peuvent être proches de celles des contaminants. Le tryptophane a une signature proche de celles du naphtalène et du carbaryl alors que la tyrosine a un maximum de fluorescence proche de celui du fluorène (Fellman et al., 2010 ; Henderson et al., 2009 ; Hudson & Reynolds, 2007). Cependant, aucun mélange n'a été testé avec ce matériel protéine-like. De ce fait, il serait intéressant, pour simuler au mieux les échantillons naturels, de rajouter, en plus des substances humiques, du tryptophane et de la tyrosine dans les mélanges standards.

Dans le chapitre IV, nous sommes intéressés aux contaminants dissous mais sans discriminer les contaminants dissous à l'état libre des contaminants dissous à l'état complexé à la matière organique. Pourtant, le degré de complexation des contaminants avec la matière organique influence fortement sur leur biodisponibilité/toxicité, leur dynamique et leur transport dans l'environnement côtier. Dans une prochaine étude, il serait donc pertinent d'évaluer la complexation de ces contaminants en utilisant des techniques adaptées comme le quenching de fluorescence ou la micro-extraction phase solide (SPME) (DePerre et al., 2014).

Dans le chapitre V, plusieurs hypothèses ont été émises sur l'impact des apports d'eaux douces du Rhône ou de l'étang de Berre dans les eaux continentales et marines. Si la dynamique saisonnière des fluorophores permet par exemple d'émettre l'hypothèse que la source autochtone du tryptophane résulte de la stimulation de la production biologique en mer par les eaux du fleuve, l'échantillonnage reste limité pour pouvoir infirmer ou affirmer toutes les hypothèses émises. Un échantillonnage à hautes fréquences dans les gradients de salinité entre le Rhône et l'étang de Vaccarès pour les eaux continentales et entre le Rhône et le canal de la Durance vers la baie de Marseille devrait permettre de répondre aux questions non résolues. De même, l'effet des pluies serait mieux cerné par un échantillonnage de faible pas, centré sur la précipitation.

Dans le chapitre VI, des mesures sur des solutions standards contenant des contaminants individuels ont été réalisées. Les temps de vie entre les substances humiques et les contaminants étaient assez différents. Il serait intéressant de réaliser des mesures sur des échantillons plus complexes (substances humiques et plusieurs contaminants), et d'évaluer la capacité de la TRSF à pouvoir mettre en évidence un important nombre de composés et de les quantifier. Cette méthode, pourrait être une bonne alternative à la méthode MEEFs-PARAFAC et pourrait être utilisée dans des environnements riches sans pour autant perdre en sensibilité. Dans le chapitre III, il a été montré que la méthode MEEFs-PARAFAC ne parvennait pas à séparer les PAHs parents des PAHs méthylés. Le temps de vie de fluorescence pourrait permettre de les séparer. Dans ce même chapitre, aucune mesure n'a été réalisée sur des échantillons naturels. Dans une prochaine étude, il serait intéressant de tester la TRFS sur de tels échantillons et de comparer les valeurs de concentrations obtenues avec une méthode de référence comme la chromatographie.

Chapitre VIII: Références

Abarnou, A., Burgeot, T., Chevreuil, M., Leboulenger, F., Loizeau, V., Madoulet-Jaouen, A., Minier, C. (2000). *Les contaminants organiques : quels risques pour le monde vivant ?* (pp. 1–35).

Aiken, G. R. (1985). *Humic substances in soil, sediment, and water: geochemistry, isolation, and characterization*. (Wiley, Ed.) (p. 692). Wiley.

Akkanen, J, Vogt, R. D., Kukkonen, J. V. K. (2004). Essential characteristics of natural dissolved organic matter affecting the sorption of hydrophobic organic contaminants. *Aquatic Sciences*, *166*, 171–177.

Akkanen, J., Tuikka, A., Kukkonen, J. V. K. (2012). On the borderline of dissolved and particulate organic matter: partitioning and bioavailability of polycyclic aromatic hydrocarbons. *Ecotoxicology and Environmental Safety*, *78*, 91–98.

Albanis, T. A., Hela, D. G., Sakellarides, T. M., Konstantinou, I. K. (1998). Monitoring of pesticide residues and their metabolites in surface and underground waters of Imathia (N. Greece) by means of solid-phase extraction disks and gas chromatography. *Journal of Chromatography A*, *823*(1–2), 59–71.

Albinet, A., Leoz-garziandia, E., Budzinski, H., Viilenave, E. (2007). Polycyclic aromatic hydrocarbons (PAHs), nitrated PAHs and oxygenated PAHs in ambient air of the Marseilles area (South of France): Concentrations and sources. *Science of the Total Environment*, *384*, 280–292.

Alostaz, M., Biggar, K., Donahue, R., Hall, G. (2008). Petroleum contamination characterization and quantification using fluorescence emission-excitation matrices (EEMs) and parallel factor analysis (PARAFAC). *Journal of Environmental Engineering and Science*, *7*(3), 183–197.

Aminot, A., Kérouel, R. (2007). *Dosage automatique des nutriments dans les eaux marines: méthodes en flux continu. Méthodes d'analyses en milieu marin, Ifremer* (p. 187). Brest, France: Quae.

Ariese, F. (1999). Application of fluorescence spectroscopic techniques in the determination of PAHs and PAH metabolites. In *Sample handling and trace analysis of polluants: techniques, applications and quality assurance* (Vol. 6, p. 789).

Azam, F., Fenchel, T., Field, J. G., Meyer-Reil, R. A., Thingstad, F. (1983). The ecological role of water column microbes in the sea. *Marine Ecology Progress Series*, *10*, 257–263.

Azimi, S., Rocher, V., Muller, M., Thevenot, D. R. (2005). Sources , distribution and variability of hydrocarbons and metals in atmospheric deposition in an urban area (Paris , France). *Science of the Total Environment*, *337*, 223–239.

Bach, M., Letzel, M., Kaul, U., Forstner, S., Metzner, G., Klasmeier, Reichenberger, S., J., Frede, H. G. (2010). Measurement and modeling of bentazone in the river Main (Germany) originating from point and non-point sources. *Water Research*, *44*(12), 3725–3733.

Baker, A., Curry, M. (2004). Fluorescence of leachates from three contrasting landfills. *Water Research*, *38*(10), 2605–2613.

Baker, A., Spencer, R. G. M. (2004). Characterization of dissolved organic matter from source to sea using fluorescence and absorbance spectroscopy. *Science of the Total Environment*, *333*(1-3), 217–232.

Baker, A., Ward, D., Lieten, S. H., Periera, R., Simpson, E. C., Slater, M. (2004). Measurement of protein-like fluorescence in river and waste water using a handheld spectrophotometer. *Water Research*, *38*(12), 2934–2938.

Balcarczyk, K. L., Jones, J. B., Jaffé, R., Maie, N. (2009). Stream dissolved organic matter bioavailability and composition in watersheds underlain with discontinuous permafrost. *Biogeochemistry*, *94*(3), 255–270.

Banas, D., Grillas, P., Auby, I., Lescuyer, F., Coulet, E., Moreteau, J. C., Millet, B. (2005). Short Time Scale Changes in Underwater Irradiance in a Wind-exposed Lagoon (Vaccarès Lagoon, France): Efficiency of Infrequent Field Measurements of Water Turbidity or Weather Data to Predict Irradiance in the Water Column. *Hydrobiologia*, *551*(1), 3–16.

Baszanowska, E., Otremba, Z., Rohde, P., Zielinski, O. (2011). Adoption of the time resolved fluorescence to oil type identiciation. *Journal of KONES powertrain and transport*, *18*(2), 25–29.

Battin, T. J., Luyssaert, S., Kaplan, L. A., Aufdenkampe, A. K., Richter, A., Tranvik, L. J. (2009). The boundless carbon cycle. *Nature Geosciences*, *2*(9), 598–600.

Beltrán, J. L., Ferrer, R., Guiteras, J. (1998). Multivariate calibration of polycyclic aromatic hydrocarbon mixtures from excitation–emission fluorescence spectra. *Analytica Chimica Acta*, *373*(2-3), 311–319.

Benitez, F. J., Acero, J. L., Real, F. J. (2002). Degradation of carbofuran by using ozone, UV radiation and advanced oxidation processes. *Journal of Hazardous Materials*, *89*(1), 51–65.

Benlahcen, K. T., Chaoui, A., Budzinski, H., Bellocq, J., Garrigues, P. (1997). Distribution and sources of polycyclic aromatic hydrocarbons in some Mediterranean coastal sediments. *Marine Pollution Bulletin*, *34*(5), 298–305.

Berlman, I. B. (1971). *Handbook of fluorescence spectra of aromatic molecules* (p. 473). New York; London: Academic Press.

Berrojalbiz, N., Dachs, J., Del Vento, S., Ojeda, M. J., Valle, M. C., Castro-Jiménez, Mariani, G., Wollgast, J., Hanke, G. (2011a). Persistent organic pollutants in Mediterranean seawater and processes affecting their accumulation in plankton. *Environmental Science & Technologycience & technology*, *45*(10), 4315–4322.

Berrojalbiz, N., Dachs, J., Ojeda, M. J., Valle, M. C., Castro-Jiménez, J., Wollgast, J., Ghiani, M., Hanke, G., Zaldivar, J. M. (2011b). Biogeochemical and physical controls on

concentrations of polycyclic aromatic hydrocarbons in water and plankton of the Mediterranean and Black Seas. *Global Biogeochemical Cycles*, *24*(4), GB4003.

Berrojalbiz, N., Lacorte, S., Calbet, A., Saiz, E., Barata, C. (2009). Accumulation and Cycling of Polycyclic Aromatic Hydrocarbons in Zooplankton. *Environmental Science & Technology*, *43*, 2295–2301.

Bertilsson, S., Jones Jr., J. B. (2003). Supply of Dissolved Organic Matter to Aquatic Ecosystems: Autochthonous Sources. In R. L. S. B. T.-A. Ecosystems (Ed.), *Aquatic Ecosystems: Interactivity of Dissolved Organic Matter* (pp. 3–24). Burlington: Academic Press.

Bieroza, M., Baker, A., Bridgeman, J. (2009). Exploratory analysis of excitation-emission matrix fluorescence spectra with self-organizing maps as a basis for determination of organic matter removal efficiency at water treatment works. *Journal of Geophysical Research: Biogeosciences*, *114*(G4), G00F07.

Birpinar, M. E., Talu, G. F., Gönençgil, B. (2009). Environmental effects of maritime traffic on the Istanbul Strait. *Environmental Monitoring and Assessment*, *152*(1-4), 13–23.

Bishop, J. K. B., Rossow, W. B. (1991). Spatial and temporal variability of global surface solar irradiance. *Journal of Geophysical Research*, *96*(C9), 16839–16858.

Blough, N. V, Del Vecchio, R. (2002). Chapter 10 - Chromophoric DOM in the Coastal Environment. In Dennis A Hansell (Ed.), *Biogeochemistry of Marine Dissolved Organic Matter* (pp. 509–546). San Diego: Academic Press.

Bocquené, G., Franco, A. (2005). Pesticide contamination of the coastline of Martinique. *Marine Pollution Bulletin*, *51*(5-7), 612–619.

Booksh, K. S., Muroski, A. R., Myrick, M. L. (1996). Single-Measurement Excitation/Emission Matrix Spectrofluorometer for Determination of Hydrocarbons in Ocean Water. 2. Calibration and Quantitation of Naphthalene and Styrene. *Analytical Chemistry*, *68*(20), 3539–3544.

Borges, A. V., Schiettecatte, L.S., Abril, G., Delille, B., Gazeau, F. (2006). Carbon dioxide in European coastal waters. *Estuarine, Coastal and Shelf Science*, *70*(3), 375–387.

Borges, A. V. (2011). Present day carbon dioxide fluxes in the coastal ocean and possible feedbacks under global change. In P. Duarte & J. M. Santana-Casiano (Eds.), *Oceans and the Atmospheric Carbon Content* (pp. 47–77). Berlin: Springer.

Borisover, M., Laor, Y., Parparov, A., Bukhanovsky, N., Lado, M. (2009). Spatial and seasonal patterns of fluorescent organic matter in Lake Kinneret (Sea of Galilee) and its catchment basin. *Water Research*, *43*(12), 3104–3116.

Borrell, A., Cantos, G., Aguilar, A., Androukaki, E., Dendrinos, P. (2007). Concentrations and patterns of organochlorine pesticides and PCBs in Mediterranean monk seals (Monachus monachus) from Western Sahara and Greece. *Science of the Total Environment*, *381*(1-3), 316–325.

Bouloubassi, I., Saliot, A. (1993). Investigation of anthropogenic and natural organic inputs in estuarine sediments using hydrocarbon markers (NAH, LAB, PAH). *Oceanologica Acta*, *16*, 145–161.

Bouloubassi, Ioanna, Saliot, A. (1991). Composition and sources of dissolved and particulate PAH in surface waters from the Rhone delta (NW Mediterranean). *Marine Pollution Bulletin*, *22*(12), 588–594.

Boyd, T. J., Osburn, C. L. (2004). Changes in CDOM fluorescence from allochthonous and autochthonous sources during tidal mixing and bacterial degradation in two coastal estuaries. *Marine Chemistry*, *89*(1-4), 189–210.

Brahima, O., Richard, C. (2003). Phototransformation of carbaryl in aqueous solution: Laser-flash photolysis and steady-state studies. *Journal of Photochemistry and Photobiology A : Chemistry*, *156*, 9–14.

Bro, R. (1997). PARAFAC. Tutorial and applications. *Chemometrics and Intelligent Laboratory Systems*, *38*(2), 149–171.

Budzinski, H., Jones, I., Bellocq, J., Piérard, C., Garrigues, P. (1997). Evaluation of sediment contamination by polycyclic aromatic hydrocarbons in the Gironde estuary. *Marine Chemistry*, *58*(1–2), 85–97.

Buet, A., Banas, D., Vollaire, Y., Coulet, E., Roche, H. (2006). Biomarker responses in European eel (Anguilla anguilla) exposed to persistent organic pollutants. A field study in the Vaccarès lagoon (Camargue, France). *Chemosphere*, *65*(10), 1846–1858.

Burel, L. (2003). Molecular and atomic ultra trace analysis by laser induced fluorescence with OPO system and ICCD camera. *Talanta*, *60*(2-3), 295–302.

Cabaniss, S. E. (1992). Synchronous Fluorescence Spectra of Metal-Fulvic Acid Complexes. *Environmental Science & Technology*, *26*(6), 1133–1139.

Cammack, W. K. L., Kalff, J., Prairie, Y. T., Smith, E. M. (2004). Fluorescent dissolved organic matter in lakes: Relationships with heterotrophic metabolism. *Limnology and Oceanography*, *49*(6), 2034–2045.

Capel, P. D., Larson, S. J., Winterstein, T. A. (2001). The behaviour of 39 pesticides in surface waters as a function of scale. *Hydrological Processes*, *15*(7), 1251–1269.

Carlson, C. A. (2002). Production and removal processes. In *Biogeochemistry of Marine Dissolved Organic Matter* (Hansell D,., pp. 91–152). San Diego: Academic Press.

Carstea, E. M., Baker, A., Bieroza, M., Reynolds, D. (2010). Continuous fluorescence excitation-emission matrix monitoring of river organic matter. *Water Research*, *44*(18), 5356–5366.

Castro-Jiménez, J., Berrojalbiz, N., Wollgast, J., Dachs, J. (2012). Polycyclic aromatic hydrocarbons (PAHs) in the Mediterranean Sea: atmospheric occurrence, deposition and

decoupling with settling fluxes in the water column. *Environmental Pollution*, *166*, 40–47.

Cauwet, G. (2002). DOM in the coastal zone. In D. A. Carlson & A. C. Hansell (Eds.), *Biogeochemistry of Marine Dissolved Organic Matter* (pp. 579–612). Academic Press.

Charizopoulos, E., Papadopoulou-Mourkidou, E. (1999). Occurrence of Pesticides in Rain of the Axios River Basin, Greece. *Environmental Science & Technology*, *33*(14), 2363–2368.

Chauvelon, P. (1996). *Hydrologie quantitative d'une zone humide méditerranéenne aménagée: Le bassin de Fumemorte en Grande Camargue, delta du Rhône*. Université de Montpellier. 274p

Chen, C. T. A., Borges, A. V. (2009). Reconciling opposing views on carbon cycling in the coastal ocean: Continental shelves as sinks and near-shore ecosystems as sources of atmospheric CO2. *Deep Sea Research Part II*, *56*, 578–590.

Chen, M., Price, R. M., Yamashita, Y., Jaffé, R. (2010). Comparative study of dissolved organic matter from groundwater and surface water in the Florida coastal Everglades using multi-dimensional spectrofluorometry combined with multivariate statistics. *Applied Geochemistry*, *25*(6), 872–880.

Chen, R. F. (1999). In situ fluorescence measurements in coastal waters. *Organic Geochemistry*, *30*, 397–409.

Chiron, S., Comoretto, L., Rinaldi, E., Maurino, V., Minero, C., Vione, D. (2009). Pesticide by-products in the Rhône delta (Southern France). The case of 4-chloro-2-methylphenol and of its nitroderivative. *Chemosphere*, *74*(4), 599–604.

Cho, B. C., Azam, F. (1990). Biogeochemical significance of bacterial biomass in the ocean's euphotic zone. *Marine Ecology Progress Series*, *63*(1989), 253–259.

Christensen, J. H., Hansen, A. B., Mortensen, J., Andersen, O. (2005). Characterization and matching of oil samples using fluorescence spectroscopy and parallel factor analysis. *Analytical chemistry*, *77*(7), 2210–2217.

Cincinelli, A., Stortini, A. M., Perugini, M., Checchini, L., Lepri, L. (2001). Organic pollutants in sea-surface microlayer and aerosol in the coastal environment of Leghorn — (Tyrrhenian Sea). *Marine Chemistry*, *76*, 77–98.

Clark, C. D., Jimenez-morais, J., Jones, G., Zanardi-lamardo, E., Moore, C. A., Zika, R. G. (2002). A time-resolved fluorescence study of dissolved organic matter in a riverine to marine transition zone. *Marine Chemistry*, *78*, 121–135.

Coble, P. G. (1996). Characterization of marine and terrestrial DOM in seawater using excitation-emission matrix spectroscopy. *Marine Chemistry*, *51*(4), 325–346.

Comoretto, L., Arfib, B., Chiron, S. (2007). Pesticides in the Rhône river delta (France): Basic data for a field-based exposure assessment. *Science of the Total Environment*, *380*(1-3), 124–132.

Cripps, G. C. (1989). Problems in the identification of anthropogenic hydrocarbons against natural background levels in the Antarctic. *Antartic Science*, *1*(4), 307–312.

Croué, J. P., Benedetti, M. F., Violleau, D., Leenheer, J. A. (2003). Characterization and copper binding of humic and nonhumic organic matter isolated from the South Platte River: evidence for the presence of nitrogenous binding site. *Environmental Science & Technology*, *37*(2), 328–336.

Dabestani, R., Ivanov, I. (1999). A Compilation of physical, spectroscopic and photophyisical properties of polycyclic aromatic hydrocarbons. *Photochemistry and Photobiologie*, *70*(1), 10–34.

Dachs, J., Bayona, J. M., Fowler, S. W., Miquel, J. C., Albaigés, J. (1996). Vertical fluxes of polycyclic aromatic hydrocarbons and organochlorine compounds in the western Alboran Sea (southwestern Mediterranean). *Marine Chemistry*, *52*, 75–86.

Dachs, J., Bayona, J. M., Raoux, C., Albaige, J. (1997). Spatial , Vertical Distribution and Budget of Polycyclic Aromatic Hydrocarbons in the Western Mediterranean Seawater. *Environmental Science & Technology*, *31*(3), 682–688.

Dachs, J., Bayona, J. M., Saliot, A., Albaiges, J. (1999). Evaluation of anthropogenic and biogenic inputs into the western Mediterranean using molecular markers. *Marine Chemistry*, *65*, 195–210.

Dachs, J., Glenn IV, T. R., Gigliotti, C. L., Brunciak, P., Totten, L. A., Nelson, E. D., Franz, T. P., Eisenreich, S. J. (2002). Processes driving the short-term variability of polycyclic aromatic hydrocarbons in the Baltimore and northern Chesapeake Bay atmosphere, USA. *Atmospheric Environment*, *36*(14), 2281–2295.

Dachs, J., Lohmann, R., Ockenden, W. A., Méjanelle, L., Eisenreich, S. J., Jones, K. C. (2002). Oceanic Biogeochemical Controls on Global Dynamics of Persistent Organic Pollutants. *Environmental Science & Technology*, *36*(20), 4229–4237.

Dachs, J., Méjanelle, L. (2010). Organic Pollutants in Coastal Waters, Sediments, and Biota: A Relevant Driver for Ecosystems During the Anthropocene? *Estuaries and Coasts*, *33*(1), 1–14.

Daughton, C. G., Ternes, T. A. (1999). Pharmaceuticals and personal care products in the environment: agents of subtle change? *Environmental Health Perspectives*, *107 Suppl*, 907–938.

De Groot, C. J., Golterman, H. (1999). Le risque d'eutrophisation de l'Etang de Vaccarès et des marais de la Camargue (Delta du Rhône, France). *Ecologie*, *30*(2), 91–100.

Delpy, F., Pagano, M., Blanchot, J., Carlotti, F., Thibault-Botha, D. (2012). Man-induced hydrological changes, metazooplankton communities and invasive species in the Berre Lagoon (Mediterranean Sea, France). *Marine pollution bulletin*, *64*(9), 1921–1932.

De Perre, C., Le Ménach, K., Ibalot, F., Parlanti, E., & Budzinski, H. (2014). Development of solid-phase microextraction to study dissolved organic matter--polycyclic aromatic hydrocarbon interactions in aquatic environment. *Analytica chimica acta*, *807*, 51–60.

Determann, S., Lobbes, J. M., Reuter, R., Rullkötter, J. (1998). Ultraviolet fluorescence excitation and emission spectroscopy of marine algae and bacteria. *Marine Chemistry*, *62*(1-2), 137–156.

Didyk, B. M., Simoneit, B. R. T., Brassel, S. C., Eglinton, G. (1978). Organic geochemical indicators of paleoenvironmental conditions of sedimentation. *Nature*, *272*, 216–222.

Dierking, J., Wafo, E., Schembri, T., Lagadec, V., Nicolas, C., Letourneur, Y., Harmelin-Vivien, M. (2009). Spatial patterns in PCBs, pesticides, mercury and cadmium in the common sole in the NW Mediterranean Sea, and a novel use of contaminants as biomarkers. *Marine Pollution Bulletin*, *58*(11), 1605–1614.

Directive 2004/850 de la Communauté Économique Européenne (2004). Journal officiel du 29/04/2004.

Directive 2013/39 de la Communauté Économique Européenne (2013). Journal officiel du 24/08/2013.

Doll, T. E., Frimmel, F. H., Kumke, M. U., Ohlenbusch, G. (1999). Interaction between natural organic matter (NOM) and polycyclic aromatic compounds (PAC)- comparison of fluorescence quenching and solid phase micro extraction (SPME). *Analytical Chemistry*, *364*, 313–319.

Douglas, A. G., Eglinton, G. (1966). Distribution of alkanes. In T. Swam (Ed.), *Comparative Phytochemistry* (pp. 57–77). London, New York: Academic Press.

Druon, J. N., Mannino, A., Signorini, S., McClain, C., Friedrichs, M., Wilkin, J., Fennel, K. (2010). Modeling the dynamics and export of dissolved organic matter in the Northeastern U.S. continental shelf. *Estuarine, Coastal and Shelf Science*, *88*(4), 488–507.

Dumbauld, B. R., Brooksà, K. M., Posey, M. H., Box, P. O., Park, O. (2001). Response of an Estuarine Benthic Community to Application of the Pesticide Carbaryl and Cultivation of Pacific Oysters (Crassostrea gigas) in Willapa Bay , Washington. *Marine Pollution Bulletin*, *42*(10), 826–844.

Durrieu de Madron, X., Denis, L., Diaz, F., Garcia, N., Guieu, C., Loye-Pilot, M., Ludwig, W., Moutin, T., Raimbault, P., Ridame, C. (2003). Nutrients and carbon budgets for the Gulf of Lion during the Moogli cruises. *Oceanologica Acta*, *26*, 421–433.

Durrieu de Madron, X., Wiberg, P. L., Puig, P. (2008). Sediment dynamics in the Gulf of Lions: The impact of extreme events. *Continental Shelf Research*, *28*(15), 1867–1876.

Eisenreich, S. (2006). Atmospheric Deposition and Marine Sedimentation Fluxes of Polycyclic Aromatic Hydrocarbons in the Eastern Mediterranean Basin, *40*(16), 4922–4927.

El Nemr, A., Abd-Allah, A. M. A. (2003). Contamination of polycyclic aromatic hydrocarbons (PAHs) in microlayer and subsurface waters along Alexandria coast, Egypt. *Chemosphere*, *52*(10), 1711–1716.

Elias, V. O., Simoneit, B. R. T., Cardoso, J. N. (1997). Even N-Alkane Predominances on the Amazon Shelf and A Northeast Pacific Hydrothermal System. *Naturwissenschaften*, *84*, 415–420.

Elkins, K. M., Nelson, D. J. (2002). Spectroscopic approaches to the study of the interaction of aluminum with humic substances. *Coordination Chemistry Reviews*, *228*(2), 205–225.

Elordui-Zapatarietxe, S., Rosell-Melé, A., Moraleda, N., Tolosa, I., Albaigés, J. (2010). Phase distribution of hydrocarbons in the water column after a pelagic deep ocean oil spill. *Marine Pollution Bulletin*, *60*(10), 1667–1673.

El-Rayyes, A. A, Htun, T. (2004). Effects of solvent on the fluorescence of 2-anilinonaphthalene. *Spectrochimica Acta Part A*, *60*(8-9), 1985–9.

Fang, F., Patterson, H. H., Cronan, C. S. (1998). A spectro Fluorimetric study of the binding of carbofuran , carbaryl , and aldicarb with dissolved organic matter. *Analytica Chimica Acta*, *373*, 139–151.

Fellman, J. B., Hood, E., Spencer, R. G. M. (2010). Fluorescence spectroscopy opens new windows into dissolved organic matter dynamics in freshwater ecosystems: A review. *Limnology and Oceanography*, *55*(6), 2452–2462.

Fernandes, M. B., Sicre, M., Broyelle, I., Lorre, A., Pont, D. (1999). Contamination by Polycyclic Aromatic Hydrocarbons (PAHs) in French and European rivers. *Hydrobiologia*, *410*, 343–348.

Ferretto, N., Tedetti, M., Guigue, C., Mounier, S., Redon, R., Goutx, M. (2014). Identification and quantification of known polycyclic aromatic hydrocarbons and pesticides in complex mixtures using fluorescence excitation–emission matrices and parallel factor analysis. *Chemosphere*, in press.

Fingas, M. F. (1995). A literature review of the physics and predictive modelling of oil spill evaporation. *Journal of Hazardous Materials*, *42*, 157–175.

Frankignoulle, M., Abril, G., Borges, A., Bourge, I., Canon, C., Delille, B., Libert, E., Théate, J. M. (1998). Carbon dioxide emission from European estuaries. *Science*, *282*, 434–436.

Frimmel, F. H., Christman, R. F. (1988). *Humic substances and their role in the environment* (p. 286). New York: Wiley.

Fromme, H., Tittlemier, S. A., Völkel, W., Wilhelm, M., Twardella, D. (2009). Perfluorinated compounds – Exposure assessment for the general population in western countries. *International Journal of Hygiene and Environmental Health*, *212*(3), 239–270.

García Reyes, J. F., Llorent Martínez, E. J., Ortega Barrales, P., Molina Díaz, A. (2004a). Multiwavelength fluorescence based optosensor for simultaneous determination of fuberidazole, carbaryl and benomyl. *Talanta*, *64*(3), 742–749.

García Reyes, J. F., Llorent Martínez, E. J., Ortega Barrales, P., Molina Díaz, A. (2004b). Continuous-flow separation and pre-concentration coupled on-line to solid-surface fluorescence spectroscopy for the simultaneous determination of o-phenylphenol and thiabendazole. *Analytical and Bioanalytical Chemistry*, *378*(2), 429–437.

Gasperi, J., Garnaud, S., Rocher, V., Moilleron, R. (2008). Priority pollutants in wastewater and combined sewer overflow. *Science of The Total Environment*, *407*(1), 263–272.

Gattuso, J. P., Frankignoulle, M., Wollast, R. (1998). Carbon and carbonate metabolism in coastal aquatic ecosystems. *Annual Review of Ecology and Systematics*, *29*, 405–433.

Gauthier, T. D., Shane, E. C., Guerin, W. F., Seitz, W. R., Grant, C. L. (1986). Fluorescence quenching method for determining equilibrium constants for polycyclic aromatic hydrocarbons binding to dissolved humic materials. *Environmental Science & Technology*, *20*(11), 1162–1166.

Giamarchi, P., Stephan, L., Salomon, S., Le Bihan, A. (2000). Multicomponent Determination of a Polyaromatic Hydrocarbon Mixture by Direct Fluorescence Measurements. *Journal of Fluorescence*, *10*(4), 393–402.

Gilliom, R. J., Barbash, J. E., Crawford, C. G., Hamilton, P. A., Martin, J. D., Nakagaki, N., Nowell, L. H., Scott, J. C., Stackelberg, P. E., Thelin, G. P., Wolock, D. M. (2006). *Pesticides in the Nation ' s Streams and Ground Water , 1992 – 2001: US Geological Survey Circular 1291* (p. 172).

Giraud, X., Le Quéré, C., da Cunha, L. C. (2008). Importance of coastal nutrient supply for global ocean biogeochemistry. *Global Biogeochemical Cycles*, *22*, GB2025.

Gohin, F. (2011). Annual cycles of chlorophyll-*a*, non-algal suspended particulate matter, and turbidity observed from space and in-situ in coastal waters. *Ocean Science*, *7*, 705–732.

Gondar, D., Thacker, S. A., Tipping, E., Baker, A. (2008). Functional variability of dissolved organic matter from the surface water of a productive lake. *Water Research*, *42*(1-2), 81–90.

Gonzalez, J. J., Vinas, L., Franco, M. A., Fumega, J., Soriano, J. A., Grueiro, G., Muniategui, S., Lopez-Mahia, P., Prada, D., Bayona, J. M., Alzaga, R., Albaigés, J. (2006). Spatial and temporal distribution of dissolved / dispersed aromatic hydrocarbons in seawater in the area affected by the Prestige oil spill. *Marine Polluition Bulletin*, *53*, 250–259.

Goutx, M., Guigue, C., Ghiglione, J. F., Pujo-Pay, M., Raybaud, V., Duflos, M., Prieur, L. (2009). Short term summer to autumn variability of dissolved lipid classes in the Ligurian sea (NW Mediterranean). *Biogeosciences*, *6*(7), 1229–1246.

Griffini, O., Bao, M. L., Barbieri, C., Burrini, D., Pantani, F. (1997). Occurrence of pesticides in the Arno River and in potable water - A survey of the period 1992-1995. *Bulletin of Environmental Contamination and Toxicology*, *59*(2), 202–9.

Guigue, C., Tedetti, M., Ferretto, N., Garcia, N., Méjanelle, L., Goutx, M. (2014). Spatial and seasonal variabilities of dissolved hydrocarbons in surface waters from the Northwestern Mediterranean Sea: Results from one year intensive sampling. *Science of The Total Environment*, *466-467*, 650–662.

Guigue, C., Tedetti, M., Giorgi, S., Goutx, M. (2011). Occurrence and distribution of hydrocarbons in the surface microlayer and subsurface water from the urban coastal marine area off Marseilles, Northwestern Mediterranean Sea. *Marine Pollution Bulletin*, *62*(12), 2741–2752.

Guitart, C., Garcia-Flor, N., Bayona, J. M., Albaige, J. (2007). Occurrence and fate of polycyclic aromatic hydrocarbons in the coastal surface microlayer. *Marine Polluition Bulletin*, *54*, 186–194.

Guo, W., He, M., Yang, Z., Lin, C., Quan, X., Wang, H. (2007). Distribution of polycyclic aromatic hydrocarbons in water , suspended particulate matter and sediment from Daliao River watershed , China. *Chemosphere*, *68*, 93–104.

Gustafsson, C., Gschwend, P. M. (1997). Aquatic colloids : Concepts , definitions , and current challenges. *Limnology and Oceanography*, *42*(3), 519–528.

Hansell, D A, Carlson, C. A. (2002). *Biogeochemistry of Marine Dissolved Organic Matter*. (A. Hansell D & A. Carlson Craig, Eds.) (p. 774). Academic Press.

Hansell, D. A, Carlson, C. A., Repeta, D. J., Schlitzer, R. (2009). Dissolved organic matter in the ocean. A controversy stimulates new insights. *Oceanography*, *22*(5), 202–211.

Harvey, G. R., Boran, D. A., Chesal, L. A., Tokar, J. M. (1983). The structure of marine fulvic and humic acids. *Marine Chemistry*, *12*(2–3), 119–132.

Hedges, J. I. (1988). Polymerization of Humic Substances in Natural Environments. In F.H. Frimmel & R. F. Christman (Eds.), *Humic substances and their role in the environment* (pp. 45–58). New York: Wiley.

Hedges, J. I. (2002). Why dissolved organics matter? In A. Hansell D & A. Carlson Craig (Eds.), *Biogeochemistry of Marine Dissolved Organic Matter* (pp. 1–33). San Diego, CA: Academic Press.

Henderson, R. K., Baker, A., Murphy, K. R., Hambly, A., Stuetz, R. M., Khan, S. J. (2009). Fluorescence as a potential monitoring tool for recycled water systems: a review. *Water Research*, *43*(4), 863–881.

Howerton, S. B., Goodpaster, J. V., McGuffin, V. L. (2002). Characterization of polycyclic aromatic hydrocarbons in environmental samples by selective fluorescence quenching. *Analytica Chimica Acta*, *459*(1), 61–73.

Hu, C., Muller-Karger, F. E., Zepp, R. G. (2002). Absorbance , absorption coefficient , and apparent quantum yield : A comment on common ambiguity in the use of these optical concepts. *Limnology and Oceanography*, *47*(4), 1261–1267.

Hudson, N., Baker, A., Ward, D., Reynolds, D. M., Brunsdon, C., Carliell-Marquet, C., Browning, S. (2008). Can fluorescence spectrometry be used as a surrogate for the Biochemical Oxygen Demand (BOD) test in water quality assessment? An example from South West England. *Science of the Total Environment*, *391*(1), 149–158.

Hudson, N., Reynolds, D. (2007). Fluorescence analysis of dissolved organic matter in natural, waste and pollutedwaters- A review. *River Research and Applications*, *23*, 631–649.

Huguet, A., Vacher, L., Relexans, S., Saubusse, S., Froidefond, J. M., Parlanti, E. (2009). Properties of fluorescent dissolved organic matter in the Gironde Estuary. *Organic Geochemistry*, *40*(6), 706–719.

Huguet, A., Vacher, L., Saubusse, S., Etcheber, H., Abril, G., Relexans, S., Ibalot, F., Parlanti, E. (2010). New insights into the size distribution of fluorescent dissolved organic matter in estuarine waters. *Organic Geochemistry*, *41*(6), 595–610.

Inman, S. M., Thibado, P., Theriault, G. A., Lieberman, S. H. (1990). Development of a pulsed-laser, fiber-optic-based fluorimeter: determination of fluorescence decay times of polycyclic aromatic hydrocarbons in sea water. *Analytica Chimica Acta*, *239*, 45–51.

Ishii, S. K. L., Boyer, T. H. (2012). Behavior of Reoccurring PARAFAC Components in Fluorescent Dissolved Organic Matter in Natural and Engineered Systems: A Critical Review. *Environmental Science & Technology*, *46*, 2006–2017.

Jeong, W.-G., Cho, S.-M. (2007). Long-term effect of polycyclic aromatic hydrocarbon on physiological metabolisms of the Pacific oyster, Crassostrea gigas. *Aquaculture*, *265*(1–4), 343–350.

Jia, G., Li, L., Qiu, J., Wang, X., Zhu, W., Sun, Y., Zhou, Z. (2007). Determination of carbaryl and its metabolite 1-naphthol in water samples by fluorescence spectrophotometer after anionic surfactant micelle-mediated extraction with sodium dodecylsulfate. *Spectrochimica Acta Part A*, *67*, 460–464.

Jiao, N., Herndl, G. J., Hansell, D. A, Benner, R., Kattner, G., Wilhelm, S. W., Kirchman, D. L., Weinbauer, M. G., Luo, T., Chen, F., Azam, F. (2010). Microbial production of recalcitrant dissolved organic matter: long-term carbon storage in the global ocean. *Nature reviews. Microbiology*, *8*, 593–599.

Jiji, D., Andersson, G. G., Booksh, K. S. (2000). Application of PARAFAC for calibration with excitation – emission matrix fluorescence spectra of three classes of environmental pollutants. *Journal of Chemometrics*, 171–185.

JiJi, R. D., Booksh, K. S. (2000). Mitigation of Rayleigh and Raman Spectral Interferences in Multiway Calibration of Excitation−Emission Matrix Fluorescence Spectra. *Analytical Chemistry*, *72*(4), 718–725.

Jiji, R. D., Cooper, G. A., Booksh, K. S. (1999). Excitation-emission matrix fluorescence based determination of carbamate pesticides and polycyclic aromatic hydrocarbons. *Analytica Chimica Acta*, *397*, 61–72.

Jolliffe, I. T. (1986). *Principal Component Analysis* (p. 487). New York, Berlin, Heidelberg, Hong Kong, London, Milan, Paris, Tokyo: Springer.

Jordan, R. E., Payne, .R. J. (1980). *Fate and weathering of petroleum spills in the marine environment: a literature review and synopsis*. (A. A. S. Publishers, Ed.) (p. 184). Ann Arbor, Michigan.

Jørgensen, L., Stedmon, C. A., Kragh, T., Markager, S., Middelboe, M., Søndergaard, M. (2011). Global trends in the fluorescence characteristics and distribution of marine dissolved organic matter. *Marine Chemistry*, *126*(1-4), 139–148.

Jos, A., Repetto, G., Ríos, J. C., del Peso, A., Salguero, M., Hazen, M. J., Fernàndez-Freire,P., Pérez-Martin, J.M.,Labrador, V., Cameán, A. (2005). Ecotoxicological evaluation of the additive butylated hydroxyanisole using a battery with six model systems and eighteen endpoints. *Aquatic Toxicology*, *71*(2), 183–192.

Joux, F., Jeffrey, W. H., Abboudi, M., Neveux, J., Pujo-Pay, M., Oriol, L., Naudin, J. (2009). Rhône River Lenses of Low Salinity and in Ultraviolet Radiation in the Rho Marine Waters of the Northwestern Mediterranean Sea : Attenuation and Effects on Bacterial Activities and Net Community Production, 783–793.

Jung, A.-V., Frochot, C., Villieras, F., Lartiges, B. S., Parant, S., Viriot, M.-L., Bersillon, J.-L. (2010). Interaction of pyrene fluoroprobe with natural and synthetic humic substances: Examining the local molecular organization from photophysical and interfacial processes. *Chemosphere*, *80*(3), 228–234.

Jurado, E., Zaldívar, J. M., Marinov, D., Dachs, J. (2007). Fate of persistent organic pollutants in the water column : Does turbulent mixing matter ? *Marine Polluition Bulletin*, *54*, 441–451.

Kalyanasundaram, K., Thomas, J. K. (1977). Environmental effects on vibronic band intensities in pyrene monomer fluorescence and their application in studies of micellar systems. *Journal of the American Chemical Society*, *99*(7), 2039–2044.

Kannan, K., Reiner, J. L., Yun, S. H., Perrotta, E. E., Tao, L., Johnson-Restrepo, B., Rodan, B. D. (2005). Polycyclic musk compounds in higher trophic level aquatic organisms and humans from the United States. *Chemosphere*, *61*(5), 693–700.

Karcher, W., Fordham, R. J., Dubois, J. J., Glaude, P. G. J. M., Lightart, J. A. (1985). *Spectral atlas of polycyclic aromatic compounds*. (K. A. P. Group, Ed.)*Environmental Pollution* (Vol. 59, p. 828). Dordrecht/Boston/Lancaster: D. Reidel Publishing Company.

Katsoyiannis, A., Sweetman, A. J., Jones, K. C. (2011). PAH Molecular Diagnostic Ratios Applied to Atmospheric Sources : A Critical Evaluation Using Two Decades of Source Inventory and Air Concentration Data from the UK. *Environmental Science & Technology*, *45*, 8897–8906.

Katsuyama, M., Ohte, N. (2002). Determining the sources of stormflow from the fluorescence properties of dissolved organic carbon in a forested headwater catchment. *Journal of Hydrology*, *268*(1-4), 192–202.

Kennish, M. J. (1992). *Ecology of Estuaries: Anthropogenic Effects*. (Crc, Ed.)*Marine Science Series* (p. 494). CRC Press.

Kim, G. B., Maruya, K. A., Lee, R. F., Lee, J. H., Koh, C. H., Tanabe, S. (1999). Distribution and sources of polycyclic aromatic hydrocarbons in sediments from Kyeonggi Bay, Korea. *Marine Pollution Bulletin*, *38*(1), 7–15.

Kim, Y., Jordan, J. A., Nahorniak, M. L., Booksh, K. S. (2005). Photocatalytic Degradation-Excitation − Emission Matrix Fluorescence for Increasing the Selectivity of Polycyclic Aromatic Hydrocarbon Analyses Photocatalytic Degradation-Excitation-Emission Matrix Fluorescence for Increasing the Selectivity of Polycyclic. *Analytical Chemistry*, *77*(23), 7679–7686.

Ko, K., Sanford, L. P., Baker, J. E. (2003). Internal cycling of particle reactive organic chemicals in the Chesapeake Bay water column. *Marine Chemistry*, *81*, 163–176.

Kolpin, D. W., Barbash, J. E., Gilliom, R. J. (2002). Atrazine and metolachlor occurence in shallow ground water of the United States, 1993 to 1995: Relations to explanatory factors 1. *Journal of the American Water Resources Association*, *38*(1), 301–311.

Kolpin, D. W., Furlong, E. T., Meyer, M. T., Thurman, E. M., Zaugg, S. D., Barber, L. B., Buxton, H. T. (2002). Pharmaceuticals, hormones, and other organic wastewater contaminants in U.S. streams, 1999-2000: a national reconnaissance. *Environmental Science & Technology*, *36*(6), 1202–1211.

Kolpin, D. W., Skopec, M., Meyer, M. T., Furlong, E. T., Zaugg, S. D. (2004). Urban contribution of pharmaceuticals and other organic wastewater contaminants to streams during differing flow conditions. *Science of The Total Environment*, *328*(1–3), 119–130.

Konstantinou, I. K., Hela, D. G., Albanis, T. A. (2006). The status of pesticide pollution in surface waters (rivers and lakes) of Greece. Part I. Review on occurrence and levels. *Environmental Pollution*, *141*(3), 555–570.

Kowalczuk, P., Durako, M. J., Young, H., Kahn, A. E., Cooper, W. J., Gonsior, M. (2009). Characterization of dissolved organic matter fluorescence in the South Atlantic Bight with use of PARAFAC model: Interannual variability. *Marine Chemistry*, *113*(3-4), 182–196.

Kowalczuk, P., Stoń-Egiert, J., Cooper, W. J., Whitehead, R. F., Durako, M. J. (2005). Characterization of chromophoric dissolved organic matter (CDOM) in the Baltic Sea by

excitation emission matrix fluorescence spectroscopy. *Marine Chemistry*, *96*(3-4), 273–292.

Kumke, M. ., Löhmannsröben, H., Roch, T. (1994). Fluorescence Quenching of Polycyclic Aromatic Compounds by Humic Acid. *Analyst*, *1*(May), 997–1001.

Kumke, M., Löhmannsröben, H., Roch, T. (1995). Fluorescence Spectroscopy of Polynuclear Aromatic Compounds in Environmental Monitoring. *Journal of Fluorescence*, *5*(2), 139–153.

Kupper, T., Plagellat, C., Brändli, R. C., de Alencastro, L. F., Grandjean, D., Tarradellas, J. (2006). Fate and removal of polycyclic musks, UV filters and biocides during wastewater treatment. *Water Research*, *40*(14), 2603–2612.

Laganà, A., Bacaloni, A., De Leva, I., Faberi, A., Fago, G., Marino, A. (2002). Occurrence and determination of herbicides and their major transformation products in environmental waters. *Analytica Chimica Acta*, *462*(2), 187–198.

Lakowicz, J. (2006). *Principles of Fluorescence Spectroscopy*. (JosephR. Lakowicz, Ed.) (p. 954). Springer US.

Lakowicz, J. R., Weber, G. (1973). Quenching of fluorescence by oxygen. A probe for structural fluctuations in macromolecules. *Biochemistry*, *12*(21), 4161–4170.

Landau-Ossondo, M., Rabia, N., Jos-Pelage, J., Marquet, L. M., Isidore, Y., Saint-Aimé, C., Martin? M., Irigaray, P., Belpomme, D. (2009). Why pesticides could be a common cause of prostate and breast cancers in the French Caribbean Island, Martinique. An overview on key mechanisms of pesticide-induced cancer. *Biomedicine & Pharmacotherapy*, *63*(6), 383–395.

Larmagnat, S., Neuweiler, F. (2011). Exploring a link between Atlantic coral mounds and Phanerozoic carbonate mudmounds: Insights from pore water fluorescent dissolved organic matter (FDOM), Pen Duick mounds, offshore Morocco. *Marine Geology*, *282*(1-2), 149–159.

Lazure, P., Dumas, F. (2008). An external–internal mode coupling for a 3D hydrodynamical model for applications at regional scale (MARS). *Advances in Water Resources*, *31*(2), 233–250.

Lee, C. L., Kuo, L. J., Wang, H. L., Hsieh, P. C. (2003). Effects of ionic strength on the binding of phenanthrene and pyrene to humic substances: three-stage variation model. *Water Research*, *37*(17), 4250–4258.

Leong, K. H., Benjamin Tan, L. L., Mustafa, A. M. (2007). Contamination levels of selected organochlorine and organophosphate pesticides in the Selangor River, Malaysia between 2002 and 2003. *Chemosphere*, *66*(6), 1153–1159.

Lepom, P., Brown, B., Hanke, G., Loos, R., Quevauviller, P., Wollgast, J. (2009). Needs for reliable analytical methods for monitoring chemical pollutants in surface water under the

European Water Framework Directive. *Journal of Chromatography. A*, *1216*(3), 302–315.

Lim, L., Wurl, O., Karuppiah, S., Obbard, J. P. (2007). Atmospheric wet deposition of PAHs to the sea-surface microlayer. *Marine Pollution Bulletin*, *54*(8), 1212–1219.

Lindsey, B. B. D., Falls, W. F., Ferrari, M. J., Zimmerman, T. M., Harned, D. A., Sadorf, E. M., Chapman, M. J. (2006). *Factors Affecting Occurrence and Distribution of Selected Contaminants in Ground Water from Selected Areas in the Piedmont Aquifer System , Eastern United States , 1993-2003* (p. 72).

Lipiatou, E., Tolosa, I., Simó, R., Bouloubassi, I., Dachs, J., Marti, S., Sicre, M. A., Bayona, J.M., Grimalt, J.O., Saliot, A., Albaiges, J. (1997). Mass budget and dynamics of polycyclic aromatic hydrocarbons in the Mediterranean Sea. *Deep Sea Research Part II*, *44*(3–4), 881–905.

Literathy, P., Haider, S., Samhan, O., Morel, G. (1989). Experimental Studies on Biological and Chemical Oxidation of Dispersed Oil in Seawater. *Water Science & Technology*, *21*, 845–856.

Liu, K. K., Atkinsion, L., Chen, C. T. A., Gao, S., Hall, J., MacDonald, R. W., Talaue-McManus, L. Quinones, R. (2000). Exploring continental margin carbon fluxes on a global scale. *Eos, Transactions American Geophysical Union*, *81*, 641–644.

Liu, K. K., Atkinson, L., Quiñones, R., Talaue-McManus, L. (2010). *Carbon and Nutrient Fluxes in Continental Margins: A Global Synthesis* (p. 772). Springer.

Liu, R., Lead, J. R., Baker, A. (2007). Fluorescence characterization of cross flow ultrafiltration derived freshwater colloidal and dissolved organic matter. *Chemosphere*, *68*(7), 1304–11.

Lønborg, C., Álvarez-Salgado, X. A., Davidson, K., Martínez-García, S., Teira, E. (2010). Assessing the microbial bioavailability and degradation rate constants of dissolved organic matter by fluorescence spectroscopy in the coastal upwelling system of the Ría de Vigo. *Marine Chemistry*, *119*(1-4), 121–129.

Lønborg, C., Álvarez-Salgado, X. A., Davidson, K., Miller, A. E. J. (2009). Production of bioavailable and refractory dissolved organic matter by coastal heterotrophic microbial populations. *Estuarine, Coastal and Shelf Science*, *82*(4), 682–688.

Loos, R., Gawlik, B. M., Locoro, G., Rimaviciute, E., Contini, S., Bidoglio, G. (2009). EU-wide survey of polar organic persistent pollutants in European river waters. *Environmental Pollution*, *157*(2), 561–568.

Loos, R., Locoro, G., Contini, S. (2010). Occurrence of polar organic contaminants in the dissolved water phase of the Danube River and its major tributaries using SPE-LC-MS(2) analysis. *Water Research*, *44*(7), 2325–35.

Lu, F., Chang, C. H., Lee, D. J., He, P. J., Shao, L. M., Su, A. (2009). Dissolved organic matter with multi-peak fluorophores in landfill leachate. *Chemosphere*, *74*(4), 575–82.

Luciani, X, Mounier, S., Paraquetti, H. H. M., Redon, R., Lucas, Y., Bois, A., Lacerda, L.D., Raynaud, M., Ripert, M. (2008). Tracing of dissolved organic matter from the Sepetiba Bay (Brazil) by PARAFAC analysis of total luminescence matrices. *Marine Environmental Research*, *65*(2), 148–157.

Luciani, Xavier. (2007). *Analyse numérique des spectres de fluorescence 3D issus de mélanges non linéaires*. Thèse dedoctorat, Université du Sud Toulon Var, France. 174p

Macdonald, R. W., Barrie, L. A., Bidleman, T. F., Diamond, M. L., Gregor, D. J., Semkin, R. G., Strachan, W. M., Li, Y., Wania, F., Alaee, M., Alexeeva, L. B., Backus, S. M., Bailey, R., Bewers, J. M., Gobeil, C., Halsall, C. J., Harner, T., Hoff, J. T., Jantunen, L. M., Lockhart, W. L., Mackay, D., Muir, D. C., Pudykiewicz, J., Reimer, K. J., Smith, J. N., Stern, G. A. (2000). Contaminants in the Canadian Arctic : 5 years of progress in understanding sources , occurrence and pathways, *Science of the Total Environment, 254*, 93-234.

Maldonado, C., Bodineau, L. (1999). Column Processes of Aliphatic and Polycyclic Aromatic Hydrocarbons in the Northwestern Black Sea Water. *Environmental Science & Technology*, *33*, 2693–2702.

Mandalakis, M., Tsapakis, M., Tsoga, A., Stephanou, E. G. (2002). Gas – particle concentrations and distribution of aliphatic hydrocarbons , PAHs , PCBs and PCDD / Fs in the atmosphere of Athens (Greece). *Atmospheric Enviroment*, *36*, 4023–4035.

Manodori, L., Gambaro, A., Piazza, R., Ferrari, S., Stortini, A. M. (2006). PCBs and PAHs in sea-surface microlayer and sub-surface water samples of the Venice Lagoon (Italy). *Marine Pollution Bulletin*, *52*, 184–192.

Manoli, E., Samara, C., Kontantinou, I., Albanis, T. (2000). Polycyclic aromatic hydrocarbons in the bulk precipitation and surface waters of Northern Greece. *Chemosphere*, *41*, 1845–1855.

Mantovani, A., Stazi, A. V, Macri, C., Maranghi, F., Ricciardi, C. (1999). Problems in testing and risk assessment of endocrine disrupting chemicals with regard to developmental toxicology. *Chemosphere*, *39*(8), 1293–1300.

Markager, S., Stedmon, C. A., Søndergaard, M. (2011). Seasonal dynamics and conservative mixing of dissolved organic matter in the temperate eutrophic estuary Horsens Fjord. *Estuarine, Coastal and Shelf Science*, *92*(3), 376–388.

Marty, J., Chiav, J., Pizay, M., Avril, B. (2002). Seasonal and interannual dynamics of nutrients and phytoplankton pigments in the western Mediterranean Sea at the DYFAMED time-series station (1991 – 1999). *Deep Sea Research Part II*, *49*, 1965–1985.

Marty, J.-C., Saliot, A. (1976). Hydrocarbons (normal alkanes) in the surface microlayer of seawater. *Deep Sea Research*, *23*(9), 863–873.

Mastral, A. M., López, J. M., Callén, M. S., García, T., Murillo, R., Navarro, M. V. (2003). Spatial and temporal PAH concentrations in Zaragoza, Spain. *Science of the Total Environment*, *307*(1-3), 111–124.

Mazurek, M. A., Simoneit, B. R. T. (1984). Characterization of biogenic and petroleum-derived organic matter in aerosols over remote, rural and urban areas. In L. H. Keith (Ed.), *Identification and analysis of organic pollutants in air* (pp. 353–370). Boston: Ann Arbor Science.

McKinlay, R., Plant, J. A., Bell, J. N. B., Voulvoulis, N. (2008). Endocrine disrupting pesticides: implications for risk assessment. *Environment International*, *34*(2), 168–183.

Meidinger, R.F., Germain, R.W. S., Dohotariu, V., Gillispie, G.D. Fluorescence of Aromatic Hydrocarbons in Aqueous Solution, Proceedings of the U.S. EPA/Air and *Waste Management Association International Symposium on Field Screening Methods for Hazardous Wastes and Toxic Chemicals*, Las Vegas, NV, 1993, pp. 395-403.

Men, B., He, M., Tan, L., Lin, C., Quan, X. (2009). Distributions of polycyclic aromatic hydrocarbons in the Daliao River Estuary of Liaodong Bay, Bohai Sea (China). *Marine Polluition Bulletin*, *58*(6), 818–826.

Menzie, C. A., Potocki, B. B., Santodonato, J. (1992). Exposure to carcinogenic PAHs in the environment. *Environmental Science & Technology*, *26*(7), 1278–1284.

Mille, G., Asia, L., Guiliano, M., Malleret, L., Doumenq, P. (2007). Hydrocarbons in coastal sediments from the Mediterranean sea (Gulf of Fos area, France). *Marine Pollution Bulletin*, *54*(5), 566–75.

Minas, H. J., Coste, B., Le Corre, P., Minas, M., Raimbault, P. (1991). Biological and geochemical signatures associated with the water circulation through the Strait of Gibraltar and in the western Alboran Sea. *Journal of Geophysical Research: Oceans*, *96*(C5), 8755–8771.

Montuori, P., Triassi, M. (2012). Polycyclic aromatic hydrocarbons loads into the Mediterranean Sea: estimate of Sarno River inputs. *Marine Pollution Bulletin*, *64*(3), 512–520.

Mopper, K., Kieber, D. J. (2002). Photochemistry and the cycling of carbon, sulphur, nitrogen and phosphorus. In D. A Hansell & C. A. Carlson (Eds.), *Biogeochemistry of Marine Dissolved Organic Matter* (pp. 455–507). San Diego: Academic Press.

Mopper, K., Stubbins, A., Ritchie, J. D., Bialk, H. M., Hatcher, P. G. (2007). Advanced instrumental approaches for characterization of marine dissolved organic matter: extraction techniques, mass spectrometry, and nuclear magnetic resonance spectroscopy. *Chemical Reviews*, *107*, 419–442.

Morra, M. J., Corapcioglu, M. O., von Wandruszka, R. M. A., Marshall, D. B., Topper, K. (1990). Fluorescence quenching and polarization studies of naphthalene and 1-naphthol interaction with humic acid. *Soil Science Society of America journal*, *54*, 1283–1289.

Mounier, S, Patel, N., Quilici, L., Benaim, J. Y., Benamou, C. (1999). Fluorescence 3D de la matière organique dissoute du fleuve Amazone (threedimensional fluorescence of the dissolved organic carbon in the Amazon River). *Water Research*, *33*(6), 1523–1533.

Mounier, Stéphane, Zhao, H., Garnier, C., Redon, R. (2010). Copper complexing properties of dissolved organic matter: PARAFAC treatment of fluorescence quenching. *Biogeochemistry*, *106*(1), 107–116.

Moutin, T., Raimbault, P., Golterman, H. L., Coste, B. (1998). The input of nutrients by the Rhône river into the Mediterranean Sea: recent observations and comparison with earlier data. *Hydrobiologia*, *373/374*, 237–246.

Munaron, D., Tapie, N., Budzinski, H., Andral, B., Gonzalez, J.-L. (2012). Pharmaceuticals, alkylphenols and pesticides in Mediterranean coastal waters: Results from a pilot survey using passive samplers. *Estuarine, Coastal and Shelf Science*, *114*, 82–92.

Muroski, A. R., Booksh, K. S., Myrick, M. L. (1996). Single-Measurement Excitation/Emission Matrix Spectrofluorometer for Determination of Hydrocarbons in Ocean Water. 1. Instrumentation and Background Correction. *Analytical Chemistry*, *68*(20), 3534–3538.

Murphy, K. R., Butler, K. D., Spencer, R. G. M., Stedmon, C. A., Boehme, J. R., Aiken, G. R. (2010). Measurement of dissolved organic matter fluorescence in aquatic environments: an interlaboratory comparison. *Environmental science & technology*, *44*(24), 9405–9412.

Murphy, K. R., Ruiz, G. M., Dunsmuir, W. T. M., Waite, T. D. (2006). Optimized Parameters for Fluorescence-Based Verification of Ballast Water Exchange by Ships. *Environmental Science & Technology*, *40*(7), 2357–2362.

Murphy, K. R., Stedmon, C. A., Waite, T. D., Ruiz, G. M. (2008). Distinguishing between terrestrial and autochthonous organic matter sources in marine environments using fluorescence spectroscopy. *Marine Chemistry*, *108*(1-2), 40–58.

Murray, K. E., Thomas, S. M., Bodour, A. A. (2010). Prioritizing research for trace pollutants and emerging contaminants in the freshwater environment. *Environmental Pollution*, *158*(12), 3462–3471.

Myklestad, S. M. (2000). Dissolved Organic Carbon from Phytoplankton. (P. J. Wangersky, Ed.)*Marine Chemistry*, *5*, 111–148.

Nagata, T. (2000). Production mechanisms of dissolved organic matter. In D. L. Kirchman (Ed.), *Microbial ecology of the oceans* (pp. 121–152). Wiley-Liss.

Nahorniak, M. L., Booksh, K. S. (2006). Excitation-emission matrix fluorescence spectroscopy in conjunction with multiway analysis for PAH detection in complex matrices. *The Analyst*, *131*(12), 1308–15.

Nhan, D. D., Carvalho, F. P., Am, N. M., Tuan, N. Q., Yen, N. T. H., Villeneuve, J.-P., Cattini, C. (2001). Chlorinated pesticides and PCBs in sediments and molluscs from freshwater canals in the Hanoi region. *Environmental Pollution*, *112*(3), 311–320.

Nicholls, R.J., P.P.Wong, V.R. Burkett, J.O. Codignotto, J.E. Hay, R.F. McLean, S. Ragoonaden, Woodroffe, C.D. (2007) Coastal systems and low-lying areas. Climate Change 2007: Impacts, Adaptation and Vulnerability. Contribution ofWorking Group II to the Fourth Assessment Report of the Intergovernmental Panel on Climate Change, M.L. Parry, O.F. Canziani, J.P. Palutikof, P.J. van der Linden and C.E. Hanson, Eds., Cambridge University Press, Cambridge, UK, 315-356.

Nijegorodov, N., Mabbs, R., Winkoun, D. P. (2003). Influence of weak and strong donor groups on the fluorescence parameters and the intersystem crossing rate constant. *Spectrochimica Acta Part A*, *59*(3), 595–606.

Nijegorodov, N., Vasilenko, V., Monowe, P., Masale, M. (2009). Systematic investigation of the influence of methyl groups upon fluorescence parameters and the intersystem crossing rate constant of aromatic molecules. *Spectrochimica Acta Part A*, *74*(1), 188–194.

Ohno, T. (2002). Fluorescence inner-filtering correction for determining the humification index of dissolved organic matter. *Environmental Science & Technology*, *36*(4), 742–746.

Oliver, R., May, E., Williams, J. (2007). Microcosm investigations of phthalate behaviour in sewage treatment biofilms. *Science of The Total Environment*, *372*(2–3), 605–614.

Olivier, J.-M., Carrel, G., Lamouroux, N., Dole-Olivier, M.-J., Malard, F., Bravard, J.-P., Amoros, C. (2009). Chapter 7 - The Rhône River Basin BT - Rivers of Europe. In *Rivers of Europe* (pp. 247–295). London: Academic Press.

Opsahl, S., Benner, R. (1997). Distribution and cycling of terrigenous dissolved organic matter in the ocean. *Nature*, *386*(6624), 480–482.

Osburn, C. L., Stedmon, C. A. (2011). Linking the chemical and optical properties of dissolved organic matter in the Baltic–North Sea transition zone to differentiate three allochthonous inputs. *Marine Chemistry*, *126*(1-4), 281–294.

Packard, T. T., Minas, H. J., Coste, B., Martinez, R., Bonin, M. C., Gostan, J., Garfield, J., Christensen, J., Dortch, Q., Minas, M., Copin-Montegut, C. (1988). Formation of the Alboran oxygen minimum zone. *Deep Sea Research Part A. Oceanographic Research Papers*, *35*(7), 1111–1118.

Pairaud, I. L., Gatti, J., Bensoussan, N., Verney, R., Garreau, P. (2011). Hydrology and circulation in a coastal area off Marseille : Validation of a nested 3D model with observations. *Journal of Marine Systems*, *88*(1), 20–33.

Palm, A., Cousins, I., Gustafsson, Ö., Axelman, J., Grunder, K., Broman, D., Brorström-Lundén, E. (2004). Evaluation of sequentially-coupled POP fluxes estimated from simultaneous measurements in multiple compartments of an air – water – sediment system. *Environmental Pollution*, *128*, 85–97.

Panagiotopoulos, C., Sempéré, R., Para, J., Raimbault, P., Rabouille, C., Charrière, B. (2012). The composition and flux of particulate and dissolved carbohydrates from the Rhone River into the Mediterranean Sea. *Biogeosciences*, *9*(5), 1827–1844.

Paoli, A. (2005). Daily variations of highly active bacteria in the Northern Adriatic Sea. *Journal of Plankton Research*, *28*(3), 325–335.

Para, J., Coble, P. G., Charrière, B., Tedetti, M., Fontana, C., Sempéré, R. (2010). Fluorescence and absorption properties of chromophoric dissolved organic matter (CDOM) in coastal surface waters of the Northwestern Mediterranean Sea (Bay of Marseilles, France). *Biogeosciences*, *7*(4), 4083–4103.

Parlanti, E., Wo, K., Geo, L., Lamotte, M. (2000). Dissolved organic matter Fluorescence spectroscopy as a tool to estimate biological activity in a coastal zone submitted to anthropogenic inputs. *Organic Chemistry*, *31*, 1765–1781.

Patel-Sorrentino, N., Mounier, S., Benaim, J. Y. (2002). Excitation – emission fluorescence matrix to study pH influence on organic matter fluorescence in the Amazon basin rivers. *Water Research*, *36*, 2571–2581.

Pegau, W. S. (2002). Inherent optical properties of the Central Arctic surface waters. *Journal of Geophysical Research*, *107*(C 10).

Peng, X., Yu, Y., Tang, C., Tan, J., Huang, Q., Wang, Z. (2008). Occurrence of steroid estrogens, endocrine-disrupting phenols, and acid pharmaceutical residues in urban riverine water of the Pearl River Delta, South China. *Science of the Total Environment*, *397*(1-3), 158–166.

Pérez, S., Dachs, J., Barceló, D. (2003). Sea breeze modulated volatilization of polycyclic aromatic hydrocarbons from the Masnou Harbor (NW Mediterranean Sea). *Environmental Science & Technology*, *37*(17), 3794–802.

Peterson, E. W., Davis, R. K., Orndorff, H. A. (2000). 17ß-Estradiol as an indicator of animal waste contamination in mantled karst aquifers. *Journal of Environmental Quality*, *29*(3), 826–834.

Peuravuori, J. (2001). Partition coefficients of pyrene to lake aquatic humic matter determined by fluorescence quenching and solubility enhancement. *Analytica Chimica Acta*, *429*(1), 65–73.

Planas, C., Caixach, J., Santos, F. J., Rivera, J. (1997). Occurrence of pesticides in Spanish surface waters. Analysis by high resolution gas chromatography coupled to mass spectrometry. *Chemosphere*, *34*(11), 2393–2406.

Plaza, C., Senesi, N., García-Gil, J. C., Polo, A. (2005). Copper(II) complexation by humic and fulvic acids from pig slurry and amended and non-amended soils. *Chemosphere*, *61*(5), 711–716.

Pujo-Pay, M., Conan, P., Joux, F., Oriol, L., Naudin, J. J., Cauwet, G. (2006). Impact of phytoplankton and bacterial production on nutrient and DOM uptake in the Rhône River plume (NW Mediterranean). *Marine Ecology Progress Series*, *315*, 43–54.

Rabouille, C., Mackenzie, F. T., Ver, L. M. (2001). Influence of the human perturbation on carbon,nitrogen, and oxygen biogeochemical cycles in the global coastal ocean. *Geochimica et Cosmochimica Acta*, *65*, 3615–3641.

Raimbault, P., Diaz, F., Pouvesle, W., Boudjellal, B. (1999a). Simultaneous determination of particulate organic carbon , nitrogen and phosphorus collected on filters , using a semi-automatic wet-oxidation method. *Marine Ecology Progress Series*, *180*, 289–295.

Raimbault, Patrick, Lantoine, F., Neveux, J. (2004). Dosage rapide de la chlorophylle a et des phéopigments a par fluorimétrie après extraction au méthanol. Comparaison avec la méthode classique d'extraction à l'acétone. *Océanis*, *30*(2), 189–205.

Raimbault, Patrick, Pouvesle, W., Sempere, R. (1999b). Wet-oxidation and automated colorimetry for simultaneous determination of organic carbon , nitrogen and phosphorus dissolved in seawater. *Marine Chemistry*, *66*, 161–169.

Readman, J. W., Fillmann, G., Tolosa, I., Bartocci, J., Villeneuve, J., Catinni, C., Mee, L. D. (2002). Petroleum and PAH contamination of the Black Sea, *44*, 48–62.

Ren, B. (1999). Solvent polarity scale on the fluorescence spectra of a dansyl monomer copolymerizable in aqueous media. *Chemical Physics Letters*, *307*(1-2), 55–61.

Reynolds, D. M. (2003). Rapid and direct determination of tryptophan in water using synchronous fluorescence spectroscopy. *Water Research*, *37*(13), 3055–3060.

Ribeiro, O., C. A., Vollaire, Y., Sanchez-Chardi, A., Roche, H. (2005). Bioaccumulation and the effects of organochlorine pesticides, PAH and heavy metals in the Eel (Anguilla anguilla) at the Camargue Nature Reserve, France. *Aquatic Toxicology*, *74*(1), 53–69.

Richards, R. P., Baker, D. B. (1993). Pesticide concentration patterns in agricultural drainage networks in the lake Erie Basin. *Environmental Toxicology and Chemistry*, *12*(1), 13–26.

Rinnan, R., Rinnan, A. (2007). Application of near infrared reflectance (NIR) and fluorescence spectroscopy to analysis of microbiological and chemical properties of arctic soil. *Soil Biology & Biochemistry*, *39*(7), 1664–1673.

Roche, H, Vollaire, Y., Martin, E., Rouer, C., Coulet, E., Grillas, P., Banas, D. (2009). Chemosphere Rice fields regulate organochlorine pesticides and PCBs in lagoons of the Nature Reserve of Camargue. *Chemosphere*, *75*(4), 526–533.

Roche, Hélène, Buet, A., Ramade, F. (2002). Accumulation of lipophilic microcontaminants and biochemical responses in eels from the Camargue Biosphere Reserve. *Ecotoxicology London England*, *11*(3), 155–164.

Rodríguez-Cuesta, M., Boqué, R., Rius, F., Picón Zamora, D., Martínez Galera, M., Garrido Frenich, A. (2003). Determination of carbendazim, fuberidazole and thiabendazole by

three-dimensional excitation–emission matrix fluorescence and parallel factor analysis. *Analytica Chimica Acta*, *491*(1), 47–56.

Romera-Castillo, C., Sarmento, H., Anton Alvarez-Salgado, X., Gasol, J. M., Marrase, C. (2010). Erratum: Production of chromophoric dissolved organic matter by marine phytoplankton. *Limnology and Oceanography*, *55*(3), 1466–1466.

Roose, P., Brinkman, U. A. T. (2005). Monitoring organic microcontaminants in the marine environment: principles, programmes and progress. *Trends in Analytical Chemistry*, *24*(11), 897–926.

Rudnick, S. M., Chen, R. F. (1998). Laser-induced fluorescence of pyrene and other polycyclic aromatic hydrocarbons (PAH) in seawater. *Talanta*, *47*(4), 907–919.

Saar, R. A., Weber, J. H. (1980). Lead(II) complexation by fulvic acid: how it differs from fulvic acid complexation of copper(II) and cadmium(II). *Geochimica et Cosmochimica Acta*, *44*(9), 1381–1384.

Salvadó, J. A., Grimalt, J. O., López, J. F., Durrieu de Madron, X., Pasqual, C., Canals, M. (2013). Distribution of organochlorine compounds in superficial sediments from the Gulf of Lion, northwestern Mediterranean Sea. *Progress in Oceanography*, *118*, 235–248.

Sarafian, T. A., Kouyoumjian, S., Tashkin, D., Roth, M. D. (2002). Synergistic cytotoxicity of Δ9-tetrahydrocannabinol and butylated hydroxyanisole. *Toxicology Letters*, *133*(2–3), 171–179.

Schwarzenbach, R. P., Gschwend, P. M., Imboden, D. M. (1993). *Environmental organic chemistry*. (J. W. & Sons, Ed.) (p. 681). New York.

Seitz, W. R. (1981). Fluorescence methods for studying of pollutants in water speciation. *Analytical chemistry*, *I*(4), 79–83.

Sempéré, R., Charrière, B., Van Wambeke, F., Cauwet, G. (2000). Carbon inputs of the Rhone River to the Mediterranean Sea: biogeochemical implications. *Global Biogeochemical Cycles*, *14*(2), 669–681.

Sicre, M.-A., Fernandes, M. B., Pont, D. (2008). Poly-aromatic hydrocarbon (PAH) inputs from the Rhône River to the Mediterranean Sea in relation with the hydrological cycle: impact of floods. *Marine Pollution Bulletin*, *56*(11), 1935–1942.

Siegel, D. A., Maritorena, S., Nelson, N. B., Behrenfeld, M. J. (2005). Independence and interdependencies among global ocean color properties: Reassessing the bio-optical assumption. *Journal of Geophysical Research: Oceans*, *110*(C7), C07011.

Siegenthaler, U., Sarmiento, J. L. (1993). Atmospheric carbon dioxide and the ocean. *Nature*, *365*, 119–125.

Singh, S., D'Sa, E. J., Swenson, E. M. (2010). Chromophoric dissolved organic matter (CDOM) variability in Barataria Basin using excitation-emission matrix (EEM)

fluorescence and parallel factor analysis (PARAFAC). *Science of the Total Environment*, *408*(16), 3211–3222.

Siron, R., Giusti, G., Blanc, F. (1987). Hydrocarbons in the water column of the Carteau Ba (Gulf of Fos-sur-mer, Mediterranean Sea). *Marine Chemistry*, *21*, 75–89.

Spencer, R. G. M., Bolton, L., Baker, A. (2007). Freeze/thaw and pH effects on freshwater dissolved organic matter fluorescence and absorbance properties from a number of UK locations. *Water Research*, *41*(13), 2941–2950.

Stedmon, C. A., Bro, R. (2008). Characterizing dissolved organic matter fluorescence with parallel factor analysis: a tutorial. *Limnology and Oceanography Methods*, *6*(3798), 572–579.

Stedmon, C. A., Osburn, C. L., Kragh, T. (2010). Tracing water mass mixing in the Baltic–North Sea transition zone using the optical properties of coloured dissolved organic matter. *Estuarine, Coastal and Shelf Science*, *87*, 156–162.

Stedmon, C. A., Bro, R. (2008). Characterizing dissolved organic matter fluorescence with parallel factor analysis: a tutorial. *Limnology and Oceanography Methods*, *6*(3798), 572–579.

Stedmon, C. A., Markager, S., Bro, R. (2003). Tracing dissolved organic matter in aquatic environments using a new approach to fluorescence spectroscopy. *Marine Chemistry*, *82*(3-4), 239–254.

Stedmon, C. A., Seredyńska-Sobecka, B., Boe-Hansen, R., Le Tallec, N., Waul, C. K., Arvin, E. (2011). A potential approach for monitoring drinking water quality from groundwater systems using organic matter fluorescence as an early warning for contamination events. *Water Research*, *45*(18), 6030–6038.

Stedmon, C. A., Markager, S. (2005a). Resolving the variability of dissolved organic matter fluorescence in a temperate estuary and its catchment using PARAFAC analysis. *Limnology and Oceanography*, *50*(2), 686–697.

Stedmon, C. A., Markager, S. (2005b). Tracing the production and degradation of autochthonous fractions of dissolved organic matter using fluorescence analysis. *Limnology and Oceanography*, *50*(5), 1415–1426.

Stedmon, C. A., Markager, S., Tranvik, L., Kronberg, L., Slätis, T., Martinsen, W. (2007). Photochemical production of ammonium and transformation of dissolved organic matter in the Baltic Sea. *Marine Chemistry*, *104*(3798), 227–240.

Steelink, C. (1985). *Humic substances in soil, sediment, and water*. (George R Aiken, R. L. MacKnight, R. . Wershaw, P. MacCarthy, Eds.) (p. 692). New York: Wiley.

Stortini, A. M., Martellini, T., Del Bubba, M., Lepri, L., Capodaglio, G., Cincinelli, A. (2009). n-Alkanes , PAHs and surfactants in the sea surface microlayer and sea water samples of the Gerlache Inlet sea (Antarctica). *Microchemical Journal*, *92*(1), 37–43.

Suffet, I. H., MacCarthy, P. (1989). *Aquatic Humic Substances. Influence on Fate and Treatment of Pollutants*. (A. C. Society, Ed.)*Advances in Chemistry* (Vol. 219, p. 864). Washington, DC.

Tedetti, M., Cuet, P., Guigue, C., Goutx, M. (2011). Characterization of dissolved organic matter in a coral reef ecosystem subjected to anthropogenic pressures (La Réunion Island, Indian Ocean) using multi-dimensional fluorescence spectroscopy. *Science of the Total Environment*, *409*(11), 2198–2210.

Tedetti, M., Guigue, C., Goutx, M. (2010). Utilization of a submersible UV fluorometer for monitoring anthropogenic inputs in the Mediterranean coastal waters. *Marine Pollution Bulletin*, *60*(3), 350–362.

Tedetti, M., Longhitano, R., Garcia, N., Guigue, C., Ferretto, N., Goutx, M. (2012). Fluorescence properties of dissolved organic matter in coastal Mediterranean waters influenced by a municipal sewage effluent (Bay of Marseilles, France). *Environmental Chemistry*, *9*, 438–449.

Tedetti, M., Sempéré, R. (2006). Penetration of ultraviolet radiation in the marine environment. A review. *Photochemistry and Photobiology*, *82*(2), 389–397.

The MerMex group, Durrieu de Madron, X., Guieu, C., Sempéré, R., Conan, P., Cossa, D., … Rabouille, C. (2011). Marine ecosystems' responses to climatic and anthropogenic forcings in the Mediterranean. *Progress in Oceanography*, *91*(2), 97–166.

Thomas, H., Bozoec, Y., Elkalay, K., de Baar, H. J. W. (2004). Comment on "Enhanced open ocean storage of CO2 from shelf sea pumping". *Science*, *304*, 1005–1008.

Thurman, E. M., Goolsby, D. A., Meyer, M. T., Kolpin, D. W. (1991). Herbicides in surface waters of the midwestern United States: the effect of spring flush. *Environmental Science & Technology*, *25*(10), 1794–1796.

Tilseth, S., Solberg, T. S., Westrheim, K. (1984). Sublethal Effects of the Water-Soluble Fraction of Ekofisk Crude Oil on the Early Larval Stages of Cod (Gadus morhua L .). *Marine Environmental Research*, *11*(1), 1-16.

Tolosa, I., Bayona, J. M., Albaigés, J. (1996). Aliphatic and Polycyclic Aromatic Hydrocarbons and Sulfur/Oxygen Derivatives in Northwestern Mediterranean Sediments: Spatial and Temporal Variability, Fluxes, and Budgets. *Environmental Science & Technology*, *30*(8), 2495–2503.

Tréguer, P., Le Corre, P. (1975). *Manuel d'analyses des sels nutritifs dans l'eau de mer: Utilisation de l'Autoanalyser II Technicon* (2nd ed.). Université de Bretagne Occidentale, Brest.

Tsapakis, M., Apostolaki, M., Eisenreich, S., Stephanou, E. G. (2006). Atmospheric Deposition and Marine Sedimentation Fluxes of Polycyclic Aromatic Hydrocarbons in the Eastern Mediterranean Basin. *Environmental Science & Technology*, *40*(16), 4922–4927.

Ulses, C., Estournel, C., Bonnin, J., Durrieu de Madron, X., Marsaleix, P. (2008). Impact of storms and dense water cascading on shelf-slope exchanges in the Gulf of Lion (NW Mediterranean). *Journal of Geophysical Research*, *113*(C2), C02010.

Ulses, C., Grenz, C., Marsaleix, P., Schaaff, E., Estournel, C., Meulé, S., Pinazo, C. (2005). Circulation in a semi-enclosed bay under influence of strong freshwater input. *Journal of Marine Systems*, *56*(1-2), 113–132.

Valavanidis, A., Vlachogianni, T., Triantafillaki, S., Dassenakis, M., Androutsos, F., Scoullos, M. (2008). Polycyclic aromatic hydrocarbons in surface seawater and in indigenous mussels (Mytilus galloprovincialis) from coastal areas of the Saronikos Gulf (Greece). *Estuarine, Coastal and Shelf Science*, *79*, 733–739.

Valero-Navarro, A., Fernández-Sánchez, J. F., Medina-Castillo, A. L., Fernández-Ibáñez, F., Segura-Carretero, A., Ibáñez, J. M., Fernández-Gutiérrez, A. (2007). A rapid, sensitive screening test for polycyclic aromatic hydrocarbons applied to Antarctic water. *Chemosphere*, *67*(5), 903–910.

Valeur, B. (2001). *Molecular Fluorescence: Principles and Applications* (p. 381). Weinheim: Wiley-VCH Verlag GmbH.

Valiela, I. (2006). *Global Coastal Change*. (Wiley-Blackwell, Ed.) (p. 368). Oxford.

Ver, L. M. B., Mackenzie F. T., Lerman A. (1999). Carbon cycle in the coastal zone: effects of global perturbations and change in the past three centuries. *Chemical Geology*, 159, 283-304.

Vodacek, A., Philpot, W. D. (1987). Environmental effects on laser-induced fluorescence spectra of natural waters. *Remote Sensing of Environment*, *21*(1), 83–95.

Vos, J. G., Dybing, E., Greim, H. A., Ladefoged, O., Lambré, C., Tarazona, J. V, Brandt, I., Vethaak, A. D. (2000). Health effects of endocrine-disrupting chemicals on wildlife, with special reference to the European situation. *Critical Reviews in Toxicology*, *30*(1), 71–133.

Wafo, E., Sarrazin, L., Diana, C., Schembri, T., Lagadec, V., Monod, J. L. (2006). Polychlorinated biphenyls and DDT residues distribution in sediments of Cortiou (Marseille, France). *Marine Pollution Bulletin*, *52*(1), 104–107.

Wakeham, S. G. (1996). Aliphatic and polycyclic aromatic hydrocarbons in Black Sea sediments. *Marine Chemistry*, *53*, 187–205.

Walsh, J. J. (1991). Importance of continental margins in the marine biogeochemical cycling of carbon and nitrogen. *Nature*, *350*, 53–55.

Walther, H.-J. (1989). J. Buffle: Complexation Reactions in Aquatic Systems; Analytical Approach. Chichester, J. Wiley & Sons Ltd./Ellis Horwood Ltd., 1988, 692 S., 247 Abb., 126 Tab., £ 69,50, ISBN 0-470-20830-9 / 085312-557-0. *Acta Hydrochimica et Hydrobiologica*, *17*(2), 230.

Wang, Y., Wang, Z., Ma, M., Wang, C., Mo, Z. (2001). Monitoring priority pollutants in a sewage treatment process by dichloromethane extraction and triolein-semipermeable membrane device (SPMD). *Chemosphere*, *43*(3), 339–346.

Wang, Z., Fingas, M. (1995). Differentiation of the source of spilled oil and monitoring of the oil weathering process using gas chromatography-mass spectrometry. *Journal of Chromatography A*, *712*, 321–343.

Wang, Z., Fingas, M., Landriault, M., Sigouin, L., Feng, Y., Mullin, J. (1997). Using systematic and comparative analytical data to identify the source of an unknown oil on contaminated birds. *Journal of Chromatography A*, *775*(1–2), 251–265.

Wang, Z., Fingas, M., Page, D. S. (1999). Oil spill identification. *Journal of Chromatography A*, *843*(1–2), 369–411.

Watkinson, R. J., Griffiths, D. (1987). Biodegradation and photo-oxidation of crude oils in a tropical marine environment. In J. Kuiper & W. J. Van der Brink (Eds.), *Fate and Effects of Oil in Marine Ecosystems* (pp. 64–77). The Hague: Martinus Nijhoff.

Weber, K., Goerke, H. (2003). Persistent organic pollutants (POPs) in antarctic fish: levels, patterns, changes. *Chemosphere*, *53*(6), 667–678.

Westerhoff, P., Wen, C., Esparza, M. (2001). Fluorescence analysis of a standard fulvic acid and tertiary treated wastewater. *Journal of Environmental Quality*, *30*(6), 2037–2046.

Wetzel, D. L., Van Vleet, E. S. (2004). Accumulation and distribution of petroleum hydrocarbons found in mussels (Mytilus galloprovincialis) in the canals of Venice, Italy. *Marine Pollution Bulletin*, *48*(9–10), 927–936.

Wilcke, W. (2007). Global patterns of polycyclic aromatic hydrocarbons (PAHs) in soil. *Geoderma*, *141*, 157–166.

Williams, P. J. le B. (2000). Heterotrophic bacteria and the dynamics of dissolved organic material. In D. L. Kirchman (Ed.), *Microbial Ecology of the Oceans* (pp. 153–200). New York: Wiley-Liss.

Williams, P. M., Druffel, E. R. M., Smith, K. L. (1987). Dietary carbon sources for deep-sea organisms as inferred from their organic radiocarbon activities. *Deep Sea Research*, *34*(2), 253–266.

Wollast, R. (1991). The coastal organic carbon cycle: Fluxes, sources, and sinks. In R. Mantoura, J. Martin, R. Wollast (Eds.), *Ocean Margin Processes in Global Change* (pp. 365–381). Berlin: Wiley-Interscience.

Wu, T., Lambert, L., Hastings, D., Banning, D. (1980). Enrichment of the agricultural herbicide atrazine in the microsurface water of an estuary. *Bulletin of Environmental Contamination and Toxicology*, *24*(1), 411–414.

Wurl, O., Obbard, J. P. (2004). A review of pollutants in the sea-surface microlayer (SML): a unique habitat for marine organisms. *Marine Pollution Bulletin*, *48*(11–12), 1016–1030.

Yamada, M., Takada, H., Toyoda, K., Yoshida, A., Shibata, A., Nombra, H., Wada, M., Nishimura, M., Okamoto, K., Ohwada, K. (2003). Study on the fate of petroleum-derived polycyclic aromatic hydrocarbons (PAHs) and the effect of chemical dispersant using an enclosed ecosystem , mesocosm. *Marine Polluition Bulletin*, *47*, 105–113.

Yamashita, Y., Cory, R. M., Nishioka, J., Kuma, K., Tanoue, E., Jaffé, R. (2010). Fluorescence characteristics of dissolved organic matter in the deep waters of the Okhotsk Sea and the northwestern North Pacific Ocean. *Deep Sea Research Part II*, *57*(16), 1478–1485.

Yamashita, Y., Jaffe, R. (2008). Assessing the dynamics of dissolved organic matter (DOM) in coastal environments by excitation emission matrix fluorescence and parallel factor analysis (EEM-PARAFAC). *Limnology and Oceanography*, *53*(5), 1900–1908.

Yamashita, Y., Maie, N., Briceño, H., Jaffé, R. (2010). Optical characterization of dissolved organic matter in tropical rivers of the Guayana Shield, Venezuela. *Journal of Geophysical Research*, *115*, G00F10.

Yamashita, Y., Panton, A., Mahaffey, C., Jaffé, R. (2011). Assessing the spatial and temporal variability of dissolved organic matter in Liverpool Bay using excitation–emission matrix fluorescence and parallel factor analysis. *Ocean Dynamics*, *61*(5), 569–579.

Yamashita, Y., Tanoue, E. (2004). In situ production of chromophoric dissolved organic matter in coastal environments. *Geophysical Research Letters*, *31*(14), 1–4.

Yao, X., Zhang, Y., Zhu, G., Qin, B., Feng, L., Cai, L., Gao, G. (2011). Resolving the variability of CDOM fluorescence to differentiate the sources and fate of DOM in Lake Taihu and its tributaries. *Chemosphere*, *82*(2), 145–155.

Zhang, Yaheng, Li, J., Dong, L., Li, Y., Chen, X. (2008). Characterization of interaction between esculin and human serum albumin in membrane mimetic environments. *Journal of Molecular Structure*, *889*(1–3), 119–128.

Zhang, Yunlin, Yin, Y., Feng, L., Zhu, G., Shi, Z., Liu, X., Zhang, Y. (2011). Characterizing chromophoric dissolved organic matter in Lake Tianmuhu and its catchment basin using excitation-emission matrix fluorescence and parallel factor analysis. *Water Research*, *45*(16), 5110–5122.

Zhang, Yunlin, Zhang, E., Yin, Y., Dijk, M. A. Van, Feng, L., Shi, Z. (2010). Characteristics and sources of chromophoric dissolved organic matter in lakes of the Yungui Plateau , China , differing in trophic state and altitude. *Limnology and Oceanography*, *55*(6), 2645–2659.

Zhou, J. L., Hong, H., Zhang, Z., Maskaoui, K., Chen, W. (2000). Multi-phase distribution of organic micropollutants in Xiamen, China, *34*(7), 2132–2150.

Zhou, Z., Guo, L., Shiller, A. M., Lohrenz, S. E., Asper, V. L., Osburn, C. L. (2013). Charachterization of oil components from the Deepwater Horizon oil spill in the Gulf of Mexico using fluorescence EEM and PARAFAC techniques. *Marine Chemistry*, *148*, 10–21.

Zsolnay, A., Baigar, E., Jimenez, M. (1999). Differentiating with fluorescence spectroscopy the sources of dissolved organic matter in soils subjected to drying. *Chemosphere, 38*(1), 45–50.

Annexes : Articles issus de la thèse

Chemosphere 107 (2014) 344–353

Contents lists available at ScienceDirect

Chemosphere

journal homepage: www.elsevier.com/locate/chemosphere

Identification and quantification of known polycyclic aromatic hydrocarbons and pesticides in complex mixtures using fluorescence excitation–emission matrices and parallel factor analysis

Nicolas Ferretto [a,*], Marc Tedetti [a], Catherine Guigue [a], Stéphane Mounier [b], Roland Redon [b], Madeleine Goutx [a]

[a] Aix-Marseille Université, Université du Sud Toulon-Var, CNRS/INSU, IRD, Mediterranean Institute of Oceanography (MIO), UM 110, 13288 Marseille Cedex 09, France
[b] Laboratoire des PROcessus de Transferts et d'Echanges dans l'Environnement (PROTEE), Université de Toulon, BP 20132, 83957 La Garde Cedex, France

HIGHLIGHTS

- Determination of PAH and pesticide fluorescence properties using EEMs.
- Discrimination of PAH and pesticide fluorescence signatures using PARAFAC analysis.
- Good correlation between PAH concentrations and fluorescence intensities in marine waters.

ARTICLE INFO

Article history:
Received 27 August 2013
Received in revised form 16 December 2013
Accepted 28 December 2013
Available online 23 January 2014

Keywords:
Fluorescence
EEM
PARAFAC
Contaminants
PAHs
Pesticides

ABSTRACT

Polycyclic aromatic hydrocarbons (PAHs) and pesticides are among the most widespread organic contaminants in aquatic environments. Because of their aromatic structure, PAHs and pesticides have intrinsic fluorescence properties in the ultraviolet/blue spectral range. In this study, excitation–emission matrix (EEM) fluorescence spectroscopy and parallel factor (PARAFAC) analysis were used to characterise and discriminate fluorescence signatures of nine PAHs and three pesticides at the μg L^{-1} level in the presence of humic substances (0.1–10 mg C L^{-1}). These contaminants displayed a diversity of fluorescence signatures regarding spectral position (λ_{Ex}: 220–335 nm, λ_{Em}: 310–414 nm), Stokes shift (39–169 nm) and number of peaks (1–8), with detection limits ranging from 0.02 to 1.29 μg L^{-1}. The EEM/PARAFAC method applied to mixtures of PAHs with humic substances validated a seven-component model that included one humic-like fluorophore and six PAH-like fluorophores. The EEM/PARAFAC method applied to mixtures of pesticides with humic substances validated a six-component model that included one humic-like fluorophore and three pesticide-like fluorophores. The EEM/PARAFAC method adequately quantified most of the contaminants for humic substance concentrations not exceeding 2.5 mg C L^{-1}. The application of this method to natural (marine) samples was demonstrated through (1) the match between the Ex and Em spectra of PARAFAC components and the Ex and Em spectra of standard PAHs, and (2) the good linear correlations between the fluorescence intensities of PARAFAC components and the PAH concentrations determined by GC–MS.

1. Introduction

Polycyclic aromatic hydrocarbons (PAHs) and pesticides are among the most widespread organic contaminants in aquatic environments (Roose and Brinkman, 2005; Lepom et al., 2009). Due to their physico-chemical properties, PAHs and pesticides are persistent and mobile, can strongly bioaccumulate in food chains and are harmful to living organisms through reprotoxic, carcinogenic, mutagenic or endocrine disrupting effects (Kennish, 1992; McKinlay et al., 2008; Landau-Ossondo et al., 2009). Thus, PAHs and pesticides are recognised by various international organizations as priority contaminants: They are included in the list of 45 priority regulated substances by the European Union (Official Journal of the EU 24/08/2013, Directive 2013/39/EU), and in the list of priority regulated substances by the US Federal Water Pollution Control Act and the US Environmental Protection Agency (EPA). PAHs are introduced into marine and fresh waters from the direct discharges of crude oil or its derivatives during sea activities, or from industrial and urban wastes routed by surface runoffs, effluents or atmospheric particles (Wurl and Obbard, 2004; Dachs and Méjanelle, 2010). Pesticides are particularly abundant near

* Corresponding author. Tel.: +33 4 91 82 90 50.
E-mail address: nicolas.ferretto@univ-amu.fr (N. Ferretto).

0045-6535/$ - see front matter © 2014 Elsevier Ltd. All rights reserved.
http://dx.doi.org/10.1016/j.chemosphere.2013.12.087

agriculture areas and enter marine and fresh waters mainly through surface runoffs (Bocquené and Franco, 2005; Jia et al., 2007). Gas or liquid chromatography coupled to mass spectrometry (GC–MS, LC–MS) is the reference analytical method to determine PAH and pesticide concentrations at $\mu g\ L^{-1}$ or $ng\ L^{-1}$ levels in natural waters (Lepom et al., 2009). However, chromatographic analyses, which require large volumes of water (1–5 L) and several sample treatment steps, such as extraction, purification or concentration, are time-consuming and cannot be applied for a large number of samples.

Due to their aromatic structures, PAHs and (to a lesser extent) pesticides have intrinsic fluorescence properties in the UV and blue spectral regions (Dabestani and Ivanov, 1999; JiJi and Booksh, 2000). Hence, fluorescence spectroscopy could be relevant for monitoring these contaminants in aquatic ecosystems. Currently, the state-of-the-art fluorescence spectroscopy technique that is used to characterise dissolved organic compounds in natural waters is fluorescence excitation–emission matrix (EEM), which involves a collection of sequential fluorescence emission (Em) spectra at successively increasing excitation (Ex) wavelengths. EEM has two significant advantages over chromatographic methods: (1) it is quick since it does not entail any sample pretreatment and (2) it only requires very small volumes of water (~5 mL). Conversely, EEM has two main limits: (1) its sensitivity, with detection limits in the $\mu g\ L^{-1}$ range and (2) its lack of selectivity, which is caused by overlapping fluorophore signatures. The overlapping in fluorescence signatures of individual compounds in multi-component mixtures, such as PAH- and pesticide-contaminated natural waters, may be important and generate complex EEMs that are difficult to interpret. Therefore, advanced multivariate statistical techniques, such as parallel factor analysis (PARAFAC), were proposed recently to decompose the EEM complex fluorescence signal into underlying individual fluorescence spectra (Stedmon and Bro, 2008).

Humic substances, which represent a major component of dissolved organic matter (DOM) in natural waters (they are particularly abundant in freshwaters and coastal ecosystems), have a strong ability to absorb light and to fluoresce (Blough and Del Vecchio, 2002). Moreover, they are known to molecularly interact and bind with organic contaminants such as PAHs and pesticides (Gauthier et al., 1986; Fang et al., 1998; Akkanen et al., 2012). Thus, the presence of humic substances in water samples containing PAHs or pesticides may cause additional difficulties in the retrieval and quantification of these contaminants by the EEM/PARAFAC method because of fluorescence signature overlapping, but also of absorbance-induced inner filtering effects and fluorescence quenching processes.

Several studies have successfully used the EEM/PARAFAC method to characterise and quantify PAHs at the $\mu g\ L^{-1}$ level from petroleum products such as gasoline, diesel, fuel, lubricating and crude oils (Christensen et al., 2005; Alostaz et al., 2008), from aqueous motor oil extract and asphalt leachate (Nahorniak and Booksh, 2006), from oceanic water enriched with gasoline (Booksh et al., 1996; Muroski et al., 1996), and from PAH mixtures in pure water (Beltrán et al., 1998; Kim et al., 2005). Also, recent works have proposed the EEM/PARAFAC method to characterise and quantify some pesticides at the $\mu g\ L^{-1}$ level from pesticide mixtures in pure water or methanol (Jiji et al., 1999; JiJi and Booksh, 2000; Rodríguez-Cuesta et al., 2003). However, to our knowledge, the EEM/PARAFAC method has never been applied on PAH or pesticide mixtures in presence of humic substances, even though this would have allowed for better reflecting the content of natural waters.

In this context, the objectives of this study are (1) to characterise the fluorescence signatures of several PAHs and pesticides of interest by using EEM spectroscopy, (2) to asses the relevancy of PARAFAC for discriminating contaminant fluorescence signatures in complex mixtures containing humic substances and (3) to apply the method on marine water samples and to compare the fluorescence intensities with concentrations of individual compounds determined by GC–MS.

2. Material and methods

2.1. Standard solutions

Nine PAHs and three pesticides of interest were chosen to conduct our study. For the PAHs, we chose naphthalene (Naph), 2,3 dimethyl naphthalene (DNaph), fluorene (Flu), 1,8 dimethyl-9H-fluorene (DFlu), phenanthrene (Phe), anthracene (Ant), pyrene (Pyr), benzo[a]anthracene (BaA) and benz(e)pyrene (BeP). For the pesticides, we selected 2-phenylphenol (Pho), carbaryl (Car) and thiabendazole (Thi). Naph, DNaph, Flu, DFlu, Phe, Ant and Pyr are among the most abundant PAHs in the dissolved phase of natural waters (Guigue et al., 2014). Because of similarities in their structure (number of rings and π electrons), isomers (Phe and Ant), parents and their alkylated homologues (Naph and DNaph, Flu and DFlu) and phenylated PAHs (BaA and BeP) should have very close fluorescence signatures. Pho, Car and Thi are used as a fungicide, but also as molluscicide, insecticide (Car), nematicide, bactericide and antibiotic (Pho) in agriculture. These pesticides have been detected in both freshwater and coastal marine environments (i.e., river of the Pearl River Delta, coastline of Martinique, Willapa Bay) (Dumbauld et al., 2001; Bocquené and Franco, 2005; Peng et al., 2008).

The PAHs and pesticides were purchased from Sigma–Aldrich ($\geqslant$98%) and were used without further purification. Stock solutions of each individual compound ($50\ mg\ L^{-1}$) were prepared by dissolving the pure solid in methanol (Rathburn HPLC grade). From the stock solutions, individual solutions with final concentrations of between 0.1 and $20\ \mu g\ L^{-1}$ were prepared in ultrapure water (i.e., Milli-Q water). In addition, PAH and pesticide mixtures were prepared from these stock solutions. The final concentrations of each compound in these mixtures were between 1 and $10\ \mu g\ L^{-1}$. Suwannee River humic (HA) (2S101H) and fulvic (FA) (2S101F) acids were purchased from the International Humic Substances Society (IHSS). The HA and FA were dissolved in sodium hydroxide and ultrapure water, respectively, to obtain HA and FA solutions of $100\ mg\ L^{-1}$. These two solutions were then mixed together to obtain a stock solution of humic substances (HA + FA) in ultrapure water of $200\ mg\ L^{-1}$. This humic substance stock solution was added to the PAH and pesticide mixtures to achieve final concentrations of HA + FA of between 0.2 and $20\ mg\ L^{-1}$, corresponding to concentrations of organic carbon of between 0.1 and $10\ mg\ C\ L^{-1}$. All solutions were made in ultrapure water and their pH was adjusted to 6.0 with sodium hydroxide. Standard (individual and mixture) solutions were stored in SCHOTT® glass bottles and in the dark at 4 °C for 48 h prior to analysis.

2.2. Natural samples

Marine water samples were collected aboard the R/V Antédon II in the morning on 6 July 2011 in the Saumaty harbour (10 samples) and on 20 July 2012 in the Port-de-Bouc harbour (20 samples), located in the Marseilles Bay (northwestern Mediterranean Sea, France). Saumaty and Port-de-Bouc harbours are known to be heavily contaminated in hydrocarbons (Guigue et al., 2011). Saumaty is a dynamic fishing port that combines trawlers, tuna boats and wholesale trading centers, whereas Port-de-Bouc is surrounded by the Marseilles–Fos petrochemical complex, which includes several chemical, petroleum and steel-work plants. Samples were taken at ~0.1 m depth (subsurface water) with 4 L

Nalgene polycarbonate bottles. The bottles were washed with 1 M HCl and ultrapure water before use, rinsed three times with the respective sample before filling and stored in the dark in the cold (4–8 °C). Back in the laboratory, samples were immediately filtered under a low vacuum (<50 mmHg) through precombusted (500 °C, 4 h) GF/F glass fibre filters (47 mm diameter, Whatman) using polysulfone filtering systems. For fluorescence measurements, filtered samples were stored in 10 mL glass tubes at 4 °C in the dark and were analysed within 24 h. For chromatographic (PAH) analyses, filtered samples were stored in 1 L SCHOTT® glass bottles at 4 °C in the dark before solvent extraction (within 48 h). All glassware was washed in 1 M HCl, rinsed with ultrapure water and heated to 500 °C for 4 h.

2.3. EEM fluorescence measurements

Fluorescence measurements were performed with a Hitachi F-7000 spectrofluorometer. The correction of spectra for instrumental response was conducted from 200 to 600 nm according to the procedure described in Tedetti et al. (2012). The samples were allowed to reach room temperature in the dark before transferring into a far UV silica quartz cuvette with a 1 cm pathlength (170–2600 nm; LEADER LAB®). The temperature was maintained at 20 °C in the cell holder with an external circulating water bath. The EEMs were collected over Ex wavelength (λ_{Ex}) of between 200 and 500 nm with a 5 nm step, and over Em wavelength (λ_{Em}) of between 280 and 550 nm with a 2 nm step. Ex and Em slit widths of 5 nm were used with a scan speed of 1200 nm min^{-1}, a time response of 0.5 s and a PMT voltage of 700 V. Blanks (ultrapure water) and quinine sulphate dihydrate solutions of between 0.5 and 50 μg L^{-1} (Fluka, purum for fluorescence) in 0.05 M H_2SO_4 were regularly measured during sample measurements. To account for inner filtering effects, absorbance measurements were performed with a Shimadzu UV–Vis 2450 spectrophotometer from 200 to 600 nm in a quartz cuvette with a 1 cm pathlength.

Each EEM was corrected for inner filtering effects by multiplying it by a correction matrix, which was calculated for each wavelength pair from the sample absorbance by assuming Ex and EM pathlengths of 0.5 cm in a 1 cm cuvette (Ohno, 2002). Next, the mean of the eleven ultrapure water EEMs was subtracted from each sample EEM. Finally, the fluorescence data were converted into quinine sulphate unit (QSU). One QSU corresponding to the fluorescence of 1 μg L^{-1} of quinine sulphate in 0.05 M H_2SO_4 at a $\lambda_{Ex}/\lambda_{Em}$ of 350/450 nm (5 nm slit widths). The conversion to QSU was made by dividing the blank-corrected EEM fluorescence data by the mean slope of the quinine linear regressions ($r^2 = 1.00$, $n = 8$), i.e., 13 arbitrary fluorescence intensity units/QSU.

2.4. PARAFAC analysis

For standard solutions, PAH and pesticide datasets were processed separately. For both contaminant types, PARAFAC was conducted first on the contaminant mixtures with and without humic substances (P^{M}_{PAHs} and $P^{M}_{pesticides}$). Next, PARAFAC was performed on the contaminant mixtures with and without humic substances and with individual contaminant solutions (P^{T}_{PAHs} and $P^{T}_{pesticides}$). These two types of datasets will provide information regarding whether the PARAFAC process is enhanced in the presence of individual EEMs. The EEM wavelength ranges that were used were 200–500 and 280–550 nm for Ex and Em, respectively. The EEMs were merged into a three-dimensional data array with the following formula: number of samples × 60 λ_{Ex} × 133 λ_{Em}. For the PAHs, the number of samples used for the PARAFAC analyses of the mixtures (P^{M}_{PAHs}) and of the mixtures plus the individual compounds (P^{T}_{PAHs}) was 40 and 121, respectively. For the pesticides, the number of samples for $P^{M}_{pesticides}$ and $P^{T}_{pesticides}$ was 40 and 67, respectively. For marine waters, 30 samples were used for PARAFAC.

PARAFAC was operated by the DOMFluor toolbox v1.6. in MATLAB® 7.10.0 (R2010a). The number of components tested ranged from 2 to 12 for standard solutions and from 2 to 6 for natural samples. For the PAH dataset, no outliers were detected. However, for the pesticide dataset, three outliers were found. These outliers corresponded to samples that contained each individual pesticide at 20 μg L^{-1}. These outliers were removed from the dataset to reduce the $P^{T}_{pesticides}$ to $P^{T*}_{pesticides}$ with 64 EEMs. The validation of the PARAFAC model (running with the non-negativity constraint) and the determination of the correct number of components were achieved through the examination of (1) the percentage of explained variance, (2) the shape of residuals, (3) the split half analysis and (4) the random initialization using the Tucker Congruence Coefficients (Stedmon and Bro, 2008).

2.5. PAH extraction and GC–MS analysis

Dissolved PAHs present in the fraction <0.7 μm were extracted from marine water using solid phase extraction (SPE) on C_{18} cartridges (Envi-18, 6 mL glass tube, 500 mg of packing, Supelco). Cartridges were conditioned with 10 mL of CH_2Cl_2, followed by 10 mL of 2-propanol and 10 mL of water-2-propanol (9:1, v/v). Then the samples were sucked through the cartridges. PAHs were eluted with 2 × 10 mL of CH_2Cl_2. Organic phases were combined and evaporated on a rotary evaporator. Deuterated standard mixtures (Naph-d_8, Phe-d_{10} and Per-d_{12}) were introduced prior to extraction, as well as a supplementary deuterated standard before injection, and used as surrogates to assess the recoveries of analytical procedures and to perform quantitation accuracy. PAHs were concentrated under a gentle stream of nitrogen and analysed by gas chromatograph-mass spectrometer (GC–MS) (TraceISQ, ThermoElectron) operating at an ionization energy of 70 eV for a m/z range of 50–600, using hydrogen as carrier gas at a flow rate of 1.2 mL min^{-1}. Compounds were identified by reference to the analysis of a standard mixture (47543-U, Supelco, USA). All concentration values were blank and recovery corrected (Guigue et al., 2011, 2014).

3. Results and discussion

3.1. Fluorescence signatures of the individual PAHs and pesticides

Table 1 shows the spectral position ($\lambda_{Ex}/\lambda_{Em}$) and the Stokes shift ($\lambda_{Em}-\lambda_{Ex}$) of the fluorescence maxima of the individual PAHs and pesticides in ultrapure water that were obtained from EEMs and peak picking technique. The linear regression parameters between the contaminant concentration and fluorescence peak intensity are also presented: slope, y intercept, coefficient of determination (r^2), and detection and quantification limits (DL and QL). The PAHs with the lowest λ_{Ex} were Naph and DNaph ($\lambda_{Ex}/\lambda_{Em}$: ~220/334 nm), while the PAH with the highest λ_{Ex} was Pyr ($\lambda_{Ex}/\lambda_{Em}$: 335/392 nm). Among PAHs, Flu and DFlu had the lowest λ_{Em} ($\lambda_{Ex}/\lambda_{Em}$: 260/310 nm) and BaA had the highest λ_{Em} ($\lambda_{Ex}/\lambda_{Em}$: 285/410 nm). Among pesticides, Car was the more blue-shifted ($\lambda_{Ex}/\lambda_{Em}$: 220/334 nm). In contrast, Pho and Thi had peaks at longer wavelengths (λ_{Ex}: 240–295 nm, λ_{Em}: 352–414 nm). The number of fluorescence maxima ranged from 1 (Flu, DFlu, Phe) to 8 (Pyr) whereas the other compounds exhibited two fluorescence peaks (Table 1). The positions of the fluorescence maxima of the parent and alkylated PAHs (Naph and DNaph, and Flu and DFlu) were analogous. However, the fluorescence maxima of the parent and phenylated PAHs (Ant and BaA, and Pyr and BeP) had different spectral positions and peak numbers. Phe and Ant, which are

Table 1
Spectral position ($\lambda_{Ex}/\lambda_{Em}$) and Stokes shift ($\lambda_{Em}-\lambda_{Ex}$) of the fluorescence maxima of the individual PAHs and pesticides in ultrapure water that were obtained from the EEM measurements and peak picking technique. The linear regression parameters between the contaminant concentration (0.1–20 μg L^{-1}) and fluorescence peak intensity (QSU) are presented: slope, *y*-intercept, determination coefficient (r^2), detection limit (DL) and quantification limit (QL). The results from previous studies are included for comparison.

PAHs and pesticides	This work							Previous studies			
	$\lambda_{Ex}/\lambda_{Em}$ (nm)	Stokes shift (nm)	Slope (QSU L μg^{-1})	*y*-intercept (μg L^{-1})	r^2	DL (μg L^{-1})	QL (μg L^{-1})	$\lambda_{Ex}/\lambda_{Em}$ (nm)	Stokes shift (nm)	Solvent	Reference
Naph	220/334	114	4.0 ± 0.1	2.4 ± 0.5	0.98	1.29	4.30	220/335	115	Water	Tedetti et al. (2010)
								225/330	105	Water	Beltrán et al. (1998)
	275/334	59	1.6 ± 0.0	0.9 ± 0.1	0.98	1.23	4.10	270/330	60	Water	Beltrán et al. (1998)
								270/335	65	Water	Tedetti et al. (2010)
								280/345	65	Water	Jiji et al. (2000)
								–/327, 337	–	Cyclohexane	Karcher et al. (1985)
DNaph	225/336	111	9.8 ± 0.2	3.3 ± 1.6	1.00	0.50	1.68				
	275/336	61	1.9 ± 0.0	0.8 ± 0.3	1.00	0.49	1.63				
Flu	260/310	50	26.5 ± 0.2	1.5 ± 1.8	1.00	0.20	0.68	260/310	50	Water	Beltrán et al. (1998)
								270/305	35	Water	Jiji et al. (2000)
								290/305	15	Water	Jiji et al. (2000)
								–/306, 315	–	Cyclohexane	Karcher et al. (1985)
DFlu	260/310	50	4.0 ± 0.1	0.4 ± 0.6	1.00	0.41	1.38				
Phe	250/366	116	11.5 ± 0.1	1.3 ± 0.6	1.00	0.16	0.52	245/360	115	Water	Tedetti et al. (2010)
								250/360	110	Water	Beltrán et al. (1998)
								270/355	85	Water	Jiji et al. (2000)
								–/346.5, 356, 364, 374	–	Cyclohexane	Karcher et al. (1985)
Ant	245/382	137	25.2 ± 0.5	−3.5 ± 4.0	1.00	0.53	1.75	245/380	135	Water	Beltrán et al. (1998)
	245/402	157	27.1 ± 0.5	−6.3 ± 4.2	1.00	0.54	1.79	245/405	60	Water	Beltrán et al. (1998)
								–/378, 399, 423, 449	–	Cyclohexane	Karcher et al. (1985)
Pyr	240/374	134	22.7 ± 0.6	8.7 ± 4.7	1.00	0.62	2.06	240/375	135	Water	Beltrán et al. (1998)
	240/392	152	22.0 ± 0.5	7.2 ± 4.0	1.00	0.54	1.80	240/395	155	Water	Beltrán et al. (1998)
	270/374	104	16.9 ± 0.4	4.7 ± 2.8	1.00	0.50	1.67	275/375	100	Water	Beltrán et al. (1998)
	270/392	122	16.2 ± 0.4	4.6 ± 2.6	1.00	0.51	1.69	275/395	120	Water	Beltrán et al. (1998)
	320/374	54	9.5 ± 0.2	2.6 ± 1.5	1.00	0.47	1.57	320/375	55	Water	Beltrán et al. (1998)
	320/392	72	9.3 ± 0.2	2.4 ± 1.4	1.00	0.46	1.54	320/395	75	Water	Beltrán et al. (1998)
	335/374	39	12.3 ± 0.3	3.2 ± 2.0	1.00	0.48	1.60	332/372	40	Ethanol	Kalyanasundaram and Thomas (1977)
	335/392	57	12.1 ± 0.2	3.2 ± 1.9	1.00	0.47	1.56	332/390	58	Ethanol	Kalyanasundaram and Thomas (1977)
								–/371.5, 378, 383, 387.5, 392, 404	–	Cyclohexane	Karcher et al. (1985)
BaA	275/390	115	14.1 ± 0.0	0.3 ± 0.2	1.00	0.06	0.19	275/390	115	Water	Beltrán et al. (1998)
	275/410	135	12.1 ± 0.0	0.2 ± 0.2	1.00	0.06	0.21	275/410	135	Water	Beltrán et al. (1998)
	285/390	105	15.8 ± 0.0	0.3 ± 0.3	1.00	0.06	0.20	290/390	100	Water	Beltrán et al. (1998)
	285/410	125	13.4 ± 0.1	0.4 ± 0.8	1.00	0.07	0.23	290/410	120	Water	Beltrán et al. (1998)
								–/387, 407.5, 433.5, 460	–	Cyclohexane	Karcher et al. (1985)
BeP	275/398	123	3.3 ± 0.0	−0.02 ± 0.01	1.00	0.02	0.07	–/388, 397.5, 409.5, 420, 433	–	Cyclohexane	Karcher et al. (1985)
	285/398	113	3.4 ± 0.0	−0.08 ± 0.02	1.00	0.04	0.14				
Pho	245/414	169	2.5 ± 0.0	1.1 ± 0.3	1.00	0.31	1.04	243/350	107	Ethanol	García Reyes et al. (2004)
	280/414	134	1.1 ± 0.0	0.3 ± 0.1	1.00	0.15	0.50	267/350	83	Ethanol	García Reyes et al. (2004)
Car	220/334	114	4.2 ± 0.0	0.6 ± 0.1	1.00	0.10	0.35	279/330	59	Methanol	Jiji et al. (1999)
	275/334	59	2.1 ± 0.0	−0.2 ± 0.2	0.99	0.36	1.20	270/320	50	Methanol	Fang et al. (1998)
								282/335	53	Methanol	García Reyes et al. (2004)
								295/335	40	Methanol	Jia et al. (2007)

(*continued on next page*)

Table 1 (*continued*)

PAHs and pesticides	This work							Previous studies			
	$\lambda_{Ex}/\lambda_{Em}$ (nm)	Stokes shift (nm)	Slope (QSU L μg^{-1})	*y*-intercept ($\mu g\ L^{-1}$)	r^2	DL ($\mu g\ L^{-1}$)	QL ($\mu g\ L^{-1}$)	$\lambda_{Ex}/\lambda_{Em}$ (nm)	Stokes shift (nm)	Solvent	Reference
Thi	240/352	112	0.7 ± 0.0	0.8 ± 0.2	0.99	0.66	2.21	250/360	110	Ethanol	García Reyes et al. (2004)
	295/354	59	1.4 ± 0.0	0.2 ± 0.3	0.99	0.71	2.37	300/340	40	Methanol	Rodríguez-Cuesta et al. (2003)
								301/360	59	Ethanol	García Reyes et al. (2004)

DL and QL of contaminants were calculated from the slope (a) and the standard deviation of the *y*-intercept (σ) of the equation of the linear regression between the contaminant concentration and the fluorescence peak intensity as following: $DL = \frac{3\sigma}{a}$ and $QL = \frac{10\sigma}{a}$.

σ was calculated according to the formula $\sigma = \sqrt{\frac{\sum(y_i - y')^2}{n-2}} \times \sqrt{\frac{\sum x_i^2}{n\sum(x_i - \bar{x})^2}}$ where n is the number of samples, x_i and y_i are the contaminant concentrations and the measured fluorescence intensities, respectively, y'_i are the fluorescence intensities calculated from the linear regression equation, and $\bar{x}$ is the mean contaminant concentration.

isomers, had similar λ_{Ex} values but different λ_{Em} values (the λ_{Em} of Ant was red-shifted). BeP and BaA had similar fluorescence maxima. Car, which is a naphthalene-derived chemical, had a fluorescence maximum that was similar to those of Naph and DNaph. The Stokes shift varied from 39 (Pyr) to 169 nm (Pho) (Table 1).

For each fluorescence maximum, a significant positive linear relationship was observed between the compound concentration and the fluorescence intensity over the range of 0.1–20 $\mu g\ L^{-1}$ ($r^2 = 0.98–1.00$, $n = 9$, $p < 0.01$) (Table 1). The DL of the PAHs was between 0.02 (BeP at $\lambda_{Ex}/\lambda_{Em}$: 275/398 nm) and 1.29 $\mu g\ L^{-1}$ (Naph at $\lambda_{Ex}/\lambda_{Em}$: 225/334 nm). The QL value was between 0.07 and 4.30 $\mu g\ L^{-1}$ for the same PAHs. Regarding pesticides, the DL was between 0.10 (Car at $\lambda_{Ex}/\lambda_{Em}$: 220/334 nm) and 0.71 $\mu g\ L^{-1}$ (Thi at $\lambda_{Ex}/\lambda_{Em}$: 240/352 nm), with corresponding QL values of 0.35 and 2.37 $\mu g\ L^{-1}$ (Table 1). The studied contaminants displayed a diversity of fluorescence signatures regarding spectral position, number of peaks, Stokes shift and the DL/QL. However, similarities were found between the parent and alkylated PAHs and between some of the PAHs and pesticides (Naph and Car) (Table 1).

The fluorescence signature of a given fluorophore is largely influenced by its conjugated π-electron system. When the number of conjugated π-electrons increases within a fluorophore, its intrinsic fluorescence capacity tends to expand through an increase in both its molar absorption coefficient (ε) and fluorescence quantum yield (Φ). In addition, an increasing number of conjugated π-electrons causes a red-shift in the absorbance wavelength as the energy decreases between the ground and excited states (Valeur, 2001). Here, we observed a significant positive linear relationship between the number of conjugated π-electrons and the λ_{Em} ($r^2 = 0.47$, $n = 29$, $p < 0.01$). Interestingly, when excluding alkylated PAHs and pesticides (i.e., the compounds that present heteroatoms, methyl, phenolic hydroxyl or carbamic acid functions), the linear correlations between the number of conjugated π-electrons and the DL, and between the number of conjugated π-electrons and λ_{Em} reached $r^2 = 0.73$ and $r^2 = 0.65$ ($n = 20$, $p < 0.01$), respectively. This result emphasises the major role of conjugated π-electron systems in controlling the magnitude and spectral domain of fluorescence for contaminants composed of only aromatic rings, such as the parent PAHs.

As mentioned above, parent and alkylated PAHs had the same fluorescence maxima positions. Nevertheless, their slopes, DL and QL were significantly different (Table 1). The number of conjugated π-electrons of these compounds (which remained unchanged) did not explain the discrepancies in fluorescence intensity. Indeed, besides the conjugated π-electron system, other parameters potentially modify Φ, including the introduction of methyl groups into the aromatic structure (Nijegorodov et al., 2003). For naphthalene, the addition of methyl groups increased its sensitivity (DL of DNaph < DL of Naph; Table 1) because the molecule symmetry was diminished and the fluorescence rate constant increased (Nijegorodov et al., 2009). In contrast, the addition of methyl groups to fluorene reduced the Φ (DL of DFLu > DL of Flu; Table 1) by increasing the intersystem crossing rate constant and by decreasing the fluorescence rate constant. These changes were attributed to the stability of the molecular symmetry (Nijegorodov et al., 2009).

The fluorescence maxima of the PAHs and pesticides found in this study were very similar to those reported in previous studies that used ultrapure water as a solvent, with differences in λ_{Ex} and $\lambda_{Em} \leqslant 5$ nm (Beltrán et al., 1998; Fang et al., 1998; Tedetti et al., 2010). Nevertheless, when the fluorescence spectra of the contaminants were measured in methanol, ethanol or hexane, blue shifts in λ_{Em} and red shifts in λ_{Ex} and λ_{Em} occurred (Table 1). Indeed, solvent polarity is known to modify the fluorescence maxima. When the solvent polarity decreased, blue shifts are observed in λ_{Em} and Φ increased due to changes in the non-radiative decay rate

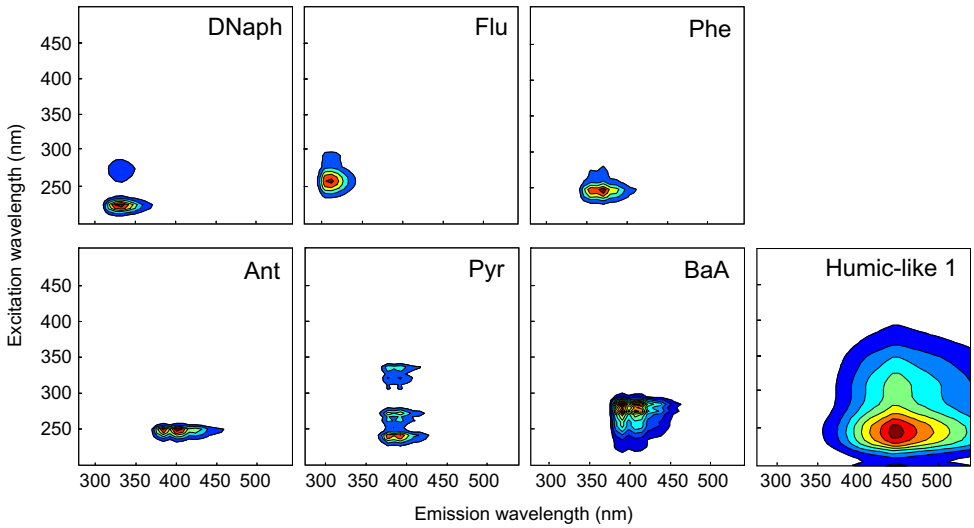

Fig. 1. Contour plots of the seven components that were validated by the PARAFAC model applied to PAH mixtures with and without humic substances plus the individual PAHs in ultrapure water (P^{T}_{PAHs}, 121 samples).

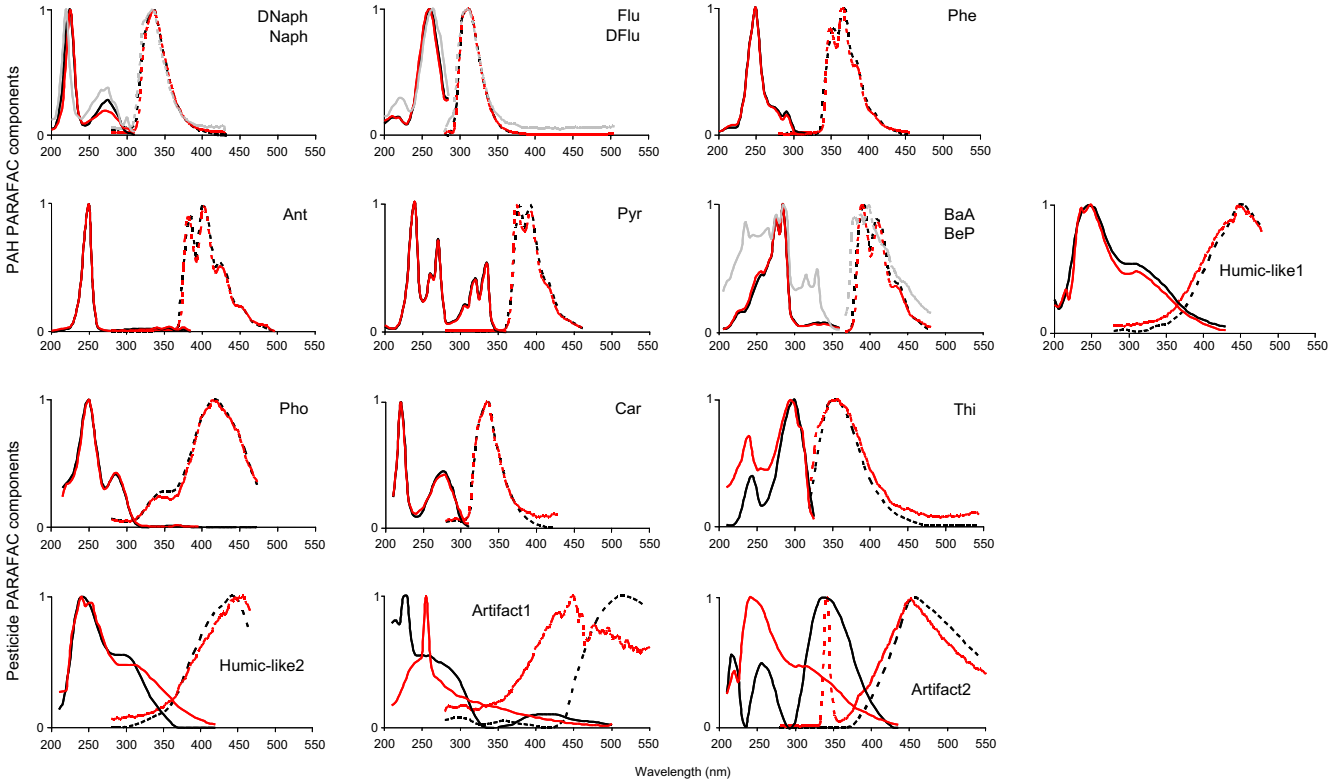

Fig. 2. Comparison between the excitation (solid line) and emission (dotted line) spectra of the PAH-, pesticide- and humic-like components that were validated by the PARAFAC models (in black) and of the individual compounds that were obtained from the EEM measurements (in red) at PAH and pesticide concentrations of 5 μg L^{-1} and at humic substance concentration of 1 mg C L^{-1}. The individual spectra of Naph, DFlu and BeP were also added (in grey). All spectra were normalised to their maximal intensities. (For interpretation of the references to colour in this figure legend, the reader is referred to the web version of this article.)

or in the conformational structure of the fluorophore (Valeur, 2001).

3.2. Discrimination of fluorescence signatures in complex mixtures

For each contaminant type, the results obtained from the two PARAFAC models (i.e., P^{M} and P^{T}) were analogous. Thus, only the PARAFAC model results from the mixtures and individual solutions are presented below (i.e., P^{T}_{PAHs} and $P^{T*}_{pesticides}$).

P^{T}_{PAHs} validated a seven-component model, which included one humic-like fluorophore (humic-like 1) and six PAH-like fluorophores (Fig. 1). To identify these fluorophores, the Ex and Em spectra of the components that were modelled by PARAFAC were compared with the Ex and Em spectra of the individual compounds acquired from the EEM measurements (Fig. 2). These comparisons showed that the six PAH-like components that were revealed by PARAFAC included DNaph, Flu, Phe, Ant, Pyr and BaA. On the other hand, Naph, DFlu and BeP did not have the corresponding

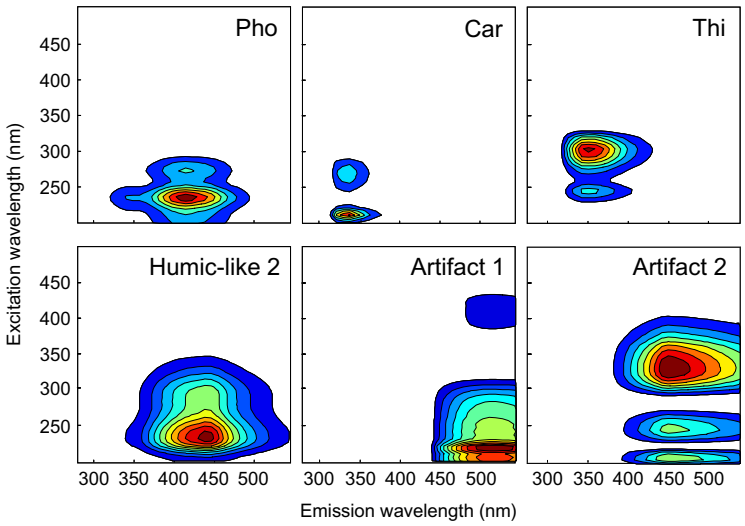

Fig. 3. Contour plots of the six components that were validated by the PARAFAC model applied to the pesticide mixtures with and without humic substances plus individual pesticides in ultrapure water ($P^{T*}_{pesticides}$, 64 samples).

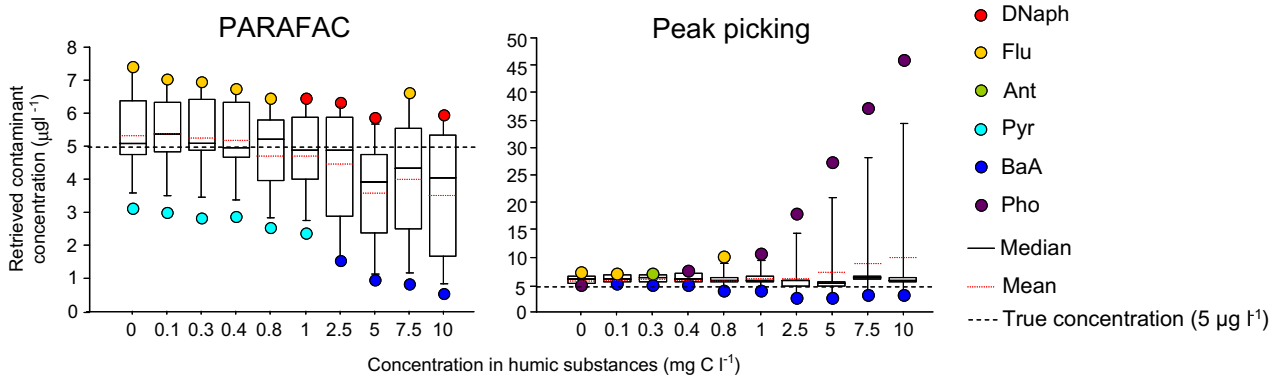

Fig. 4. Box-and-whisker plots of the PAH (DNaph, Flu, Phe, Ant, Pyr, BaA) and pesticide (Pho, Car) concentrations obtained from PARAFAC and peak picking methods, with regard to the humic substance concentrations (from 0 to 10 mg C L^{-1}). These individual contaminant concentrations were retrieved from mixtures containing true contaminant concentrations of 5 µg L^{-1}. The Thi concentrations, which were greater than the other compound concentrations, are not included in this figure.

components identified in the PARAFAC model. Indeed, the EEM spectra of DNaph and Flu fitted the Naph-like and Flu-like components better than the EEM spectra of Naph and DFlu (Fig. 2). Hence, the PARAFAC analysis applied on PAH mixtures was not able to separate the parent and alkylated compounds (i.e., the fluorophores that had the same fluorescence maxima). The compounds that had the highest fluorescence were "selected" by the PARAFAC: DNaph and Flu (Table 1). As previously mentioned, BaA and BeP had similarities in their fluorescence domains. Likewise, the PARAFAC model selected BaA (Figs. 1 and 2), which was more fluorescent than BeP according to the linear regression parameters (Table 1).

$P^{T*}_{pesticides}$ validated a six-component model that included one humic-like fluorophore (humic-like 2), three pesticide-like fluorophores and two fluorophores considered as artifacts (Fig. 3). The three pesticides, Pho, Car and Thi, were identified by comparing the measured EEM spectra with the modelled PARAFAC spectra (Fig. 2). The greatest discrepancies between the measured and modelled spectra were observed for Thi, which presented the lowest fluorescence (Table 1). Fig. 2 also show the good correspondence between the spectra of the two humic-like components ("humic-like 1" for the PAH model and "humic-like 2" for the pesticide model) and the spectra of the pure humic substance solution. By opposition, the spectra of the two artifacts derived from the pesticide model did not fit at all with the spectra of the pure humic substance.

The contaminant concentrations in the mixtures that were determined from peak picking and PARAFAC techniques were compared to the true contaminant concentrations, with regard to the humic substance concentrations (Fig. 4). For peak picking method, the contaminant concentrations in the mixtures were calculated using linear regression parameters between the individual contaminant concentrations (0.1–20 µg L^{-1} for PAHs and pesticides) and their corresponding EEM fluorescence intensities (data reported in Table 1). For PARAFAC method, the contaminant concentrations in the mixtures were calculated using linear regression parameters between the individual contaminant concentrations (0.1–20 µg L^{-1} for PAHs, 0.1–10 µg L^{-1} for pesticides) and their corresponding PARAFAC component intensities (data not shown). Whatever the true contaminant concentration in the mixtures (1, 2, 5 or 10 µg L^{-1}), the trends of retrieved concentrations were similar. Thus, only the results relating to the 5 µg L^{-1} concentration are presented here (Fig. 4). When considering all humic substance concentrations, the mean contaminant concentration that was derived from PARAFAC analysis (4.7 ± 0.7 µg L^{-1}) was much closer to the true contaminant concentration than that derived from peak

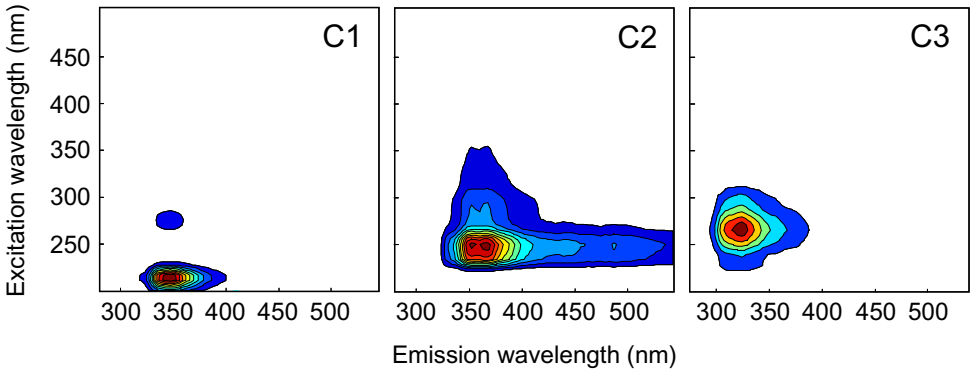

Fig. 5. Contour plots of the three components that were validated by the PARAFAC model applied to 30 marine samples collected in two harbours in the Marseilles Bay (northwestern Mediterranean Sea, France).

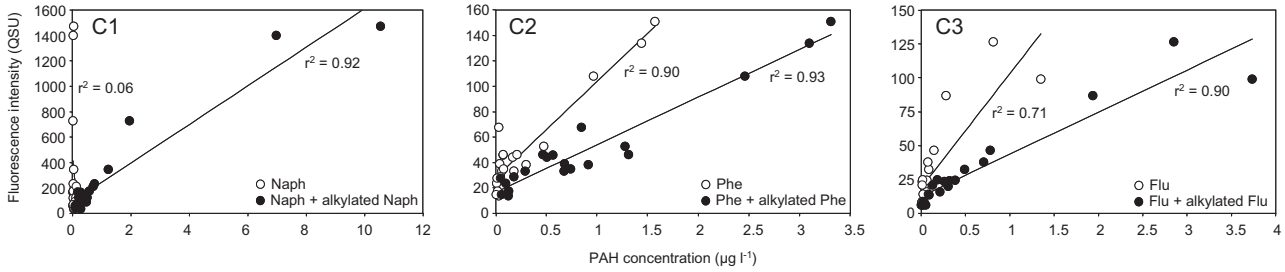

Fig. 6. Comparison between the fluorescence intensities of PARAFAC components and the concentrations of PAHs determined by GC–MS (parent Naph, Phe and Flu in white or sum of parent + alkyltated Naph, Phe and Flu in black) for marine samples collected in two harbours in the Marseilles Bay (northwestern Mediterranean Sea, France).

picking (7.1 ± 1.7 µg L^{-1}). Clearly, concentrations were overestimated with the peak picking method due to overlapping fluorescence signatures. As shown in Fig. 4, this overestimation increased with increasing humic substance concentrations. The Pho concentration was the most overestimated because its fluorescence signature was very close to that of humic substances (Table 1; Fig. 3).

In contrast, the PARAFAC-derived concentrations tended to decrease with increasing humic substance concentration (Fig. 4). Taken into account that samples were corrected for inner filtering effects, this decrease in PARAFAC-derived concentrations may be explained by fluorescence quenching processes induced by the presence of humic substances (Kumke et al., 1994; Fang et al., 1998; Peuravuori, 2001; Lee et al., 2003; Jung et al., 2010). Pyr and BaA, which were always underestimated (Fig. 4), would be particularly sensitive to these quenching processes. Other compounds such as Phe, Ant and Car are also known to be affected by quenching (Kumke et al., 1994; Fang et al., 1998; Peuravuori, 2001; Lee et al., 2003; Jung et al., 2010). On the contrary, regardless of the humic substance concentration, the PARAFAC-derived Flu and DNaph concentrations were always overestimated. PARAFAC was unable to discriminate the fluorescence signatures of the parent and alkylated PAHs. Therefore, the fluorescence intensities of DFlu and Naph were very likely superimposed on those of Flu and DNaph. Consequently, these results show that the EEM/PARAFAC identification and quantification of PAHs and pesticides at the µg L^{-1} level is efficient but, due to organic matter quenching processes, its efficiency is limited to aquatic systems containing humic substance amount not exceeding 2.5 mg C L^{-1} (Fig. 4).

3.3. Application to marine samples

Three components were validated by the PARAFAC model applied to 30 marine samples collected in two harbours in the Marseilles Bay (northwestern Mediterranean Sea, France) (Fig. 5). We found that the fluorescence maxima of C1 ($\lambda_{Ex}/\lambda_{Em}$: 225, 285/340 nm), C2 ($\lambda_{Ex}/\lambda_{Em}$: 250/356, 372 nm) and C3 ($\lambda_{Ex}/\lambda_{Em}$: 265/324 nm) were very close to fluorescence maxima of Naph, Phe and Flu or of their alkylated compounds, respectively (Table 1; Fig. 1). Interestingly, these components were very similar to the three oil-related components ascertained by Zhou et al. (2013) in the water column of the Gulf of Mexico during the Deepwater Horizon oil spill: C1 ($\lambda_{Ex}/\lambda_{Em}$: 226/340 nm), C2 ($\lambda_{Ex}/\lambda_{Em}$: 236/360 nm) and C6 ($\lambda_{Ex}/\lambda_{Em}$: 252/311 nm). These components would be derived from crude and weathered oil (Zhou et al., 2013). The concentration in dissolved organic carbon of our marine samples ranged from 0.85 to 2.3 mg C L^{-1}. Thus, their organic carbon content was not high enough to induce significant fluorescence quenching effects.

On the same marine samples, individual parent and alkylated (methyl, dimethyl and trimethyl) PAH concentrations were determined by chromatographic analysis (GC–MS). Total (parent + alkylated) PAH concentrations ranged from 0.2 to 18 µg L^{-1}. Major (parent + alkylated) compounds were Phe, comprising 20–60% of total PAHs, followed by Naph (12–54% of total PAHs) and Flu (6–29% of total PAHs). The fluorescence intensities of PARAFAC components C1, C2 and C3 were thus compared to the concentrations of parent Naph, Phe and Flu and to the concentrations of parent + alkylated Naph, Phe and Flu (Fig. 6). We observed that the fluorescence intensities were much better correlated to parent + alkylated concentrations (r^2 = 0.92, 0.93, 0.90 for respectively Naph, Phe and Flu) than to parent concentrations (r^2 = 0.06, 0.90, 0.71 for respectively Naph, Phe and Flu). The good correlations between these two techniques implied that the EEM/PARAFAC method could substitute chromatographic analysis for predominant PAHs in highly contaminated aquatic environments. Our study confirms the importance of alkylated (methyl, dimethyl and trimethyl) compounds in the pool of dissolved PAHs (Guigue et al., 2011, 2014) and highlights their strong contribution to the PAH fluorescence signal in marine coastal waters.

4. Conclusion

In this study, we combined the EEM and PARAFAC methods to discriminate and quantify PAHs (DNaph, Flu, Phe, Ant, Pyr, BaA) and pesticides (Pho, Car) at the $\mu g\ L^{-1}$ level in the presence of humic substances (at relevant freshwater concentrations). We underlined the quenching effect on PAHs and pesticides for humic substance concentrations exceeding 2.5 mg C L^{-1}. The application of this method to natural (marine) samples was demonstrated through the highlight of fluorescence signatures of PAH and the good linear correlations between spectrofluorimetry and GC–MS results. The PAH fluorescence signal in marine coastal waters was mainly due to alkylated compounds. Although this combined fluorescence spectroscopy/multi-way analysis method cannot replace standard chromatographic techniques to measure organic contamination at trace levels ($ng\ L^{-1}$), it may be useful as low cost, efficient screening method to monitor PAH and pesticide concentrations in the $\mu g\ L^{-1}$ range in chronically or sporadically contaminated natural waters.

Acknowledgements

We acknowledge D. Lefèvre and A. Robert for the use of the Shimadzu spectrophotometer. We thank B. Charrière for DOC analyses. We are grateful to two anonymous reviewers for their helpful comments and suggestions. This study is part of the "IBISCUS" research project that was funded by the Agence Nationale de la Recherche (ANR) – ECOTECH program (project ANR-09-ECOT-009-01). This work also contributes to Work Package 3 (Action C3A) of the CNRS-INSU MISTRALS "MERMEX" project.

References

Akkanen, J., Tuikka, A., Kukkonen, J.V.K., 2012. On the borderline of dissolved and particulate organic matter: partitioning and bioavailability of polycyclic aromatic hydrocarbons. Ecotoxicol. Environ. Saf. 78, 91–98.

Alostaz, M., Biggar, K., Donahue, R., Hall, G., 2008. Petroleum contamination characterization and quantification using fluorescence emission–excitation matrices (EEMs) and parallel factor analysis (PARAFAC). J. Environ. Eng. Sci. 7, 183–197.

Beltrán, J.L., Ferrer, R., Guiteras, J., 1998. Multivariate calibration of polycyclic aromatic hydrocarbon mixtures from excitation–emission fluorescence spectra. Anal. Chim. Acta 373, 311–319.

Blough, N.V., Del Vecchio, R., 2002. Chapter 10 – Chromophoric DOM in the Coastal Environment. In: Hansell, D.A. (Ed.), Biogeochemistry of Marine Dissolved Organic Matter. Academic Press, San Diego, pp. 509–546.

Bocquené, G., Franco, A., 2005. Pesticide contamination of the coastline of Martinique. Mar. Pollut. Bull. 51, 612–619.

Booksh, K.S., Muroski, A.R., Myrick, M.L., 1996. Single-measurement excitation/emission matrix spectrofluorometer for determination of hydrocarbons in ocean water. 2. Calibration and quantitation of naphthalene and styrene. Anal. Chem. 68, 3539–3544.

Christensen, J.H., Hansen, A.B., Mortensen, J., Andersen, O., 2005. Characterization and matching of oil samples using fluorescence spectroscopy and parallel factor analysis. Anal. Chem. 77, 2210–2217.

Dabestani, R., Ivanov, I., 1999. A Compilation of physical, spectroscopic and photophyisical properties of polycyclic aromatic hydrocarbons. Photochem. Photobiol. 70, 10–34.

Dachs, J., Méjanelle, L., 2010. Organic pollutants in coastal waters, sediments, and biota: a relevant driver for ecosystems during the anthropocene? Estuaries Coasts 33, 1–14.

Dumbauld, B.R., Brooksà, K.M., Posey, M.H., Box, P.O., Park, O., 2001. Response of an estuarine benthic community to application of the pesticide carbaryl and cultivation of Pacific Oysters (*Crassostrea gigas*) in Willapa Bay, Washington. Mar. Pollut. Bull. 42, 826–844.

Fang, F., Patterson, H.H., Cronan, C.S., 1998. A spectro fluorimetric study of the binding of carbofuran, carbaryl, and aldicarb with dissolved organic matter. Anal. Chim. Acta 373, 139–151.

García Reyes, J.F., Llorent Martınez, E.J., Ortega Barrales, P., Molina Dıaz, A., 2004. Multiwavelength fluorescence based optosensor for simultaneous determination of fuberidazole, carbaryl and benomyl. Talanta 64, 742–749.

García Reyes, J.F., Llorent Martínez, E.J., Ortega Barrales, P., Molina Díaz, A., 2004. Continuous-flow separation and pre-concentration coupled on-line to solid-surface fluorescence spectroscopy for the simultaneous determination of o-phenylphenol and thiabendazole. Anal. Bioanal. Chem. 378, 429–437.

Gauthier, T.D., Shane, E.C., Guerin, W.F., Seitz, W.R., Grant, C.L., 1986. Fluorescence quenching method for determining equilibrium constants for polycyclic aromatic hydrocarbons binding to dissolved humic materials. Environ. Sci. Technol. 20, 1162–1166.

Guigue, C., Tedetti, M., Giorgi, S., Goutx, M., 2011. Occurrence and distribution of hydrocarbons in the surface microlayer and subsurface water from the urban coastal marine area off Marseilles, Northwestern Mediterranean Sea. Mar. Pollut. Bull. 62, 2741–2752.

Guigue, C., Tedetti, M., Ferretto, N., Garcia, N., Méjanelle, L., Goutx, M., 2014. Spatial and seasonal variabilities of dissolved hydrocarbons in surface waters from the Northwestern Mediterranean Sea: results from one year intensive sampling. Sci. Total Environ. 466–467, 650–662.

Jia, G., Li, L., Qiu, J., Wang, X., Zhu, W., Sun, Y., Zhou, Z., 2007. Determination of carbaryl and its metabolite 1-naphthol in water samples by fluorescence spectrophotometer after anionic surfactant micelle-mediated extraction with sodium dodecylsulfate. Spectrochim. Acta 67, 460–464.

JiJi, R.D., Booksh, K.S., 2000. Mitigation of Rayleigh and Raman Spectral interferences in multiway calibration of excitation–emission matrix fluorescence spectra. Anal. Chem. 72, 718–725.

Jiji, R.D., Cooper, G.A., Booksh, K.S., 1999. Excitation–emission matrix fluorescence based determination of carbamate pesticides and polycyclic aromatic hydrocarbons. Anal. Chim. Acta 397, 61–72.

Jiji, D., Andersson, G.G., Booksh, K.S., 2000. Application of PARAFAC for calibration with excitation–emission matrix fluorescence spectra of three classes of environmental pollutants. J. Chemom., 171–185.

Jung, A.-V., Frochot, C., Villieras, F., Lartiges, B.S., Parant, S., Viriot, M.-L., Bersillon, J.-L., 2010. Interaction of pyrene fluoroprobe with natural and synthetic humic substances: examining the local molecular organization from photophysical and interfacial processes. Chemosphere 80, 228–234.

Kalyanasundaram, K., Thomas, J.K., 1977. Environmental effects on vibronic band intensities in pyrene monomer fluorescence and their application in studies of micellar systems. J. Am. Chem. Soc. 99, 2039–2044.

Karcher, W., Fordham, R.J., Dubois, J.J., Glaude, P.G.J.M., Lightart, J.A., 1985. Spectral atlas of polycyclic aromatic compounds, Environmental Pollution. D. Reidel Publishing Company, Dordrecht/Boston/Lancaster.

Kennish, M.J., 1992. Ecology of Estuaries: Anthropogenic Effects, Marine Science Series. CRC Press.

Kim, Y., Jordan, J.A., Nahorniak, M.L., Booksh, K.S., 2005. Photocatalytic degradation-excitation–emission matrix fluorescence for increasing the selectivity of polycyclic aromatic hydrocarbon analyses photocatalytic degradation–excitation–emission matrix fluorescence for increasing the selectivity of polycyclic. Anal. Chem. 77, 7679–7686.

Kumke, M., Löhmannsröben, H., Roch, T., 1994. Fluorescence quenching of polycyclic aromatic compounds by humic acid. Analyst 1, 997–1001.

Landau-Ossondo, M., Rabia, N., Jos-Pelage, J., Marquet, L.M., Isidore, Y., Saint-Aimé, C., Martin, M., Irigaray, P., Belpomme, D., 2009. Why pesticides could be a common cause of prostate and breast cancers in the French Caribbean Island, Martinique. An overview on key mechanisms of pesticide-induced cancer. Biomed. Pharmacother. 63, 383–395.

Lee, C.-L., Kuo, L.-J., Wang, H.-L., Hsieh, P.-C., 2003. Effects of ionic strength on the binding of phenanthrene and pyrene to humic substances: three-stage variation model. Water Res. 37, 4250–4258.

Lepom, P., Brown, B., Hanke, G., Loos, R., Quevauviller, P., Wollgast, J., 2009. Needs for reliable analytical methods for monitoring chemical pollutants in surface water under the European Water Framework Directive. J. Chromatogr. A 1216, 302–315.

McKinlay, R., Plant, J.A., Bell, J.N.B., Voulvoulis, N., 2008. Endocrine disrupting pesticides: implications for risk assessment. Environ. Int. 34, 168–183.

Muroski, A.R., Booksh, K.S., Myrick, M.L., 1996. Single-measurement excitation/emission matrix spectrofluorometer for determination of hydrocarbons in ocean water. 1. Instrumentation and background correction. Anal. Chem. 68, 3534–3538.

Nahorniak, M.L., Booksh, K.S., 2006. Excitation–emission matrix fluorescence spectroscopy in conjunction with multiway analysis for PAH detection in complex matrices. Analyst 131, 1308–1315.

Nijegorodov, N., Mabbs, R., Winkoun, D.P., 2003. Influence of weak and strong donor groups on the fluorescence parameters and the intersystem crossing rate constant. Spectrochim. Acta Part A Mol. Biomol. Spectrosc. 59, 595–606.

Nijegorodov, N., Vasilenko, V., Monowe, P., Masale, M., 2009. Systematic investigation of the influence of methyl groups upon fluorescence parameters and the intersystem crossing rate constant of aromatic molecules. Spectrochim. Acta. A. Mol. Biomol. Spectrosc. 74, 188–194.

Ohno, T., 2002. Fluorescence inner-filtering correction for determining the humification index of dissolved organic matter. Environ. Sci. Technol. 36, 742–746.

Peng, X., Yu, Y., Tang, C., Tan, J., Huang, Q., Wang, Z., 2008. Occurrence of steroid estrogens, endocrine-disrupting phenols, and acid pharmaceutical residues in urban riverine water of the Pearl River Delta, South China. Sci. Total Environ. 397, 158–166.

Peuravuori, J., 2001. Partition coefficients of pyrene to lake aquatic humic matter determined by fluorescence quenching and solubility enhancement. Anal. Chim. Acta 429, 65–73.

Rodríguez-Cuesta, M., Boqué, R., Rius, F., Picón Zamora, D., Martınez Galera, M., Garrido Frenich, A., 2003. Determination of carbendazim, fuberidazole and thiabendazole by three-dimensional excitation–emission matrix fluorescence and parallel factor analysis. Anal. Chim. Acta 491, 47–56.

Roose, P., Brinkman, U.A.T., 2005. Monitoring organic microcontaminants in the marine environment: principles, programmes and progress. Trends Anal. Chem. 24, 897–926.
Stedmon, C.A., Bro, R., 2008. Characterizing dissolved organic matter fluorescence with parallel factor analysis: a tutorial. Limnol. Oceanogr. Methods 6, 572–579.
Tedetti, M., Guigue, C., Goutx, M., 2010. Utilization of a submersible UV fluorometer for monitoring anthropogenic inputs in the Mediterranean coastal waters. Mar. Pollut. Bull. 60, 350–362.
Tedetti, M., Longhitano, R., Garcia, N., Guigue, C., Ferretto, N., Goutx, M., 2012. Fluorescence properties of dissolved organic matter in coastal Mediterranean waters influenced by a municipal sewage effluent (Bay of Marseilles, France). Environ. Chem. 9, 438–449.
Valeur, B., 2001. Molecular Fluorescence: Principles and Applications. Wiley-VCH Verlag GmbH, Weinheim.
Wurl, O., Obbard, J.P., 2004. A review of pollutants in the sea-surface microlayer (SML): a unique habitat for marine organisms. Mar. Pollut. Bull. 48, 1016–1030.
Zhou, Z., Guo, L., Shiller, A.M., Lohrenz, S.E., Asper, V.L., Osburn, C.L., 2013. Charachterization of oil components from the Deepwater Horizon oil spill in the Gulf of Mexico using fluorescence EEM and PARAFAC techniques. Mar. Chem. 148, 10–21.

Science of the Total Environment 466-467 (2014) 650–662

Contents lists available at SciVerse ScienceDirect

Science of the Total Environment

journal homepage: www.elsevier.com/locate/scitotenv

Spatial and seasonal variabilities of dissolved hydrocarbons in surface waters from the Northwestern Mediterranean Sea: Results from one year intensive sampling

Catherine Guigue [a,*], Marc Tedetti [a], Nicolas Ferretto [a], Nicole Garcia [a], Laurence Méjanelle [b], Madeleine Goutx [a]

[a] Aix-Marseille University, Mediterranean Institute of Oceanography (MIO), 13288 Marseille, Cedex 9, France; Université du Sud Toulon-Var, 83957 La Garde Cedex, France; CNRS-INSU/IRD UM 110
[b] CNRS-University Paris 6, UMR 8222, Laboratoire d'ECObiogéochimie Benthique (LECOB), Observatoire Océanologique, F-66650 Banyuls/mer, France

HIGHLIGHTS

- Spatio-temporal distribution of dissolved hydrocarbons in the NW Mediterranean Sea
- Sources, transport and removing processes affecting AHs and PAHs are uncoupled.
- Anthropogenic signatures (both petrogenic and pyrogenic) increased in winter.
- Dissolved hydrocarbons originated mainly from the Rhône River and the atmosphere.

ARTICLE INFO

Article history:
Received 5 June 2013
Received in revised form 24 July 2013
Accepted 24 July 2013
Available online xxxx

Editor: D. Barcelo

Keywords:
Aliphatic hydrocarbons
Polycyclic aromatic hydrocarbons
Dissolved contaminants
Northwestern Mediterranean sea
Marseilles coastal area
Rhône River

ABSTRACT

Dissolved aliphatic hydrocarbons (AHs) and polycyclic aromatic hydrocarbons (PAHs) were analysed from surface water collected in continental, harbour and off-shore marine sites from Marseilles coastal area (Northwestern Mediterranean Sea) from February 2011 to February 2012. AH and PAH concentrations were in the range of 0.04–0.53 μg l^{-1} and 8.1–405 ng l^{-1}, respectively. They both displayed seasonal and spatial variations in their concentrations and molecular composition. The lowest AH concentrations were found in summer and the highest PAH concentrations in winter. Both natural and anthropogenic (pyrogenic and petrogenic) hydrocarbon sources were identified. In winter, concentrations and composition patterns highlighted an increase in the signature of unburned and combusted fossil fuels, while they suggested an enhancement of weathering processes in summer months. Hydrocarbon inputs to the dissolved phase seemed to originate mainly from the atmosphere and the Rhône River. Hydrocarbon additional sources were identified only at the harbour site, emphasising the intense shipping traffic and industrial activities occurring in one of the most important Mediterranean harbours. This study underscores the strong dynamics of dissolved hydrocarbons and the uncoupling of the sources, transport and removing processes affecting AHs and PAHs. It also demonstrates the pertinence of taking this dynamics into account for the budget assessments of organic pollutants in coastal environments.

1. Introduction

Hydrocarbons, including aliphatic hydrocarbons (AHs) and polycyclic aromatic hydrocarbons (PAHs), are among the most widespread organic contaminants found in the marine environment. Some of them are harmful to living organisms with reprotoxic, carcinogenic and mutagenic effects (Kennish, 1992; Scarlett et al., 2007). Hydrocarbons are introduced in the coastal marine waters mainly through atmospheric exchanges/depositions, rivers, municipal/industrial effluents and surface runoffs (Tolosa et al., 1996; Lipiatou et al., 1997; Castro-Jiménez et al., 2012). AHs and PAHs may be both of biogenic or anthropogenic origin, although PAHs are almost exclusively considered of anthropogenic origin, especially in highly urbanised and industrialised areas. Moreover, PAHs are sensitive indicators of petrogenic (uncombusted petroleum) and pyrogenic (incomplete combustion of fossil fuels) sources (see reviews by Wang et al., 1999; Wurl and Obbard, 2004). The uncoupling of the sources, transport and removing processes affecting these two hydrocarbon classes has already been evoked (Bouloubassi and Saliot, 1993; Wakeham, 1996). Thus, the simultaneous analysis of AHs and PAHs constitutes a powerful and indispensable approach for the comprehensive assessment of various inputs as well as for the

* Corresponding author at: Aix-Marseille University, Mediterranean Institute of Oceanography (MIO), 13288 Marseille, Cedex 9, France. Tel.: +33 4 91 82 90 62; fax: +33 4 91 82 90 51.
E-mail address: catherine.guigue@univ-amu.fr (C. Guigue).

0048-9697/$ – see front matter © 2013 Elsevier B.V. All rights reserved.
http://dx.doi.org/10.1016/j.scitotenv.2013.07.082

determination of their environmental behaviour, especially in estuarine and coastal regions.

Because of their low water solubility, AHs and PAHs are considered to be preferentially associated with particles in the coastal marine waters. This is highlighted by the large number of studies dealing with hydrocarbons in coastal sediments and particles while hydrocarbons in the dissolved phase of the water column have been much less investigated. However, in some systems with a low suspended matter load, the concentrations of PAHs in the dissolved phase were similar or even higher than those recorded in the particulate phase (Bouloubassi and Saliot, 1991; Guigue et al., 2011). In addition, dissolved hydrocarbons in the marine coastal environment are subjected to various transformation processes including evaporation, interactions with dissolved organic matter, bio-degradation and photo-degradation (Jordan and Payne, 1980; Schwarzenbach et al., 1993; Tsapakis et al., 2006). A better knowledge of the distribution and fate of hydrocarbons in the dissolved phase of the water column is essential for a more accurate estimation of their fluxes and budgets within marine ecosystems.

Dissolved hydrocarbons and their degradation products bioconcentrate into organisms by passive diffusion and respiration (Berrojalbiz et al., 2009, 2011). For small organisms at the basis of many marine trophic chains, dissolved hydrocarbons are much more bio-available and therefore more likely to have toxic effects on the biota than hydrocarbons present in particles, which are bioaccumulated through ingestion (Tilseth et al., 1984; Akkanen et al., 2012). Documenting dissolved hydrocarbon concentrations, which are presently scarce in marine waters, is relevant for assessments of toxicological effects within coastal marine ecosystems.

Marseilles (Southern France) is the first Mediterranean harbour for goods traffic and the Marseilles–Fos petrochemical complex is the world's third oil port. Marseilles is also the second most populated city in France, and thus generates important industrial, shipping, nautical and tourism activities. Hence, the Marseilles coastal area (Northwestern Mediterranean Sea) is exposed to numerous sources of contamination such as urban and industrial wastes, petroleum inputs and atmospheric depositions from transports, pyrogenic residues, and industrial and harbour activities. Moreover, the Marseilles coastal area is highly influenced by the Rhône River, which is the most significant source of freshwater in the Mediterranean Sea (Durrieu de Madron et al., 2003; Pairaud et al., 2011). Indeed, the Rhône River is the largest French river in terms of water discharge, and represents a considerable transport pathway for contaminants to the marine environment.

Numerous works have reported on the concentrations of hydrocarbons in waters and sediments from the Northwestern Mediterranean Sea (Benlahcen et al., 1997; Lipiatou et al., 1997; Dachs et al., 1997, 1999; Pérez et al., 2003; Mille et al., 2007; Berrojalbiz et al., 2011). However, little is known about the concentrations of dissolved AHs and PAHs in surface water of the Rhône River (Sicre et al., 2008), the Rhône Delta (Bouloubassi and Saliot, 1991, 1993) and the Bay of Marseilles (Marty and Saliot, 1976; Siron et al., 1987; Guigue et al., 2011). The main objectives of the present work are (i) to assess the spatial and temporal variabilities of dissolved AHs and PAHs in the surface waters of the Marseilles coastal area in term of concentration, molecular composition, origin and fate and (ii) to better understand the influence of the Rhône River on their distribution.

2. Material and methods

2.1. Study sites

Two continental (Arles and Vaccarès) and three marine (Port-de-Bouc, Couronne and Sofcom) sites were studied in the Marseilles coastal area neighbouring according to their different potential levels and sources of contamination (Fig. 1; Table 1). Arles station (AR) is located in the Rhône River, which is 812 km long and has a drainage basin of approximately 97,800 km^2. The Rhône delta has a surface area of ~1750 km^2 and is composed mainly of wetlands, ponds and salt marshes. The central part of the delta, known as the 'Camargue' (~750 km^2), comprises farmlands and salted ponds. The Vaccarès pond (VA, 12 km long, 6500 km^2, <2 m depth) is the largest pond of Camargue. It is the main element of the control system of the Rhône delta waters. VA is thus directly under the influence of the Rhône River. It is also subjected to pesticides and hydrocarbons from agricultural operation and nearby industrial areas such as the Marseilles–Fos petrochemical complex through atmospheric transport.

Port-de-Bouc (PB) is a harbour situated in the Gulf of Fos-sur-mer and surrounded by the Marseilles–Fos petrochemical complex, which includes several chemical, petroleum and steel-work plants. The Gulf of Fos-sur-mer receives some freshwater inputs coming from the Rhône River and the Berre Lagoon (Ulses et al., 2005). In addition, PB is positioned on the route of oil cargo ships going to the Berre Lagoon through the Caronte channel. Couronne (COU) is a nearshore site off PB. COU is located close to the Rhône River plume whose extent depends on Rhône water discharges and wind conditions (Pairaud et al., 2011). Sofcom (SOF), situated in the Bay of Marseilles near the Frioul Islands (~7 km off Marseilles), is a nearshore observation site of the national Service d'Observation en Milieu LITtoral (SOMLIT; http://www.domino.u-bordeaux.fr/somlit_national/). It is located much farther from the Rhône River and was selected as marine reference by comparison to the other anthropogenically impacted sites.

2.2. Sampling strategy

All sites were sampled ca bi-monthly from February 2011 to February 2012 in the morning between 8:00 and 12:00 am (Table 1). Freshwater samples (AR and VP) were taken directly from the edge while marine samples (PB, COU and SOF) were collected from the R/V Antédon II. AR, VA and PB were sampled only at 0.1 m depth (subsurface water, SSW) whereas offshore marine sites (COU and SOF) were sampled at 0.1 and 5 m depths. SSW samples were collected directly in 4 l Nalgene® polycarbonate bottles. The bottles were opened below the water surface to avoid the sampling of the surface microlayer. Five m depth samples were taken by means of a 5 l Niskin bottle equipped with silicon ribbons and Viton o-rings. They were then transferred into Nalgene® bottles. The bottles were washed with 1 M hydrochloric acid (HCl) and ultrapure water (i.e., Milli-Q water from Millipore system, final resistivity: 18.2 MΩ cm^{-1}) before use, rinsed three times with the respective sample before filling and stored in the dark in the cold (4–8 °C).

2.3. Filtration of samples

Back in the laboratory, samples were immediately filtered under a low vacuum (<50 mm Hg) through precombusted (500 °C, 4 h) GF/F (~0.7 μm) glass fibre filters (47 mm diameter, Whatman) using polysulfone filtering systems for hydrocarbons (AHs and PAHs) and all-glassware systems for biogeochemical parameters, i.e., nitrates (NO_3^-), chlorophyll *a* (Chl-*a*) and particulate organic carbon (POC). The hydrocarbons present in the particulate matter, which was retained on the filters, are not presented here. The material that passes through GF/F filters consists in truly dissolved and colloidal matters, which can be each subjected to specific processes (Gustafsson and Gschwend, 1997). However, as it is difficult to separate operationally these two fractions, most of the environmental studies (including the present one) consider the material presents in GF/F filtered water simply as the 'dissolved matter'. It is worth noting that hydrocarbon concentrations in the truly dissolved phase would be lower than those reported here. Filtered samples for dissolved hydrocarbon analyses were stored in 2 l SCHOTT® glass bottles with 50 ml dichloromethane (CH_2Cl_2) at 4 °C in the dark before solvent extraction (within 48 h). Filtered samples for NO_3^- and filters for Chl-*a* and POC were stored frozen until

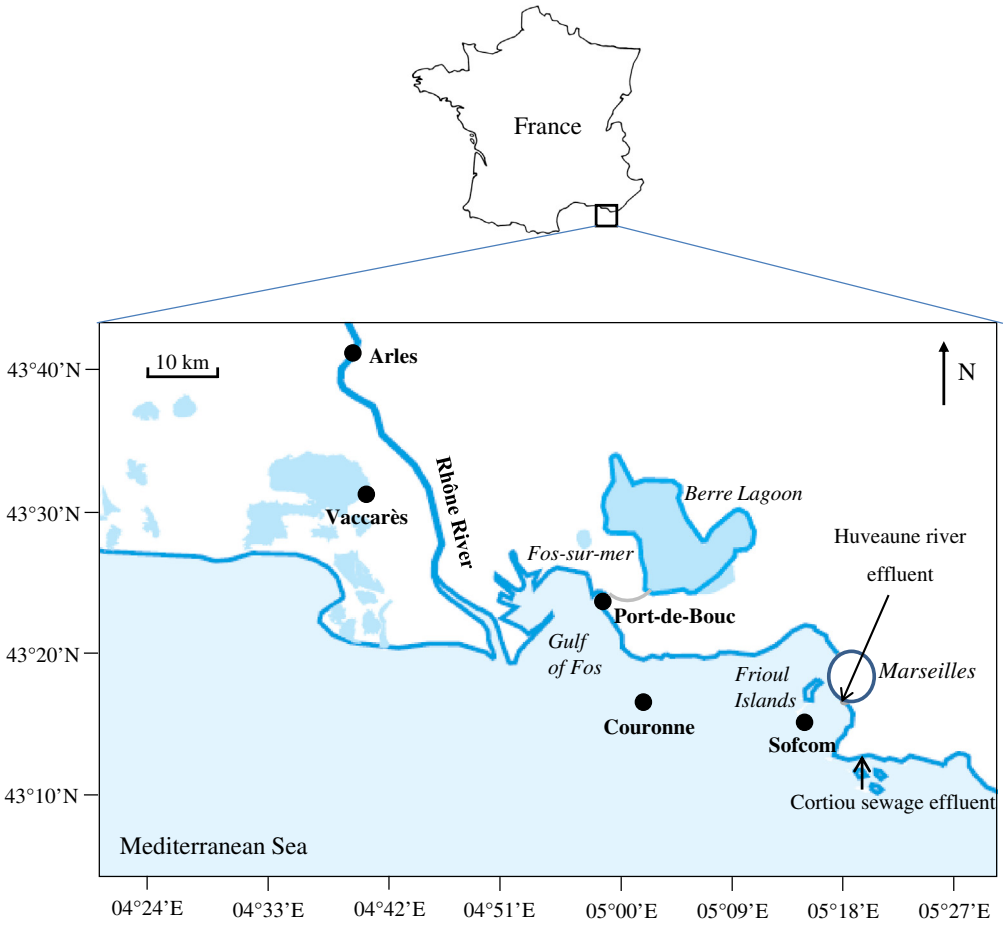

Fig. 1. Location of the five study sites in the Marseilles coastal area (Northwestern Mediterranean Sea, France): Arles (AR), Vaccarès (VA), Port-de-Bouc (PB), Couronne (COU) and Sofcom (SOF). The detailed characteristics of these sites are provided in Table 1.

analysis. During the experiments and analyses, gloves were worn and care was taken to avoid contaminations. All the glassware was washed with 1 M HCl and ultrapure water and combusted at 500 °C during 4 h. All the materials that could not be baked were washed with 1 M HCl and ultrapure water and dried at room temperature.

2.4. Hydrocarbon extraction and purification

Dissolved hydrocarbons present in the fraction of <0.7 μm were extracted from water by liquid–liquid extraction with CH_2Cl_2 (2 × 80 ml per litre). Organic phases were combined and evaporated on a rotary evaporator. Prior to purification, solvent was change to *n*-hexane. Hexane solubilised extracts were then purified to separate AHs (fraction 1, F1) from PAHs (fraction 2, F2). Extracts were fractionated on a 500 mg silica column. Silica gel (extra pure, Merck) was activated at 500 °C for 4 h followed by partially deactivation with 4% water by weight. F1 was eluted with 2 ml *n*-hexane while F2 was eluted with 3 ml *n*-hexane/CH_2Cl_2 (3:1 v/v). All solvents were of organic trace analysis quality (Rathburn, Interchim).

2.5. Analysis of hydrocarbons by gas chromatography (GC–MS)

Both F1 and F2 fractions were concentrated under a gentle stream of nitrogen and analysed by gas chromatograph–mass spectrometer (GC–MS) (TraceISQ, ThermoElectron) operating at an ionisation energy of 70 eV for a m/z range of 50–600, using hydrogen as carrier gas at a flow rate of 1.2 ml min^{-1}. The injector (used in splitless mode) and detector temperatures were 250 and 320 °C, respectively. The initial column temperature was held for 3 min at 70 °C, then ramped at 15 °C min^{-1} (ramp 1) to 150 °C and then at 7 °C min^{-1} (ramp 2) to a final temperature of 320 °C, which was held for 10 min. Data were carried out using selected ion monitoring (SIM) mode.

2.6. Determination of hydrocarbon indices and ratios

For AHs, we determined R, which corresponds to the sum of the concentrations of the resolved *n*-alkane series from *n*-C_{15} to *n*-C_{36} with two isoprenoids, pristane (Pr) and phytane (Phy). We also determined the UCM concentrations by integrating the hump (when present) using

Table 1
Characteristics of the study sites, located in the Marseilles coastal area (Northwestern Mediterranean Sea, France) and sampled from February 2011 to February 2012.

Name	Abbreviation	Water type	Position	Depth of the water column	Sampling depth
Arles	AR	Freshwater	43°40.7′N, 04°37.3′E	2 m	0.1 m
Vaccarès	VA	Freshwater	43°31.4′N, 04°38.1′E	0.5 m	0.1 m
Port-de-Bouc	PB	Harbour water	43°24.1′N, 04°59.0′E	5 m	0.1 m
Couronne	COU	Marine coastal water	43°16.5′N, 05°02.1′E	90 m	0.1 and 5 m
Sofcom	SOF	Marine coastal water	43°14.3′N, 05°17.3′E	60 m	0.1 and 5 m

the mean response factor of the resolved compounds (relationship between the area of the peak and the mass of each AH). The UCM hump corresponds to a mixture of many structurally complex isomers and homologues of branched and cyclic hydrocarbons that cannot be resolved by capillary GC columns (Bouloubassi and Saliot, 1993). Its relative importance, expressed as the ratio of unresolved to resolved compounds (UCM/R), is commonly used as diagnostic criteria of pollutant inputs (Mazurek and Simoneit, 1984).

Concerning PAHs, we determined the concentrations of 17 parent PAHs (PAHs-$_P$), namely naphthalene (Naph), acenaphthylene (Acy), acenaphtene (Ace), fluorene (Flu), dibenzothiophene (DBT), phenanthrene (Phe), anthracene (Ant), fluoranthene (Flt), pyrene (Pyr), benz[*a*]anthracene (BaA), chrysene (Chr), benzo[*b*]fluoranthene (BbF), benzo[*k*]fluoranthene (BkF), benzo[*a*]pyrene (BaP), dibenz[*a,h*]anthracene (DBA), benzo[*g,h,i*]perylene (BP), indeno[1,2,3-*cd*]pyrene (IndP), as well as the concentrations of alkylated homologues (methyl = C_1, dimethyl = C_2, trimethyl = C_3) of the five target compounds Naph, Flu, Phe, Pyr and Chr, which lead to a total of 32 PAHs (PAHs-$_{P+A}$). Naph, Acy, Ace, Flu, DBT, Phe and Ant are low molecular weight (LMW) compounds (2–3 rings) while Flt, Pyr, BaA, Chr, BbF, BkF, BaP, DBA, BP and IndP are high molecular weight (HMW) compounds (4–6 rings). In order to assess the contamination sources (petrogenic or pyrogenic), we determined not only the isomer ratios Phe/Ant and Flt/Pyr but also Alk/Par ratio (Budzinski et al., 1997; Readman et al., 2002; Mille et al., 2007; Azimi et al., 2005).

2.7. Quality assurance/Quality control

Deuterated standard mixtures (C_{16}-d_{34}, C_{24}-d_{50}, and C_{36}-d_{74} for AHs, and Naph-d_8, Phe-d_{10}, and Per-d_{12} for PAHs) were introduced prior to extraction, as well as a supplementary deuterated standard before injection, and used as surrogates to assess the recoveries of analytical procedures and to perform quantitation accuracy. The C_{16}-d_{34}, C_{24}-d_{50} and C_{36}-d_{74} average recoveries were of 30, 63 and 85%, respectively, while Naph-d_8, Phe-d_{10}, and Per-d_{12} average recoveries were of 38, 74 and 88%, respectively. Cautions were taken during the evaporation under nitrogen because dryness could lead to the total loss of the more volatile compounds. In addition, blanks were run for the whole procedure including extraction, solvent concentration and purification. They ranged from 0.01 to 0.02 μg l^{-1} and from 2.0 to 3.1 ng l^{-1} for AHs and PAHs, respectively. All concentration values were blank and recovery corrected. Detection limits for individual compounds varied from 0.5 to 15 pg l^{-1}.

Compounds were identified and quantified by reference to the analysis of standard mixtures (04071, Fluka and 47543-U, Supelco among others). Calibration curves were made for all target compounds analysed except for the alkylated homologues that were quantified with their parent compound calibration curves. The calibration was performed in SIM mode. The correlation coefficients were >0.99 for all the compounds studied.

Samples were treated and analysed as the sampling was performed. Variations in calibration curves over one year study were not significant (including after maintenance operations, i.e., essentially consumable changes). However, at the end of the study, a few samples from each sites and seasons were injected again under exactly the same conditions to confirm the spatial and temporal variabilities of the results.

2.8. Ancillary data

For marine sites, profiles of temperature and salinity were obtained from a 19*plus* conductivity temperature depth (CTD) profiler (Seabird Electronics Inc., USA). Because the deployment of the CTD profiler was not possible in shallow freshwaters, salinity at AR and VA was measured on 0.1 m depth discrete samples using a refractometer (MASTER-S/Millα, Atago, Tokyo). Concerning biogeochemical parameters, NO_3^- were analysed using an automated colourimetric method (Aminot and Kérouel, 2007). The detection limit was 0.05 μM. Chl-*a* was analysed by fluorescence method following a methanol extraction (Raimbault et al., 2004). POC was determined using wet-oxidation procedure of Raimbault et al. (1999).

2.9. Statistics

A one-way analysis of variance (ANOVA) performed with StatView 5.0 was used to compare the means of independent data groups (normally distributed). The significance threshold was set at $p < 0.05$.

3. Results

3.1. Hydrological and biogeochemical description of the study sites

Hydrological and biogeochemical data are reported in Table 2. The lowest salinities were found at the continental sites. Salinity was constant at AR (0) and ranged from 0 to 15 at VA. These latter values confirmed the (natural or anthropogenically constrained) mixing between the Rhône River waters and the Mediterranean marine waters. At PB, COU-0.1 m and COU-5 m, salinity ranged 24.8–36.8, 34.7–38.1 and 37.3–38.0, respectively, which pointed out Rhône water intrusions into these sites. On the contrary, at SOF salinity values (37.7–38.2, except on 12/12/2011) were typical of Mediterranean marine waters.

POC concentrations ranged from 6.0 to 125 μM (flood) and from 12 to 278 μM at AR and VA, respectively. For marine waters, POC concentrations ranged from 6.0 to 39 μM at PB, from 2.1 to 83 μM at COU-0.1 m, from 1.9 to 33 μM at COU-5 m, from 1.4 to 12.5 μM at SOF-0.1 m and from 1.2 to 9.0 μM at SOF-5 m.

NO_3^- concentrations ranged from 69 to 125 μM and from 0.75 to 34 μM at AR and VA, respectively. For marine waters, NO_3^- concentrations ranged from 0.04 to 13 μM at PB, from 0.0 to 13 μM at COU-0.1 m, from 0.0 to 3.7 μM at COU-5 m, from 0.0 to 2.1 μM at SOF-0.1 m and from 0.0 to 2.4 μM at SOF-5 m.

Chl-*a* concentrations ranged from 0.41 to 16 μg l^{-1} and from 0.51 to 26 μg l^{-1} at AR and VA, respectively. For marine waters, Chl-*a* concentrations ranged from 0.62 to 5.7 μg l^{-1} at PB, from 0.20 to 3.2 μg l^{-1} at COU-0.1 m, from 0.29 to 1.3 μg l^{-1} at COU-5 m, from 0.16 to 2.2 μg l^{-1} at SOF-0.1 m and from 0.21 to 1.8 μg l^{-1} at SOF-5 m.

With regard to these hydrological and biogeochemical characteristics, it appears that the study sites were quite different one from another, except COU and SOF. Salinity was negatively correlated to POC, NO_3^- and Chl-*a* ($r = -0.49$ at -0.74, $p < 0.0001$, $n = 117$), while Chl-*a* was positively correlated to POC and NO_3^- ($r = 0.20$–0.66, $p < 0.001$–0.03, $n = 117$). These results confirmed that the Rhône River is a source of nutrients and drains large amounts of material (both dissolved and particulate) and that hydrological and biogeochemical parameters may be used as tracers of the Rhône River plume, either by direct inputs (lower salinities associated with increases in POC, NO_3^- and/or Chl-*a* concentrations), or by inducing in situ primary production (Pujo-Pay et al., 2006). Because of the geomorphology of the drainage basin, VA and PB were intensively impacted by the Rhône River (Ulses et al., 2005). COU, located off PB, and SOF were impacted occasionally (salinity < 37.8) under specific wind conditions (Pairaud et al., 2011) and quite weakly (Para et al., 2010), respectively, by the Rhône River plume.

3.2. Spatial and seasonal variations of dissolved AHs

3.2.1. Concentration levels

At all sites, the concentrations of resolved alkanes (R) ranged from 0.04 to 0.58 μg l^{-1} (mostly <0.30 μg l^{-1}; Table 3). No significant differences were found for R concentrations, neither between 0.1 and 5 m depths at COU and SOF ($p = 0.52$, $n = 14$), nor within the five sites ($p = 0.07$–0.95, $n = 13$–29). R concentrations were not correlated to hydrological and biogeochemical parameters ($r = -0.10$–0.10, $p =$

Table 2
Hydrological and biogeochemical parameters.

		2011																			2012		
		17/02	24/02	10/03	24/03	18/04	03/05	17/05	09/06	27/06	05/07	18/07	05/09	15/09	10/10	24/10	03/11	17/11	01/12	12/12	09/01	23/01	06/02
AR 0.1 m	Salinity	0	0	0	0	0	0	0	0	0	0	0	0	0	0	0	0	0	0	0	0	0	0
	POC (μM)	14	11	7.3	21	18	36	28	27	10	14	10	8.1	8.1	10	6.0	8.1	12	8.1	24	125	32	24
	NO_3^- (μM)	115	122	125	104	106	86	87	84	69	69	70	70	76	77	81	83	81	90	100	111	120	111
	Chl-*a* (μg l^{-1})	2.3	16	9.7	1.9	2.3	11	3.7	4.9	15	2.9	2.5	1.7	1.8	NA	NA	NA	0.49	0.41	1.1	3.0	1.3	1.1
VA 0.1 m	Salinity	7	7	15	4	4	1	2	4	1	0	0	2	2	14	14	3	0	0	8	5	13	
	POC (μM)	18	17	12	132	236	158	70	278	143	78	89	58	50	97	30	137	78	72	48	62	66	
	NO_3^- (μM)	2.4	2.1	1.6	4.0	34	28	20	0.75	9.6	20	16	12	9.4	2.0	2.1	6.4	4.0	1.8	3.0	9.1	11	
	Chl-*a* (μg l^{-1})	21	10	4.5	20	11	19	10	26	0.51	8.6	7.5	4.9	9.6	NA	NA	NA	6.9	7.4	2.8	6.4	6.0	
		10/02	15/02	17/03	28/03	08/04	09/05	01/05	07/06	28/06	07/07	19/07	07/09	21/09	14/10	21/10		22/11	09/12	12/12	11/01	25/01	
PB 0.1 m	Salinity (1 m)	24.8	32.3	33.4		29.1	28.2	34.8	NA	35.8	36.0		30.0	29.9	32.0	26.7		34.6	36.8		31.0	33.6	
	POC (μM)	6.1	9.0	16		21	17	17	29	32	23		39	24	17	21		12	18		16	6.0	
	NO_3^- (μM)	13	7.6	5.9		1.3	0.4	0.67	0.29	0.06	0.04		0.42	0.75	2.5	2.3		3.5	1.5		8.1	9.3	
	Chl-*a* (μg l^{-1})	0.75	1.0	1.6		0.82	0.78	1.9	4.7	NA	2.7		5.7	3.0	NA	NA		2.4	2.1		0.95	0.62	
COU 0.1 m	Salinity	38.0	NA	37.9	37.6	37.8	37.7	36.8		36.2	37.6		37.5	36.1	38.1	37.8		38.0	34.7		37.8	37.6	
	POC (μM)	3.0	3.8	4.4	11.5	9.8	7.4	26		83	29		6.8	9.0	3.5	3.5		2.4	7.1		2.1	2.6	
	NO_3^- (μM)	0.83	1.13	0.77	0.44	0.0	0.04	0.14		0.05	1.2		0.0	4.9	0.04	0.72		0.37	13		3.7	3.1	
	Chl-*a* (μg l^{-1})	0.54	0.58	0.66	1.1	0.20	0.32	2.0		0.66	3.2		0.39	1.0	NA	NA		0.33	0.66		0.33	0.31	
COU 5 m	Salinity	38.0	NA	37.9	37.6	37.9	37.8	38.0		37.7	37.0		37.7	37.7	38.1	37.8		38.0	37.3		37.8	37.6	
	POC (μM)	3.0	3.1	4.5	11	8.5	8.1	12		33	19		6.4	5.4	3.8	3.3		2.1	5.0		1.9	2.1	
	NO_3^- (μM)	0.85	1.2	0.76	0.59	0.00	0.05	0.02		0.05	0.01		0.0	0.60	0.05	0.76		0.42	2.4		3.7	2.7	
	Chl-*a* (μg l^{-1})	0.50	0.78	0.73	0.75	0.46	0.37	1.1		3.5	0.47		0.29	0.50	NA	NA		0.34	1.3		0.31	0.31	
SOF 0.1 m	Salinity	38.0	38.0	38.0	NA	37.9	37.8	38.0	37.8	37.9	37.7	NA	NA	38.1	38.1	38.2		38.0	37.8	37.1	38.2	38.2	
	POC (μM)	3.2	3.3	4.1	5.7	8.4	7.8	4.4	7.7	4.5	3.5	9.0	4.2	2.6	5.0	3.1		2.4	4.5	12.5	1.7	1.4	
	NO_3^- (μM)	0.93	1.1	1.3	0.40	0.00	0.20	0.19	0.38	0.5	0.02	0.01	0.0	0.0	0.05	0.07		0.33	0.31	1.15	2.1	1.4	
	Chl-*a* (μg l^{-1})	0.55	0.64	0.49	0.40	0.59	0.50	0.30	0.78	0.25	0.16	0.53	0.18	0.12	NA	NA		0.33	1.0	2.20	0.34	0.37	
SOF 5 m	Salinity	38.0	38.0	37.9	NA	37.9	37.8	38.0	37.9	38.1	37.8	NA	NA	38.0	38.1	38.2		38.0	37.8		38.1	38.2	
	POC (μM)	2.6	4.2	4.0	6.1	8.2	7.1	3.9	7.6	4.0	4.5	9.0	4.5	2.6	4.7	3.5		2.6	5.0		1.4	1.2	
	NO_3^- (μM)	1.0	1.1	0.82	0.41	0.00	0.17	0.13	0.40	0.43	0.32	0.00	0.00	0.00	0.04	0.08		0.38	0.53		2.4	1.7	
	Chl-*a* (μg l^{-1})	0.69	0.56	0.57	0.78	0.19	0.57	0.30	0.82	1.8	0.27	0.66	0.21	0.25	NA	NA		0.34	0.50		0.37	0.28	

POC: particulate organic carbon; NO_3^-: nitrates; Chl-*a*: chlorophyll *a*.
NA: not available.

0.31–0.69, n = 105) during the sampling period. However, they were significantly lower in summer compared to the other 3 seasons (p = 0.0013–0.05, n = 24–30), which exhibited comparable values (p = 0.17–0.69, n = 24–30), suggesting less inputs and/or more removing processes during the warmer months.

3.2.2. Composition patterns and ratios

AH composition patterns are presented in Fig. 2. They displayed bimodal distributions showing spatial and seasonal variations. For the lighter compounds (<*n*-C_{20}), patterns exhibited very variable maximum alternating between *n*-C_{16}–*n*-C_{17} + Pr (from spring to fall) and *n*-C_{19} (fall and winter) as well as a general depletion in *n*-C_{18}. For the heavier compounds (≥*n*-C_{20}), patterns were centred on *n*-C_{28}–*n*-C_{30}. In spring and winter, all sites exhibited predominance (more or less marked) of even over odd carbon numbered *n*-alkanes in the range *n*-C_{20}–*n*-C_{36} especially at offshore sites (COU and SOF). This predominance tended to reduce/disappear in summer and fall at AR, VA and PB but remained visible at COU and SOF. Thus, even *n*-alkane predominance was related to season and affected riverine waters as well as marine sites with no river influence. Besides, one can notice the dominance of *n*-C_{27}, *n*-C_{29}, and *n*-C_{31} typically originating from epicuticular waxes of higher plants in fall at VA (Douglas and Eglinton, 1966). Finally, UCM was noticeable in the range of 0.13–1.6 μg l^{-1} with UCM/R ratios varying from 0.51 to 5.7. UCM occurrences were too scarce to perform statistical tests.

3.3. Spatial and seasonal variations of dissolved PAHs

PAHs-$_P$ (sum of 17 parent PAHs) and PAHs-$_{P+A}$ (sum of PAHs-$_P$ + alkylated homologues of 5 target PAHs) concentrations are reported Table 4. Although PAHs-$_P$ represent essential data to assess a preliminary level of hydrocarbon contaminations in the environment and to establish comparisons with literature data, PAHs-$_{P+A}$ are more relevant to investigate more deeply the distribution and dynamics of hydrocarbons (Wang and Fingas, 1995) as well as to assess their toxicological effects on marine ecosystems. While both PAHs-$_P$ and PAHs-$_{P+A}$ concentrations are described, statistical tests and distribution patterns were performed only on the PAHs-$_{P+A}$ dataset.

3.3.1. Concentration levels

The potential enrichment in aromatic compounds due to alkylated homologues (PAHs-$_{P+A}$/PAHs-$_P$) varied from 1.3 to 3.9. PAHs-$_P$ and PAHs-$_{P+A}$ concentrations ranged from 6.1 to 101 ng l^{-1} and from 12 to 241 ng l^{-1}, respectively at AR, while they varied from 9.4 to 115 and from 15 to 360 ng l^{-1}, respectively at VA. At marine sites, PAHs-$_P$ and PAHs-$_{P+A}$ concentrations ranged from 6.3 to 135 ng l^{-1} and from 13 to 364 ng l^{-1}, respectively at PB, while they varied from 4.8 to 151 ng l^{-1} and from 8.1 to 324 ng l^{-1}, respectively at COU (both depths) and from 4.7 to 80 ng l^{-1} and from 8.9 to 217 ng l^{-1}, respectively at SOF (both depths). It is worth noting that on 07/07/2012, sporadic high values were recorded at PB and COU showing a specific contamination. Correspondingly to AHs, no significant differences were recorded for PAHs-$_{P+A}$ concentrations between 0.1 and 5 m depths at COU and SOF (p = 0.80, n = 36) but, contrary to AHs, significant differences were found among sites. PAHs-$_{P+A}$ concentrations were higher at PB than at the other 4 sites (p = 0.001–0.03, n = 17–38) while AR, VA, COU and SOF depicted no difference from each other (p = 0.08–0.96, n = 17–38). In addition, PAHs-$_{P+A}$ concentrations were higher in winter than during the other 3 seasons (p = <0.001–0.003, n = 26–44) while no significant differences were found between spring, summer and fall (p = 0.26–0.76, n = 26–44). PAHs-$_{P+A}$ concentrations were not correlated to hydrological and biogeochemical parameters (r = −0.37–0.03, p = 0.65–0.99, n = 17–38).

3.3.2. Composition patterns and ratios

Spatial and seasonal variations of the PAHs-$_{P+A}$ composition patterns are presented in Fig. 3. These patterns were highly dominated by light compounds (2–3 rings). On the whole dataset, 2–3 ring compounds represented 90 ± 5% of PAHs-$_{P+A}$, for which naphthalenes (sum of Naph, C_1-Naph, C_2-Naph and C_3-Naph) were the major components (49 ± 20%) followed by phenanthrenes and fluorenes (15 ± 7 and 11 ± 4%, respectively). Moreover, heavy compounds like C_2- and C_3-Pyr, C_1-, C_2- and C_3-Chr, BbF, BkF, BaP, DBA, BP and IndP were almost

Table 3
Concentrations of AHs and UCM (μg l^{-1}), and UCM/R ratio.

		2011																2012		
		10/03	24/03	18/04	03/05	09/06	27/06	05/07	18/07	05/09	15/09		24/10	03/11	17/11	01/12	12/12	09/01	23/01	06/02
AR 0.1 m	R (μg l^{-1})	0.28	0.28	0.19	0.12	0.13	0.15	0.18	0.15	0.10	0.22		0.16	0.11	0.16	0.17	0.17	0.18	0.16	0.16
	UCM (μg l^{-1})							0.62	0.87		1.6			0.38	0.27					
	UCM/R							3.5	5.5		5.7			2.9	1.8					
VA 0.1 m	R (μg l^{-1})	0.39	0.29	0.15	0.14	0.19	0.24	0.13	0.06	0.09	0.16		0.15	0.10	0.31	0.53	0.15	0.16	0.13	
	UCM (μg l^{-1})							0.29							0.49					
	UCM/R							2.3							1.6					
		17/03	28/03	08/04	09/05	07/06	28/06	07/07	19/07	07/09	21/09	14/10	21/10		22/11	09/12		11/01	25/01	
PB 0.1 m	R (μg l^{-1})	0.21		0.20	0.12	0.12	0.07	0.08		0.09		0.19	0.15		0.24	0.20		0.10		
	UCM (μg l^{-1})														0.25					
	UCM/R														1.0					
COU 0.1 m	R (μg l^{-1})	0.20	0.08	0.13	0.23		0.13	0.04		0.11	0.58	0.07	0.17		0.10	0.18		0.10	0.10	
	UCM (μg l^{-1})										0.76									
	UCM/R										1.2									
COU 5 m	R (μg l^{-1})	0.20	0.07	0.13	0.17		0.10	0.05		0.07	0.29	0.04	0.17		0.13	0.21		0.09	0.16	
	UCM (μg l^{-1})										0.29									
	UCM/R										1.0									
SOF 0.1 m	R (μg l^{-1})	0.22	0.13	0.25	0.28		0.22	0.06	0.08	0.08	0.29		0.08		0.14	0.15		0.11	0.12	
	UCM (μg l^{-1})										0.30		0.18		0.13					
	UCM/R																			
SOF 5 m	R (μg l^{-1})	0.25	0.13	0.24	0.24		0.22	0.09	0.09	0.09	0.26	0.45	0.11		0.11	0.22		0.19	0.09	
	UCM (μg l^{-1})											0.23	0.28							
	UCM/R											0.51	2.7							

R: resolved aliphatic hydrocarbons (sum of *n*-alkanes from C_{15} to C_{36} with two isoprenoids, pristane and phytane); UCM: unresolved complex mixture; UCM/R: unresolved complex mixture over resolved aliphatic hydrocarbon concentration ratio.

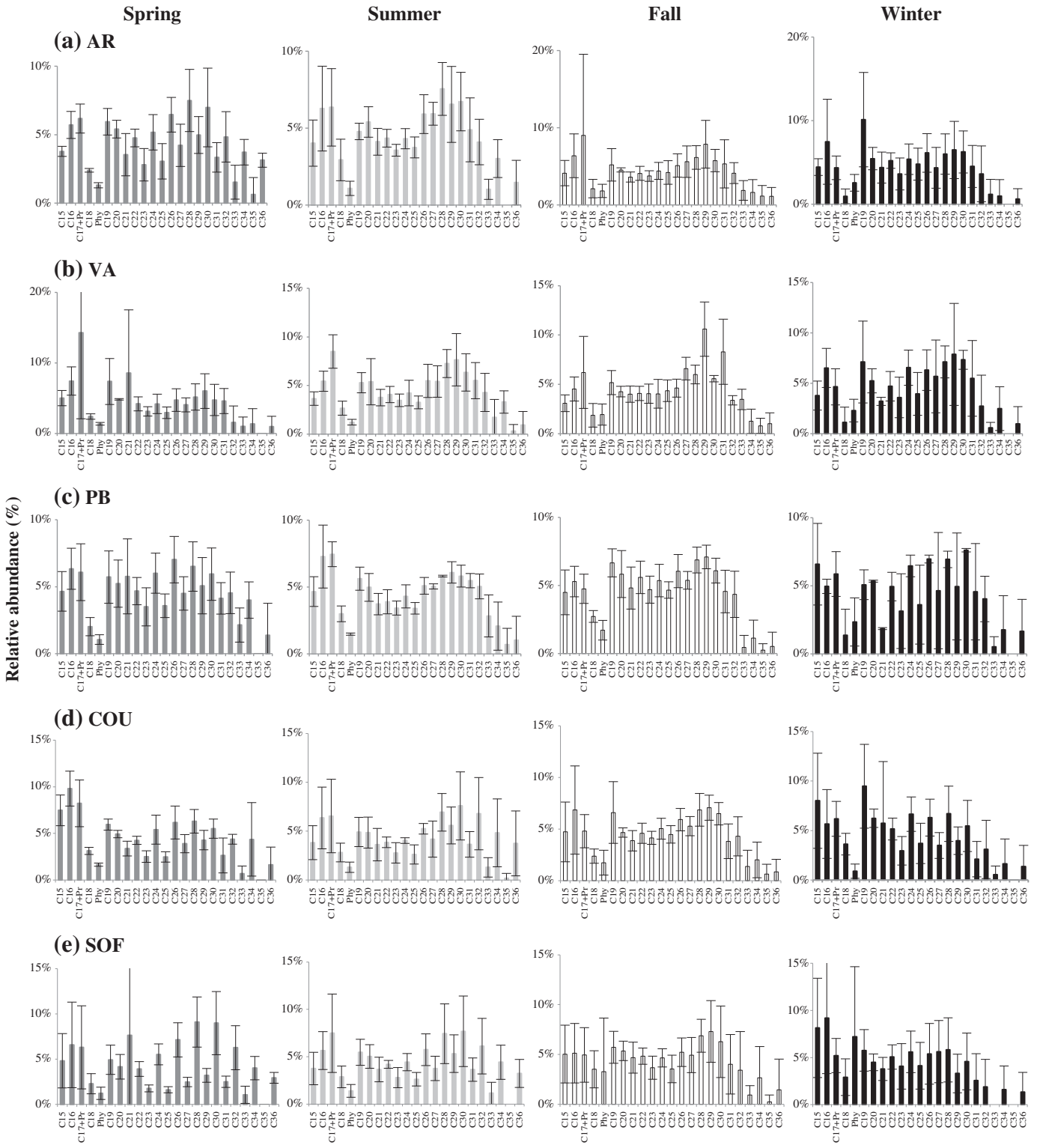

Fig. 2. Composition patterns of dissolved AHs (in %) at AR (a), VA (b), PB (c), COU (d) and SOF sites (e). Pr = Pristane; Phy = Phytane.

never detected. Interestingly, spatial and seasonal variation patterns were due mainly to the distribution within naphthalenes. The similar seasonal evolution in the PAHs-$_{P+A}$ composition at AR, VA, COU and SOF suggested a common dynamics at these sites. On the contrary, at PB, the composition patterns were different from the other sites and between seasons (alternating dominance between Naph and its alkylated homologues). This pointed out more local and variable sources. Besides, on 07/07/2011, the PAHs-$_{P+A}$ composition exhibited unusual profiles at PB, COU-0.1 m and COU-5 m with Naph reaching 49, 52 and 61% of PAHs-$_{P+A}$, respectively, followed by C_1-Naph, C_2-Naph, and C_3-Naph in a decreasing order (sum of naphthalenes = 82–91%). These latter patterns associated with the high concentration levels, can be explained by a sporadic spillage from industrial activities and/or the use of light oil (e.g., gasoline) shortly before.

Table 4
Concentrations of 17 parent PAHs (PAHs-$_P$) and 32 parents + alkylated PAHs (PAHs-$_{P+A}$) (ng l^{-1}), and Phe/Ant, Flt/Pyr and Alk/Par ratios.

		2011																		2012		
		17/02	24/02	10/03	24/03	18/04	03/05	17/05	09/06	27/06	05/07	18/07	05/09	15/09	10/10	24/10	03/11	17/11	01/12	12/12	09/01	23/01	06/02
AR 0.1 m	PAHs-$_P$	53	38	23	18	16	13	11	10	16	19	19	17	13	6.1	23	10	13	40	101	93	33	40
	PAHs-$_{P+A}$	91	63	40	37	28	23	20	20	30	33	35	27	23	12	36	20	22	70	241	223	66	84
	Phe/Ant	5.4	11	13	8.8	11	11	11	14	14	15	11	8.7	8.0	10	11	12	9.1	6.9	4.4	4.0	5.1	5.4
	Flt/Pyr	0.4	0.4	0.4	0.5	0.5	0.5	0.4	0.4	0.5	0.5	0.5	0.4	0.5	0.5	1.3	0.5	0.4	0.5	0.4	0.4	0.5	0.5
	Alk/Par	1.1	0.8	1.0	1.4	1.0	1.1	1.2	1.2	1.2	1.0	1.3	0.9	1.2	1.5	0.8	1.3	0.9	1.1	2.0	2.0	1.5	1.5
VA 0.1 m	PAHs-$_P$	75	41	25	27	19	12	9.4	11	12	27	12	14	15	10	25	13	18	52	115	114	30	
	PAHs-$_{P+A}$	136	76	43	45	43	25	15	22	24	36	19	22	25	17	44	24	31	116	352	360	73	
	Phe/Ant	6.8	12	19	9.3	9.0	9.4	6.3	16	17	4.5	11	14	12	15	15	15	12	5.7	5.4	6.6	4.6	
	Flt/Pyr	0.3	0.3	0.7	0.5	0.4	0.3	0.4	0.3	0.4	0.3	0.4	0.4	0.3	0.4	0.3	0.3	0.4	0.5	0.5	0.5	0.7	
	Alk/Par	1.0	1.0	0.8	0.8	1.6	1.5	0.7	1.3	1.3	0.5	0.9	0.8	0.8	0.9	0.9	1.1	0.8	1.6	2.8	2.9	2.1	
		10/02	15/02	17/03	28/03	08/04	09/05	01/05	07/06	28/06	07/07	19/07	07/09	21/09	14/10	21/10		22/11	09/12	12/12	11/01	25/01	
PB 0.1 m	PAHs-$_P$	105	73	56		28	26	19	9.6	21	62		11	7.0	6.3	16		18	82		135	27	
	PAHs-$_{P+A}$	405	192	221		58	60	37	22	47	106		20	18	13	32		41	225		364	63	
	Phe/Ant	14	11	18		10	15	12	11	19	11		12	8.6	12	15		7.8	5.7		4.5	5.5	
	Flt/Pyr	0.3	0.3	0.5		0.6	0.4	0.3	0.3	0.3	0.3		0.3	0.2	0.3	0.3		0.2	0.6		0.4	0.6	
	Alk/Par	3.7	1.9	3.6		1.3	1.6	1.1	1.7	1.4	0.7		1.0	1.8	1.4	1.3		1.6	2.3		2.3	2.0	
COU 0.1 m	PAHs-$_P$	31	20	9.8	10	16	12	10		8.8	41		10	7.6	5.3	7.2		7.3	65		119	61	
	PAHs-$_{P+A}$	49	39	18	16	25	21	18		14	64		16	13	8.8	12		13	154		324	127	
	Phe/Ant	13	16	17	13	13	5.3	14		16	16		13	12	13	11		5.9	7.3		4.9	6.3	
	Flt/Pyr	0.3	0.3	0.5	0.4	0.5	0.4	0.4		0.3	0.5		0.4	0.3	0.2	0.3		0.2	0.6		0.5	0.7	
	Alk/Par	0.7	1.1	1.0	0.7	0.7	1.1	1.0		0.9	0.6		0.8	0.9	0.9	0.8		1.0	1.9		2.4	1.6	
COU 5 m	PAHs-$_P$	22	17	8.5	10	15	11	12		9.1	151		10	4.8	5.6	8.6		5.4	49		106	61	
	PAHs-$_{P+A}$	38	32	15	16	24	19	22		15	221		16	8.1	11	13		8.8	123		269	180	
	Phe/Ant	10	13	12	11	12	10	13		15	16		14	9.5	10	11		6.8	6.3		4.6	5.3	
	Flt/Pyr	0.3	0.3	0.5	0.5	0.5	0.2	0.4		0.4	0.5		0.3	0.3	0.2	0.2		0.3	0.6		0.5	0.5	
	Alk/Par	0.9	1.1	0.8	0.7	0.7	0.9	1.0		0.9	0.5		0.8	0.9	1.2	0.7		0.8	2.0		2.2	2.8	
SOF 0.1 m	PAHs-$_P$	26	25	12	9.1	13	10	8.5	8.9	8.0	7.8	8.0	7.6	6.0	6.7	8.0		5.3	37		54	36	
	PAHs-$_{P+A}$	53	43	21	16	20	19	16	18	15	13	13	13	9.8	12	13		9.2	95		136	87	
	Phe/Ant	6.0	13	12	14	10	11	11	15	15	11	12	12	14	16	13		12	13		5.7	6.0	
	Flt/Pyr	0.3	0.3	0.4	0.4	0.4	0.4	0.3	0.3	0.3	0.2	0.5	0.3	0.3	0.2	0.3		0.3	0.4		0.5	0.5	
	Alk/Par	1.2	0.8	0.9	0.9	0.5	1.1	1.1	1.2	1.1	0.7	0.8	1.1	0.8	1.2	0.9		0.9	1.3		2.1	2.1	
SOF 5 m	PAHs-$_P$	5.9	22	12	8.8	12	7.3	9.8	7.9	7.0	18	8.5	7.7	6.4	6.6	7.2		4.7	55		80	46	
	PAHs-$_{P+A}$	12	45	19	15	19	13	17	16	15	23	13	12	11	12	13		8.9	145		217	112	
	Phe/Ant	3.9	14	11	12	11	12	16	17	15	11	15	12	16	13	7.5		13	6.1		5.2	5.2	
	Flt/Pyr	0.1	0.2	0.4	0.4	0.5	0.3	0.3	0.4	0.3	0.3	0.4	0.3	0.2	0.3	0.3		0.2	0.5		0.5	0.6	
	Alk/Par	1.4	1.3	0.8	0.8	0.6	0.9	1.0	1.3	1.4	0.4	0.7	0.8	0.8	1.2	1.1		1.1	2.3		2.5	2.1	

PAHs-$_P$: 17 parent polycyclic aromatic hydrocarbons (PAHs); PAHs-$_{P+A}$: sum of 17 parents and 15 alkylated homologues PAHs; Phe/Ant: phenanthrene (Phe) over anthracene (Ant) concentration ratio. Flt/Pyr: fluoranthene (Flt) over pyrene (Pyr) concentration ratio; Alk/Par: alkylated homologues over parent PAH concentration ratio.

At all sites, Phe/Ant ratios ranged from 3.9 to 19 and were lower in winter than in spring and summer ($p = 0.0002$–0.004, $n = 26$–44) while Flt/Pyr ratios ranged from 0.1 to 1.3 and were higher in winter than in fall ($p = 0.007$, $n = 30$–44). In addition, at all sites, Alk/Par ratios were 1.2 ± 0.6 and were higher in winter ($p < 0.0001$–0.0203, $n = 26$–44). Fig. 4 presents the cross plot between Phe/Ant and Flt/Pyr ratios. From April to November 2011 (spring to fall), when PAH concentrations were the lowest, hydrocarbons were rather of strictly petrogenic origin. In February–March 2011 and from December 2011 to February 2012 (late fall and winter), when PAH concentrations were the highest, mixed origin PAHs dominated.

3.4. Relationship between dissolved AHs and PAHs-$_{P+A}$

When considering the whole dataset, AH and PAHs-$_{P+A}$ concentrations were not correlated ($r = -0.1$, $p = 0.33$, $n = 105$). In addition, sporadic increases in concentrations of one hydrocarbon class were not associated with fluctuations from the other class. For instance, the higher AH values at offshore sites (both depths) on 21/09/2011, along with low CPI_{21-33} values especially at COU, were not associated with an increase in PAHs-$_{P+A}$ concentrations. In the same way, the PAHs-$_{P+A}$ contamination observed on 07/07/2011 as well as the higher PAHs-$_{P+A}$ values recorded in winter were not combined with a rise in AH concentrations.

4. Discussion

4.1. Significance of AH and PAH concentrations

Due to their hydrophobic properties, it is considered that AHs are preferentially adsorbed onto particles, thus dissolved *n*-alkane concentrations are less widespread than dissolved PAH concentrations in the literature (Cincinelli et al., 2001; Stortini et al., 2009). Comparison with the literature must be carried out with caution because the number of studied compounds as well as the definition of the particulate and the dissolved phases may vary between authors. Considering this, the concentrations reported in this study for a series of resolved C_{15}–C_{36} *n*-alkanes and 2 isoprenoids (0.04–0.53 μg l^{-1}) are in the same range than those recorded in Antarctic surface waters (0.11 to 0.30 μg l^{-1}; Stortini et al., 2009), in the coastal Tyrrhenian Sea (0.14–0.82 μg l^{-1}; Cincinelli et al., 2001) and in the Marseilles coastal waters (0.04–0.41 μg l^{-1}; Guigue et al., 2011). It appears surprising to record levels comparable to those from Antarctic surface waters for which there are no major local anthropogenic sources. However, the authors of this study explain that slightly higher AH concentrations in the Gerlache Inlet Sea may originate from phytoplankton as well as research station activities and shipping. In addition, long range atmospheric transport and subsequent depositions associated with a sequestration by low water temperatures and degradation processes of lower magnitude, as

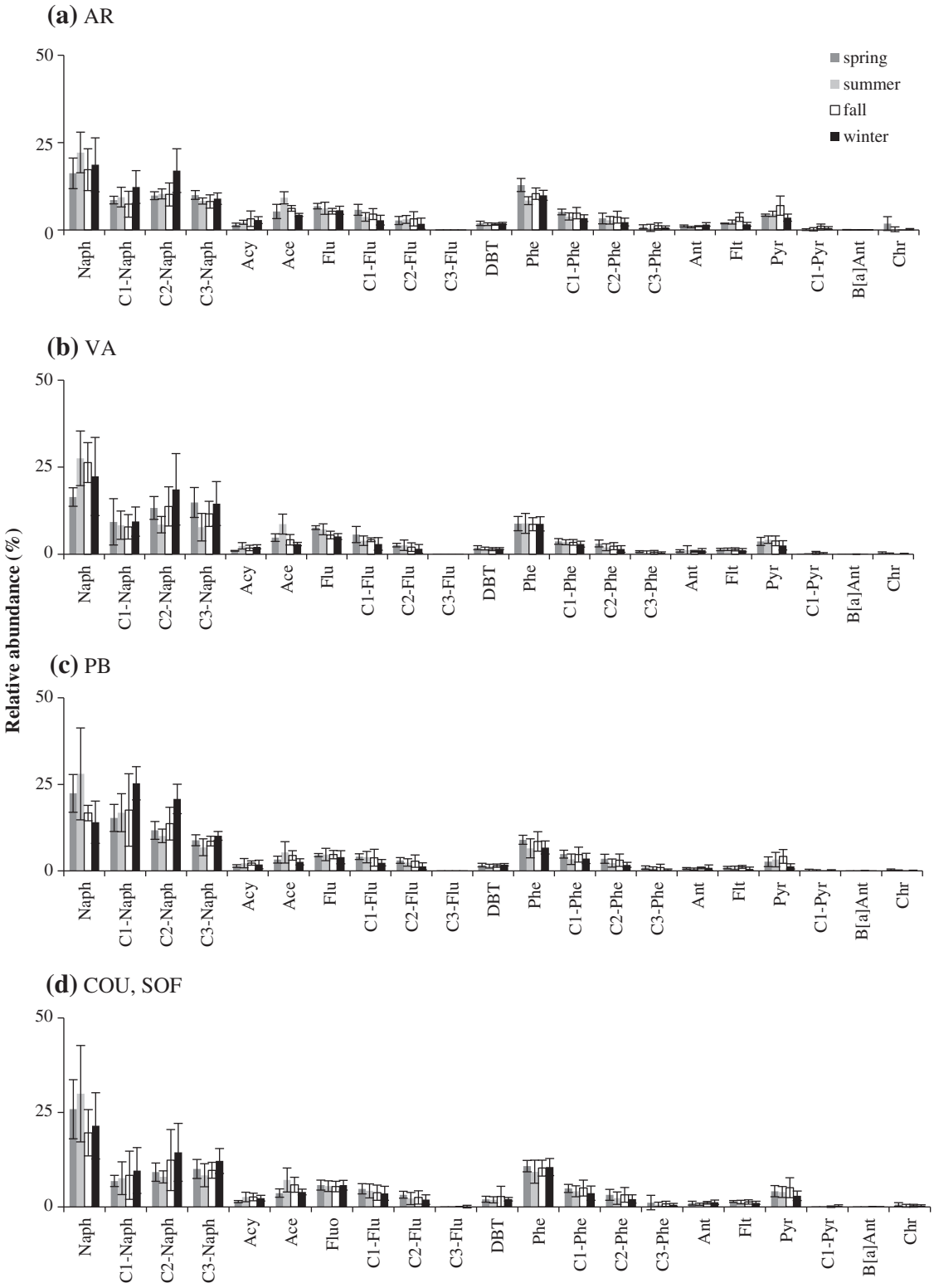

Fig. 3. Composition patterns of dissolved PAHs (in %) at AR (a), VA (b), PB (c), COU and SOF sites (d). Naph: naphthalene; C_1-Naph: methylnaphthalenes; C_2-Naph: dimethylnaphthalenes; C_3-Naph: trimethylnaphthalenes; Acy: Acenaphthylene; Ace: Acenaphtene; Flu: Fluorene; C_1-Flu: methylfluorenes; C_2-Flu: dimethylfluorenes; C_3-Flu: trimethylfluorenes; DBT: dibenzothiophene; Phe: phenanthrene; C_1-Phe: methylphenanthrenes; C_2-Phe: dimethylphenanthrenes; C_3-Phe: trimethylphenanthrenes; Ant: anthracene; Flt: fluoranthene; Pyr: pyrene; C_1-Pyr: methylpyrene; B[a]Ant: benz[a]anthracene; Chr: chrysene.

it has been highlighted for the Arctic (MacDonald et al., 2000), may be an additional explanation. On the other side, dissolved AH concentrations of the present work were one order of magnitude higher than those reported for the Northwestern Black Sea (0.012–0.05 μg l^{-1}; Maldonado et al., 1999) but they were one order of magnitude lower than those measured by Marty and Saliot (1976) for the Northwestern Mediterranean Sea (0.70–2.4 μg l^{-1}). One can assume that this decrease in AH concentrations might be linked to the MARPOL 73/78

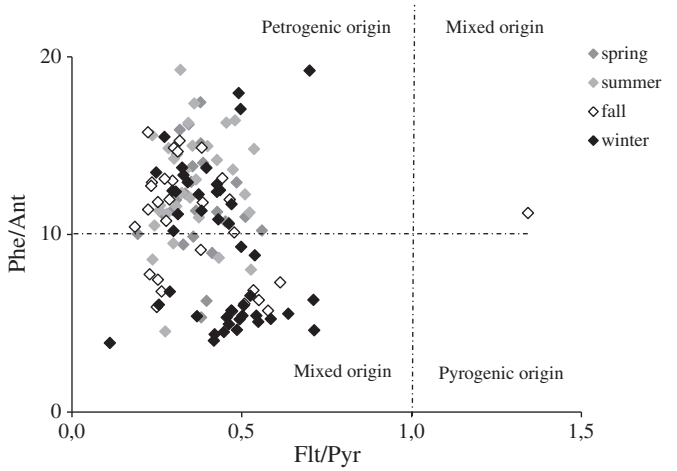

Fig. 4. Cross plot of Phe/Ant versus Flt/Pyr ratios for all sites.

convention, adopted in 1973 and modified several times so far, which deals with the prevention of the hydrocarbon pollution from tankers. Indeed, over the last 40 years, accidental spills of hydrocarbons from ships have been reduced by a factor four in the world ocean. Moreover, since 1987, the Marseilles sewage treatment plant treats wastewaters and run-offs from low rain waters (diverting rivers, such as the Huveaune River that previously flowed into the coastal waters; Fig. 1) from Marseilles and 15 surrounding municipalities. The effluent, after several treatments including oil removing, flows into the Cortiou Creek in the South Bay of Marseilles.

The dissolved PAH concentrations (PAHs-$_P$: 4.7–151 ng l^{-1}; PAHs-$_{P+A}$: 8.1–405 ng l^{-1}) from these Northwestern Mediterranean surface waters were of the same order of magnitude than those previously recorded in this area (Bouloubassi and Saliot, 1991; Tedetti et al., 2010; Guigue et al., 2011) and in other Mediterranean coastal waters (El Nemr and Abd-Allah, 2003; Manodori et al., 2006; Valavanidis et al., 2008). Moreover, a previous study focused on the Rhône River reported the same range of concentrations (PAHs-$_P$: 3.1–89 ng l^{-1}; Sicre et al., 2008). A recent study covering the whole Mediterranean Basin reported lower concentrations in the Western basin (PAHs-$_P$: 0.15–0.81 ng l^{-1}) and in the Eastern basin including the Black Sea, the Marmara Sea and the Nile River mouth (PAHs-$_P$: 0.56–8.80 ng l^{-1}; Berrojalbiz et al., 2011). Similarly, the present results are above PAHs-$_P$ concentrations in coastal waters offshore Barcelona (Spain) and Banyuls-sur-mer (France) (PAHs-$_P$: 4.3–31 ng l^{-1}; Guitart et al., 2007). On the other hand, our PAH concentrations remained far below the concentrations recorded by Zhou et al. (2000) and Guo et al. (2007) from the Xiamen Harbour (106–945 ng l^{-1}) and the Daliao River watershed (946–13,448 ng l^{-1}), respectively (China). According to these comparisons, Marseilles coastal area may be considered as moderately contaminated in PAHs. Several months after the *Prestige* oil spillage, Gonzáles et al. (2006) measured dissolved PAHs-$_{P+A}$ in surface waters from 350 to 580 ng l^{-1} and, 3 years after the *Prestige* wrecks had been sealed for leaks, Elordui-Zapatarietxe et al. (2010) still measured dissolved PAHs-$_{P+A}$ from 31 to 188 ng l^{-1}. With regard to these latter information, dissolved PAH concentrations we recorded in the Marseilles coastal area (up to 405 ng l^{-1} for PAHs-$_{P+A}$), especially during the colder months, reflected an anthropogenic forcing of the same order as that observed several months after a tanker oil spill.

Despite some similarities observed between these two hydrocarbon classes such as the seasonal variations and some contribution from anthropogenic sources (detailed below), AH and PAHs-$_{P+A}$ concentrations were not correlated. Since the concentration levels and molecular composition reflect the balance between the source, transport and removing processes, the miscorrelation between these two classes of dissolved hydrocarbons mirrored the uncoupling of their dynamics, as already mentioned in sediments (Bouloubassi and Saliot, 1993; Wakeham, 1996). Thus, the simultaneous analysis of dissolved AHs and PAHs is supposed to reveal complementary information for a better comprehensive assessment of various natural and anthropogenic inputs as well as for the determination of their environmental behaviour.

4.2. Sources of hydrocarbons

4.2.1. Biogenic sources

AH biogenic fingerprints (planktonic, bacterial and terrigeneous) showed marked spatial and seasonal variations. Indeed, some planktonic contributions (n-C_{17} + Pr) increased from spring to fall while others (n-C_{19}; Wakeham, 1996) increased in winter at all sites except PB. The occurrence of Pr may also be a planktonic signature (Didyk et al., 1978). Furthermore, the predominance of odd or even n-alkanes reflected rather a biogenic origin, while its absence is a sign of an anthropogenic origin. The predominance of even compounds, which is much less common than the odd one, comes from direct microorganism contribution (bacteria, fungi, and yeast) and from their action on algal detritus. This contribution from microorganisms was especially marked at COU and SOF in spring and has already been reported for dissolved water (passing through 1.2 μm porosity filter) in the range n-C_{16}–n-C_{31} (Elias et al., 1997 and reference therein). This signature was more marked at offshore sites where the inputs of petroleum hydrocarbons carried by the Rhône River masked less the biogenic even n-alkanes.

Finally, terrigeneous hydrocarbons were present mostly at VA in fall and underscored that VA was the most terrigeneous impacted site. Terrigeneous signatures were scarcely recorded in the dissolved phase and were only evidenced in sediments and particles in this area (Mille et al., 2007; Guigue et al., 2011). One reason for this is that hydrophobic long chain n-alkanes from higher plants, such as n-C_{27}, n-C_{29} and n-C_{31}, have very high affinity for particles/sediments, and even in the case of turbulence they are not easily transferred to the dissolved phase.

It should be noticed that a few PAHs (especially Naph and Phe) may be biologically produced in plants, soils and sediments, which could have some influence on the distribution of PAHs in continental waters (Wilke, 2007 and references therein). Their similar distribution in continental and offshore marine sites failed to evidence an obvious continental source of these PAHs. This observation is in accordance with the study by Wilke (2007) showing that PAHs in temperate area soils are mainly from anthropogenic origin.

4.2.2. Anthropogenic sources

In summer and fall, chronic petroleum inputs of AHs affected all studied sites, especially in the Rhône and adjacent waters at AR, VA and PB (molecular composition patterns without even or odd n-alkane predominance). An additional fingerprint of degraded petroleum, UCM, was occasionally evidenced only in the Rhône River (UCM/R values of 5.5 and 5.7 on July and September 2011; Mazurek and Simoneit, 1984). This confirmed that the Rhône River drains significant amounts of anthropogenic contaminants (Sicre et al., 2008).

Whatever the site and the season, unburned fossil fuel inputs was the dominant PAH source (Fig. 3; predominance of 2–3 ring compounds with a high proportion of alkylated homologues; Cripps, 1989). This result was in line with previous characterisation of PAHs in the Mediterranean Sea (Manoli et al., 2000; Berrojalbiz et al., 2011). Such PAH profile, in addition to result from unburned petroleum, may be also the consequence of the partitioning of LMW and HMW PAHs between the dissolved and particulate phases, directly related to their difference in K_{ow}. Because they have close K_{ow}, PAH isomers have the same partitioning between the dissolved and particulate phases. Thus, the ratios between isomer compounds (Phe/Ant and Flt/Pyr) seem to be relevant indexes of PAH sources. However, when samples are collected far from defined sources, bio-degradation may affect their ratios (Wang et al., 1999; Katsoyiannis et al., 2011). In the present study, plots of isomer ratios show petrogenic and mixed origins of PAHs-$_{P+A}$ over

the year. These ratios suggested an increase in pyrogenic sources in winter, while another fingerprint (Alk/Par ratios) indicated meanwhile an increase in petrogenic signatures during the colder months. These conflicting results reflected the increase in both inputs. It is well known that unburned and incompletely combusted petroleum PAHs originating industrial/domestic heating increase in winter (Palm et al., 2004). The petrogenic and mixed origins of PAHs were also reported by Manodori et al. (2006) for the Venice lagoon and consistent with a highly urbanised and industrialised area.

Even though isomer ratios did not distinguish PB from the other sites, composition patterns and significant higher PAHs-$_{P+A}$ concentrations indicated recent petroleum sources, especially in winter (Gonzáles et al., 2006). The contamination of PB site from petrogenic additional sources is suspected to come from industrial activities/wastes and shipping traffic. Overall, the overlap of signatures identified various sources of hydrocarbons in the dissolved phase.

4.3. Fate of dissolved hydrocarbons in surface waters

Identifying explicitly the fate of hydrocarbons is difficult in the marine environment because a wide variety of processes including evaporation, bio- and photo-degradation, adsorption onto suspended particles, integration into the food web are interacting during transport (Jordan and Payne, 1980; Tsapakis et al., 2006). The hydrocarbon pattern that we observed over the year in the surface continental and marine waters close to Marseilles suggested some major transport pathways (including the Rhône River and the atmospheric circulation) and several removing processes (see sections that follow).

4.3.1. Major transport pathways

According to hydrological and biogeochemical parameters, VA and PB were highly impacted by the Rhône River inputs (characterised at AR), while COU and SOF were impacted occasionally and weakly, respectively. In addition, AH molecular patterns suggested a Rhône influence at AR, VA and PB (Fig. 2) while COU and SOF evoked different sources and transport pathway. Besides, PAH concentration increases in winter and PAH composition patterns characterised both continental and offshore marine sites, suggesting a more widespread source of hydrocarbons than the Rhône River. Exchange with the atmosphere might be this source of dissolved hydrocarbons in surface coastal waters.

Indeed, it is very well admitted that a major source of dissolved LMW *n*-alkanes ($<n$-C_{24}) and 2–3 ring PAHs in the surface marine waters are gaseous atmospheric depositions (Mandalakis et al., 2002; Tsapakis et al., 2006; Castro-Jiménez et al., 2012). Most inputs/outputs (with highest fluxes for LMW compounds) from the atmosphere are due to diffusive exchanges with surface waters and are subjected to strong seasonal variations (Jurado et al., 2007). In winter, at low temperature, the air–water partitioning favours higher PAH concentrations in surface waters (Palm et al., 2004).

Finally, an additional source of dissolved hydrocarbons can be the sediment remobilisation (resuspension, refocus). The influence of sediment is very likely more important in shallow sites such as AR, VA and PB (Table 1). Moreover, at PB, the AH distribution in the dissolved phase is very similar to that recorded in the sediments (Mille et al., 2007). However, the influence of sediment is more difficult to highlight for PAHs, whose composition over this area is characterised by enrichment in ≥3-ring compounds which hardly partition to dissolved water (Benlahcen et al., 1997; Mille et al., 2007).

4.3.2. Hydrocarbon removing from surface waters

Several studies showed that weathering processes (i.e., evaporation, bio-degradation and photo-degradation) induced a preferential loss of LMW hydrocarbons (Wang and Fingas, 1995; Dachs et al., 1999, 2002; Yamada et al., 2003; Tsapakis et al., 2006). Evaporation to the atmosphere is the most important process that hydrocarbons undergo after their introduction/deposition to surface waters and it affects both AHs and PAHs with regard to their vapour pressure (Yamada et al., 2003). Degradation by marine bacteria and photo-degradation lead to synergetic reactions that enhance the degradation (Watkinson and Griffiths, 1987; Litheraty et al., 1989). Seasonal variations of removing processes have also been widely described. In summer, with the temperature increase, there is a net volatilisation of LMW hydrocarbons (Fingas, 1995; Dachs et al., 2002; Palm et al., 2004). Moreover, lower concentrations of LMW hydrocarbons in summer have been often ascribed to higher rates of photo- and bio-degradations (Yamada et al., 2003; Palm et al., 2004). In our study area (the Mediterranean Sea), the amplitudes in the sea surface temperature and in the solar irradiance received at the surface between winter and summer (13 and 26 °C, and 144 and 540 W m^{-2}, respectively) are very likely to promote more intense weathering of dissolved hydrocarbons from surface waters in summer. Indeed, we found that, along with lower concentrations, 2-ring PAHs-$_{P+A}$ proportions were lower in spring, summer and fall ($51 \pm 9\%$) compared to winter ($60 \pm 8\%$) ($p < 0.0001$, $n = 26$–44), highlighting an increase in weathering effects during the warmer months. In a previous study, Albinet et al. (2007) recorded PAHs derivatives associated with photo-chemical processes (nitrated and oxygenated PAHs) originating mainly from gasoline and diesel engines in the ambient air of Marseilles.

Hydrocarbons can also be removed from surface waters by sorption onto biogenic and/or atmospherically deposited particles (Dachs et al., 1996, 2002; Ko et al., 2003; Berrojalbiz et al., 2009). This process is likely to concern HMW compounds and follows the (organic) particle seasonal cycle. Although biogeochemical parameters pointed out significantly higher POC concentrations in spring relative to winter due to biological activity (Table 2; $p = 0.019$, $n = 26$), we found no relationship between the dissolved AH, PAHs-$_{P+A}$ and POC concentrations throughout the year. Thus, adsorption onto particles was not the main driver of the decrease in dissolved LMW PAHs-$_{P+A}$ (and AHs) we observed during the warmer months.

5. Conclusions

This one year study highlights that the Marseilles coastal area is moderately contaminated in hydrocarbons compared to other coastal environments, except Port-de-Bouc Harbour which, subjected to an intense shipping traffic and industrial activities/wastes, may reach PAHs-$_{P+A}$ levels encountered several months after oil spillages. Our results underline various natural and anthropogenic sources of hydrocarbons along with different transport pathway and removing processes. The major entering pathways for allochthonous dissolved hydrocarbons in this coastal area seemed to be the atmosphere and the Rhône River (limited to the plume extent) while some autochthonous biogenic hydrocarbon were also evidenced. We show a seasonal variation of inputs and removing processes, with higher inputs from unburned petroleum/incompletely combusted emissions and higher surface run-offs and less weathering processes in winter, whereas the opposite pattern was observed in summer (less inputs and more evaporation/degradation). Interestingly, no differences were found between 0.1 and 5 m depth, neither for biogeochemical and hydrological parameters, nor for hydrocarbon concentrations. This study demonstrates the complexity and the pertinence of investigating the dynamics of organic pollutants in the dissolved phase of the water column since it provides access to complementary information that is not available when studying settling/sinking particles and sediments. Dissolved organic pollutants may interact with natural organic matter (especially humic substances) to form different complexes. These complexes are known to modify their bioavailability/toxicity and their transport in the coastal environment. Hence, further investigations taking into account the complexation between pollutants and organic matter are necessary to get a global picture of the dynamics of dissolved organic pollutants in marine coastal waters.

Acknowledgements

We are grateful to the captain and crew of the R/V Antédon II, as well as to the Service d'Observation of the Mediterranean Institute of Oceanography and to the core parameter platform, both managed by P. Raimbault, for their excellent cooperation. The authors are grateful to two anonymous reviewers for their comments and suggestions. This study is part of "IBISCUS" and "VASQUE" projects, labelled by the Competitivity Cluster Mer PACA. IBISCUS received the financial support from the Agence Nationale de la Recherche (ANR) — ECOTECH programme (project ANR-09-ECOT-009-01). VASQUE was funded by the Direction Générale de la Compétitivité, de l'Industrie et des Services (DGCIS) — Eco industries programme. This work also contributes to Work Package 3 of the CNRS-INSU MISTRALS "MERMEX" project.

References

Akkanen J, Tuikka A, Kukkonen JVK. On the borderline of dissolved and particulate organic matter: partitioning and bioavailability of polycyclic aromatic hydrocarbons. Ecotoxicol Environ Saf 2012;78:91–8.

Albinet A, Leoz-Garziandia E, Budzinski H, Villenave E. Polycyclic aromatic hydrocarbons (PAHs), nitrated PAHs and oxygenated PAHs in ambient air of the Marseilles area (South of France): concentrations and sources. Sci Total Environ 2007;384:280–92.

Aminot A, Kérouel R. Dosage automatique des nutriments dans les eaux marines: méthodes en flux continu. Méthodes d'analyses en milieu marin, Ifremer. France: Brest; 2007.

Azimi S, Rocher V, Muller M, Moilleron R, Thevenot DR. Sources, distribution and variability of hydrocarbons and metals in atmospheric deposition in an urban area (Paris, France). Sci Total Environ 2005;337:223–39.

Benlahcen KT, Chaoui A, Budzinski H, Bellocq J, Garrigues P. Distribution and sources of polycyclic aromatic hydrocarbons in some Mediterranean coastal sediments. Mar Pollut Bull 1997;34:298–305.

Berrojalbiz N, Lacorte S, Calbet A, Saiz E, Barata C, Dachs J. Accumulation and cycling of polycyclic aromatic hydrocarbons in zooplankton. Environ Sci Technol 2009;43:2295–301.

Berrojalbiz N, Dachs J, Ojeda. MJ, Valle MC, Castro-Jiménez J, Wollgast J, et al. Biogeochemical and physical controls on concentrations of polycyclic aromatic hydrocarbons in water and plankton of the Mediterranean and Black Seas. Global Biogeochem Cycles 2011;25(GB4003). http://dx.doi.org/10.1029/2010GB003775.

Bouloubassi I, Saliot A. Composition and sources of dissolved and particulate PAHs in surface waters from the Rhone Delta (NW Mediterranean). Mar Pollut Bull 1991;22:588–94.

Bouloubassi I, Saliot A. Investigation of anthropogenic and natural organic inputs in estuarine sediments using hydrocarbon markers (NAH, LAB, PAH). Oceanol Acta 1993;16:145–61.

Budzinski H, Jones I, Bellocq J, Piérard C, Garrigues P. Evaluation of sediment contamination by polycyclic aromatic hydrocarbons in the Gironde estuary. Mar Chem 1997;58:85–97.

Castro-Jiménez J, Berrojalbiz N, Wollgast J, Dachs J. Polycyclic aromatic hydrocarbons (PAHs) in the Mediterranean Sea: atmospheric occurrence, deposition and decoupling with settling fluxes in the water column. Environ Pollut 2012;16:40–7.

Cincinelli A, Stortini AM, Perugini M, Checcini L, Lepri L. Organic pollutants in sea-surface microlayer and aerosol in the coastal environment of Leghorn (Tyrrhenian Sea). Mar Chem 2001;76:77–98.

Cripps GC. Problems in the identification of anthropogenic hydrocarbons against natural background levels in the Antarctic. Antarct Sci 1989;14:307–12.

Dachs J, Bayona JM, Fowler SW, Miquel JC, Albaigés J. Vertical fluxes of polycyclic aromatic hydrocarbons and organochlorine compounds in the western Alboran Sea (southwestern Mediterranean). Mar Chem 1996;52:75–86.

Dachs J, Bayona JM, Raoux C, Albaigés J. Spatial, vertical distribution and budget of polycyclic aromatic hydrocarbons in the western Mediterranean seawater. Environ Sci Technol 1997;31:682–8.

Dachs J, Bayona JM, Fillaux J, Saliot A, Albaigés J. Evaluation of anthropogenic inputs into the western Mediterranean using molecular markers. Mar Chem 1999;65:195–210.

Dachs J, Lohman R, Ockenden WA, Méjanelle L, Eisenrich S, Jones KC. Oceanic biogeochemical controls on global dynamics of persistent organic pollutants. Environ Sci Technol 2002;36:4229–37.

Didyk BM, Simoneit BRT, Brassel SC, Eglinton G. Organic geochemical indicators of paleoenvironmental conditions of sedimentation. Nature 1978;272:216–22.

Douglas AG, Eglinton G. Distribution of alkanes. In: Swam T, editor. Comparative phytochemistry. London, New York: Academic Press; 1966. p. 57–77.

Durrieu de Madron X, Denis L, Diaz F, Garcia N, Guieu C, Loye-Pilot M, Ludwig W, Moutin T, Raimbault P, Ridame C. Nutrients and carbon budgets for the Gulf of Lion during the Moogli cruises. Oceanol Act 2003;26:421–33.

El Nemr A, Abd-Allah AMA. Contamination of polycyclic aromatic hydrocarbons (PAHs) in microlayer and subsurface waters along Alexandria coast, Egypt. Chemosphere 2003;52:1711–6.

Elias VO, Simoneit BRT, Cardoso JN. Even *n*-alkanes on the Amazon Shelf and a northeast Pacific hydrothermal system. Naturwissenschaften 1997;84:415–20.

Elordui-Zapatarietxe S, Rosell-Melé A, Moraleda N, Tolosa I, Albaigés J. Phase distribution of hydrocarbons in the water column after a pelagic deep ocean oil spill. Mar Pollut Bull 2010;60:1667–73.

Fingas MF. A literature review of the physics and predictive modelling of oil spill evaporation. J Hazard Mater 1995;42:157–75.

Gonzáles JJ, Vinãs L, Franco MA, Fumega J, Soriano JA, Grueiro G, Muniategui S, López-Mahiá P, Prada D, Bayona JM, Alzaga R, Albaigés J. Spatial and temporal distribution of dissolved:dispersed aromatic hydrocarbons in seawater in the area affected by the *Prestige* oil spill. Mar Pollut Bull 2006;53:250–9.

Guigue C, Tedetti M, Giorgi S, Goutx M. Occurrence and distribution of hydrocarbons in the surface microlayer and subsurface water from the urban coastal marine area off Marseilles, Northwestern Mediterranean Sea. Mar Pollut Bull 2011;62:2741–52.

Guitart C, García-Flor N, Bayona JM, Albaigés J. Occurrence and fate of polycyclic aromatic hydrocarbons in the coastal surface microlayer. Mar Pollut Bull 2007;54:186–94.

Guo W, He M, Yang Z, Lin C, Quan X, Wang H. Distribution of polycyclic aromatic hydrocarbons in water, suspended particulate matter and sediment from Daliao River watershed, China. Chemosphere 2007;68:93–104.

Gustafsson, Gschwend. Aquatic colloids: concepts, definitions and current challenges. Limnol Oceanogr 1997;42:519–28.

Jordan RE, Payne JR. Fate and weathering of petroleum spills in the marine environment: a literature review and synopsis. Ann Arbor, Michigan: Ann Arbor Science Publishers; 1980.

Jurado E, Zaldívar JM, Marinov D, Dachs J. Fate of persistent organic pollutants in the water column: does turbulent mixing matter? Mar Pollut Bull 2007;54:441–51.

Katsoyiannis A, Sweetman AJ, Jones KC. PAH molecular diagnostic ratios applied to atmospheric sources: a critical evaluation using two decades of source inventory and air concentration data from the UK. Environ Sci Technol 2011;45:8897–906.

Kennish MJ. Poly-nuclear aromatic hydrocarbons. Ecology of estuaries: anthropogenic effects. Boca Raton: CRC Press; 1992. p. 133–81.

Ko K, Sanford LP, Baker JE. Internal cycling of particle reactive organic chemicals in the Chesapeake Bay water column. Mar Chem 2003;81:163–76.

Lipiatou E, Tolosa I, Simó R, Bouloubassi I, Dachs J, Marti S, Sicre MA, Bayona JM, Grimalt JO, Saliot A, Albaigés J. Mass budget and dynamics of polycyclic aromatic hydrocarbons in the Mediterranean Sea. Deep Sea Res Part II 1997;44:881–905.

Litheraty P, Haider S, Samhan O, Morel G. Experimental studies on biological and chemical oxidation of dispersed oil in seawater. Water Sci Technol 1989;21:845–56.

MacDonald RW, Barrie LA, Bidleman TF, Diamond ML, Gregor DJ, Semkin RG, et al. Contaminants in the Canadian Arctic: 5 years of progress in understanding sources, occurrence and pathways. Sci Total Environ 2000;254:93–234.

Maldonado C, Bayona JM, Bodineau L. Sources, distribution, and water column processes of aliphatic and polycyclic hydrocarbons in the Northwestern Black Sea water. Environ Sci Technol 1999;33:2693–702.

Mandalakis M, Tsapakis M, Tsoga A, Stephanou EG. Gas–particle concentrations and distribution of aliphatic hydrocarbons, PAHs, PCBs and PCDD/Fs in the atmosphere of Athens (Greece). Atmos Environ 2002;36:4023–35.

Manodori L, Gambaro A, Piazza R, Ferrari S, Stortini AM, Moret I, Capodaglio G. PCBs and PAHs in the sea-surface microlayer and sub-surface water samples of the Venice Lagoon (Italy). Mar Pollut Bull 2006;52:184–92.

Manoli E, Samara C, Konstantinou I, Albanis T. Polycyclic aromatic hydrocarbons in the bulk precipitation and surface waters of Northern Greece. Chemosphere 2000;41:1845–55.

Marty JC, Saliot A. Hydrocarbons (normal alkanes) in the surface microlayer of sea water. Deep-Sea Res 1976;23:863–73.

Mazurek MA, Simoneit BRT. Characterization of biogenic and petroleum-derived organic matter in aerosols over remote, rural and urban areas. In: Keith LH, editor. Identification and analysis of organic pollutants in air. Boston: Ann Arbor Science; 1984. p. 353–70.

Mille G, Asia L, Guiliano M, Malleret L, Doumenq P. Hydrocarbons in coastal sediments from the Mediterranean Sea (Gulf of Fos area, France). Mar Pollut Bull 2007;54:566–75.

Pairaud IL, Gatti J, Bensoussan N, Verney R, Garreau P. Hydrology and circulation in a coastal area off Marseille: validation of a nested 3D model with observations. J Mar Syst 2011;88:20–33.

Palm A, Cousins I, Gustafsson Ö, Axelman J, Grunder K, Broman D, Brorström-Lundén E. Evaluation of sequentially-coupled POP fluxes estimated from simultaneous measurements in multiple compartments of an air–water–sediment system. Environ Pollut 2004;128:85–97.

Para J, Coble PG, Charrière B, Tedetti M, Fontana C, Sempéré R. Fluorescence and absorption properties of chromophoric dissolved organic matter (CDOM) in coastal surface waters of the northwestern Mediterranean Sea, influence of the Rhône River. Biogeosciences 2010;7:4083–103.

Pérez S, Dachs J, Barceló D. Sea breeze modulated volatilization of polycyclic aromatic hydrocarbons from the Masnou Harbor (NW Mediterranean Sea). Environ Sci Technol 2003;37:3794–802.

Pujo-Pay M, Conan P, Joux F, Oriol L, Naudin JJ, Cauwet G. Impact of phytoplankton and bacterial production on nutrient and DOM uptake in the Rhône River plume (NW Mediterranean). Mar Ecol Prog Ser 2006;315:43–54.

Raimbault P, Diaz F, Boudjellal B. Simultaneous determination of particulate forms of carbon, nitrogen and phosphorus collected on filters using a semiautomatic wet-oxidation procedure. Mar Ecol Prog Ser 1999;180:289–95.

Raimbault P, Neveux J, Lantoine F. Dosage rapide de la chlorophylle *a* et des phaeopigments *a* par fluorimétrie après extraction au méthanol. Comparaison avec la méthode classique d'extraction à l'acétone. Oceanis 2004;30:189–205.

Readman JW, Fillmann G, Tolosa I, Bartocci J, Villeneuve JP, Catinni C, Mee LD. Petroleum and PAH contamination of the Black Sea. Mar Pollut Bull 2002;44:48–62.

Scarlett A, Galloway TS, Rowland SJ. Chronic toxicity of unresolved complex mixture (UCM) of hydrocarbons in the marine sediments. J Soils Sediments 2007;7:200–6.

Schwarzenbach RP, Gschwend PM, Imboden DM. Environmental organic chemistry. New York: John Wiley & Sons; 1993.

Sicre MA, Fernandes MB, Pont D. Poly-aromatic hydrocarbon (PAH) inputs from the Rhône River to the Mediterranean Sea in relation with the hydrological cycle: impact of floods. Mar Pollut Bull 2008;56:1935–42.
Siron R, Giusti. G, Blanc F. Hydrocarbons in the water column of the Carteau Bay (Gulf of Fos-sur-mer, Mediterranean Sea). Mar Chem 1987;21:75–89.
Stortini AM, Martellini T, Del Bubba M, Lepri L, Capodaglio G, Cincinelli A. *n*-Alkanes, PAHs and surfactants in the sea surface microlayer and sea water samples of the Gerlache Inlet Sea (Antarctica). Microchem J 2009;92:37–43.
Tedetti M, Guigue C, Goutx M. Utilization of a submersible UV fluorometer for monitoring anthropogenic inputs in the Mediterranean coastal waters. Mar Pollut Bull 2010;60: 350–62.
Tilseth S, Solberg TS, Westrheim K. Sublethal effects of the water-soluble fraction of Ekofisk crude oil on the early larval stages of cod (*Gadus morhua* L.). Mar Environ Res 1984;11:1–16.
Tolosa I, Bayona JM, Albaigés J. Aliphatic and polycyclic aromatic hydrocarbons and sulfur/oxygen derivatives in Northwestern Mediterranean sediments: spatial and temporal variability, fluxes, and budgets. Environ Sci Technol 1996;30:2495–503.
Tsapakis M, Apostolaki M, Eisenreich S, Stephanou EG. Atmospheric deposition and marine sedimentation fluxes of polycyclic aromatic hydrocarbons in the eastern Mediterranean Basin. Environ Sci Technol 2006;40:4922–7.
Ulses C, Grenz C, Marsaleix P, Schaaff E, Estournel S, Meulé S, Pinazo C. Circulation in a semi-enclosed bay under influence of strong freshwater input. J Mar Syst 2005;56: 113–32.
Valavanidis A, Vlachogianni T, Triantafillaki S, Dassenakis M, Androutsos F, Scoullos M. Polycyclic aromatic hydrocarbons in surface seawater and indigenous mussels (*Mytilus galloprovincialis*) from coastal areas of the Saronikos Gulf (Greece). Estuar Coast Shelf Sci 2008;79:733–9.
Wakeham SG. Aliphatic and polycyclic aromatic hydrocarbons in Black Sea sediments. Mar Chem 1996;53:187–205.
Wang Z, Fingas M. Differentiation of the source of spilled oil and monitoring of the oil weathering process using gas chromatography–mass spectrometry. J Chromatogr A 1995;712:321–43.
Wang Z, Fingas M, Page DS. Oil spill identification. J Chromatogr A 1999;843:369–411.
Watkinson RJ, Griffiths D. Biodegradation and photo-oxidation of crude oils in a tropical marine environment. In: Kuiper J, Van der Brink WJ, editors. Fate and effects of oil in marine ecosystems. The Hague: Martinus Nijhoff Publishers; 1987.
Wilke W. Global patterns of polycyclic aromatic hydrocarbons (PAHs) in soil. Geoderma 2007;141:157–66.
Wurl O, Obbard JP. A review of pollutants in the sea-surface microlayer (SML): a unique habitat for marine organisms. Mar Pollut Bull 2004;48:1016–30.
Yamada M, Takada H, Toyoda K, Yoshida, Shibata A, Nombra H, Wada M, Nishimura M, Okamoto K, Ohwada K. Study of the fate of petroleum-derived polycyclic aromatic hydrocarbons (PAHs) and the effect of chemical dispersant using an enclosed ecosystem. Mar Pollut Bull 2003;47:105–13.
Zhou JL, Hong H, Zhang Z, Maskaoui K, Chen W. Multi-phase distribution of organic micropollutants in Xiamen Harbour, China. Water Res 2000;34:2132–50.